2018

Drying Inhomogeneity during Film Formation of Waterborne Latex Systems – A Mechanistic Study on Skin Layer Formation

Hao Huang
Lehigh University

Drying Inhomogeneity during Film Formation of Waterborne Latex Systems – A Mechanistic Study on Skin Layer Formation

by

Hao Huang

A Dissertation

Presented to the Graduate and Research Committee

of Lehigh University

in Candidacy for the Degree of

Doctor of Philosophy

in

Chemical Engineering

Lehigh University

May 2018

Certificate of Approval

Approved and recommended for acceptance as a dissertation in partial fulfillment of the requirements for the degree of Doctor of Philosophy.

Date

Dr. Mohamed S. El-Aasser
Professor in Charge and Advisor

Accepted Date

Committee Members

Prof. Mohamed S. El-Aasser
Chairman and Advisor

Prof. H. Daniel Ou-Yang
Co-advisor

Dr. Willie Lau

Prof. James F. Gilchrist

Prof. Mark A. Snyder

Acknowledgments

The author wishes to express sincere gratitude to:

- ✧ Professor Mohamed S. El-Aasser for invaluable guidance and advice throughout this project, for proofreading the drafts of my dissertation, and for engaging me in learning and gaining comprehensive knowledge of emulsion polymerization and latex systems.
- ✧ Professor H. Daniel Ou-Yang for invaluable guidance and advice throughout this project, for suggestions on experiment design, and for directing me in learning about optics, confocal microscopies and systematic knowledge of colloidal dynamics.
- ✧ Dr. Willie Lau, the chief scientist of Beijing Oriental Yuhong Waterproof Technology Co., Ltd (Oriental Yuhong), for bringing and supporting this project, for providing vital advice, as well as for serving on the Dissertation Committee.
- ✧ Professor James F. Gilchrist and Professor Mark A. Snyder for appreciable discussions and suggestions, as well as for serving on the Dissertation Committee.
- ✧ Professor Chao Zhou and Mr. Yongyang Huang for providing and educating me about the optical coherence tomography (OCT) and for profound collaboration in this project.
- ✧ Dr. Eric S. Daniels, Mr. Tom Madle (from Dow Chemical Company) and Mr. Joseph Rokowski (from Oriental Yuhong) for instructing me about technologies of latex and coatings, as well as for helpful discussions.
- ✧ Mr. Zhiyu Jiang for participation in latex synthesis and helpful discussions, as well as Mr. Chong Shen and Mr. Krittanon Sirorattanakul for helpful discussions.
- ✧ All other faculty members, colleagues and friends for their helps.
- ✧ Beijing Oriental Yuhong Waterproof Technology Co., Ltd and Emulsion Polymers Institute for financial and technical support.

Dedication

To my parents, Xiaoshi Huang and Xiulan Jia

Table of Contents

List of Tables

List of Figures

Glossary of Symbols

A_{coal}	coalesced layer thickening prefactor ($\mu m/\min^{1/2}$)
CMC	critical micelle concentration (mM)
CMC_{serum}	CMC of surfactant in aqueous phase of latex (mM)
$c_{sur,aq}$	surfactant concentration in aqueous phase of latex, where "sur" can be "SLS" or "TTX" to represent the SLS or TTX surfactant, respectively (mM)
D_p	diameter of latex particle (nm)
d_n	number average diameter of latex particles (nm)
d_s	surface average diameter of latex particles (nm)
d_v	volume average diameter of latex particles (nm)
d_w	weight average diameter of latex particles (nm)
d_{in}	average inter-distance between latex particles (nm)
e	Euler's number
$\dot{E}$	water receding rate, or velocity of water surface falling during drying (nm/s)
h_{skin}	skin layer thickness (μm)
h_{coal}	coalesced layer thickness (μm)
H	wet film thickness (mm)
H_{dry}	dried film thickness (mm)
I	ionic strength of aqueous medium (mM)
J	water flux (water mass loss per unit area per unit time) through a dried latex film, a skin layer or a coalesced layer ($g/(cm^2 \cdot min)$)
k_B	Boltzmann constant (J/K)
k_{FCC}	% solids content of face-centered cubic (FCC) lattice of latex particles

k_{s0}	initial % solids content of latex
k_s	% solids content of latex at a point of time during drying
$k_{sur/s}$	weight ratio of surfactant versus solid in latex, where "sur" can be "SLS" or "TTX" to represent the SLS or TTX surfactant, respectively
$k_{add/s}$	weight ratio of water-soluble additive versus solid in latex, where "add" can be "SLS", "TTX", "APA" or "PEG" additive
k_w	film water content
$k_{w,infl}$	film water content at inflection point
$k_{w,2k}$	film water content at 2000 min
k_w^*	water content in wet domain
K_D	partition coefficient, i.e. ratio of the molar amount of adsorbed surfactant on latex particles' surface versus the amount of surfactant in aqueous phase
K_{spc}	speckle contrast value
M_{sur}	molecular weight of surfactant, where "sur" can be "SLS" or "TTX" to represent the SLS or TTX surfactant, respectively (g/mol)
N_A	Avogadro constant (mol^{-1})
p_0	equilibrium water vapor pressure (Pa)
PDI	polydispersity index of particle size distribution
Pe	Peclet number
q_e	elementary charge (C)
ΔRH	difference of relative humidity on two sides of a dried latex film, a skin layer or a coalesced layer
R_{abs}	relative absorbed water mass

$\tilde{R}_{abs}$	water absorption efficiency ($\mathrm{day}^{-1/2}$)
R_p	radius of latex particle (nm)
SD	standard deviation of diameter of latex particles (nm)
SC_{carb}	% of particles' surface coverage by chemically bound carboxyl groups
SC_{sulf}	% of particles' surface coverage by chemically bound sulfate groups
SC_{sur}	% of particles' surface coverage by surfactant molecules, where "sur" can be "SLS" or "TTX" to represent the SLS or TTX surfactant, respectively
T	temperature (°C)
t_{coal}	time point when coalesced layer begins thickening (min)
t_{infl}	inflection point (min)
Δt_{del}	coalescence delay time (min)
$\widetilde{\Delta t}_{del}$	coalescence delay efficiency (min/(1%))
T_g	glass transition temperature of polymer (°C)
WVP	water vapor permeability of a dried latex film, a skin layer or a coalesced layer ($\mathrm{g}/(\mathrm{cm} \cdot \mathrm{min} \cdot \mathrm{Pa})$)
$w(t)$	drying curve, i.e. water weight loss per area as a function of time ($\mathrm{g/cm^2}$)
$dw(t)/dt$	drying rate curve, i.e. derivative of $w(t)$ versus time ($\mathrm{g}/(\mathrm{cm}^2 \cdot \mathrm{min})$)
$\phi_w(t)$	drying extent curve, i.e. percentage of the evaporated water versus the total water in the initial latex film as a function of drying time
$k_w(t)$	film water content curve, i.e. weight percentage of water in the latex film as a function of time
γ	interfacial tension (Dynes/cm)
ε_m	permittivity of aqueous medium (F/m)

$\bar{\lambda}$	$\bar{\lambda}$ factor, i.e. ratio of drying rate versus particle deformation rate
μ	viscosity of water (Pa · s)
v_0	initial drying rate of latex film ($g/(cm^2 \cdot min)$)
ρ	density of latex (g/cm^3)
ρ_s	density of solid or polymer in latex (g/cm^3)
ρ_w	density of water or aqueous phase in latex (g/cm^3)
φ_{acid}	number density of acid groups on particle surface (nm^{-2})
φ_{carb}	number density of carboxyl groups on particle surface (nm^{-2})
φ_{sulf}	number density of sulfate groups on particle surface (nm^{-2})
$\varphi_{sur,p}$	number density of surfactant molecules adsorbed on particle surface, where "sur" can be "SLS" or "TTX" to represent SLS or TTX surfactant (nm^{-2})
$\tilde{\varphi}_{sur}$	surfactant adsorption efficiency, where "sur" can be "SLS" or "TTX" to represent the SLS or TTX surfactant, respectively (nm^{-2}/mM)
$\varphi_{sur,p,max}$	maximum number density of surfactant molecules adsorbed on particle surface, where "sur" can be "SLS" or "TTX" to represent the SLS or TTX surfactant, respectively (nm^{-2})

Abstract

Drying inhomogeneity of latex is the phenomenon where the spatial distribution of latex particles is non-uniform and evolving with time during the drying process. In order to study this phenomenon, this dissertation research employed the optical coherence tomography (OCT), a 3D microscopic imaging technique, to visualize the dynamics and the structure of latex in real time. The gravimetric and video analysis were also integrated to OCT (called "OCT-Gravimetry-Video" method) to simultaneously monitor the drying process of latex.

For the polystyrene model latex (with T_g = 106 °C), multiple types of drying inhomogeneity were observed at room temperature. Vertical packing and horizontal drying front were the packing processes of particles from the top of latex and the edge of latex, respectively. Shear bands and cracks were the dislocations of latex structure after particles became packed, due to the lack of particles' deformation to relax the internal stress.

For the film-forming low-T_g model latexes (acrylate copolymer latexes with $T_g < 0$ °C) at room temperature, the particles on the top of drying latex are readily deformed and coalesced early into a polymer layer (called "skin layer"). The low-permeable skin layer impedes drying and retains water in the wet domain beneath skin. The film drying time can extend to weeks which is unacceptable in paint applications. In the architectural or roof coatings with millimeter-thick films, ~15 wt% water can be trapped beneath skin, leading to poor adhesion to substrate and bubbles inside films. The real-time OCT images show four drying stages: I) packing of particles, II) consolidation of particles, III) formation and maturation of incipient skin, IV) thickening of coalesced latex polymer layer (coalesced layer, which includes skin). The gravimetry shows a dramatic decrease of drying rate after Stage III, and the film appears white and opaque in the video. The entire film drying time

can be dominated by Stage IV. The coalesced layer thickness (h_{coal}) is found to increase with the square root of time, and the "coalesced layer thickening model" is developed.

It is found that, the post-added (added after polymerization) surfactant into the low-T_g latex can delay the maturation of skin layer (Stage III), accelerate the increment of h_{coal} with time, and shorten the film drying time. A mechanism is proposed that, besides other chemical species in aqueous phase, the surfactant molecules adsorbed on particles' surface (which increase repulsive forces between particles) and the surfactant molecules desorbed from particles' surface (which are trapped within the interstices between particles) can delay the coalescence between particles. The longer the delay time for particles' coalescence (Δt_{del}), the more water evaporates before the packed particles on top coalesce into a matured skin, thus the water content in the wet domain beneath skin (k_w^*) is reduced. According to the mathematical model, lower k_w^* leads to faster increase of h_{coal} with time, and less time for drying the entire latex film. Based on the measured drying curves, Δt_{del} is found to increase linearly with the percentage of latex particles' surface coverage by surfactant (SC_{sur}). At the same SC_{sur}, the anionic sodium lauryl sulfate surfactant gives a longer Δt_{del} than the nonionic Triton X-100 surfactant does. For both the model latexes and the commercial latex studied in this dissertation research, with the appropriate type and amount of surfactant post-added into latex, not only is the film drying time significantly shortened, but also the water-resistance of the dried latex film is not compromised.

Drying inhomogeneity is complex, which is not only determined by the physical properties of latex, but also influenced by the water-soluble molecules and their molecular interactions. The OCT-Gravimetry-Video method can be a useful tool to study the drying process and film formation of latex systems with more details.

1 Chapter 1 Introduction

1.1 Waterborne latex and coatings

Latex, or emulsion polymer, is a colloidal system of polymer particles suspended in water. Milk, secreted by mammals, is a latex containing protein aggregates in aqueous medium[1]. Flowering plants also exude latex to protect damaged tissues[2]. The most famous latex in nature is "natural rubber"[3], produced from rubber trees and composed of poly(cis-1,4-isoprene) particles with diameters from 0.08 to 2 μm. Natural rubbers, widely used as adhesives and elastomers since ancient times, have inspired people to make synthetic latexes through the process of emulsion polymerization[4–6]. Industrially developed from 1930s, emulsion polymerization is a free-radical-initiated chain polymerization in an aqueous phase, in the presence of surfactants, initiators, monomer droplets and sometimes chain transfer agents. Surfactant molecules can adsorb on polymer particles to prevent aggregation and keep stability; initiator produces free radicals, while monomer droplets provide reservoirs of monomer and chain transfer agent controls molecular weight. Micellar nucleation, homogeneous nucleation and droplet nucleation were three proposed mechanisms to form polymer particles in water. Considering product stability and shipping cost, the particle sizes (diameters) are controlled within tens to hundreds of nanometers, and the solids contents of latexes are around 50 wt% or higher. Global demand for latex was 10.2 million metric tons in 2015, and forecast to rise 4.2% per year to 12.5 million metric tons in 2020 (valued at $37.2 billion)[7]. The majority of latexes go to industries of paints, coatings and adhesives. They are also used as inks, cosmetics and pharmaceuticals. With nearly zero emission of volatile organic compounds (VOC), waterborne latex is

becoming more and more popular than solvent-borne polymers. By drying a pool of liquid latex at a temperature higher than polymer's glass transition temperature (T_g), the colloidal polymer particles can be transformed into a continuous polymer film, which covers a material surface for protective, aesthetic, medical and other purposes. Pigments, fillers, water-soluble additives, coalescing agents and rheological modifiers are always mixed with latexes to improve the mechanical, coloring and leveling properties of waterborne coatings. Ideally, by drying waterborne latex homogeneously (i.e. latex particles distribute uniformly in space during the whole drying process), a uniform and transparent polymer film can be formed without obvious structural defects. Nevertheless, real applications always suffer drying inhomogeneity, resulting in defects such as drying front, shear bands, cracks, detachment and skin layer. This dissertation develops the "OCT (optical coherence tomography)-Gravimetry-Video" method to investigate the drying inhomogeneity in both microscopic and macroscopic ways. This dissertation focuses on studying the mechanism of skin layer formation, where during the drying process, the latex particles near the top surface of latex film (film/air interface) get dried early and form a polymer skin that impedes water evaporation from underneath. This dissertation also studies the effects of post-added (added after polymerization) surfactants and other water-soluble additives on the skin layer formation and the film formation process, in order to solve the slow-drying problem caused by skin. Concerning the water resistance of dried latex film, the water absorptions of dried films are also examined.

1.2 Latex film formation

Compared to the drying process of solvent-borne polymers during which polymer molecule chains become concentrated and entangled, the drying process of latex particles is more complex. It transforms liquid suspension of separated polymer particles into a coherent solid polymer film, which is called "latex film formation". Since 1951 when Dillon et al.[8] borrowed the idea of sintering of powered metals and firstly proposed the concept of fusion of polymer particles, theoretical and experimental researches[9–16] have abounded in studying the mechanism of latex film formation. Basically, the film formation process contains four sequential states (shown in Figure 1.1). Initially, particles are separately suspended in water, with surfactants and water-soluble molecules either adsorbed on particle surfaces or dissolved in aqueous medium (State 1). With free water evaporation, particles get closer until touching each other or being packed (State 2). At State 2, particles are usually not as regularly packed as shown in Figure 1.1, instead, they should be randomly packed because of fast drying rate and non-uniform particle size distribution. With further loss of water within particles' interstices, and when the particles are soft enough or drying temperature is higher than polymer's T_g, particles deform into hexagonal shapes to fill the voids (State 3). At State 3, the boundaries between particles are clear and enriched with surfactant and other water-soluble molecules; the mechanical strength of the film is still weak. Afterwards, the polymer chains in each particle reptate to break up the boundary, and get entangled with those in neighboring particles (State 4). When the interdiffusion depth reaches around one gyration radius of polymer chain, the film's strength becomes fully developed. Water-soluble molecules at State 4 are either trapped within polymer matrix, or exuded toward film top (film/air interface) and film bottom

(film/substrate interface). Since the amount of water-soluble molecules is usually less than 1% of polymer mass and the sizes of molecule aggregates are usually less than visible light wavelength, the film looks transparent. To sum up, latex film formation experiences three major steps: packing of particles (from State 1 to 2), deformation of particles (from State 2 to 3) and coalescence of particles (from State 3 to 4).

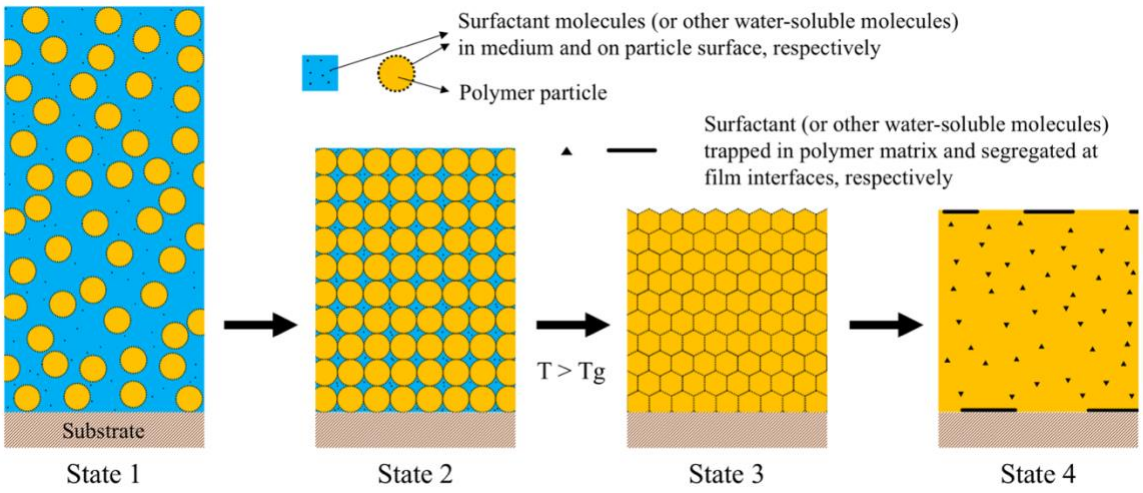

Figure 1.1: Schematic illustration of major states of latex film formation, from the start of free water evaporation to the end of polymer interdiffusion: State 1 – suspended particles, State 2 – packed particles, State 3 – deformed particles, State 4 – coalesced polymer film.

1.3 Drying inhomogeneity

If the drying processes at all locations on a pool of latex are the same as Figure 1.1, the resulting dried film should be continuous, smooth and uniform. However, in reality, drying is always inhomogeneous in both the horizontal direction (parallel to film surface) and vertical direction (perpendicular to film surface), during which the spatial distribution of latex particles is non-uniform and evolving with drying time.

1.3.1 Horizontal drying front and vertical packing

During the initial period of drying when particles are becoming packed (from State 1 to 2 in Figure 1.1), particles preferentially accumulate at both the film edge and the film top, which herein are named "horizontal drying front" and "vertical packing", respectively (shown as Figure 1.2). For the former one, more commonly known as "coffee ring effect", particles are dragged by the outward capillary flow due to the pinning of liquid contact line on the substrate[17]; the capillary pressure within the front packed particles also causes the water recession into the film[18]. Such drying front can lead to poor film leveling and short open time for coating repair[19]. For the latter one, also known as "snow plow effect", particles are not concentrated uniformly along the vertical direction, but start packing from the film top and propagate to the film bottom. This happens when the drying rate is faster than the particle's diffusion rate, i.e. Peclet number (Pe) larger than one[20], which is always seen under room drying condition. In the dilute limit with the Stokes-Einstein diffusion equation applied, Pe is expressed as:

$$Pe = \frac{6\pi\mu R_p H\dot{E}}{k_B T} \qquad (1.1)$$

where μ is the water viscosity, R_p is the particle radius, H is the wet film thickness, $\dot{E}$ is the water receding rate (the velocity of water surface falling during drying), k_B is the Boltzmann constant and T is the temperature. For a typical drying under 25 ℃ and 40% RH with $R_p = 100\ \mathrm{nm}$, $H = 1\ \mathrm{mm}$ and $\dot{E} = 30\ \mathrm{nm/s}$, Pe is calculated as 12, large enough to form vertical packing.

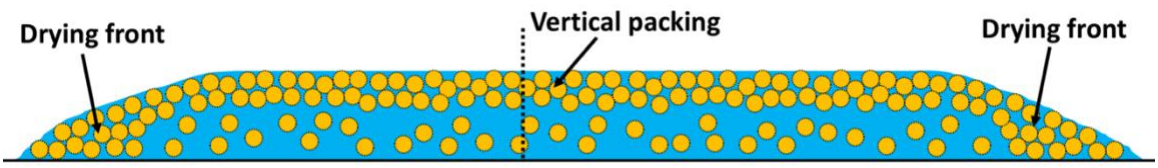

Figure 1.2: Schematic illustration of particles packing in both horizontal ("drying front") and vertical directions ("vertical packing").

1.3.2 Cracks, detachment, shear bands and skin layer formation

After the packing state where particles contact each other (State 2 in Figure 1.1), further water evaporation exerts forces to compress particles. These forces, induced by interfacial tensions, are categorized into three types: wet sintering (polymer/water interface), dry sintering (polymer/air interface) and capillary force (air/water interface)[16]. They are several or tens of times of γ/R_p, where γ is the interfacial tension. Assuming $R_p = 100$ nm and $\gamma = 35$ mN/m, $\gamma/R_p = 0.35$ MPa. Routh and Russel[13] derived the dimensionless parameter $\bar{\lambda}$ to predict the modes of film formation, expressed as the ratio of the drying rate over the particle deformation rate:

$$\bar{\lambda} = \frac{\eta R_p \dot{E}}{\gamma H} \qquad (1.2)$$

where η is the viscosity of polymer.

When $\bar{\lambda} > 1$, which usually happens when polymer is hard (with T_g higher than room temperature), water recedes faster than particles' deformation, leaving a porous structure filled with air and residual water between particles. The compressive forces induced between each pair of particles (either by particle surface tension or by water/air interfacial tension) point over all directions[14,21]. Such internal stresses accumulate until

cracks form to relax forces. Due to poor adhesion between hard particles and substrate, part of the latex can be bent up and detach from the substrate. In this dissertation, shear banding was also observed under the optical coherence tomography (OCT) microscopic imaging (see Figure 3.6 in Chapter 3). Shear bands have the bifurcation shapes in the cross-section of latex (shown in Figure 1.3A, similar to shear-banding failure of plastic materials[22] and shear deformation in geology[23]). Although shear bands developing along the horizontal direction during drying colloids were reported recently[28,29], this dissertation research is the first time to find the apparent shear bands developing along the vertical direction (in the cross-section of latex). They are believed as dislocations where intense shearing strains occur, induced by the vertical component of internal compressive stresses.

When $\bar{\lambda} < 1$, which occurs when polymer is soft (with T_g lower than room temperature), as soon as water surface recedes, latex particles on film top exposed to air deform and even coalesce so fast that a dried continuous polymer skin layer is formed (shown as Figure 1.3B). The skin layer usually has a very low water vapor permeability (WVP), and thus the further drying of the film is impeded. Such slow-drying problem becomes more serious if the latex film is thick, because more water is trapped in the wet domain underneath the skin. For example, in the architectural or roof coatings with millimeter-thick films, ~15 wt% water can be trapped beneath skin, which can take weeks to get dried. The trapped water can lower the mechanical strength and the adhesion to substrate, and cause bubbles inside film, which are detrimental to the coating product. According to the experimental measurements in this dissertation, the model PEM latex film (studied in Chapter 4) and the commercial PLB latex film (studied in Chapter 6) with an initial wet film thickness of ~2 mm (with latex solids of about 50% and a final dried film

thickness expected to be 1 mm) took more than 4 days and 12 days to get 95% of water evaporated, respectively, which is unacceptable in real applications.

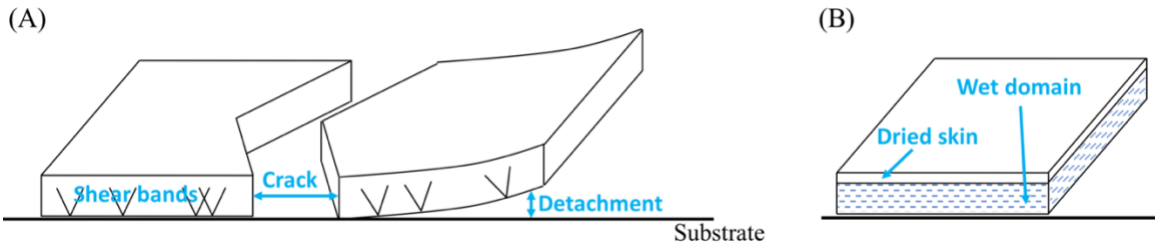

Figure 1.3: Schematic illustrations of (A) cracks, detachment and shear bands for a high-T_g latex, as well as (B) skin layer formation for a low-T_g latex.

1.4 Objectives

Drying inhomogeneity sometimes compromises the final properties of latex coatings, making them non-uniform and producing defects, which cannot be overcome without understandings of the mechanisms responsible for such inhomogeneity. Drying latex is such a complex process that interactions between particles, water-soluble molecules, interfacial tensions and deformability of particles all affect the drying process and film formation[13,14,18,20,24–27]. This makes developing a universal theoretical model almost impossible. Many experimental methods have been used to monitor the motions of particles and morphological changes of films[16], however, they have limitations, such as low resolution of microscopy, or incapability of detecting particles inside a film, or destruction to latex sample. Therefore, besides the basic methods (such as gravimetry and videography), a non-invasive tool needs to be employed to image the internal structure of film both microscopically and three-dimensionally. This helps fundamental studies of drying inhomogeneity, based on which a solution to solve a drying problem can be found. Regarding the focus of this dissertation – skin layer formation, both the mechanism of

drying process and the strategies to promote the drying of a skin-forming film will be investigated. The drying processes of latexes in this dissertation are conducted at room temperature and humidity. The objectives of this dissertation include:

1. Develop a non-invasive and non-destructive experimental method to characterize the drying inhomogeneity of latex system in real time, combining microscopic 3D imaging with macroscopic measurements.
2. Study the mechanism of skin layer formation and film formation of thick low-T_g latex film, including analysis of latex particles' mobility and distribution, correlation between skin layer and drying rate, and kinetic evolution of coalesced latex polymer layer. Mathematical model needs to be established on describing the latex film formation process with skin layer formation.
3. Investigate the effects of post-added water-soluble additives (especially surfactants) on the skin layer formation, the film formation process and the film drying time, in order to provide a guideline in solving the slow-drying problem caused by skin. A minor amount of water-soluble additives can change the drying profile enormously and be an effective solution in real applications.

Based on those objectives, this dissertation contains the following six chapters, including the introductory Chapter 1 herein. In Chapter 2, model latex systems are synthesized and characterized. In Chapter 3, optical coherence tomography (OCT) is developed to image the structure and the particles' mobility inside a drying latex film, based on the reflected light intensity; by combining OCT with gravimetric measurement and videography (called "OCT-Gravimetry-Video" method), the film's internal structure,

the drying curve and the film appearance can be monitored simultaneously. Using this method, different types of drying inhomogeneity can be characterized. In Chapter 4, the mechanism of skin layer formation and the mathematical model of latex film formation are proposed based on the results of the studies using the "OCT-Gravimetry-Video" method. In Chapter 5, the effects of post-added surfactants on the skin layer formation and the drying process of latex film are investigated. In Chapter 6, the skin layer formation and film formation of a commercial latex with a severe slow-drying problem are studied, plus the effects of post-added surfactants and other water-soluble additives. In Chapters 5 and 6, the water resistances (or water absorptions) of dried films are measured, in cases some additives do not compromise the water resistance of dried film while others do. In Chapter 7, conclusions of all chapters are summarized, and future recommendations of this dissertation are stated.

1.5 References

1. Fox, P. F., Uniacke-Lowe, T., McSweeney, P. L. H. & O'Mahony, J. A. *Dairy Chemistry and Biochemistry*. (Springer International Publishing, 2015).
2. Agrawal, A. A. & Konno, K. Latex: A Model for Understanding Mechanisms, Ecology, and Evolution of Plant Defense Against Herbivory. *Annu. Rev. Ecol. Evol. Syst.* **40,** 311–331 (2009).
3. Schmidt, T., Lenders, M., Hillebrand, A., van Deenen, N., Munt, O., Reichelt, R., Eisenreich, W., Fischer, R., Prüfer, D. & Schulze Gronover, C. Characterization of rubber particles and rubber chain elongation in Taraxacum koksaghyz. *BMC Biochem.* **11,** 11 (2010).
4. Kohjiya, S. & Ikeda, Y. *Chemistry, manufacture and applications of natural rubber*. (Elsevier/Woodhead Publ, 2014).
5. van Herk, A. M. *Chemistry and Technology of Emulsion Polymerisation*. (Wiley, 2013).
6. Lovell, P. A. & El-Aasser, M. S. *Emulsion Polymerization and Emulsion Polymers*. (Wiley, 1997).
7. *Global Emulsion Polymers Market by Product, Market and Country, 7th Edition*. (The Freedonia Group, 2016).
8. Dillon, R. E., Matheson, L. A. & Bradford, E. B. Sintering of synthetic latex particles. *J. Colloid Sci.* **6,** 108–117 (1951).
9. Sheetz, D. P. Formation of films by drying of latex. *J. Appl. Polym. Sci.* **9,** 3759–3773 (1965).
10. Vanderhoff, J. W., Bradford, E. B. & Carrington, W. K. The transport of water through latex films. *J. Polym. Sci. Polym. Symp.* **41,** 155–174 (1973).

11. Zhao, C. L., Wang, Y., Hruska, Z. & Winnik, M. A. Molecular aspects of latex film formation: an energy-transfer study. *Macromolecules* **23,** 4082–4087 (1990).

12. Kim, K. D., Sperling, L. H., Klein, A. & Wignall, G. D. Characterization of film formation from direct miniemulsified polystyrene latex particles via SANS. *Macromolecules* **26,** 4624–4631 (1993).

13. Routh, A. F. & Russel, W. B. Deformation Mechanisms during Latex Film Formation: Experimental Evidence. *Ind. Eng. Chem. Res.* **40,** 4302–4308 (2001).

14. Tirumkudulu, M. S. & Russel, W. B. Cracking in Drying Latex Films. *Langmuir* **21,** 4938–4948 (2005).

15. Carter, F. T., Kowalczyk, R. M., Millichamp, I., Chainey, M. & Keddie, J. L. Correlating Particle Deformation with Water Concentration Profiles during Latex Film Formation: Reasons That Softer Latex Films Take Longer to Dry. *Langmuir* **30,** 9672–9681 (2014).

16. Keddie, J. & Routh, A. F. *Fundamentals of Latex Film Formation: Processes and Properties*. (Springer Netherlands, 2010).

17. Deegan, R. D., Bakajin, O., Dupont, T. F., Huber, G., Nagel, S. R. & Witten, T. A. Capillary flow as the cause of ring stains from dried liquid drops. *Nature* **389,** 827–829 (1997).

18. Routh, A. F. & Russel, W. B. Horizontal drying fronts during solvent evaporation from latex films. *AIChE J.* **44,** 2088–2098 (1998).

19. Ludwig, I. *Drying, film formation and open time of aqueous polymer dispersions: an investigation of different aspects by rheometry and Inverse-Micro-Raman-Spectroscopy (IMRS)*. (Universitätsverlag, 2008).

20. Routh, A. F. & Zimmerman, W. B. Distribution of particles during solvent evaporation from films. *Chem. Eng. Sci.* **59,** 2961–2968 (2004).

21. Lee, W. P. & Routh, A. F. Why Do Drying Films Crack? *Langmuir* **20,** 9885–9888 (2004).

22. Bigoni, D. *Nonlinear solid mechanics: bifurcation theory and material instability*. (Cambridge University Press, 2012).

23. Fossen, H., Schultz, R. A., Shipton, Z. K. & Mair, K. Deformation bands in sandstone: a review. *J. Geol. Soc.* **164,** 755–769 (2007).

24. Gromer, A., Nassar, M., Thalmann, F., Hébraud, P. & Holl, Y. Simulation of Latex Film Formation Using a Cell Model in Real Space: Vertical Drying. *Langmuir* **31,** 10983–10994 (2015).

25. Visschers, M., Laven, J. & van der Linde, R. Forces operative during film formation from latex dispersions. *Prog. Org. Coat.* **31,** 311–323 (1997).

26. Okuzono, T., Ozawa, K. & Doi, M. Simple Model of Skin Formation Caused by Solvent Evaporation in Polymer Solutions. *Phys. Rev. Lett.* **97,** (2006).

27. König, A. M., Weerakkody, T. G., Keddie, J. L. & Johannsmann, D. Heterogeneous Drying of Colloidal Polymer Films: Dependence on Added Salt. *Langmuir* **24,** 7580–7589 (2008).

28. Yang, B., Sharp, J. S. & Smith, M. I. Shear Banding in Drying Films of Colloidal Nanoparticles. *ACS Nano* 9, 4077–4084 (2015).

29. Kiatkirakajorn, P.-C. & Goehring, L. Formation of Shear Bands in Drying Colloidal Dispersions. *Phys. Rev. Lett.* 115, (2015).

2 Chapter 2 Synthesis and Characterizations of Model Latex Systems

2.1 Introduction

Latex film formation is a complex drying process, during which the evaporation of water and thermal fluctuations of polymer chains drive the transformation from colloidal polymer particles to a continuous polymer film. Besides room temperature, humidity and wind that affect the drying rate, multiple intrinsic properties of latexes determine the film formation process, such as polymer T_g, polymer composition, particle size, particle surface property, surfactants and water vapor permeability (WVP) of dried latex film. In order to study the latex film formation process, it is untenable without synthesizing latexes and characterizing them.

In this Chapter, following the introductions on emulsion polymerization processes and characterizations for latex systems, the experimental details of synthesis and characterizations of the model latex systems used in this study will be presented with the results and data analysis.

2.1.1 Emulsion polymerization

Latexes, or emulsion polymers, are majorly produced by the process of emulsion polymerization[1,2]. Other latexes are made via microemulsion polymerization[3], miniemulsion polymerization[4–6], dispersion polymerization[7,8], suspension polymerization[9] and emulsion-solvent removal method[10,11]. Emulsion polymerization is a free-radical-initiated chain polymerization in an aqueous medium, in the presence of initiators,

monomers and surfactants. Sometimes, chain transfer agents are added to control the molecular weight of polymers.

At the start of emulsion polymerization, typically half of the weight is water, serving to maintain a low viscosity and transfer the heat; the other half is monomer (such as styrene with a relatively low water solubility, and/or other monomers with relatively higher water solubility). In some emulsion polymerization systems, the ratio of the monomer to the total mass can be varied in the range of 10 – 55 wt% in order to control the final latex solids content. With mechanical stirring and surfactant in water, monomers are in the form of large droplets (from one to tens of microns in diameter). The other components, which are in minor amounts (usually <1 wt% for each), include initiator, surfactant and chain transfer agent. Chain transfer agent (such as n-dodecyl mercaptan) is normally aliphatic and can be mixed with monomers. Surfactant molecules (such as sodium lauryl sulfate), which are amphiphilic with a hydrophobic tail and a hydrophilic head in molecular structure, are mainly distributed in three locations: 1) dissolved freely in water, 2) assembled as micelles (several to tens of nanometers in diameter), and 3) adsorbed on monomer droplets. Initiator (such as sodium persulfate) is normally water-soluble and generates free radicals in water phase.

When a conventional emulsion polymerization process is initiated, small-size polymer particles (nuclei) on the order of 5-10 nanometers-in-diameter are formed via one or more particle nucleation mechanisms. In general, two well-known particle nucleation mechanisms are applicable: namely, micellar nucleation[12,13] and homogeneous nucleation[14,15].

In micellar nucleation, initiator radicals enter the monomer-swollen surfactant micelles to polymerize and form small polymer particle nuclei. These small nuclei grow quickly via propagation reaction of the monomer which is supplied to these sites by diffusion from the larger monomer droplets. This nucleation mechanism is usually predominant when monomers have relatively low water solubility (<15 mM) and surfactant concentration is above the critical micelle concentration (CMC) to form micelles.

In homogeneous nucleation, radicals add monomer units directly in the aqueous phase, creating oligomers. After the length of oligomers reaches the solubility limit, they precipitate out and aggregate to form small polymer particle nuclei. The nuclei grow via two mechanisms: limited aggregation of the smaller nuclei and/or simultaneous propagation reaction to form larger polymer particles. This nucleation mechanism is usually predominant when monomers have relatively high water solubility (>170 mM) or surfactant concentration is lower than CMC.

It should be mentioned that both nucleation mechanisms may take place simultaneously in emulsion polymerization processes when the concentration of surfactant is above the CMC, but to different extents depending on the water-solubility of the monomers: the lower the water-solubility of the monomer, the higher the proportion of particle nucleation via micellar nucleation; the reverse is true for monomers with higher water-solubility.

Besides reactions in micelles and water phase, the chances are low that radicals enter monomer droplets to form large polymer particles (microns in diameter) – droplet nucleation[16], because these large size monomer droplets have small overall surface area relative to large surface areas of micelles and nuclei particles. However, in the cases when

the polymerization starts with pre-emulsified colloidally stable small monomer-in-water droplets in the diameter range of 50 – 500 nm, particle nucleation is found to take place predominantly in these fine droplets. This process is referred to as "miniemulsion" polymerization[1,4,5,6], which found wide range of applications in polymerization of hydrophobic monomers or oligomers, as well as encapsulation of inorganic or organic materials with very low or no water solubility.

Following the nucleation step (regardless of the nucleation mechanism), radicals continue to be produced in aqueous phase and enter the growing latex particles, and polymerization continues within these particles via propagation reaction of the monomers that diffuse through water from monomer droplets. Surfactants from micelles that do not form particles or from monomer droplets' surfaces that shrink, transport through water and get adsorbed onto surfaces of growing polymer particles. With the adsorbed surfactant molecules and/or sulfate groups (from initiator radicals) on particles' surface, the colloidal stability can be maintained. Furthermore, a minor amount (<1 wt%) of monomer acid (such as acrylic acid or methacrylic acid) can be added in monomers. In this way, carboxyl groups can be grafted on particles' surface[17]. By keeping the aqueous medium at relatively high pH (>7) via bases, extra charges from carboxyl groups can enhance particles' stability. At the end of polymerization, almost all the monomer is converted to polymers in latex particles, although a relatively small amount of water-soluble oligomers and micron-size particles (from droplet nucleation) exist.

In practice, the "seeding stage" procedure[1,2] is used in emulsion polymerization process in order to have a better control on the process reproducibility, by avoiding the irreproducibility in the particle nucleation stage. In this process, less than 10 wt% of the

total monomer is polymerized first to form "latex particle seeds", followed by the addition of the remaining monomer in either batch or semi-batch mode. Besides the classical water-soluble initiators (such as persulfate salts which produce free radicals in water by heating), oil-soluble initiators and redox initiators are sometimes used[1,28,29]. Upon heating, oil-soluble initiators preferentially generate two radicals/initiator molecules within the monomer-swollen particles. The desorption of one of the two initiator radicals from polymer particles causes the remaining radical to initiate polymerization of new polymer chains and maintains the propagation reaction of monomers. The exiting radical to the aqueous phase may re-enter into monomer-swollen particles. Redox initiators are also used in emulsion polymerization which involve using oxidizing and reducing agents to generate radicals at low temperatures. They can be applied when polymers with high molecular weights and low branching levels are sought, or used as "chaser" in order to reduce the residual monomer within the latex particles at the end of the polymerization. The radicals generated in water can enter particles directly if they are hydrophobic or after some degree of polymerization if they are hydrophilic.

The model latexes used in this dissertation were synthesized via the standard procedures of semi-batch emulsion polymerization, in which the monomers, surfactant and initiator were added continuously following the formation of seeds that were created in situ by first polymerizing 2.5% of the monomer to high conversion. Subject to various needs of basic latex properties, polymer composition and particle size were adjusted by varying the monomers and the amount of surfactant.

2.1.2 Compositions and characterizations of latex

As discussed above about the emulsion polymerization, the resulting latex is a complex colloidal system with a variety of compositions, as shown in Figure 2.1. Typically, more than 95 wt% of latex is made of polymer particles and water, each occupying about half of the mass. The remaining less-than 5 wt% mass consists of carboxyl groups, initiator groups, surfactant and other water-soluble molecules (such as oligomers and ions). Polymer chains in latex particles are not simply linear repetition of monomer units, instead they may have branches and crosslinks with adjacent polymer chains. Moreover, initiator groups (such as anionic sulfate groups, resulting from free radicals) and carboxyl groups (resulting from monomer acid) are incorporated into polymer chains. Since those groups are hydrophilic, a large portion of them can migrate onto surfaces of particles to help stabilize the colloid. Surfactant molecules have a distribution equilibrium between particle surface and aqueous medium (called "surfactant adsorption isotherm"). The surfactant adsorbed on particle surface, which provide electrostatic repulsive force (due to ionic surfactants) or steric repulsions (due to non-ionic surfactants), serve a major role in preventing aggregation of particles. During emulsion polymerization, homogeneous nucleation can leave a minor amount of water-soluble oligomers that do not form particles. They are amphiphilic polymers that can also adsorb on particle surfaces and even interact with surfactant molecules[18]. Other species, like buffer solution (such as sodium carbonate) and base (such as sodium hydroxide or ammonia) for increasing the pH of latex, can increase the amount of salt ions in the aqueous medium.

Considering such complex compositions, major characterizations of the latex systems in this dissertation include: solids content (k_{s0}) of latex, glass temperature (T_g) of

polymer, diameter of particles (D_p), number densities of carboxyl groups and sulfate groups on particle surface (φ_{acid} and φ_{sulf}), surfactant adsorption isotherm and water vapor permeability (WVP) of dried latex film. Those are key factors in determining the drying process and film formation of latexes. Solids content (k_{s0}), which is the weight percentage of solids (mostly polymer) in latex, directly relates to the viscosity of latex[19]. Polymer T_g correlates with the polymer's viscosity and particles' deformability at room temperature[20]. Particle size influences the packing process of latex particles[21]. Carboxyl groups can affect the distribution of particles during drying and improve the strength of film through hydrogen bonding[22]. Both carboxyl groups and sulfate groups also affect particle's surface charge and electrostatic interaction between particles. Surfactant molecules, not only provide repulsive interactions between particles, but also control the onset of particles' coalescence during film formation[23]. WVP of dried film is determined by the hydrophobicity of polymer, the extent of coalescence, the hydrophilic molecules and the structural defects of film. Since skin is a coalesced latex film on top, WVP can determine the film drying time if any water is trapped under skin.

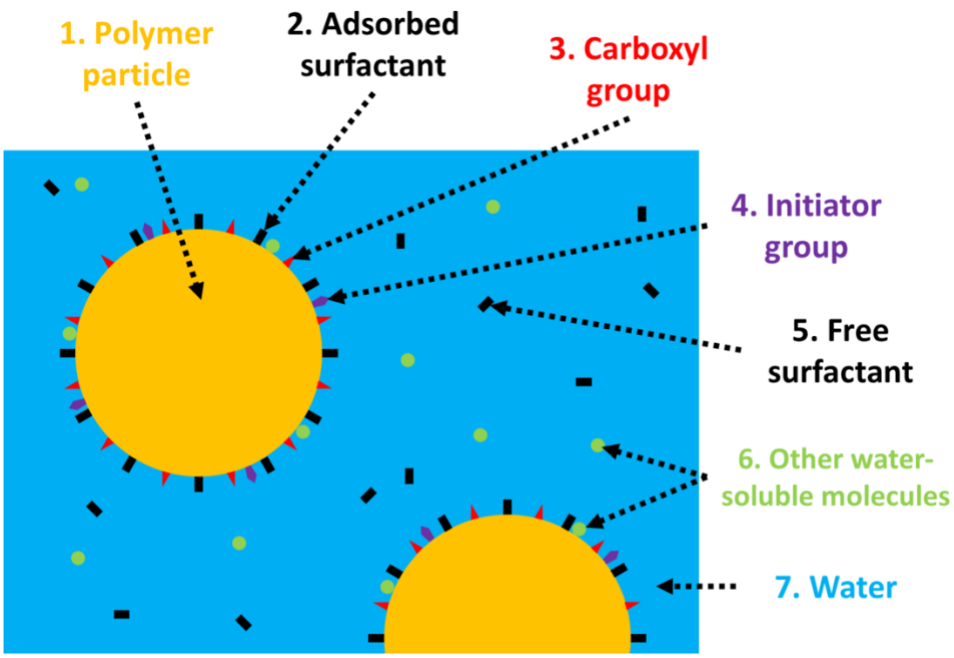

Figure 2.1: schematic illustration of the compositions of a typical latex: 1) polymer particles; 2) surfactant molecules adsorbed on particle surface; 3) carboxyl groups grafted on particle surface (such as methacrylic acid units); 4) initiator groups grafted on particle surface (such as sulfate groups from free radicals of sodium persulfate); 5) free surfactant molecules dissolved in water; 6) other water-soluble molecules (such as oligomers and ions), either dissolved in water or adsorbed on particle surface; 7) water.

2.2 Synthesis of model latexes

In this dissertation, all latex systems are synthesized by the semi-batch emulsion polymerization with the seeding stage. The model latex most frequently used for drying and film formation studies in this dissertation is an acrylic copolymer system, which is widely used as a binder in coatings industry due to its outstanding resistance to corrosion and weathering[24]. The polymer compositions in the model latex particles have 64 wt% of 2-ethylhexyl acrylate (EHA) units, 35 wt% of methyl methacrylate (MMA) units and 1 wt% of methacrylic acid (MAA) units. The model latex is designated as "poly(64EHA/35MMA/1MAA) latex", or "PEM latex" for short. The latex has a low T_g (-19 °C), which means that the particles can be deformed and coalesced very fast during drying at room temperature. Therefore, PEM latex is a good candidate for studying the drying inhomogeneities of low-T_g latex – mainly the processes of particles' packing and skin layer formation. In skin layer formation, the top surface of film dries early and forms a skin that traps water underneath. PEM latex is also a model system for studying the surfactants' effects on skin layer formation. PEM latex will be covered in Chapter 4 and 5.

The other series of latex systems with relatively soft polymer particles have copolymer compositions of n-butyl acrylate (BA) units, MMA units and 1 wt% MAA units. Their ratios of BA versus MMA are varied to achieve varied polymer T_g's. They are designated as "poly(77BA/22MMA/1MAA) latex" ("PBM1" for short) with -25 °C T_g, "poly(60BA/39MMA/1MAA) latex" ("PBM2" for short) with -3 °C T_g, and "poly(45BA/54MMA/1MAA) latex" ("PBM3" for short) with 23 °C T_g. Average particle diameters of PEM, PBM1, PBM2 and PBM3 are between 170 nm and 190 nm. In addition, a latex with the same polymer composition as PBM2 but doubled in particle diameter (360

nm) is synthesized by utilizing the PBM2 latex as seed and adding the appropriate amount of monomers, surfactant and initiator to achieve the targeted particle diameter, which is named as "D-PBM2". PBM1, PBM2, PBM3 and D-PBM2 are used to investigate the effects of solids content, polymer T_g and particle size on the drying process of latex films, which will be discussed in Chapter 4.

For comparison, two latexes with a high T_g (much higher than room temperature) are synthesized. They have the same polymer compositions – 99 wt% of styrene (St) units and 1 wt% of MAA units, designated as "poly(99St/1MAA) latex", or "PS latex" for short. However, their particle sizes are different. The latex with larger average particle diameter (125 nm) is called "L-PS latex"; the other latex with smaller average particle diameter (53 nm) is called "S-PS latex". Since the polymer T_g is higher than 100 °C, their particles almost do not deform under room conditions. Although there is no skin formation during drying of PS latexes, they can be a useful model to study the film formation process before the deformation stage. They are also good candidates for investigating the drying inhomogeneities of high-T_g latex, such as particles' packing, cracks and shear bands. In Chapter 3, the drying processes of PS latexes will be studied with the new "OCT-Gravimetry-Video" method.

2.2.1 Materials

EHA, BA, MMA and St monomers (purchased from ACROS Organics, USA) and MAA monomer (purchased from Sigma-Aldrich, USA), all monomers have purities higher than 99% and are used directly without further purification. n-dodecyl mercaptan (DDM), purchased from Sigma-Aldrich, is used as the chain transfer agent. Sodium lauryl sulfate

(SLS), from Alfa Aesar (USA), is used as the ionic surfactant to form micelles and stabilize particles. Sodium persulfate (NaPS), from Sigma-Aldrich, is used as the thermal initiator. Sodium formaldehydesulfoxylate dihydrate (SFS) from ACROS Organics, t-butyl peroxide (tBHP, 70% aqueous solution) from Alfa Aesar, and ferrous sulfate heptahydrate ($FeSO_4$) from Fisher Scientific (USA) are used as the combination of redox initiator, serving as a "chaser" in order to reduce the residual monomer in the latex particles during the final stage of emulsion polymerization. Sodium carbonate (Na_2CO_3), from ACROS Organics, is used as the buffer to maintain the pH during synthesis. Sodium hydroxide (NaOH) from AMRESCO (USA) or 28% aqueous ammonia (NH_3) from VWR (USA), is used to neutralize the carboxyl groups after latex synthesis. 37% aqueous formaldehyde, from AMRESCO, is used as the biocide to inhibit growth of bacteria after synthesis. Deionized (DI) water (with electrical resistivity of 18.2 $M\Omega \cdot cm$ at 25 °C) is made by Milli-Q water purification system.

2.2.2 Semi-batch emulsion polymerization

Different from the batch process where all reactants are added before reaction, the semi-batch process is where only small part of recipe is added at start of reaction and then the remaining majority is added continuously[1]. In this way, the particle size and the polymer compositions can be controlled facilely. In this dissertation, synthesis of the model poly(64EHA/35MMA/1MAA) latex (or PEM latex) follows the semi-batch emulsion polymerization procedures. First, less than 5 wt% of monomers are added into the reactor to form polymer seeds. Second, the remaining monomers are added with controlled speed to grow the seeds into larger particles, while the number of particles remains the same.

Third, after majority of monomers are reacted, hydrophobic redox initiator (called "chaser") is added to polymerize residual monomers inside particles.

All synthesis is performed in a 1-liter four-neck flask, connected with a polytetrafluoroethylene (PTFE) stirrer, a reflux condenser, a feeding tube and an adaptor that connects a nitrogen inlet and a thermocouple. Considering the volume of the reactor, the overall recipe of the PEM latex is designed as given in Table 2.1. The detailed steps of synthesis are as follows:

1) Mix 288 g EHA, 157.5 g MMA, 4.5 g MAA and 0.45 g DDM uniformly; dissolve 1.67 g SLS in 196 g water; emulsify the monomers' mixture in the SLS aqueous solution by the homogenizer (T25, IKA, USA) to form a monomer emulsion.
2) Add 160 g water in the reactor; dissolve 0.58 g SLS and 1.8 g Na_2CO_3 in it; keep stirring the liquid; heat the reactor and maintain the temperature at 88 °C by the heating mantle (Glas-Col, USA) and the temperature controller (J-KEM, USA).
3) Dissolve 1.58 g NaPS in 8 g water; add 16.2 g monomer emulsion (2.5 wt% of total monomers) and the NaPS solution into the reactor; run the polymerization for 10 min to form polymer latex seeds at high conversion, during which the system turns from white to blue.
4) Dissolve 0.22 g NaPS in 20 g water; feed the NaPS solution by the syringe pump (Harvard Apparatus, USA) and feed the remaining monomer emulsion by the metering pump (FMI, US) continuously over 70 min; afterwards, wait 30 min for ongoing polymerization.
5) Dissolve 0.9 g 70% tBHP solution in 17.5 g water; dissolve 0.45 g SFS in 18.4 g water; make a 0.15% $FeSO_4$ aqueous solution.

6) Cool the reactor and maintain at 70 °C; add 1.5 g 0.15% $FeSO_4$ solution into the reactor; charge the tBHP solution and the SFS solution continuously over 20 min for the "chaser" purpose.
7) Cool the reactor to room temperature; make 5% NaOH aqueous solution; mix 18 g of the NaOH solution in the latex to increase the pH to around 8; add and mix 0.12 g 37% formaldehyde solution in the latex.

The resultant PEM latex is uniform and stable, with no coagulum formation.

As for the series of PBM and PS latexes, the synthesis procedures are almost the same. Table 2.2 and Table 2.3 show their recipes. During the synthesis of D-PBM2 latex, PBM2 latex is used as the "seed" with more monomers added and polymerized in order to grow the particles to larger size. The mass ratio of the added monomers to the polymer in PBM2 seed is 7.5. Since the number of particles is about constant, the particle diameter of D-PBM2 would be 2.04 ($= 8.5^{1/3}$) times that of PBM2, which agrees with the ratio of particle diameter measured by dynamic light scattering (360 nm/175 nm = 2.06, as shown in Table 2.4 or 2.5). During the synthesis of PS latexes, the surfactant added for making S-PS latex is more than that used for making L-PS latex, in order to make particles with the targeted smaller diameter.

Table 2.1: Recipe for the synthesis of the model poly(64EHA/35MMA/1MAA) latex (or PEM latex)

Ingredient	**Amount (g)**	**Weight percentage (%)**
DI water	439	48.9
EHA	288	32.1
MMA	157.5	17.6
MAA	4.5	0.50
DDM	0.45	0.05
SLS	2.25	0.25 (17.8 mM)[a]
NaPS	1.8	0.20 (17.2 mM)[a]
Na_2CO_3	1.8	0.20 (38.7 mM)[a]
tBHP	0.63	0.07 (15.9 mM)[a]
SFS	0.45	0.05 (6.7 mM)[a]
$FeSO_4$	0.0023	0.0003
NaOH	0.9	0.10 (51.3 mM)[a]
Formaldehyde	0.044	0.005
Total	897.3	100

[a] Concentrations based on the water phase

Table 2.2: Recipes for the synthesis of poly(BA/MMA/MAA) latexes (or PBM latex series) with different polymer compositions (PBM1, PBM2, PBM3) and different particle size (D-PBM2)

	PBM1 latex		PBM2 latex	
Ingredient	**Amount (g)**	**Weight percentage (%)**	**Amount (g)**	**Weight percentage (%)**
DI water	425	48.1	425	48.1
BA	346.5	39.2	270	30.6
MMA	99	11.2	175.5	19.9
MAA	4.5	0.51	4.5	0.51
DDM	0	0.00	0	0.00
SLS	2.25	0.25 (18.4 mM)[a]	2.25	0.25 (18.4 mM)[a]
NaPS	1.8	0.20 (17.8 mM)[a]	1.8	0.20 (17.8 mM)[a]
Na_2CO_3	1.8	0.20 (40.0 mM)[a]	1.8	0.20 (40.0 mM)[a]
tBHP	0.63	0.07 (16.4 mM)[a]	0.63	0.07 (16.4 mM)[a]
SFS	0.45	0.05 (6.9 mM)[a]	0.45	0.05 (6.9 mM)[a]
$FeSO_4$	0.0023	0.0003	0.0023	0.0003
NH_3	0.89	0.10 (123 mM)[a]	0.89	0.10 (123 mM)[a]
Formaldehyde	0.044	0.005	0.044	0.005
Total	882.8	100	882.8	100

	PBM3 latex	
Ingredient	**Amount (g)**	**Weight percentage (%)**
DI water	425	48.1
BA	202.5	22.9
MMA	243	27.5
MAA	4.5	0.51
DDM	0	0.00
SLS	2.25	0.25 (18.4 mM)[a]
NaPS	1.8	0.20 (17.8 mM)[a]
Na_2CO_3	1.8	0.20 (40.0 mM)[a]
tBHP	0.63	0.07 (16.4 mM)[a]
SFS	0.45	0.05 (6.9 mM)[a]
$FeSO_4$	0.0023	0.0003
NH_3	0.89	0.10 (123 mM)[a]
Formaldehyde	0.044	0.005
Total	882.8	100

Ingredient	D-PBM2 latex	
	Amount (g)	Weight percentage (%)
"Seed" PBM2 [b]	120	13.7
DI water	296	33.9
BA	270	30.9
MMA	175.5	20.1
MAA	4.5	0.52
DDM	0	0.00
SLS	1.665	0.19 (16.2 mM)[a]
NaPS	1.8	0.21 (21.2 mM)[a]
Na_2CO_3	1.8	0.21 (47.7 mM)[a]
tBHP	0.63	0.07 (19.6 mM)[a]
SFS	0.45	0.05 (8.2 mM)[a]
$FeSO_4$	0.0023	0.0003
NH_3	0.89	0.10 (146.9 mM)[a]
Formaldehyde	0.044	0.005
Total	873.3	100

[a] Concentrations based on the water phase

[b] 120 g of PBM2 latex was used as the seed for the synthesis of D-PBM2 latex. The mass ratio of the added monomers to the PBM2 seed's polymer is 7.5; enough to double the size of the seed particles. The overall copolymer composition is the same as the initial seed.

Table 2.3: Recipes for the synthesis of L-PS and S-PS latexes

	L-PS latex		S-PS latex	
Ingredient	**Amount (g)**	**Weight percentage (%)**	**Amount (g)**	**Weight percentage (%)**
DI water	455	59.8	574	64.5
St	297	39.1	297	33.4
MAA	3	0.39	3	0.34
DDM	0	0	0	0
SLS	1.5	0.20 (11.4 mM)[a]	12	1.35 (72.5 mM)[a]
NaPS	1.5	0.20 (13.8 mM)[a]	1.2	0.13 (8.8 mM)[a]
Na_2CO_3	1.2	0.16 (24.9 mM)[a]	1.2	0.13 (19.7 mM)[a]
tBHP	0.42	0.06 (10.2 mM)[a]	0.42	0.05 (8.1 mM)[a]
SFS	0.3	0.04 (4.3 mM)[a]	0.3	0.03 (3.4 mM)[a]
$FeSO_4$	0.0015	0.0002	0.0015	0.0002
NaOH	0.6	0.08 (33.0 mM)[a]	0.6	0.07 (26.1 mM)[a]
Formaldehyde	0.030	0.004	0.030	0.003
Total	760.6	100	889.8	100

[a] Concentrations based on the water phase

2.3 Characterizations of model latex systems

As mentioned in the introduction part of this chapter, the properties of model latexes that influence the film formation process will be characterized with respect to six items: 1) solids content (k_{s0}), the weight percentage of solids in latex; 2) T_g of polymer, the temperature near which the polymer changes from glass state to rubbery state; 3) particle size (D_p), the diameter of particles, including the average size, the polydispersity index (PDI) and the statistical size distribution; 4) number densities of carboxyl and sulfate groups on particle surface (φ_{carb} and φ_{sulf}), how many carboxyl and sulfate molecules per nm^2 grafted on particles' surface; 5) surfactant adsorption isotherm, the equilibrium distribution between the number density of surfactant molecules adsorbed on particles' surface versus the concentration of surfactant molecules free in water; 6) water vapor permeability (WVP) of dried latex film, the permeability of film through which water molecules diffuse.

For the PS and PBM latexes, the first three properties were characterized: namely, solids content, T_g and particle size. PS particles do not deform or form polymer film at room temperature, but can form structures of packing, cracks and shear bands that will be studied in Chapter 3. PBM latexes vary in T_g and particle size, which are important factors affecting the film formation process and will be investigated in Chapter 4. However, for the PEM latex, all the six latex properties listed above are characterized, because this is the major model latex system used in this dissertation to study the skin layer formation (Chapter 4), and the effects of surfactants on film formation (Chapter 5). The results of all latex particle sizes are given in Tabled 2.4. All the characterization results and the latexes' properties are summarized in Table 2.5.

2.3.1 Solids content, polymer T_g and particle size

2.3.1.1 Experimental details

***Latex solids content* (k_{s0}):**

k_{s0} is the ratio of the fully-dried-latex's mass over the initial latex's mass. First, about 3-ml latex is added in a clean aluminum crinkle dish (VWR, USA). The dish weight (m_{dis}) and the total weight of initial latex plus dish (m_{tot0}) are measured by the digital balance with a 0.0001-g precision (AGN200, Torbal, USA). Then, the aluminum dish with the latex is placed in an oven and air-dried at 95 ℃ for 24 h. Finally, the total weight of dried latex plus dish (m_{tot1}) is measured. The solids content is calculated as:

$$k_{s0} = \frac{m_{tot1} - m_{dis}}{m_{tot0} - m_{dis}} \times 100\% \qquad (2.1)$$

***T_g of polymer*:**

The polymer T_g is the transition temperature separating the hard glass region at lower temperatures and the soft rubber region at higher temperatures. The common characterization is measuring the heat capacity as a function of temperature, via differential scanning calorimetry (DSC). At the transition, the heat capacity increases abruptly with increasing temperature. T_g can be determined as the temperature where one-half of heat capacity's increase occurs. First, 30 mg latex is added in a DSC sample pan and dried at 95 ℃ for 24 h. Then, the sample is sealed and transferred to the DSC instrument (Q2000, TA Instruments, USA). The measurement is automatic and gives the value of T_g.

***Latex Particle size (D_p)*:**

The particle size (diameter, D_p) and size distribution are measured in two ways – dynamic light scattering (DLS) and transmission electron microscopy (TEM). DLS measures the diffusion coefficient of diluted colloidal particles based on the scattered light fluctuations, from which the hydrodynamic diameter (d_{LS}) and its estimated standard deviation (SD) of spheres are given (ISO22412:2008). TEM measures the physical diameter and its distribution of dried particles in vacuum. Normally, the particle size determined from DLS is larger than that from TEM, since the particles in water can have surfactant, oligomers and hydrated layer on the particle surface.

For DLS, the latex is diluted to 0.1 wt% with 10 mM KNO_3 aqueous solution. 1 mL diluted latex is added in a glass tube and placed in the DLS setup (ALV/CGS-3 Goniometer System, ALV GmbH, Germany) for measurement.

For TEM, phosphotungstic acid (PTA) from Fisher Scientific is used to protect particles from deformation and to increase the contrast of particle's boundary. An aqueous mixture with 0.1 wt% PTA and 0.025 wt% latex particles is prepared. One small drop of the mixture is taken and dried on a carbon-film-coated TEM grid (01814-F, TED PELLA, USA) at room temperature. The grid is carefully placed in the TEM setup (JEM-1200EX, JEOL, USA) to take the electron transmission images. The particle diameter and size distribution are determined by measuring 1000 particles in ImageJ. Besides the exact size distribution, there are some statistical diameters that are commonly used. First, which is most familiar, is the number average diameter (d_n), defined as:

$$d_n = \frac{\sum n_i d_i}{\sum n_i} \quad (2.2)$$

where n_i is the number of particles with diameter of d_i. Then the standard deviation (SD) is computed as:

$$\mathrm{SD} = \sqrt{\frac{\sum n_i (d_i - d_n)^2}{(\sum n_i) - 1}} \quad (2.3)$$

Since the particle size distribution is usually asymmetric, it is reasonable to calculate surface-area average (d_s), weight average (d_w) and volume average diameters (d_v) to compare them with d_n. They are defined as:

$$d_s = \frac{\sum n_i d_i^3}{\sum n_i d_i^2} \quad (2.4)$$

$$d_w = \frac{\sum n_i d_i^4}{\sum n_i d_i^3} \quad (2.5)$$

$$d_v = \left(\frac{\sum n_i d_i^3}{\sum n_i}\right)^{1/3} \quad (2.6)$$

The polydispersity index (PDI) is then calculated as:

$$\mathrm{PDI} = \frac{d_w}{d_n} \quad (2.7)$$

2.3.1.2 Results and data analysis

A summary of the characterization results and properties of the latex systems are given in Table 2.4 for latex particle sizes and Table 2.5 for all other latex properties. More details are reported and discussed below.

Latex solids content (k_{s0}) and copolymers' densities:

The % solids contents (k_{s0}) for PEM, L-PS, S-PS, PBM1, PBM2, PBM3 and D-PBM2 latexes are 50.37, 40.11, 33.43, 52.27, 50.61, 51.07 and 57.89, respectively. k_{s0} could be varied within ±0.5% error for different synthesis batches. Among the solids (containing polymers, surfactant, salts and so on), 98 wt% is polymers for PEM, PBM series and L-PS, while 95 wt% for S-PS, according to the recipes in Tables 2.1, 2.2 and 2.3. For drying and film formation studies in following chapters, it is assumed that all solids in latex are polymers. According to the densities of homopolymers[30], the copolymer densities of poly(64EHA/35MMA/1MAA), poly(99St/1MAA), poly(77BA/22MMA/1MAA), poly(60BA/39MMA/1MAA) and poly(45BA/54MMA/1MAA) are estimated to be 1.03 g/cm^3, 1.05 g/cm^3, 1.02 g/cm^3, 1.06 g/cm^3 and 1.09 g/cm^3, respectively, which are close to but slightly heavier than water. In our calculation of film thickness and latex particles' volume fraction, the density of polymer (or solids, ρ_s) and the density of latex (ρ) are set to be about the same as that of water ($\rho = \rho_s = \rho_w = 1\ \mathrm{g/cm^3}$).

***T_g of polymer*:**

The glass transition temperatures (T_g) of dried latex polymers for PEM, L-PS, S-PS, PBM1, PBM2, PBM3 and D-PBM2 latexes are measured as -19 ℃, 107 ℃, 106 ℃, -

25 ℃, -3 ℃, 23 ℃ and 0 ℃, respectively. Thus, during drying at room temperature, the particles of PEM latex and PBM series can deform, while particles of PS latexes are too hard to deform.

Latex Particle size (D_p):

Table 2.4 gives the various average particle diameters and standard deviations (SD) of the prepared latex systems as determined by DLS and TEM.

For PBM1, PBM2, PBM3 and D-PBM2 latexes, the particle diameters (D_p) measured by DLS are 189 nm , 175 nm , 187 nm and 360 nm, respectively, with all SD's listed in Table 2.4.

For PEM, L-PS and S-PS latexes, the particle diameters (D_p's) measured by DLS are 176 nm , 125 nm and 53 nm , respectively. The number average diameters measured by TEM are 182 nm, 113 nm, and 31 nm, respectively. All SD's and PDI's measured by TEM are listed in Table 2.4. The results measured by DLS and TEM are generally similar (within about 20 nm difference). However, as expected, there are some differences between various average diameters (d_n, d_s, d_v and d_w) measured by TEM (shown in Table 2.4). Figures 2.2 A, B and C show the TEM micrographs of the above three latexes, together with their particle size distributions based on both number percentage and weight percentage. The size distribution for each latex system was constructed based on measuring 1000 particles by TEM. According to both DLS and TEM results, the PDI's and SD's (in Table 2.4) show that the particle diameter of PEM latex is relatively uniform, while the particle size distributions of L-PS and S-PS latexes are broader. The TEM images of both PS latexes (Figure 2.2B and C) clearly show abundance of smaller particles and broader

size distribution, particularly for the S-PS latex. Because of the well-known limitation of the DLS[31] in capturing the sizes of smaller particles in the presence of larger particles, it's not surprising that for S-PS latex, the average diameter measured by DLS is larger than the d_n, d_s, d_v and d_w measured by TEM. Moreover, the surfactant and polymeric molecules adsorbed on surface of particles in water may make the size measured by DLS larger than that by TEM[32].

In the following chapters, the particle diameters measured by DLS will be used to represent the particle sizes of latex systems, since DLS measured all latexes while TEM only measured three latexes listed in Figure 2.4. The PEM, L-PS and S-PS latexes with both DLS and TEM measurements will be the main latexes studied in Chapter3, 4 and 5. The PBM1, PBM2, PBM3 and D-PBM2 with only DLS measurement will also be investigated in Chapter 4.

Table 2.4: Comparative results of DLS and TEM measurements of particle sizes of all model latex systems, given as particle diameters (D_p)

Latex[a]	D_p by DLS		D_p by TEM					
	d_{LS} (nm)	SD (nm)	d_n (nm)	SD (nm)	d_w (nm)	PDI	d_s (nm)	d_v (nm)
PEM	176	18	182	28	194	1.07	190	186
L-PS	125	23	113	28	127	1.12	124	119
S-PS	53	7	31	11	42	1.37	39	35
PBM1	189	20	/	/	/	/	/	/
PBM2	175	23	/	/	/	/	/	/
PBM3	187	21	/	/	/	/	/	/
D-PBM2	360	71	/	/	/	/	/	/

[a] Polymer compositions (in weight ratios of polymerized monomers) of all the latexes listed from top to bottom are poly(64EHA/35MMA/1MAA), poly(99St/1MAA), poly(99St/1MAA), poly(77BA/22MMA/1MAA), poly(60BA/39MMA/1MAA), poly(45BA/54MMA/1MAA), and poly(60BA/39MMA/1MAA), respectively. Note: EHA, BA, MMA, St and MAA are 2-ethylhexyl acrylate, n-butyl acrylate, methyl methacrylate, styrene, and methacrylic acid, respectively.

A

PEM latex

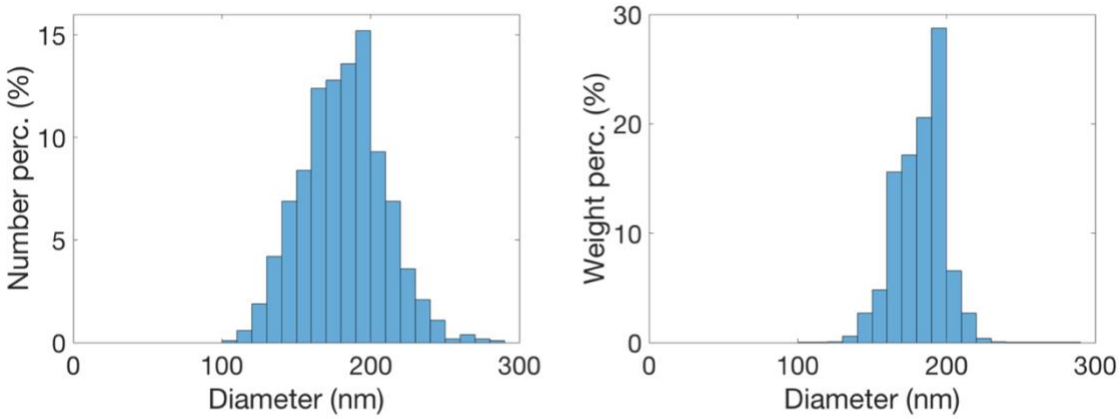
Number perc. (%)
15
10
5
0
0
100
200
300
Diameter (nm)
Weight perc. (%)
30
20
10
0
0
100
200
300
Diameter (nm)

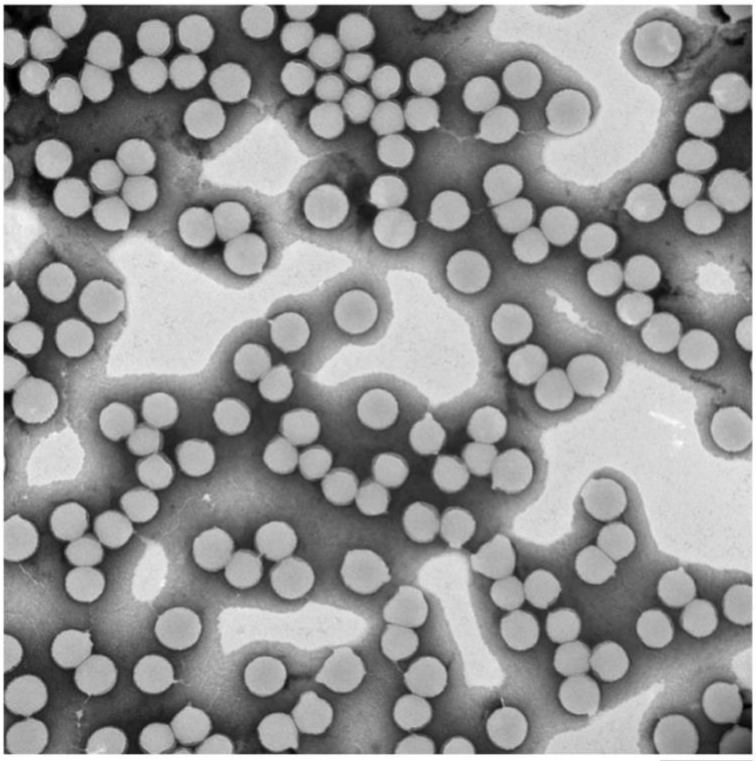
500 nm

B L-PS latex

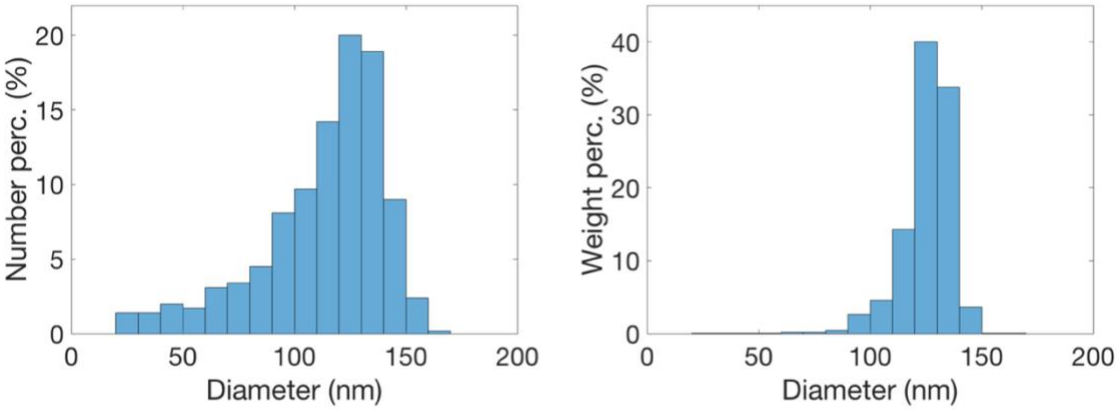
Number perc. (%)
0
5
10
15
20
0
50
100
150
200
Diameter (nm)
Weight perc. (%)
0
10
20
30
40
0
50
100
150
200
Diameter (nm)

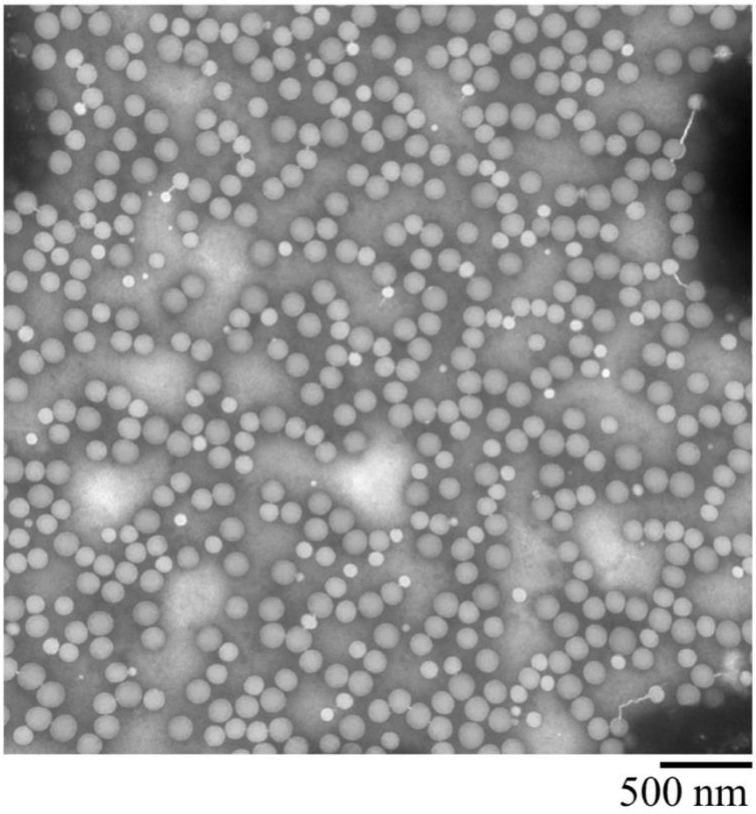
500 nm

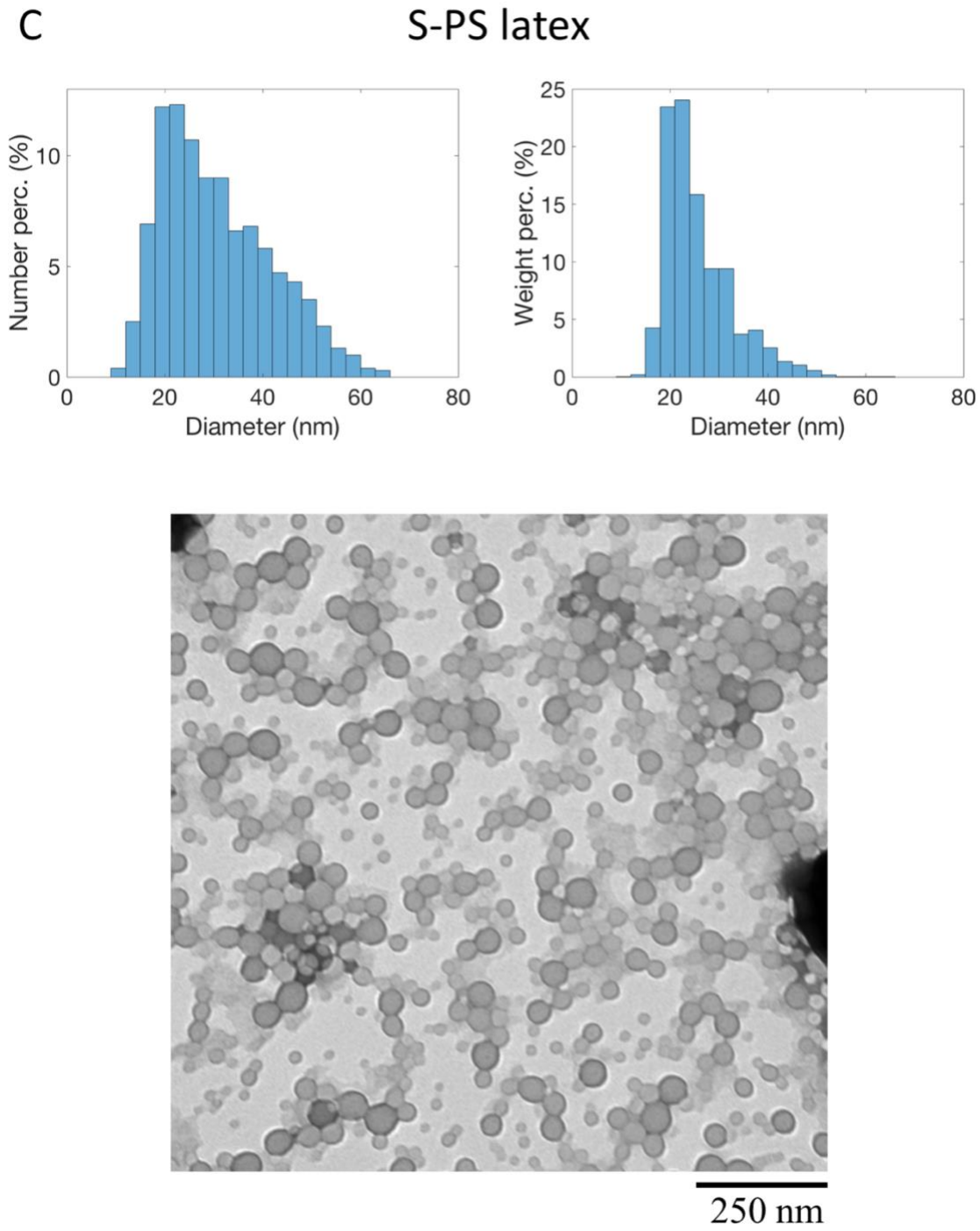

Figure 2.2: Particle size distributions (based on both number percentage and weight percentage) and TEM micrographs of (A) PEM, (B) L-PS and (C) S-PS latexes; in all cases 1000 particles were measured for each latex by TEM. The scale bars at the bottom right corners of TEM images denote 500 nm for PEM and L-PS, and 250 nm for S-PS.

2.3.2 Number densities of carboxyl and sulfate groups on latex particles' surface

2.3.2.1 Experimental details

The measurement of the number densities of carboxyl groups and sulfate groups on particle surface follows the standard procedure – "serum replacement" plus conductometric titration[17,25]. First, serum replacement pumps DI water through the latex in a cell via a semi-permeable membrane. The pore size of the membrane should not be larger than particles' diameter, so that water-soluble molecules and oligomers are washed away while particles remain inside the cell. After serum replacement, it is a system of polymer particles suspended in pure water. On particles' surface, there are grafted carboxyl groups (from MAA) and sulfate groups (from NaPS). Next, in order to eliminate the residual positive ions (such as Na^+ or K^+) near those acidic groups and replace them with H^+, either dilute hydrochloric acid or ion-exchange resin can be used. Finally, conductometric titrations are used on both cleaned latex and DI water (with the same volume) in parallel by adding volumetric solution of NaOH dropwise, giving curves of system's electrical conductivity as a function of added amount of NaOH with known molar concentration. Based on the inflection points on these curves, the numbers of carboxyl groups (weak acids) and sulfate groups (strong acids) on particles' surface can be derived.

In the experiment, the PEM latex was diluted by DI water to around 2% solids content and then washed by the serum replacement method until the latex conductivity was close to DI water. The membrane was chosen with a pore size of 0.1 μm (Whatman® Nuclepore™ Track-Etched Membrane, Sigma-Aldrich), so that PEM latex particles (D_p = 176 nm) remain within the serum replacement cell while water-soluble molecules and

oligomers are washed away. The latex was further purified by the ion exchange resin (Rexyn I-300, ACROS Organics), which is a mixture of OH^- and H^+ forms and the resin was cleaned with DI water before mixing it with latex. The solids content of the final cleaned latex was re-measured as 1.55%. The cleaned latex was further diluted by 10 times to get latex with 0.155% solids content. The conductometric curves of both diluted cleaned latex and DI water were measured by dripping 0.02 M NaOH solution into 100 g sample, using the conductometric setup (Schott Gerate, Germany).

2.3.2.2 Results and data analysis

Figure 2.3 shows the conductometric curves of both DI water and the diluted cleaned PEM latex. For DI water, the conductivity increases linearly with the volume of added NaOH solution, because of increasing concentrations of ions. For the diluted cleaned latex, the curve is no longer linear. Within the initial 0.075 ml of added NaOH solution, the conductivity drops, corresponding to the neutralization of strong acids (or sulfate groups) on particles' surface. With more NaOH added, the conductivity increases, but not as fast as DI water does until around 1.4 ml. This indicates the reaction between the weak acids (or carboxyl groups) and NaOH. After 1.4 ml, the 0.466 ml volume difference between those two curves represents the total amount of NaOH needed to neutralize both sulfate and carboxyl groups. Therefore, the NaOH volume to neutralize the sulfate groups is (V_{sulf}) is 0.075 ml, and that to neutralize the carboxyl groups (V_{carb}) is 0.466 – 0.075 ml = 0.391 ml.

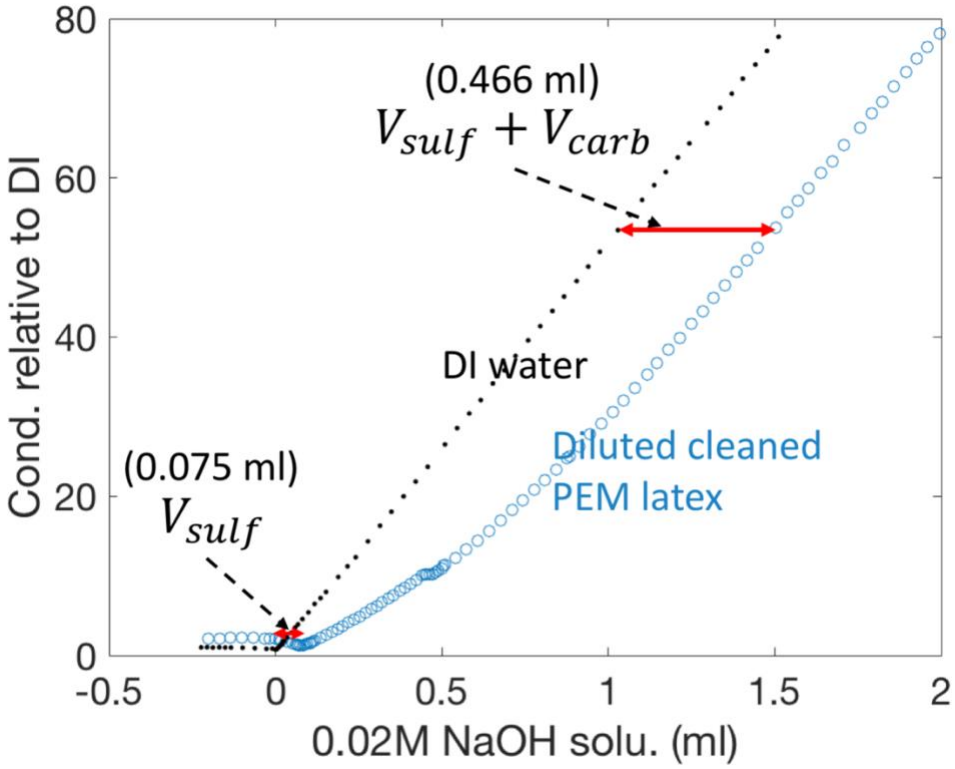

Figure 2.3: conductometric curves of both DI water (black dots) and the diluted cleaned PEM latex with 0.155% solids content (blue circles): relative conductivity of sample versus DI water, as a function of added volume of 0.02 M NaOH solution. The short red double-headed arrow denotes the volume of NaOH needed to neutralize strong acids (sulfate groups); the long red double-headed arrow denotes the volume of NaOH needed to neutralize both strong acids (sulfate groups) and week acids (carboxyl groups).

With the known diluted cleaned latex mass ($m_{clean} = 100$ g), its solids content ($k_{clean} = 0.155\%$), particle size (where volume average diameter is used as $D_p = d_v = 186$ nm), density of polymer (ρ_s being about 1 g/cm^3) and Avogadro's number ($N_A = 6.022 \times 10^{23}$), the calculation of acid groups can be done based on the added volume of NaOH solution (V_{vol}) and its concentration ($c_{vol} = 0.02$ M), as follows:

1) the total surface area of particles is:

$$A_p = \frac{6m_{clean}k_{clean}}{\rho_s D_p} \quad (2.8)$$

2) the number of added NaOH molecules or monoacid groups on all particles is:

$$N_{acid} = V_{vol}c_{vol}N_A \quad (2.9)$$

3) By dividing Equation (2.9) by Equation (2.8), the number density of acid groups on particle surface is:

$$\varphi_{acid} = \frac{N_{acid}}{A_p} = \frac{V_{vol}c_{vol}N_A\rho_s D_p}{6m_{clean}k_{clean}} \quad (2.10)$$

For sulfate groups where $V_{vol} = V_{sulf} = 0.075$ ml, $\varphi_{sulf} = 0.181\ \text{nm}^{-2}$; for carboxyl groups where $V_{vol} = V_{carb} = 0.391$ ml, $\varphi_{carb} = 0.942\ \text{nm}^{-2}$. Therefore, grafted on the particle surface of PME latex, there are 0.181 sulfate groups and 0.942 carboxyl groups per nm^2. Given the total amounts of NaPS and MAA added during synthesis (see Table 2.1) and by calculating acid groups in the original PEM latex based on φ_{sulf} and φ_{carb}, results show that 45.9% of all MAA and 30.3% of all sulfate are grafted on particles' surface, while the remaining amounts are either buried inside particles or in the aqueous phase.

2.3.3 Surfactant adsorption isotherm

2.3.3.1 Experimental details

In a surfactant solution, surfactant molecules either stay in the bulk of water, or reside at the interface between water and air (denoted as water/air interface). Compared to the amount of molecules in bulk, the single-layer molecules at water/air interface is a relatively negligible amount, but it can lower the water/air interfacial tension dramatically. Before the critical micelle concentration (CMC), both the bulk concentration and the interface's number density increase with an increasing amount of added surfactant. The interfacial tension decreases because of more surfactant molecules accumulated at the interface. When the added amount of surfactant exceeds CMC in the aqueous phase, the state of surfactant molecules at the interface is at the densest accumulation (monolayer), and thus any extra surfactant molecules can only form micelles in the aqueous phase. The interfacial tension no longer changes. Therefore, by measuring the surface tension as a function of surfactant concentration, the CMC can be determined at the break point.

As for the latex system, besides a negligible amount at the water/air interface, almost all surfactant molecules are either in the aqueous bulk or adsorbed on particles' surface (which is enormous due to small particle diameters). There exists an equilibrium distribution of surfactant molecules between the bulk concentration and the number density on particle surface. Before the CMC of latex, surfactant molecules are adsorbed on particles' surface, while some freely soluble in the aqueous phase with no micelles' formation; with further increase in the amount of surfactant, both the bulk concentration and the number density on particle surface increase, and the latex/air interfacial tension decreases. After

the CMC, molecules on the particle surface reach the densest adsorption, and those in the aqueous phase can form micelles; at this point, the latex/air interfacial tension also no longer changes. The CMC of the latex should be higher than that of only serum (aqueous phase extracted from latex), because more surfactant is needed for particles' adsorption. Based on such concept[26], the difference of latex's CMC (concentration based on the aqueous phase in latex) and serum's CMC indicates the maximum amount of surfactant molecules adsorbed onto particles' surface under the prevailing experimental conditions. Although filtration, colorimetry and NMR have been used to quantify the adsorption isotherm curve[18], the surface tension measurement is much easier, faster and lower-cost.

In the experiment, first, the PEM latex is diluted 5 times using DI water to 10.07% solids content (k_{dil}). Second, the serum is separated out from the diluted latex by centrifuge, which takes 3 hours at 8,500 RPM in AccuSpin 400 Centrifuge (Fisher Scientific) until the supernatant becomes transparent. Given the facts that the density of PEM is 1.03 g/cm^3 (see Section 2.3.1.2) and the weight average particle diameter (d_w) is 194 nm (see Table 2.4), the latex particles should sediment under the above centrifugation condition, leading to the separation of clear serum at the top of the centrifugation tube. Third, the surface tensions of both the diluted latex and the serum at different added surfactant concentrations (based on the aqueous phase), called "surface tension curves" are measured by DuNouy Tensiometer (CSC Scientific, USA) at around 23 °C. Based on the difference of those two surface tension curves and the CMC's, the surfactant adsorption isotherm curve is derived by plotting the number density of surfactant molecules on particle surface ($\varphi_{sur,p}$) as a function of the molar concentration in the aqueous medium ($c_{sur,aq}$) (see Figure 2.4C).

2.3.3.2 Results and data analysis

Figure 2.4A shows the surface tension curves of both serum and 5x diluted PEM latex (10% solids) as a function of added SLS surfactant, in which the aqueous phase in the diluted latex has the same mass as the serum. The CMC's are determined as 2.39 mM for the serum (CMC_{ser}) and 8.45 mM for the latex (CMC_{lat}, concentration based on the aqueous phase in latex). In theory, both curves should start (when no surfactant is added) at a same high surface tension, and end (after surfactant reaches CMC) at a same low surface tension. However, particles at the latex/air interface can also affect the surface tension, making the two curves in Figure 2.4A start and end at different surface tension values. In order to derive the surfactant adsorption isotherm curve, two assumptions are made: 1) the surface tension curves of both serum and latex start and end at same surface tension values; 2) with the added amount of surfactant, the surface tension drops linearly before CMC and becomes flat after CMC. Therefore, the surface tension curves can be modified as shown in Figure 2.4B. ΔC in Figure 2.4B denotes the equivalent concentration (amount per unit volume of the aqueous phase) of adsorbed surfactant on particle surface at the corresponding surfactant concentration in the aqueous phase ($c_{sur,aq}$). ΔC increases proportionally with $c_{sur,aq}$ and stops at ΔC_{max} after CMC_{ser}, indicating a linear isotherm curve before CMC. Thus, regarding this specific latex sample (5x diluted PEM), the partition coefficient (K_D) can be defined as the ratio of the equivalent concentration of adsorbed surfactant versus the concentration of surfactant in aqueous phase, calculated from Figure 2.4B as:

$$K_D = \frac{\Delta C}{c_{sur,aq}} = \frac{\Delta C_{max}}{CMC_{ser}} = \frac{CMC_{lat} - CMC_{ser}}{CMC_{ser}} = \frac{8.45}{2.39} - 1 = 2.54 \qquad (2.11)$$

In the latex with 1 L aqueous phase which has 1 mM surfactant ($c_{sur,aq}$ = 1 mM), the number of adsorbed surfactant molecules on all particles is:

$$N_{sur} = \frac{\Delta C \cdot N_A}{c_{sur,aq}} = K_D \cdot N_A \qquad (2.12)$$

In the latex with 1 L aqueous phase, the overall surface area of particles (according to Equation 2.8) is:

$$A_p = \frac{6\rho k_{dil}}{\rho_s D_p (1 - k_{dil})} = \frac{6k_{dil}}{D_p (1 - k_{dil})} \qquad (2.13)$$

where the diluted latex solids content is $k_{dil} = 10.07\%$, and the latex density is about $\rho = \rho_s = \rho_w = 1\ \mathrm{g/cm^3}$.

Thus, the "surfactant adsorption efficiency" ($\tilde{\varphi}_{sur}$), defined as the number density of surfactant molecules on particle surface per 1 mM c_{sur}, is:

$$\tilde{\varphi}_{sur} = \frac{N_{sur}}{A_p} = K_D \cdot \frac{N_A D_p (1 - k_{dil})}{6k_{dil}} \qquad (2.14)$$

, giving $\tilde{\varphi}_{sur} = 0.401\ \mathrm{nm^{-2}/mM}$.

It should be noted that, in the original 5x diluted PEM latex, there is 0.5 g/L (or 1.93 mM based on the aqueous phase in latex) of SLS molecules based on Table 2.1. According to Equation 2.11, of the 1.93mM SLS, 0.54 mM is in the serum while the remaining 1.39 mM SLS molecules are adsorbed on particles' surfaces (that is $\tilde{\varphi}_{sur} \cdot 0.54\ \text{mM} = 0.22\ \text{nm}^{-2}$ on particle surface). Therefore, for the PEM latex system, the total CMC of the aqueous phase is:

$$CMC_{serum} = CMC_{ser} + 0.54\ \text{mM} = 2.93\ \text{mM} \qquad (2.15)$$

, and the maximum number density of surfactant molecules on particle surface is:

$$\varphi_{sur,p,max} = \tilde{\varphi}_{sur} CMC_{serum} = 1.175\ \text{nm}^{-2} \qquad (2.16)$$

To sum up, the curve of surfactant adsorption isotherm is shown in Figure 2.4C, which is expressed as:

$$\varphi_{sur,p}(c_{sur,aq}) = \begin{cases} \tilde{\varphi}_{sur} c_{sur,aq}, & 0 < c_{sur,p} \le CMC_{serum} \\ \varphi_{sur,p,max}, & c_{sur,p} > CMC_{serum} \end{cases} \qquad (2.17)$$

where $\tilde{\varphi}_{sur} = 0.401\ \text{nm}^{-2}/\text{mM}$, $CMC_{serum} = 2.93$ mM, and $\varphi_{sur,p,max} = 1.175\ \text{nm}^{-2}$, in which the subscript of "sur" is "SLS" herein. Such curve will be used to explain the effects of surfactant on the drying process of film formation in following chapters.

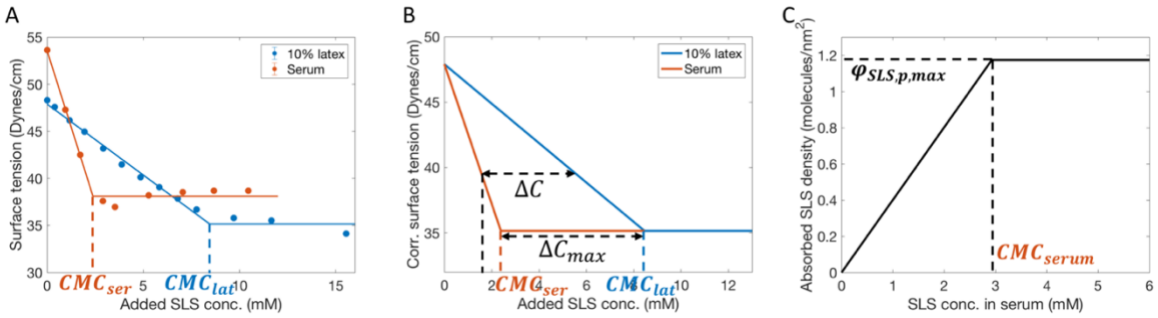

Figure 2.4: (A) measured surface tension curves of 5x diluted PEM latex and its serum – surface tensions as a function of added SLS concentrations (based on the aqueous phase). (B) modified surface tension curves of 5x diluted PEM latex and its serum. (C) SLS adsorption isotherm curve of the PEM latex system.

2.3.4 Water vapor permeability (WVP) of dried latex film

2.3.4.1 Experiment details

WVP characterizes the ability for water molecules to transport through a dried latex polymer film. It is expressed as[27]:

$$\text{WVP} = \frac{JH_{dry}}{p_0 \cdot \Delta RH} \qquad (2.18)$$

where J is the water flux (water mass loss per unit film area per unit time), H_{dry} is the dried film thickness, p_0 is the equilibrium vapor pressure at room temperature, and ΔRH is the difference of relative humidities on two sides of film. In the experiment, 30.6 g PEM latex ($k_{s0} = 50.37\%$) is dried in a 14 cm-in-diameter Petri dish with Teflon liner (Fluoro Lab, USA) at room condition, in order to get a dried film with 1 mm thickness. After drying for more than 14 days at room temperature when the film looks transparent and the measured weight shows < 2% of water remains in film, the film is peeled off. The film is cut into a

circle to fit in the permeability cup (with a drying area of 10 cm^2, BYK, USA). The permeability cup is filled with the commercial latex (that will be used in Chapter 6) and the circular film is placed above. The measurement is performed in a weathertight container (The Container Store, USA) with the relative humidity controlled at 40 RH% by potassium carbonate's saturated solution. The temperature during measurement is 21±1 °C. Within 10 hours, the gap between the film and the cup edge can be sealed by the commercial latex which is dried in the gap. After that, the water evaporation rate through the circular film becomes constant, which is used to calculate the value of WVP.

2.3.4.2 Results and analysis

The weight of the permeability cup was measured every 24 hours and gave the water evaporation rate as $(6.0 \pm 0.5) \times 10^{-6}$ g/min . Thus, $J = (6.0 \pm 0.5) \times 10^{-7}$ $\mathrm{g/(min \cdot cm^2)}$. With $H = 0.1$ cm, $p_0 = 2493$ Pa at 21 °C and $\Delta RH = 1 - 40\% = 0.6$, the WVP of dried PEM latex film is calculated based on Eq. 2.18 and found to be $(4.0 \pm 0.3) \times 10^{-11}$ $\mathrm{g/(cm \cdot min \cdot Pa)}$. This value will be used to correlate with the drying rate through skin layer in the following chapters.

2.4 Conclusions

Semi-batch emulsion polymerization process has been employed to synthesize the PEM latex, the PS latex series (i.e. L-PS and S-PS) and the PBM latex series (i.e. PBM1, PBM2, PBM3 and D-PBM2). During synthesis, SLS is used as surfactant and NaPS is used as initiator. Basic characterizations of solids content (k_{s0}), polymer T_g and particle diameter (D_p) were performed on all latexes. Among them, D_p's were measured by DLS (on all

latexes) and TEM (on PEM, L-PS and S-PS latexes only). In addition, the number densities of carboxyl and sulfate groups on particle surface (φ_{acid} and φ_{sulf}) and the surfactant adsorption isotherm curve of the PEM latex, and the water vapor permeability (WVP) of the dried PEM latex film were also measured. All the experimental results are summarized in Tables 2.4 and 2.5.

The PS latex series have the same polymer composition of 99St/1MAA, but with different particle diameters (D_p = 125 nm for L-PS and D_p = 53 nm for S-PS, as measured by DLS). Their polymer T_g's are so high (> 100 °C) that particles do not deform at room temperature. They will be used in Chapter 3 to study the drying behaviors of high-T_g latexes with the newly-established OCT-Gravimetry-Video method. The PEM latex has polymer composition of 64EHA/35MMA/1MAA with T_g = -19 °C. The PBM latex series have polymer composition of xBA/(99-x)MMA/1MAA, where x varies to adjust T_g from -25 °C to 23 °C. PEM, PBM1, PBM2 and PBM3 have similar particle diameters (D_p = 175 – 189 nm, measured by DLS). D-PBM2 has the same polymer composition as PBM2, but with larger D_p = 360 nm (measured by DLS). PBM latex series will be used to examine the effects of T_g and D_p on the drying profiles of low-T_g latexes in Chapter 4. PEM latex will be the major model latex system to study the process of skin layer formation in Chapter 4 and the effects of surfactants in Chapter 5, where the OCT-Gravimetry-Video characterizations will also be applied.

Table 2.5: Characterizations results and properties of all model latex systems synthesized for studies in this dissertation

Latex	Polymer composition (weight ratios of polymerized monomers)[a]	Solids content k_{s0} (%)	Poly-mer T_g (°C)	Particle diameter, D_p	
				by DLS (nm)	d_n by TEM[b] (nm)
PEM	64EHA/35MMA/1MAA	50.37	-19	176 (SD=18)[c]	182(SD=28)
L-PS	99St/1MAA	40.11	107	125 (SD=23)	113(SD=28)
S-PS	99St/1MAA	33.43	106	53 (SD=7)	31 (SD=11)
PBM1	77BA/22MMA/1MAA	52.27	-25	189 (SD=20)	/
PBM2	60BA/39MMA/1MAA	50.61	-3	175 (SD=23)	/
PBM3	45BA/54MMA/1MAA	51.07	23	187 (SD=21)	/
D-PBM2	60BA/39MMA/1MAA	57.89	0	360 (SD=71)	/

Latex	φ_{carb} (nm^{-2})[d]	φ_{sulf} (nm^{-2})[d]	SLS adsorption isotherm			WVP ($g/(cm \cdot min \cdot Pa)$)
			$\tilde{\varphi}_{SLS,p}$ (nm^{-2}/mM)[e]	CMC_{serum} (mM)[e]	$\varphi_{SLS,p,max}$ (nm^{-2})[e]	
PEM	0.942	0.181	0.401	2.93	1.18	$(4.0 \pm 0.3) \times 10^{-11}$

[a] EHA, BA, MMA, St and MAA in polymer compositions represent units of 2-ethylhexyl acrylate, n-butyl acrylate, methyl methacrylate, styrene and methacrylic acid, respectively.
[b] The number average diameter (d_n) of latex particles, measured by TEM (see Table 2.4).
[c] SD means standard deviation.
[d] Number densities of carboxyl groups (φ_{carb}) and sulfate groups (φ_{sulf}) on particle surface.
[e] Three parameters of the surfactant isotherm curve (see Equation 2.17)

2.5 References

1. Lovell, P. A. & El-Aasser, M. S. *Emulsion Polymerization and Emulsion Polymers*. (Wiley, 1997).
2. van Herk, A. M. *Chemistry and Technology of Emulsion Polymerisation*. (Wiley, 2013).
3. Antonietti, M., Basten, R. & Lohmann, S. Polymerization in microemulsions — a new approach to ultrafine, highly functionalized polymer dispersions. *Macromol. Chem. Phys.* **196,** 441–466 (1995).
4. Miller, C. M., Blythe, P. J., Sudol, E. D., Silebi, C. A. & El-Aasser, M. S. Effect of the presence of polymer in miniemulsion droplets on the kinetics of polymerization. *J. Polym. Sci. Part Polym. Chem.* **32,** 2365–2376 (1994).
5. El-Aasser, M. S. Miniemulsions: Overview of Research and Applications (2002 Roy W. Tess Award). *J. Coat. Technol. Res.* **1,** 20–31 (2004).
6. Landfester, K. Miniemulsion Polymerization and the Structure of Polymer and Hybrid Nanoparticles. *Angew. Chem. Int. Ed.* **48,** 4488–4507 (2009).
7. Arshady, R. Suspension, emulsion, and dispersion polymerization: A methodological survey. *Colloid Polym. Sci.* **270,** 717–732 (1992).
8. Tseng, C. M., Lu, Y. Y., El-Aasser, M. S. & Vanderhoff, J. W. Uniform polymer particles by dispersion polymerization in alcohol. *J. Polym. Sci. Part Polym. Chem.* **24,** 2995–3007 (1986).
9. Brooks, B. Suspension Polymerization Processes. *Chem. Eng. Technol.* **33,** 1737–1744 (2010).

10. Vanderhoff, J. W., El-Aasser, M. S. & Ugelstad, J. Polymer emulsification process. *U. S. Pat.* **US 4,177,177,** (1979).

11. Freitas, S., Merkle, H. P. & Gander, B. Microencapsulation by solvent extraction/evaporation: reviewing the state of the art of microsphere preparation process technology. *J. Controlled Release* **102,** 313–332 (2005).

12. Harkins, W. D. A General Theory of the Mechanism of Emulsion Polymerization [1]. *J. Am. Chem. Soc.* **69,** 1428–1444 (1947).

13. Smith, W. V. & Ewart, R. H. Kinetics of Emulsion Polymerization. *J. Chem. Phys.* **16,** 592 (1948).

14. Priest, W. J. Partice Growth in the Aqueous Polymerization of Vinyl Acetate. *J. Phys. Chem.* **56,** 1077–1082 (1952).

15. Hansen, F. K. & Ugelstad, J. Particle nucleation in emulsion polymerization. I. A theory for homogeneous nucleation. *J. Polym. Sci. Polym. Chem. Ed.* **16,** 1953–1979 (1978).

16. Ugelstad, J., El-Aasser, M. S. & Vanderhoff, J. W. Emulsion polymerization: Initiation of polymerization in monomer droplets. *J. Polym. Sci. Polym. Lett. Ed.* **11,** 503–513 (1973).

17. Loncar, F. Analysis, Kinetics and Alkali-swellability of Carboxylated Latexes. (Lehigh University, 1985).

18. Colombié, D., Landfester, K., Sudol, E. D. & El-Aasser, M. S. Competitive Adsorption of the Anionic Surfactant SLS and the Nonionic Surfactant Triton X-405 on Polystyrene Latex Particles. *Langmuir* **16,** 7905–7913 (2000).

19. Laun, H. M. Rheological properties of aqueous polymer dispersions. *Angew. Makromol. Chem.* **123,** 335–359 (1984).

20. Carter, F. T., Kowalczyk, R. M., Millichamp, I., Chainey, M. & Keddie, J. L. Correlating Particle Deformation with Water Concentration Profiles during Latex Film Formation: Reasons That Softer Latex Films Take Longer to Dry. *Langmuir* **30,** 9672–9681 (2014).

21. Routh, A. F. & Zimmerman, W. B. Distribution of particles during solvent evaporation from films. *Chem. Eng. Sci.* **59,** 2961–2968 (2004).

22. Tang, J., Daniels, E. S., Dimonie, V. L., Klein, A. & El-Aasser, M. S. Influence of Carboxyl Groups on the Morphology and Surface Properties of Films Prepared from Model Carboxylated Latex Blends. in *Film Formation in Coatings* (eds. Provder, T. & Urban, M. W.) **790,** 212–232 (American Chemical Society, 2001).

23. Pohl, K., Adams, J. & Johannsmann, D. Correlation between Particle Deformation Kinetics and Polymer Interdiffusion Kinetics in Drying Latex Films. *Langmuir* **29,** 11317–11321 (2013).

24. Koleske, J. V. *Paint and Coating Testing Manual: Fifteenth Edition of the Gardner-Sward Handbook*. (ASTM International, 2012).

25. Ahmed, S. M., El-Aasser, M. S., Pauli, G. H., Poehlein, G. W. & Vanderhoff, J. W. Cleaning latexes for surface characterization by serum replacement. *J. Colloid Interface Sci.* **73,** 388–405 (1980).

26. Maron, S. H., Elder, M. E. & Ulevitch, I. . Determination of surface area and particle size of synthetic latex by adsorption I. Latices containing fatty acid soaps. *J. Colloid Sci.* **9,** 89–103 (1954).

27. Topçuoğlu, Ö., Altinkaya, S. A. & Balköse, D. Characterization of waterborne acrylic based paint films and measurement of their water vapor permeabilities. *Prog. Org. Coat.* **56,** 269–278 (2006).

28. Asua, J. M., Rodriguez, V. S., Sudol, E. D. & El-Aasser, M. S. The free radical distribution in emulsion polymerization using oil-soluble initiators. *J. Polym. Sci. Part Polym. Chem.* 27, 3569–3587 (1989).

29. Lamb, D. J., Fellows, C. M. & Gilbert, R. G. Radical entry mechanisms in redox-initiated emulsion polymerizations. *Polymer* 46, 7874–7895 (2005).

30. Mark, J. E. *Physical Properties of Polymers Handbook*. (Springer New York, 2007).

31. Collins, E. A. Measurement of Particle Size and Particle Size Distribution. In Emulsion Polymerization and Emulsion Polymers (ed. Lovell, P. A. & El-Aasser, M. S.) 386–432 (Wiley, 1997).

32. Schärtl, W. *Light Scattering from Polymer Solutions and Nanoparticle Dispersions*. (Springer Berlin Heidelberg, 2007).

3 Chapter 3 OCT(Optical Coherence Tomography)-Gravimetry-Video Method to Study the Drying Process of Latex Systems, and Drying Inhomogeneity of High-T_g Latexes

This chapter is the basis for an article for publication in Scientific Reports, submitted on January 8th, 2018 (Manuscript #: SREP-17-56506)

3.1 Introduction

Latex has been widely used in waterborne coatings, adhesives and paints, as well as inks, cosmetics, pharmaceuticals and so forth. By drying a pool of latex with a specific thickness (from tens of microns to several millimeters), a polymer film can be formed to cover a material surface for protective, adhesive and aesthetic purposes. Ideally, it is expected that particles distribute homogeneously in space during drying, so that a uniform film with no obvious defects can be formed (Figure 1.1 in Chapter 1). However, real applications suffer "drying inhomogeneity", in which the spatial distribution of latex particles is non-uniform and changes with drying time[1] (Figures 1.2 and 1.3 in Chapter 1). In the horizontal direction, the "coffee ring effect"[2] packs particles near the circumferential edge, causing short open time for film leveling[3–5]; in the vertical direction, the "snow plow effect"[6,7] packs particles near the top surface, causing skin layer formation[8,9]; with loss of water, interfacial tensions (or capillary forces) between particles build up the internal compressive stresses that tend to shrink the volume of latex, leading to the formation of cracks and shear bands[10–13]. All these drying defects sometimes compromise the mechanical properties and break up the

integrity of final dried coatings. To solve the drying problems, it is necessary to understand the mechanism of drying inhomogeneity of latex films.

Theoretical models on the drying inhomogeneity were established to simulate the time-evolution of non-uniform distribution of simple hard spheres[3,6,8,11]. More recent studies show that interactions between particles, water-soluble molecules and interfacial tensions all influence the spatial distribution of latex particles[7,14,15]. Even more complex, the changing concentration and distribution of water-soluble molecules (such as surfactants and ions) can alter particles' interactions during drying[16–18]. This makes developing a universal theoretical model almost impossible.

Therefore, experimental approaches need to be developed to monitor the drying process and investigate the drying inhomogeneity. In macroscopic ways, gravimetric analysis and videography are most common and simplest methods[5,19]. They record water mass loss and film appearance as a function of time respectively, showing global views of film drying. Optical cantilever-bending technique, which measures the deflection of the compliant substrate, gives the overall internal stresses of film[20]. In microscopic ways (with microns or sub-micron resolutions), environmental scanning electron microscopy (ESEM), ellipsometry, atomic force microscopy (AFM) and diffusing wave spectroscopy were used to detect the packing process of particles, during which particles become concentrated and contact each other, and their Brownian motions become restricted[7,21–24]. However, those methods can only observe the top surface of film (low penetration within 50 μm). Traction force microscopy was used to map out the stress distribution of film, but only at the film/substrate interface[25,26]. In order to visualize structures inside a film, cryogenic scanning electron microscopy (Cryo-SEM) was used to view the cross-section of latex and

observed the packing of particles, but with a concern of damaging the sample[27]. Confocal laser scanning microscopy was used to profile the spatial distribution of particles[28], but the fluorescence-labeling process can alter particles' properties. Nuclear magnetic resonance profiling[9], Raman microspectrometer[29] and infrared microscopy[30] can non-destructively measure the distribution of water concentration inside the latex, but lack the resolution to see latex particles.

Optical coherence tomography (OCT), a non-destructive and non-invasive optical imaging technique, is capable of obtaining cross-sectional and volumetric images inside a sample with sufficient penetration up to 1-2 mm depths due to near-infrared light illumination[31–34]. OCT relies on low-coherence interferometry to detect back-scattered light signals within the sample and provides reconstructed image of scattered light intensity with micron-scale resolutions. OCT has been widely adopted for ophthalmological[35] and cardiological imaging[36,37]. In order to get a 3D volumetric image, confocal microscopies have to scan the light in both horizontal and vertical directions. But Fourier-Domain type of OCT (FdOCT) only needs to scan along the horizontal direction, since the information along the vertical direction (light beam) is encoded in the spectrum of light source[38]. This makes the OCT's scanning speed much faster than confocal microscopies. In studies of drying waterborne colloids, OCT was used to track motions of micron-size particles that represented the fluid flow in an evaporating drop[39,40]. Other studies reported using OCT to monitor the evolutions of thickness, refractive index and surface roughness by drying varnish coatings[41,42]. However, none of those OCT studies investigated the mobility of latex particles or the internal microstructures of latex film at different drying stages.

In this dissertation, in order to non-destructively characterize the drying process of a latex film in both macroscopic and microscopic ways, an integrated system is developed. It combines OCT, gravimetric measurement and video camera together, being called the "OCT-Gravimetry-Video" method. First, the time-lapse OCT imaging shows not only the thickness change of film, but also the internal microstructure at a local scanning spot, based on back-scattered light intensity. The imaging can be cross-sectional in 2D dimension, or volumetric in 3D dimension. Besides, a speckle contrast analysis[43] on OCT images can differentiate the mobility of particles in order to visualize the packing processes of particles – vertical packing ("snow plow effect") and horizontal drying front. Second, the video camera records latex's macroscopic appearance from the top view. It shows the drying boundary and cracks that propagated along the horizontal surface of film. Third, the gravimetry, using a digital balance, measures the global drying curve, from which the drying rates and the water contents in latex at different times are derived. They can be correlated with different drying stages observed in OCT images and video photos.

In this chapter, two polystyrene (PS) latexes with diameters of 125 nm and 53 nm (the L-PS and S-PS latexes synthesized in Chapter 2) are used. The drying processes of those hard particles (with T_g > 100 °C) are studied by the OCT-Gravimetry-Video method. Although they don't deform to form a continuous polymer film at room temperature, they are good models to investigate the crack formation or the drying stages before particles' deformation. Results show the drying inhomogeneities on both horizontal and vertical directions, including drying boundary and cracks characterized by video and gravimetry, as well as horizontal drying front, vertical packing and apparent shear bands observed by OCT. Particle size is found to significantly affect the packing, cracking and shear banding

phenomena. In Chapters 4 – 6, latexes with soft and deformable particles (the PEM latex and PBM latex series synthesized in Chapter 2 and the commercial PLB latex in Chapter 6) will be used. They have T_g's below 0 °C and skin layer can be easily formed on the top surface of film. Besides packing of particles, OCT shows the process of skin layer formation, since the skin has a low light scattering while the wet domain below has a higher light scattering. The skin layer formation is also correlated with the drying curve and the film's appearance.

3.2 Materials and methods

3.2.1 Polystyrene Latex samples

The latexes to be studied in this chapter are L-PS and S-PS. According to Table 2.5 (Chapter 2), the solids content (k_{s0}), the polymer T_g and the average particle diameter (D_p, by DLS) of L-PS are 40.11%, 107 °C and 125 nm, respectively; those of S-PS are 33.43%, 106 °C and 53 nm, respectively. The synthetic recipes of both latexes are shown in Table 2.3 (Chapter 2), from which major compositions of latexes can be inferred.

3.2.2 OCT-Gravimetry-Video method

Figure 3.1 shows the schematic diagram of OCT-Gravimetry-Video setup, integrating an optical coherence tomography (OCT) system, a digital balance, and a video camera. OCT acquires cross-sectional or volumetric images of the latex with micron resolutions by detecting back-scattered light intensity via low coherence interferometry. The digital balance measures the water mass loss of the latex over time. The video camera records

changes of the overall appearance of the latex under white light. Drying of a latex was conducted under room conditions.

For OCT imaging, the FdOCT was constructed using a superluminescent diode (SLD, SLD1325, Thorlabs, USA) with a central wavelength of 1320 nm and a spectral range of 110 nm. The light was transmitted through a 50/50 optical coupler, with 50% power to the sample arm and the other half of power to the reference arm. A 2D galvanometer (Galvo, GVS 002, Thorlabs) was utilized on the sample arm to scan the light beam on the latex film along the horizontal direction. A lens with a focal length of 50 mm (AC254-050-C, Thorlabs) was used as the objective. The beam size on the objective lens was measured to be 5.0 mm, yielding an effective numerical aperture (NA) of 0.05. The depth of field (DOF) of the OCT system was calculated to be 500 μm. Above the objective, a wedge (PS814-C, Thorlabs) was used to adjust the incident angle of the beam on the sample to minimize surface reflection from the latex. The light reflected from the latex and then from the mirror above the latex (M2) was then interfered at the 50/50 optical coupler with the light reflected from the reference mirror (M1). The interfered light signals were detected by a custom spectrometer which consists of a diffraction grating, an F-theta lens (FTH100-1064, Thorlabs) and a line-scan camera (SU1024LDH2, Sensors Unlimited, USA), operating at an axial scan (A-scan) rate of 20.7 kHz. The maximum imaging depth of the OCT system was measured to be 3.4 mm in the air with a refractive index value (RI) of 1. The axial resolution of the system was measured to be 6.7 μm in the air, and the transverse resolution was measured to be 14 μm. The sensitivity of the OCT system was measured to be ~101 dB.

Besides OCT imaging, OCT-Gravimetry-Video method can perform gravimetric measurement and video recording. The gravimetric measurement was achieved using a digital balance with a 0.001 g precision (AD60, Torbal, USA). A specific mass of latex was weighed and spread uniformly onto the Petri dish (8.52 cm in diameter and 0.85 cm in wall height, Kord-Valmark, USA). In this chapter, 5.7 g of L-PS or S-PS latex was used so that the initial latex thickness was 1 mm. A video camera (HERO Session, GoPro, USA) was used to capture top-view time-lapse photos of the latex under white light. A hygrometer/thermometer (TH0165, Perfect Prime, USA) was installed nearby to track changes of environment's temperature and humidity. All setups were connected and controlled by a computer. All measurements were synchronized so that data measured from all setups were acquired at the same time.

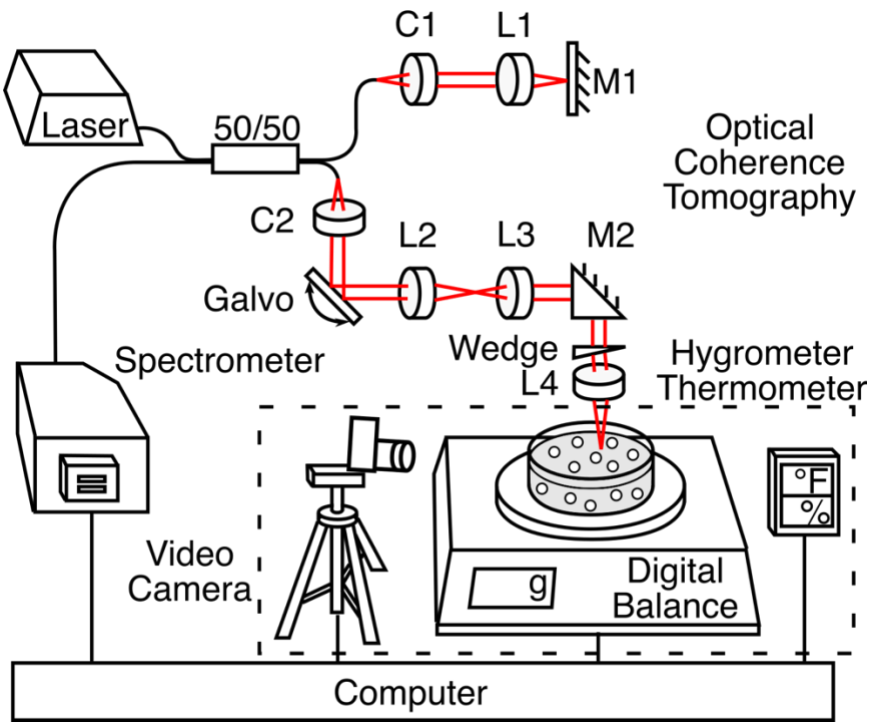

Figure 3.1: Schematic diagram of OCT-Gravimetry-Video setup.

3.2.3 Data acquisition and processing

3.2.3.1 Cross-sectional OCT structural imaging – "2D OCT structural image" and "time-lapse OCT intensity profile"

OCT imaging was started after the latex was weighed and spread uniformly in the Petri dish. Time-lapse OCT datasets were acquired and processed[38] every 2 min. For each dataset, 100 two-dimensional images were repeatedly taken on the same cross-sectional area of latex within 1 second. Each image contains $N_x \times N_z$ pixels, with N_x pixels corresponding to the number of light scanning points along the horizontal direction (x-axis), and N_z pixels corresponding to the signal points encoded in the spectrum of light along the vertical direction (z-axis). The pixel size of x-axis is calibrated as 10 μm. The

pixel size of z-axis is 6.7 μm for the air with RI = 1. In this chapter, the RI of PS (1.57) is used for latex, and thus the z-axis's pixel size becomes 6.7/1.57 = 4.3 μm. For a typical image, $N_x = 200$ (with a length of 1 mm) and $N_z = 512$ (with a length of 2.2 mm). Of course, N_x can be larger in order to scan a larger area on the latex. Then, these 100 images were averaged regarding the light intensity to improve the signal to noise ratio. The image was also rotated by vertical shifting each column of pixels by Matlab, so as to make sure the Petri dish surface was leveled in the image. In this way, a "2D OCT structural image" was obtained. Furthermore, by averaging each 2D OCT structural image along the horizontal direction, the "time-lapse OCT intensity profile" was obtained to show the time-evolution of backscattering intensity distribution in the vertical direction.

3.2.3.2 Cross-sectional OCT speckle imaging – "2D OCT speckle image" and "time-lapse OCT speckle profile"

Speckle contrast analysis[43] was performed on each 2D OCT structural image to distinguish the mobility of particles in the latex's cross-section, in order to characterize the packing process of particles. First, a sub-image for each given pixel was extracted from the 2D OCT structural image using the moving window method. For 2D OCT speckle analysis, each sub-image was composed of 11 × 11 pixels. For time-lapse OCT speckle analysis, each sub-image consisted of a row of pixels at a certain depth of the 2D OCT structural image, which was N_x × 1 pixels. Define I_k as the OCT scattered light intensity of each pixel within the sub-image, where $k = 1, 2, \dots, N$, and N was the total number of pixels in each sub-image. Thus, $N = 121$ for 2D speckle analysis and $N = N_x$ for time-lapse speckle

analysis. Then, the average intensity $\langle I \rangle$ and the average intensity square $\langle I^2 \rangle$ were calculated, respectively, as:

$$\langle I \rangle = \sum_{k=1}^{N} I_k / N \qquad (3.1)$$

and

$$\langle I^2 \rangle = \sum_{k=1}^{N} {I_k}^2 / N \qquad (3.2)$$

Then, the standard deviation of intensity for each sub-image was calculated as:

$$\sigma_{spc} = \{\langle I^2 \rangle - [\langle I \rangle]^2\}^{1/2} \qquad (3.3)$$

Finally, the speckle contrast (K_{spc}) for each pixel was derived from its corresponding sub-image as:

$$K_{spc} = \sigma_{spc} / \langle I \rangle \qquad (3.4)$$

In OCT speckle images, a high speckle contrast (K_{spc}) indicates low mobility of particles, which means that the motions of particles are restricted. On the other hand, a low K_{spc} indicates high mobility of particles, which means that the particles remain separately suspended and freely moving in the water.

By doing 2D speckle analysis, the "2D OCT speckle image" was obtained to show the 2D distribution of K_s in the cross-section of film. By doing 1D speckle analysis, the "time-lapse OCT speckle profile" was obtained as the time-evolution of K_{spc} in the vertical direction. By monitoring the distribution of speckle contrast changing with drying time, the behaviors of particles' vertical packing and horizontal drying front can be captured.

For an example of the vertical packing process (such as Figure 3.4c and Figure 3.4d1-d3), a domain boundary can be distinguished that separated the high K_{spc} region ("packed layer") and the low K_{spc} region ("suspension layer"). To determine the domain boundary curve in the time-lapse OCT speckle profile, we first calculated the average K_{spc} value of packed layer and that of suspension layer. Then, a threshold K_{spc} value was defined as the mean of both of these K_{spc}'s. The pixels with the same value as the threshold K_{spc} were determined as the packing boundary curve (dotted curve in Figure 3.4c). After determining the domain boundary in the time-lapse OCT speckle profile, the curve of the packed layer thickness changing with time was measured (dotted curve in Figure 3.4e). The other way to define domain boundary was based on the differences of scattered light intensity in OCT intensity profile, since the packed layer and suspension layer have different scattering properties. Setting the threshold intensity value as the mean of intensities of packing and suspension layers in the time-lapse OCT intensity profile (Figure 3.4b), the domain boundary curve (dotted curve in Figure 3.4b) and the curve of packed layer thickness (solid curve in Figure 3.4e) were determined.

3.2.3.3 Volumetric OCT structural imaging – "3D OCT structural image"

In 2D OCT structural image, the light beam scanned N_x points along x-axis in the horizontal direction. At each point, the scattered light intensities at N_z points along z-axis in the vertical direction were decoded in the spectrum of interfered scattered light. In the volumetric structural imaging, the light beam scanned in a two-dimensional fashion along the horizontal surface – N_x points on x-axis and N_y points on y-axis. In this way, a "3D OCT structural image" with $N_x \times N_y \times N_z$ pixels was obtained. N_z is always 512, the same as 2D OCT structural image; while N_x and N_y can be adjusted to a desired scanning area.

3.2.3.4 Gravimetry – "drying curve", "drying rate curve" and "film water content curve"

The total weight of the latex film was measured as a function of time ($W_{\text{latex}}(t)$), starting from when latex was transferred into the Petri dish ($t = 0$). Data were taken every 2 min after the sample was placed on the balance. With a known drying area ($A = \pi(8.52\ \text{cm}/2)^2 = 57.01\ \text{cm}^2$), the latex weight per area and the initial latex weight per area are defined as $w_{\text{latex}}(t) = W_{\text{latex}}(t)/A$ and $w_{\text{latex0}} = W_{\text{latex}}(t = 0)/A$, respectively. Thus, the drying curve, defined as the weight loss per area of the latex film, was measured as a function of time:

$$w(t) = w_{\text{latex0}} - w_{\text{latex}}(t) \qquad (3.5)$$

Then the drying rate curve was derived as:

$$\text{Drying rate} = dw(t)/dt \quad (3.6)$$

With the known initial solids content (k_{s0}) of latex, the drying extent curve (the percentage of the evaporated water versus the total water in the initial latex film) was calculated as:

$$\phi_w(t) = w(t)/\left(w_{\text{film0}}(1 - k_{s0})\right) \quad (3.7)$$

And the film water content curve (the weight percentage of water in the latex film as a function of time) was derived as:

$$k_w(t) = 1 - \frac{w_{\text{latex0}} k_{s0}}{w_{\text{latex0}} - w(t)} \quad (3.8)$$

For comparison, the drying rate of deionized (DI) water (with electrical resistivity of 18.2 MΩ · cm at 25 °C) in the Petri dish was measured under the same condition. At the same time, temperature and humidity of the experimental environment was monitored by a hygrometer/thermometer.

3.2.3.5 Video recording

Video recording was initiated before weighing the latex. Time-lapse photos of the latex film were recorded every 2 min. The photos had a resolution of 0.17 mm. The color change of latex film was correlated to different drying stages. The drying boundaries and cracks were also observed.

3.3 Results and discussions

3.3.1 OCT-Gravimetry-Video characterizations on drying processes of L-PS and S-PS latexes – "vertical packing", "consolidation", "detachment", "cracking", "drying boundary" and "apparent shear bands"

Figure 3.2 and Figure 3.3 present the time-lapse OCT-Gravimetry-Video measurements on the drying processes of L-PS and S-PS, respectively. The local internal microstructure at the OCT scanning spot (1 mm in this section), the global drying curve and the top-view visual appearance of the whole latex (8.52 cm for Petri dish) were characterized simultaneously. Characterization results from different measurements were correlated to provide insights of drying inhomogeneities in each state of the drying process. During drying of those two latexes, the room temperature and humidity were measured as 26 ± 1 ◦C and 45 ± 1% RH.

3.3.1.1 PS latex with larger particles (L-PS, particle size: 125 nm)

For L-PS latex, from 0 min to ~186 min, the video shows that the top surface of latex was smooth, and its color changed from opaque white to transparent blue (Figures 3.2b1-b3). The color change was because the interstices between particles decreased as the water evaporated so that short-wavelength light had stronger scattering compared to long-wavelength light due to Rayleigh scattering[5,44]. This drying state is referred as "initial drying" state in Figure 3.2c. In this state, the measured global drying rate was constant (Figure 3.2a). The drying rate was the same as that of de-ionized (DI) water ($(2.0 \pm 0.1) \times 10^{-4}\,\mathrm{g/(cm^2 \cdot min)}$) measured under the same room condition. In Figure

3.2d, the film thickness was defined as the distance between the film bottom and the film top along the vertical direction (the difference of the two vertical positions of film bottom and film top at a specific time). From 0 min to 186 min, the film thickness as measured along the vertical lines (e1 and a line at 186 min in Figure 3.2d), respectively, decreased linearly from ~1100 μm to ~720 μm. This agrees with the measured constant drying rate.

After ~186 min, the video shows that cracks appeared in the middle of the Petri dish and propagated to the dish wall until ~220 min (Figure 3.2b3-b7), which is referred to as the "crack formation and propagation" state in Figure 3.2c. During this time, L-PS was broken up into pieces. At ~190 min, when cracks appeared at the OCT scanning spot (Figure 3.2b4), the time-lapse OCT intensity profile shows the latex detached and moved up off the dish substrate (Figure 3.2d, the "detachment" state in Figure 3.2f). From ~186 min to ~220 min, the water content of the whole latex (k_w) decreased from 36.4% to 29.1% (Figure 3.2a). Before the detachment of the latex, the substrate exerted the tensile stresses to the latex to counteract its volume shrinkage caused by the internal compressive stress (due to the interfacial tensions or capillary forces between particles). Such tensile stresses induced the formation of cracks later on, even though there were more than 30% of water inside the latex[11,25].

From ~210 min to ~278 min, which took ~68 min, the video shows that a clear drying boundary appeared in the middle of the Petri dish and propagated to the dish wall (Figures 3.2b5-b8). The drying boundary separated the enclosed white drier region from the outside blue wetter area, with the enclosed region expanding over time. The whitening of the enclosed region can be attributed to air infiltration into the latex, causing a change of its scattering property. This drying state was named the "drying boundary propagation"

state in Figure 3.2c. Although 13.1% water was in the latex at ~278 min, the latex kept white and barely changed afterwards in the video (Figures 3.2b8-b10). Since the structure of latex was so porous, the packed particles did not inhibit drying. Ideally, if drying was uniform everywhere on the horizontal surface, the drying rate should drop abruptly from free water evaporation to zero at the time point when all water evaporated. However, it took ~72 min for the drying rate to decrease from ~1.7×10^{-4} g/(cm^2 · min) at ~276 min to nearly 0 at ~348 min (Figure 3.2a, the "drying rate decrease" state in Figure 3.2c). The reason is that the horizontal drying inhomogeneity causes the dryings at different positions to stop at different times. The period of "drying rate decrease" state (~72 min) is also close to that of "drying boundary propagation" state (~68 min), shown in Figure 3.2c. After ~348 min, the latex was dried out due to nearly zero drying rate and zero water content.

Interestingly, as the drying boundary reached the OCT scanning spot (the location marked with a black cross in Figure 3.2b1) at ~212 min, 2D OCT structural image shows that apparent shear bands were formed in the cross-section of the latex (Figure 3.2e4, referred as the "formation of apparent shear bands" state in Figure 3.2f). Yang et al.[12] and Kiatkirakajorn et al.[13] reported and explained the finding of shear-banding structures developed along the horizontal direction, seen from the top view, by drying colloidal silica and polystyrene particles. However, the apparent shear bands in Figure 3.2e4 were developing along the vertical direction, seen from the cross-sectional view. They can be attributed to the vertical component of compressive stresses within the latex, although the water content is high (k_w = 30.9% at 212 min). The apparent shear bands lasted for ~68 minutes and disappeared at ~280 min. Details on the shapes and patterns of apparent shear bands will be investigated in Section 3.3.2.2 by scanning a larger area with OCT. Between

~190 min and ~314 min, the time-lapse OCT intensity profile shows the latex moved up and down with formation of cracks and apparent shear bands. During that period, the latex kept relaxing internal stresses. Thus, this drying state was called the “stress relaxation” in Figure 3.2f. After ~314 min, the latex at the OCT scanning spot barely changed and remained detached (Figures 3.2e5-e6), corresponding to the “final drying” state in Figure 3.2f.

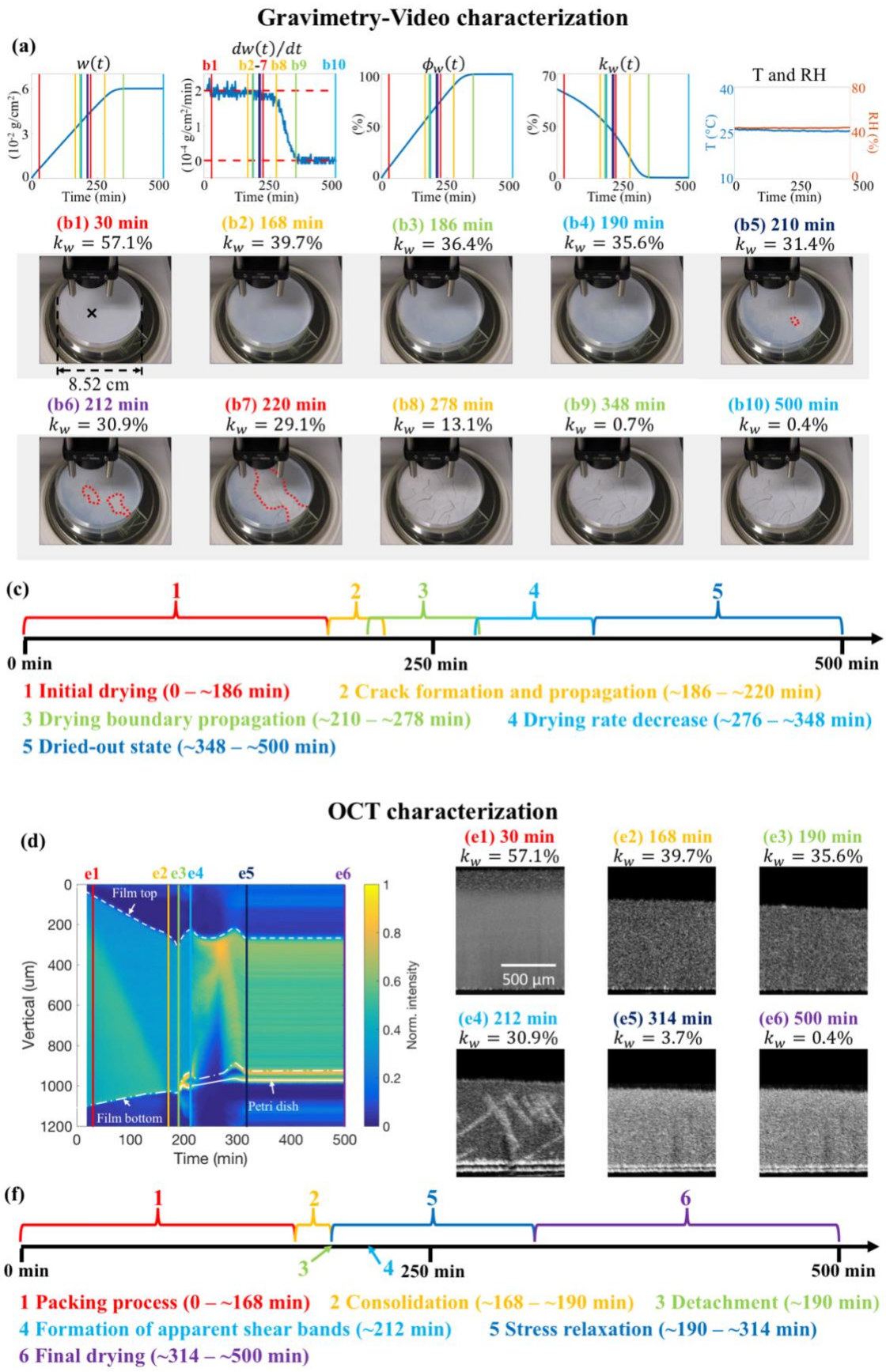
Gravimetry-Video characterization
(a)
w(t)
dw(t)/dt
b1 b2-7 b8 b9 b10
φw(t)
kw(t)
T and RH
Time (min)
(b1) 30 min
kw = 57.1%
(b2) 168 min
kw = 39.7%
(b3) 186 min
kw = 36.4%
(b4) 190 min
kw = 35.6%
(b5) 210 min
kw = 31.4%
8.52 cm
(b6) 212 min
kw = 30.9%
(b7) 220 min
kw = 29.1%
(b8) 278 min
kw = 13.1%
(b9) 348 min
kw = 0.7%
(b10) 500 min
kw = 0.4%
(c)
1
2
3
4
5
0 min
250 min
500 min
1 Initial drying (0 – ~186 min)
2 Crack formation and propagation (~186 – ~220 min)
3 Drying boundary propagation (~210 – ~278 min)
4 Drying rate decrease (~276 – ~348 min)
5 Dried-out state (~348 – ~500 min)
OCT characterization
(d)
e1 e2 e3 e4 e5 e6
Film top
Film bottom
Petri dish
Vertical (um)
Time (min)
Norm. intensity
(e1) 30 min
kw = 57.1%
(e2) 168 min
kw = 39.7%
(e3) 190 min
kw = 35.6%
500 μm
(e4) 212 min
kw = 30.9%
(e5) 314 min
kw = 3.7%
(e6) 500 min
kw = 0.4%
(f)
1
2
3
4
5
6
0 min
250 min
500 min
1 Packing process (0 – ~168 min)
2 Consolidation (~168 – ~190 min)
3 Detachment (~190 min)
4 Formation of apparent shear bands (~212 min)
5 Stress relaxation (~190 – ~314 min)
6 Final drying (~314 – ~500 min)

Figure 3.2: **OCT-Gravimetry-Video characterizations on L-PS latex**. (a) drying curve ($w(t)$), drying rate curve ($dw(t)/dt$), drying extent curve ($\phi_w(t)$) and film water content curve ($k_w(t)$), with the monitored temperature and relative humidity. (b1-b10) video photos at 30, 168, 186, 190, 210, 212, 220, 278, 348 and 500 min. (c) Drying states from the start of drying to the end of being fully dried, defined by Gravimetry-Video characterization. (d) Time-lapse OCT intensity profile. (e1-e6) 2D OCT structural images at 30, 168, 190, 212, 314 and 500 min. (f) Drying states, defined by OCT characterization. Black cross in (b1): Scanning spot of OCT. Red dotted curves in (b5-b7): drying boundary separating the white drier area and the blue wetter area.

3.3.1.2 PS latex with smaller particles (S-PS, particle size: 53 nm)

For S-PS latex, from 0 min to ~200 min, the video shows that the top surface of latex was smooth (Figures 3.3b1-b3), corresponding to the "initial drying" in Figure 3.3c. And its color was bluer and more transparent as compared to L-PS latex because smaller interstices between smaller particles led to stronger scattering of short-wavelength light than scattering of long-wavelength light[5,44]. The drying rate was the same as that of DI water (Figure 3.3a). Starting from ~200 min, cracks appeared and propagated to the Petri dish wall until ~310 min (Figures 3.3b3-b7), corresponding to the "crack formation and propagation" state in Figure 3.3c. When the cracks reached the OCT scanning spot at ~220 min (Figure 3.3b4), the time-lapse OCT intensity profile shows the start of latex's detachment away from the substrate (Figure 3.3d, the "detachment" state in Figure 3.3f). The water content of S-PS latex changed from 44.5% at 200 min to 18.3% at 310 min (Figure 3.3a).

From ~276 min to ~392 min, which took ~116 min, the video shows that a clear drying boundary emerged and propagated to the Petri dish wall (Figures 3.3b5-b8), corresponding to the "drying boundary propagation" in Figure 3.3c. After ~392 min, the latex stayed white and barely changed (Figures 3.3b8-b10). From ~292 min to ~406 min, which took ~114 min, the drying rate decreased from ~$1.7 \times 10^{-4}\ \mathrm{g/(cm^2 \cdot min)}$ to nearly 0 (Figure 3.3a), corresponding to the "drying rate decrease" in Figure 3.3c. The period of "drying rate decrease" state (~114 min) is close to that of "drying boundary propagation" state (~116 min). When the drying boundary reached the OCT scanning spot at ~292 min, the 2D OCT structural image shows the formation of apparent shear bands along the vertical direction (Figure 3.3e4, the "formation of apparent shear bands" state in Figure

3.3f). The apparent shear bands lasted for ~34 minutes and disappeared at ~326 min. Between ~220 min and ~326 min, the time-lapse OCT intensity profile shows the latex moved up and down (the "stress relaxation" state in Figure 3.3f). Afterwards, the latex at the OCT scanning spot remained unchanged and detached (Figures 3.3e5-e6, the "final drying" state in Figure 3.3f).

By comparing the crack patterns of L-PS (Figure 3.2b10) and S-PS (Figure 3.3b10), the broken-up pieces of S-PS are generally smaller than those of L-PS. The average of crack areas (defined as area of a broken-up piece surrounded by cracks) were 66.8 mm^2 (standard deviation = 60.3 mm^2) for L-PS and 27.4 mm^2 (standard deviation = 24.1 mm^2) for S-PS. Such difference can be explained by the different compressive stresses, which are about inversely proportional to the particle size[1,11]. Therefore, the smaller the particles are, the higher the internal stresses will be, therefore the more cracks will be needed to release the accumulated stress energy.

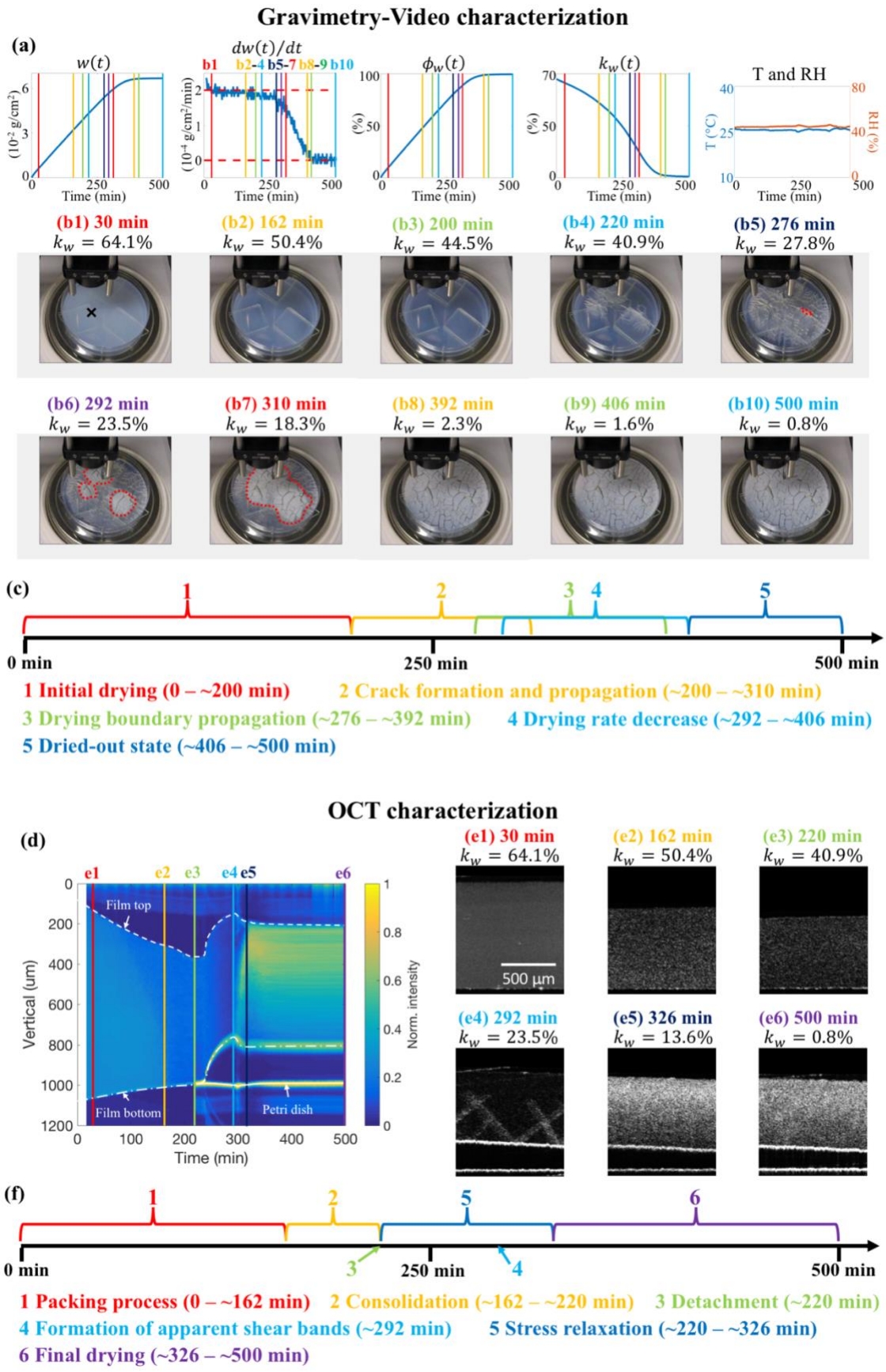
Gravimetry-Video characterization
(a)
w(t)
dw(t)/dt
b1 b2-4 b5-7 b8-9 b10
φw(t)
kw(t)
T and RH
Time (min)
(b1) 30 min
kw = 64.1%
(b2) 162 min
kw = 50.4%
(b3) 200 min
kw = 44.5%
(b4) 220 min
kw = 40.9%
(b5) 276 min
kw = 27.8%
(b6) 292 min
kw = 23.5%
(b7) 310 min
kw = 18.3%
(b8) 392 min
kw = 2.3%
(b9) 406 min
kw = 1.6%
(b10) 500 min
kw = 0.8%
(c)
0 min
250 min
500 min
1 Initial drying (0 – ~200 min)
2 Crack formation and propagation (~200 – ~310 min)
3 Drying boundary propagation (~276 – ~392 min)
4 Drying rate decrease (~292 – ~406 min)
5 Dried-out state (~406 – ~500 min)
OCT characterization
(d)
e1 e2 e3 e4 e5 e6
Film top
Film bottom
Petri dish
Vertical (um)
Time (min)
Norm. intensity
(e1) 30 min
kw = 64.1%
(e2) 162 min
kw = 50.4%
(e3) 220 min
kw = 40.9%
500 μm
(e4) 292 min
kw = 23.5%
(e5) 326 min
kw = 13.6%
(e6) 500 min
kw = 0.8%
(f)
0 min
250 min
500 min
1 Packing process (0 – ~162 min)
2 Consolidation (~162 – ~220 min)
3 Detachment (~220 min)
4 Formation of apparent shear bands (~292 min)
5 Stress relaxation (~220 – ~326 min)
6 Final drying (~326 – ~500 min)

Figure 3.3: **OCT-Gravimetry-Video characterizations on S-PS latex**. (a) drying curve ($w(t)$), drying rate curve ($dw(t)/dt$), drying extent curve ($\phi_w(t)$) and film water content curve ($k_w(t)$), with the monitored temperature and relative humidity. (b1-b10) video photos at 30, 162, 200, 220, 276, 292, 310, 392, 406 and 500 min. (c) Drying states from the start of drying to the end of being fully dried, defined by Gravimetry-Video characterization. (d) Time-lapse OCT intensity profile. (e1-e6) 2D OCT structural images at 30, 162, 220, 292, 326 and 500 min. (f) Drying states, defined by OCT characterization. Black cross in (b1): Scanning spot of OCT. Red dotted curves in (b5-b7): drying boundary separating the white drier area and the blue wetter area.

3.3.1.3 Visualization of particles' vertical packing process using OCT

The dynamic process of particles' packing can be visualized in time-lapse OCT images of both L-PS and S-PS latexes. Figure 3.4a illustrates the vertical packing process of particles, known as the snow plow effect. At the beginning, particles in latex are separated by large distances and move freely in space. As water continues to evaporate, the latex becomes divided into two domains in the vertical direction: in the upper domain (named "packed layer"), particles are in contact with each other with smaller interstices and low mobility; in the lower domain (named "suspension layer"), particles remain separately suspended and freely move in water with larger distance. At the end of packing, all particles are packed and their motions are restricted.

Figures 3.4b and 3.4f (or Figure 3.2d and 3.3d) show the time-lapse OCT intensity profiles of L-PS and S-PS, respectively. Within the initial 180 min, a domain boundary curve was observed in the latex's cross-section, which was shown as dotted curves in Figure 3.4b and 3.4f, respectively. The curve separated the upper domain with lower scattered light intensity and the lower domain with higher scattered light intensity, which suggested that these two domains had different internal structures. To verify it, speckle contrast analysis was performed on 2D OCT structural images and time-lapse OCT intensity profiles, by which the mobility of particles in these two domains can be differentiated. The higher the speckle contrast (K_{spc}) is, the lower the mobility of particles is. Figure 3.4c and 3.4g show the time-lapse OCT speckle profiles of L-PS and S-PS latexes, respectively. In those two figures, domain boundary curves can be easily identified based on K_{spc} (shown as dotted curves in Figure 3.4c and 3.4g). Above the boundary, K_{spc} is high with low particles' mobility; below it, K_{spc} is low with high particles' mobility.

Such domain boundaries can be also observed in 2D OCT speckle images (Figures 3.4d1-d3, h1-h3). These results of the speckle contrast analysis indicated that the upper and lower domains of the latex in both time-lapse OCT intensity and speckle profiles are the packed layer and the suspension layer, respectively.

Based on either light intensity (Figures 3.4b and 3.4f) or speckle contrast (Figures 3.4c and 3.4g), the packed layer thickness of latex film was determined by the distance between its top surface and its domain boundary curve. For L-PS latex (Figure 3.4e), the packing process started from the beginning, and the packed layer thickness was observed to increase linearly most of the time. The packing process was finished at ~168 min, according to the speckle analysis. Thus, we referred the period between 0 min and ~168 min to the "packing process" state in Figure 3.2f. Both the growth curves of packed layer thickness, determined by the intensity and the speckle contrast, overlapped very well. For S-PS (Figure 3.4i), the packed layer was not evident during the initial about 50 min, where the packed layer was too thin to be resolved by OCT. After that, the packed layer thickness began to increase fast with time. The packing process was finished at ~162 min. However, we observed that, although the two curves determined by the intensity and the speckle contrast had the same growing trend, they did not overlap well. This is because the intensity contrast between packed layer and suspension layer in Figure 3.4f is so small that the domain boundary cannot be clearly defined. On the other hand, the speckle analysis is more sensitive to particle's mobility, so that it can provide higher contrast to define the domain boundary in Figure 3.4g.

Besides the different growth curves of packed layer thickness between L-PS and S-PS latexes, there are other differences between these two samples, in regard to the packing

behaviors. One is that the film water contents (k_w) when all particles get packed in the OCT speckle profiles are different: k_w = 39.7% at 168 min for L-PS (Figure 3.2e2) and k_w = 50.4% at 162 min for S-PS (Figure 3.3e2). Both of those k_w values are higher than 26% (void fraction of densest regular packing) or 36% (void fraction of closely random packing)[45], indicating that particles are either loosely random packed or spaced apart when the packing process ended. Afterwards, for L-PS between ~168 min and ~190 min (Figure 3.2d) and for S-PS between ~162 min and ~220 min (Figure 3.3d), the latex thicknesses kept decreasing. This indicates that particles became further packed with reduced water contents. Thus, we called this period as the "consolidation" state in Figure 3.2f and Figure 3.3f. Another difference is that in OCT speckle images, L-PS has a sharper domain boundary (Figure 3.4c) than S-PS does (Figure 3.4g). In another word, the packing/suspension boundary transition along the vertical direction in OCT speckle images is faster for L-PS than that for S-PS. Routh and Zimmerman[6] developed a numerical model to simulate the particles' packing process based on the Peclet number (Pe). In the dilute limit where Stokes-Einstein equation determines the diffusion coefficient of particles, Pe can be written as Equation 1.1 in Chapter 1 ($Pe = 6\pi\mu R_0 H\dot{E}/(k_B T)$). According to their model, the larger Pe is, the easier the particles get packed, and the sharper the packing/suspension domain boundary will be. If $Pe \geq 10$, the domain boundary was so sharp that the transition from packed layer to suspension layer is asymptotic. In our experiments, Pe for L-PS and S-PS are calculated as 8.9 and 3.5, respectively. This explains the difference of the boundary sharpness, shown in Figure 3.4c and 3.4g. Note that, the simulation results by Routh and Zimmerman did not consider interactions between particles. In reality, electrostatic or steric repulsive interactions, which are related to

surfactants and salts, can dramatically change the diffusion coefficient of particles[7,46]. In addition, as mentioned before, at the end of particles' packing, k_w of S-PS (50.4%) is higher than k_w of L-PS (39.7%), both larger than 36% that Routh and Zimmerman assumed in their model. Therefore, in order to precisely predict the profile of particles' distribution during drying, particles' interaction and void fraction of packed state need to be taken into account.

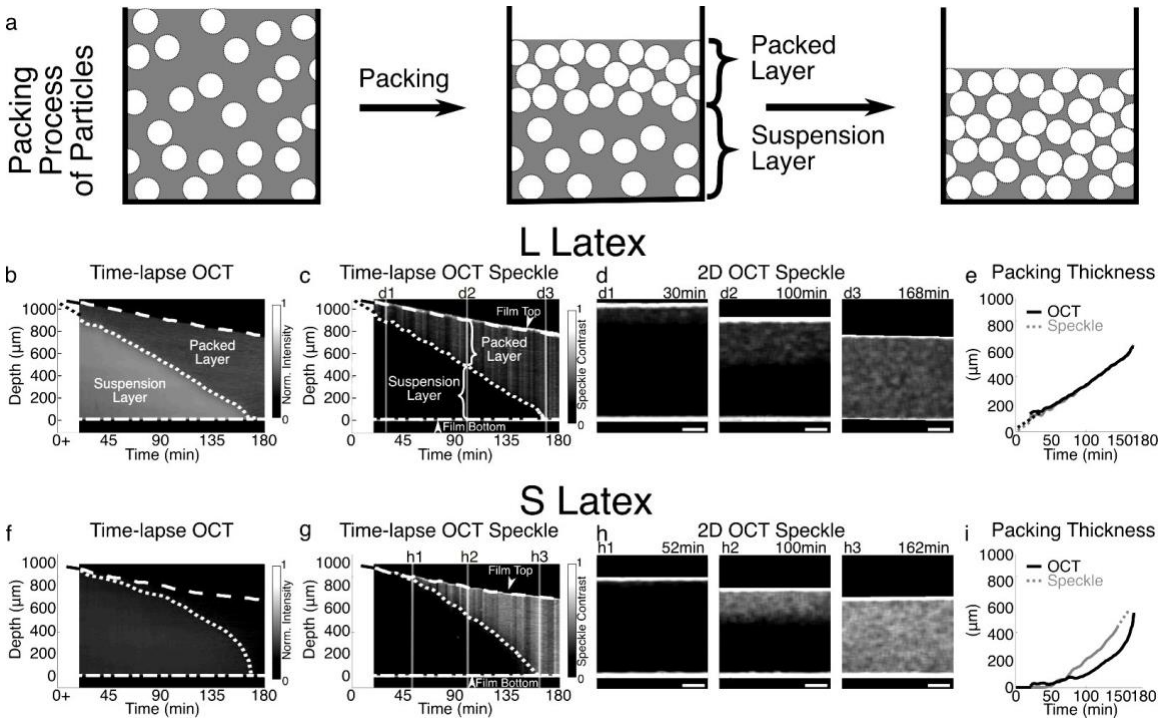

Figure 3.4: **Visualization of particles' vertical packing process using OCT.** (a) Schematic illustration of the packing process of particles. (b,f) Time-lapse OCT intensity profiles of L-PS and S-PS (Figure 3.2d and Figure 3.3d). (c,g) Time-lapse OCT speckle profiles of L-PS and S-PS. The domain boundary curves separating the upper packed layer and the lower suspension layer, shown as dotted curves inside the latexes in (b,f,c,g), were determined according to the scattered light intensities in (b,f) or the speckle contrast values in (c,g). (d1-d3) 2D OCT speckle images at 30, 100 and 168 min of L-PS latex. (h1-h3) 2D OCT speckle images at 52, 100 and 162 min of S-PS latex. (e) L-PS latex: two curves of packed layer thickness as a function of drying time, which are derived from the boundary curves by the light intensity in (b) and by the speckle analysis in (c), respectively. (i) S-PS latex: two curves of packed layer thickness as a function of drying time, which are derived from the boundary curves by the light intensity in (f) and by the speckle analysis in (g), respectively.

3.3.2 Large-area OCT characterizations on drying processes of L-PS and S-PS latexes

For OCT images in Figure 3.2 and Figure 3.3, the OCT scanning area was in the length of 1 mm ($N_x = 200$). In order to investigate the internal structures of drying latex in more details, a large scanning area is set with the length of 5 mm ($N_x = 500$, $N_y = 500$). In this section, the "horizontal drying front" and the "vertical packing" are visualized by scanning a latex droplet; the shapes and patterns of "apparent shear bands" are analyzed by scanning a latex film in Petri dish.

3.3.2.1 "Horizontal drying front" and "vertical packing"

A latex film in a Petri dish was confined by the dish wall (Figure 3.2b1 and Figure 3.3b1), so that the "coffee ring effect" (drying front) was not evinced. However, in real applications, the edges of coatings are always thin and pinned on the substrate without wall's confinement. Thus, the drying of a latex droplet on a substrate can represent real applications where the drying fronts dominate the horizontal drying inhomogeneity.

Drying front is a region of packed particles that propagates horizontally from the edge toward the center of a latex film. Although theoretical models explained the formation and propagation of drying front[2,3,47], the real development of drying fronts of latex particles has not been observed in three dimensions by experiments. Based on analysis of particles' packing process (Figure 3.4), large-area OCT images (~4mm in length) were taken to show the cross-sectional profiles of packing in a latex droplet in Figure 3.5. For both L-PS and S-PS, the horizontal drying fronts propagated at a similar speed, which is much faster than the vertical packing process. The vertical packing of L-PS (Figure 3.5a) was readier than

that of S-PS (Figure 3.5b), since it did not start until ~500 s for S-PS while it started from the beginning for L-PS (similar to observations in Figure 3.4e and 3.4i). Near the end of drying (~400 s for L-PS in Figure 3.5a and ~610 s for S-PS in Figure 3.5b), the whole droplet became donut-shaped due to the continuous dragging of particles from center toward edge.

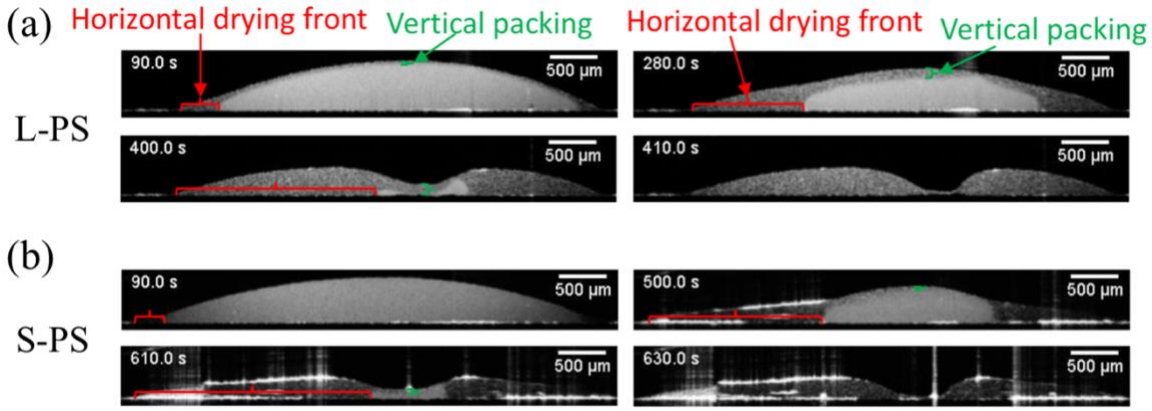

Figure 3.5: (a) 2D OCT structural images of L-PS droplet's cross-section at 90 s, 280 s, 400 s and 410 s. (b) 2D OCT structural images of S-PS droplet's cross-section at 90 s, 500 s, 610 s and 630 s. Horizontal red brackets in figures: horizontal drying fronts. Vertical green brackets in figures: vertical packing.

3.3.2.2 "Apparent shear bands" in cross-sectional view and top view

Large-area 3D OCT structural images in Figure 3.6 show the volumetric structures of apparent shear bands, where the latex was dried in the Petri dish. In the cross-section, the apparent shear bands have bifurcation shapes (cross-sections in Figures 3.6a and 3.6b). They are caused by the vertical component of compressive stresses in the film. The bifurcations grew from the "seeds" on film bottom and upward to the film top, although not reaching the top. Since shear bands always occur at structural defects[48], this indicates that the particles near the film top were more densely packed with less defects than the film

bottom. The bifurcation angles (θ, defined as the angle between the shear band surface and the line orthogonal to the film bottom) and the seed distances (defined as distance between two adjacent bifurcation seeds) were then measured. For L-PS (Figure 3.6a), the bifurcation angles are 39° (standard deviation = 3.5°) and the seed distances are 501 μm (standard deviation = 169 μm); for S-PS (Figure 3.6b), they are 32° (standard deviation = 4°) and 250 μm (standard deviation = 82 μm), respectively. Thus, S-PS has more apparent shear bands than L-PS, which can be explained by the higher internal stresses induced by S-PS.

When seen from the top view of latex film, the projections of apparent shear bands show net-working patterns along the horizontal surface (top views in Figures 3.6a and 3.6b). The bright curves in the patterns are called "ridges" herein. They indicate the horizontal components of compressive stresses in the latex, which should be about orthogonal to the tangential lines of those ridges. The directions of horizontal stresses are shown as blue arrows in top views of Figure 3.6, all of which point away from the crack boundaries. The distances between ridges (or seed distances) indicate the magnitude of the stresses. Therefore, by imaging the shear bands' patterns, the directions and magnitudes of compressive stresses within the film can be potentially mapped out.

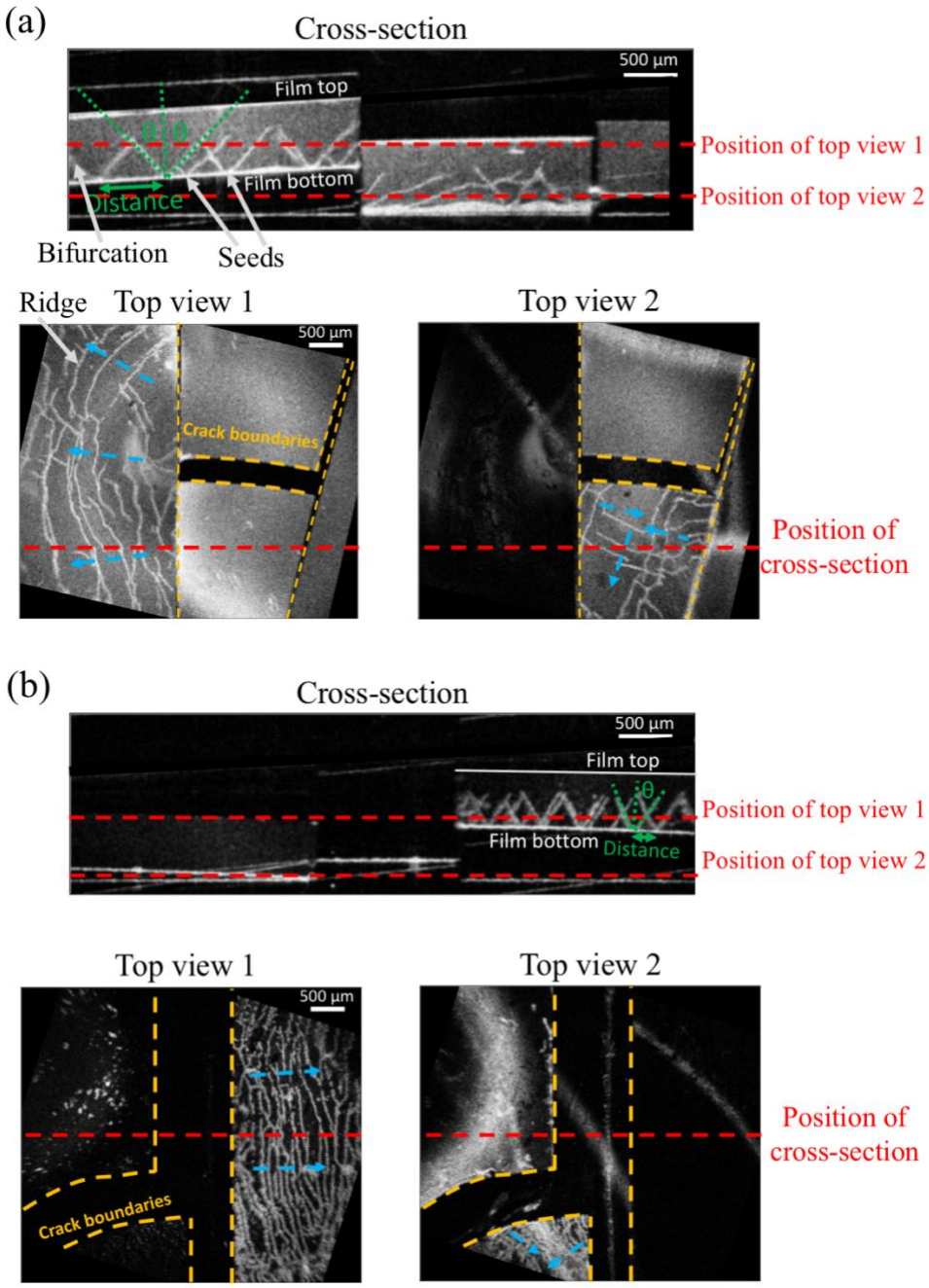

Figure 3.6: cross-sectional images and top-view images of (a) L-PS and (b) S-PS, derived from the 3D OCT structural images during the formation of apparent shear bands. Red dash lines: the OCT scanning planes of corresponding cross-sectional and top-view images. Green dotted lines and θ in the cross-section: the bifurcation shape of apparent shear bands, and the bifurcation angle between the apparent shear band's surface and the line vertical to the film bottom. Green double-headed arrows in the cross-section: seed distance between adjacent bifurcations. Yellow lines in top-view images: boundaries of cracks. Blue arrows in top-view images: directions of horizontal compressive stresses, orthogonal to the ridges (bright curves) of apparent shear bands.

3.4 Conclusions

Drying inhomogeneity is a universal phenomenon that the spatial distribution of latex particles is non-uniform and changes with drying time, resulting in the formation of drying defects in latex films. A new method by combining optical coherence tomography with gravimetric and video analysis ("OCT-Gravimetry-Video" method) has been demonstrated to characterize the drying inhomogeneity of polystyrene latex systems, which are L-PS and S-PS in this chapter.

OCT collects back-scattered light from sample and constructs the cross-sectional and volumetric images of latex film with microns' resolution. The OCT scanning area on the film surface can be from 1 mm to 5 mm in length. The time-lapse OCT images show drying inhomogeneities in both vertical and horizontal directions. Vertical packing process and horizontal drying fronts of particles were monitored with time. Horizontal drying fronts were obvious and propagated fast from film edge to film center, while vertical packing was slower. L-PS started the vertical packing from the beginning of drying, while S-PS started late. The packing/suspension domain boundary of L-PS was sharper than that of S-PS, corresponding to the larger Peclet number during drying of L-PS. Cracks, film detachment off substrate, and apparent shear bands were observed. The apparent shear bands indicate internal compressive stresses in both vertical and horizontal directions during drying a film. S-PS formed a denser population of apparent shear bands than L-PS did, indicating larger internal stresses within S-PS. The patterns of apparent shear bands can be potentially used to map out the directions and magnitudes of internal stresses.

Gravimetry measures the global water mass loss as a function of drying time, from which the drying rate and the film water content evolving with time can be derived. The

drop of drying rate from initial free water evaporation to final nearly zero indicates the drying process in the vertical direction. The transition time of such drying rate's drop indicates the propagation of drying boundaries along the horizontal direction. Video takes time-lapse photos of the latex from the top view, showing color changes, drying boundaries and cracks formation. S-PS presented smaller crack areas than L-PS, indicating larger internal stresses within S-PS. All the three characterizations of "OCT-Gravimetry-Video" method can be correlated with each other at each stage of latex's drying process.

OCT-Gravimetry-Video method is of great value since it offers novel insights of various drying inhomogeneities. In Chapters 4 – 6, the process of skin layer formation will be studied with low-T_g latexes, mostly based on the "OCT-Gravimetry-Video" characterizations. OCT shows the film's internal structure evolving with time. Gravimetry measures the drying curve to correlate its inflection point with the OCT imaging. The video shows drying boundaries along the film surface. The effects of water-soluble additives (especially surfactants) on the film's drying profiles will be also investigated.

3.5 References

1. Keddie, J. & Routh, A. F. *Fundamentals of Latex Film Formation: Processes and Properties*. (Springer Netherlands, 2010).
2. Deegan, R. D., Bakajin, O., Dupont, T. F., Huber, G., Nagel, S. R. & Witten, T. A. Capillary flow as the cause of ring stains from dried liquid drops. *Nature* **389,** 827–829 (1997).
3. Routh, A. F. & Russel, W. B. Horizontal drying fronts during solvent evaporation from latex films. *AIChE J.* **44,** 2088–2098 (1998).
4. Ludwig, I. *Drying, film formation and open time of aqueous polymer dispersions: an investigation of different aspects by rheometry and Inverse-Micro-Raman-Spectroscopy (IMRS)*. (Universitätsverlag, 2008).
5. Divry, V., Gromer, A., Nassar, M., Lambour, C., Collin, D. & Holl, Y. Drying Mechanisms in Plasticized Latex Films: Role of Horizontal Drying Fronts. *J. Phys. Chem. B* **120,** 6791–6802 (2016).
6. Routh, A. F. & Zimmerman, W. B. Distribution of particles during solvent evaporation from films. *Chem. Eng. Sci.* **59,** 2961–2968 (2004).
7. König, A. M., Weerakkody, T. G., Keddie, J. L. & Johannsmann, D. Heterogeneous Drying of Colloidal Polymer Films: Dependence on Added Salt. *Langmuir* **24,** 7580–7589 (2008).
8. Routh, A. F. & Russel, W. B. Deformation Mechanisms during Latex Film Formation: Experimental Evidence. *Ind. Eng. Chem. Res.* **40,** 4302–4308 (2001).

9. Carter, F. T., Kowalczyk, R. M., Millichamp, I., Chainey, M. & Keddie, J. L. Correlating Particle Deformation with Water Concentration Profiles during Latex Film Formation: Reasons That Softer Latex Films Take Longer to Dry. *Langmuir* **30,** 9672–9681 (2014).
10. Price, K., Wu, W., McCormick, A. V. & Francis, L. F. Measurements of Stress Development in Latex Coatings. in *Protective Coatings: Film Formation and Properties* (eds. Wen, M. & Dušek, K.) 225–240 (Springer International Publishing, 2017).
11. Tirumkudulu, M. S. & Russel, W. B. Cracking in Drying Latex Films. *Langmuir* **21,** 4938–4948 (2005).
12. Yang, B., Sharp, J. S. & Smith, M. I. Shear Banding in Drying Films of Colloidal Nanoparticles. *ACS Nano* **9,** 4077–4084 (2015).
13. Kiatkirakajorn, P.-C. & Goehring, L. Formation of Shear Bands in Drying Colloidal Dispersions. *Phys. Rev. Lett.* **115,** (2015).
14. Gromer, A., Nassar, M., Thalmann, F., Hébraud, P. & Holl, Y. Simulation of Latex Film Formation Using a Cell Model in Real Space: Vertical Drying. *Langmuir* **31,** 10983–10994 (2015).
15. Okuzono, T., Ozawa, K. & Doi, M. Simple Model of Skin Formation Caused by Solvent Evaporation in Polymer Solutions. *Phys. Rev. Lett.* **97,** (2006).
16. Belaroui, F., Grohens, Y., Boyer, H. & Holl, Y. Depth profiling of small molecules in dry latex films by confocal Raman spectroscopy. *Polymer* **41,** 7641–7645 (2000).
17. Gundabala, V. R., Zimmerman, W. B. & Routh, A. F. A Model for Surfactant Distribution in Latex Coatings. *Langmuir* **20,** 8721–8727 (2004).
18. NAPOLEON Film Formation Team & Keddie, J. L. Mapping the route from wet to dry. *Eur. Coat. J.* **11,** 28–32 (2009).

19. Croll, S. Drying of latex paint. *J. Coat. Technol.* **58,** 41–49 (1986).

20. Petersen, C., Heldmann, C. & Johannsmann, D. Internal Stresses during Film Formation of Polymer Latices. *Langmuir* **15,** 7745–7751 (1999).

21. Donald, A. M. The use of environmental scanning electron microscopy for imaging wet and insulating materials. *Nat. Mater.* **2,** 511–516 (2003).

22. Keddie, J. L., Meredith, P., Jones, R. A. L. & Donald, A. M. Kinetics of Film Formation in Acrylic Latices Studied with Multiple-Angle-of-Incidence Ellipsometry and Environmental SEM. *Macromolecules* **28,** 2673–2682 (1995).

23. Wang, Y., Juhue, D., Winnik, M. A., Leung, O. M. & Goh, M. C. Atomic force microscopy study of latex film formation. *Langmuir* **8,** 760–762 (1992).

24. Brun, A., Dihang, H. & Brunel, L. Film formation of coatings studied by diffusing-wave spectroscopy. *Prog. Org. Coat.* **61,** 181–191 (2008).

25. Xu, Y., Engl, W. C., Jerison, E. R., Wallenstein, K. J., Hyland, C., Wilen, L. A. & Dufresne, E. R. Imaging in-plane and normal stresses near an interface crack using traction force microscopy. *Proc. Natl. Acad. Sci.* **107,** 14964–14967 (2010).

26. Xu, Y., German, G. K., Mertz, A. F. & Dufresne, E. R. Imaging stress and strain in the fracture of drying colloidal films. *Soft Matter* **9,** 3735–3740 (2013).

27. Ma, Y., Davis, H. T. & Scriven, L. E. Microstructure development in drying latex coatings. *Prog. Org. Coat.* **52,** 46–62 (2005).

28. Prasad, V., Semwogerere, D. & Weeks, E. R. Confocal microscopy of colloids. *J. Phys. Condens. Matter* **19,** 113102 (2007).

29. Loussert, C., Bouchaudy, A. & Salmon, J.-B. Drying dynamics of a charged colloidal dispersion in a confined drop. *Phys. Rev. Fluids* **1,** (2016).

30. Guigner, D., Fischer, C. & Holl, Y. Film Formation from Concentrated Reactive Silicone Emulsions. 1. Drying Mechanism. *Langmuir* **17,** 3598–3606 (2001).

31. Huang, D., Swanson, E., Lin, C., Schuman, J., Stinson, W., Chang, W., Hee, M., Flotte, T., Gregory, K., Puliafito, C. & Fujimoto, J. Optical coherence tomography. *Science* **254,** 1178–1181 (1991).

32. Drexler, W., Liu, M., Kumar, A., Kamali, T., Unterhuber, A. & Leitgeb, R. A. Optical coherence tomography today: speed, contrast, and multimodality. *J. Biomed. Opt.* **19,** 071412 (2014).

33. Fujimoto, J. & Swanson, E. The Development, Commercialization, and Impact of Optical Coherence Tomography. *Investig. Opthalmology Vis. Sci.* **57,** OCT1-OCT13 (2016).

34. de Boer, J. F., Leitgeb, R. & Wojtkowski, M. Twenty-five years of optical coherence tomography: the paradigm shift in sensitivity and speed provided by Fourier domain OCT [Invited]. *Biomed. Opt. Express* **8,** 3248 (2017).

35. Potsaid, B., Gorczynska, I., Srinivasan, V. J., Chen, Y., Jiang, J., Cable, A. & Fujimoto, J. G. Ultrahigh speed Spectral / Fourier domain OCT ophthalmic imaging at 70,000 to 312,500 axial scans per second. *Opt. Express* **16,** 15149–15169 (2008).

36. Tearney, G. J., Waxman, S., Shishkov, M., Vakoc, B. J., Suter, M. J., Freilich, M. I., Desjardins, A. E., Oh, W.-Y., Bartlett, L. A., Rosenberg, M. & Bouma, B. E. Three-Dimensional Coronary Artery Microscopy by Intracoronary Optical Frequency Domain Imaging. *JACC Cardiovasc. Imaging* **1,** 752–761 (2008).

37. Suter, M. J., Nadkarni, S. K., Weisz, G., Tanaka, A., Jaffer, F. A., Bouma, B. E. & Tearney, G. J. Intravascular Optical Imaging Technology for Investigating the Coronary Artery. *JACC Cardiovasc. Imaging* **4,** 1022–1039 (2011).

38. Wojtkowski, M., Srinivasan, V. J., Ko, T. H., Fujimoto, J. G., Kowalczyk, A. & Duker, J. S. Ultrahigh-resolution, high-speed, Fourier domain optical coherence tomography and methods for dispersion compensation. *Opt. Express* **12,** 2404 (2004).

39. Manukyan, S., Sauer, H. M., Roisman, I. V., Baldwin, K. A., Fairhurst, D. J., Liang, H., Venzmer, J. & Tropea, C. J. Imaging internal flows in a drying sessile polymer dispersion drop using Spectral Radar Optical Coherence Tomography (SR-OCT). *J. Colloid Interface Sci.* **395,** 287–293 (2013).

40. Davidson, Z. S., Huang, Y., Gross, A., Martinez, A., Still, T., Zhou, C., Collings, P. J., Kamien, R. D. & Yodh, A. G. Deposition and drying dynamics of liquid crystal droplets. *Nat. Commun.* **8,** 15642 (2017).

41. Saccon, F. A. M., Oliveira, F. M. D. R. de, Ribas, M. O., Jr, P. Z.; Muller, M. & Fabris, J. L. Kinetics of varnish long-term drying process monitored by a heterogeneous optical sensor system. *Meas. Sci. Technol.* **24,** 094013 (2013).

42. Lawman, S. & Liang, H. High precision dynamic multi-interface profilometry with optical coherence tomography. *Appl. Opt.* **50,** 6039 (2011).

43. Boas, D. A. & Dunn, A. K. Laser speckle contrast imaging in biomedical optics. *J. Biomed. Opt.* **15,** 011109 (2010).

44. van Tent, A. & te Nijenhuis, K. Turbidity study of the process of film formation of thin films of aqueous acrylic dispersions. *Prog. Org. Coat.* **20,** 459–470 (1992).

45. Liu, A. J. & Nagel, S. R. *Jamming and Rheology: Constrained Dynamics on Microscopic and Macroscopic Scales*. (Taylor & Francis, 2001).

46. Lovell, P. A. & El-Aasser, M. S. *Emulsion Polymerization and Emulsion Polymers*. (Wiley, 1997).

47. Deegan, R. D., Bakajin, O., Dupont, T. F., Huber, G., Nagel, S. R. & Witten, T. A. Contact line deposits in an evaporating drop. *Phys. Rev. E* **62,** 756–765 (2000).

48. Bigoni, D. *Nonlinear solid mechanics: bifurcation theory and material instability*. (Cambridge University Press, 2012).

4 Chapter 4 Skin Layer and Film Formation during Drying of Thick Films of Low-T_g Model Latex System of Poly(64EHA/35MMA/1MAA) and Other Latex Systems of Poly(BA/MMA/1MAA)

4.1 Introduction

Drying a waterborne latex film always inflicts "drying inhomogeneity", during which the non-uniform time-evolving spatial distribution of latex particles sometimes damages the integrity and mechanical properties of final dried coatings. Chapter 3 establishes the OCT-Gravimetry-Video method and studies the drying inhomogeneities of polystyrene (PS) latex systems with a polymer T_g much higher than room temperature. PS latexes are good models to investigate the mechanisms of particles' packing process, cracks and shear bands. This chapter studies the drying process of latex systems with polymer T_g's near and lower than room temperature. The polymer particles of lower T_g's are more viscoelastic than PS particles at room temperature, so that the film's internal stresses during drying can be relaxed by the deformation of particles. Thus, neither cracks nor shear bands are expected to be observed. The particles' deformation closes up the voids, making the film transparent; the coalescence (polymer chains' interdiffusion) breaks up boundaries and entangle all deformed particles, making the film continuous and strengthened. As shown in Figure 1.1 (Chapter 1), the process of latex film formation takes place in three steps: packing, deformation and coalescence of the latex particles.

In coating applications, it should be expected that all of water in the latex evaporates so that the film would be void-free, transparent and cohesive. However, if particles are soft enough, the film can retain water which takes longer time to dry. The drying time of latex film has been found to inversely correlate with the viscosity or T_g of polymers[1]. The reason, which has been studied both theoretically[2–4] and experimentally[5–8,1], is the "skin layer formation". As introduced in Chapter 1, the skin layer formation is one type of drying inhomogeneity in the vertical direction, commonly seen by drying low-T_g latexes. The formation of skin layer during drying of a latex film depends on two dimensionless parameters – Peclet number (Pe) and $\bar{\lambda}$. Although there are complex modifications on these two parameters considering particles' interactions and permeability through particles' interstices[12,13], the simple expressions of Equations 1.1 and 1.2 (defined in Chapter 1, also given below) are most frequently used and were experimentally validated[1,7]:

$$Pe = \frac{6\pi\mu R_p H\dot{E}}{k_B T}$$

and

$$\bar{\lambda} = \frac{\eta R_p \dot{E}}{\gamma H}$$

where μ is the water viscosity, R_p is the particle radius, H is the wet film thickness, $\dot{E}$ is the water receding rate (the velocity of water surface falling during drying), k_B is the Boltzmann constant, T is the temperature, η is the polymer viscosity and γ is the interfacial tension.

When $Pe > 1$ and $\bar{\lambda} < 1$, the packed particles on the film top that are exposed or close to air will deform and even coalesce fast into a polymer film before all the water within the latex film evaporates, which means the film formation process on film top happens earlier than that below. Thus, the top dried coalesced latex polymer film, known as "skin", traps the remaining water underneath it. Shown as in Figure 1.3B (Chapter 1), the resulting film structure has two layers – the skin layer above and the "wet domain" below; also there can be a transition zone between them. The film looks opaque and white due to the strong light scattering in the wet domain with the existence of water. Since the skin usually has a very low water vapor permeability (WVP), the diffusion of water molecules through skin becomes so slow that the drying rate of film is only negligible to that of initial free water evaporation. It will take a long time for particles in the wet domain to transform into a dried coalesced latex polymer film. The drying problem caused by skin can be more severe when thick latex films (from ~500 μm to millimeters in wet thickness) for architectural and protective coatings are applied, because more water can be retained under the skin which takes longer time to dry. In this dissertation, experiments on drying low-T_g latexes under room condition were carried out using the PEM latex (studied in this chapter and Chapter 5) and the commercial PLB latex (studied in Chapter 6) with a wet film thickness of 2 mm. The results of these two latex systems show that it takes >4 days and >12 days to get 95% of water evaporated, respectively, which is too long for coating applications.

Besides the criteria of skin layer formation (Equation 1.1 and 1.2 in Chapter 1) which take polymer T_g and particle size into account, the dynamic processes of skin formation and latex film formation need to be studied further. It should be noted that,

besides polymer T_g and particle size, chemical compositions in latex (such as surfactants, ions, and particles' surface groups) can affect the drying process of film (see Section 2.1 in Chapter 2). Moreover, understanding the mechanism of skin formation process lays basis for controlling the drying process of latex film as well as for solving the drying problem caused by skin. In macroscopic studies, gravimetric analysis and video characterization were commonly used[5,6,9,10]. The skin layer formation correlates with the turning point of drying curve (at which the drying rate decreased significantly) and the opaqueness of film appearance. In microscopic studies, heterogeneous optical sensor system (HSS), nuclear magnetic resonance (NMR) profiling, near infrared (NIR) measurement and diffusing wave spectroscopy (DWS) were used in recent years[1,8,11,12]. NMR measured the vertical distribution of water concentration and showed a dried polymer skin without water on the film top. NIR measured the mean water content in film and found a significant slowdown of evaporation when skin formed. However, in both methods, the thickness of skin and the time-evolution of film structure could not be determined clearly due to limited resolutions. HSS was able to measure the skin thickness as a function of time, based on the reflectivity difference between skin and wet domain; however, the result was only qualitatively described without theoretical explanations. By combining DWS and NMR, skin formation was found to occur when latex particles on the film top became static. However, DWS only detects particles on the top surface and is unable to penetrate inside the film[12]. Therefore, in order to understand thoroughly the drying process and skin layer formation of latex film, both the internal microstructure of film and the macroscopic measurements need to be combined and synchronized to monitor the drying process.

In this chapter, the OCT-Gravimetry-Video method (constructed and applied to study high-T_g latexes, reported in Chapter 3) is employed to study the drying process and skin layer formation of low-T_g latex system. OCT (optical coherence tomography) collects back-scattered light from the sample and reconstructs the internal structure based on light intensity. The OCT images and profile along the vertical direction at a specific OCT scanning spot are used to map out the particles' packing process and to visualize the formation of skin layer and the transformation of wet domain into dried coalesced latex polymer layer. Since the skin and the coalesced latex polymer layer ("coalesced layer" for short) are transparent with much lower reflectivity than the opaque wet domain, the thicknesses of skin and coalesced layer as a function of time can be measured based on the light intensity difference. It should be noted that the coalesced layer's thickness includes the thickness of skin which is also part of coalesced latex film. Gravimetry measures the global drying curve, from which the drying rate curve and the film water content curve as a function of time are derived. Video shows the latex's macroscopic appearance from the top view, from which the color change of latex and the propagation of drying boundary (the boundary separating the more opaque white area and more transparent blue area in the horizontal direction) are observed.

This chapter mainly reports the studies of the dying process and skin layer formation process of the model PEM (poly(64EHA/35MMA/1MAA)) latex system. The latex has a -19 °C T_g and 176 nm average particle diameter (measured by DLS in Section 2.3.1.1 in Chapter 2), stabilized by sodium lauryl sulfate (SLS) surfactant as well as sulfate and carboxyl groups on particles' surface (see Tables 2.4 and 2.5 in Chapter 2). The OCT-Gravimetry-Video method was used to monitor the drying process of PEM latex at room

temperature and humidity. The OCT profile with microns' resolution shows the packing, the consolidation, the formation of apparent skin, and the thickening of coalesced latex polymer layer ("coalesced layer") in the vertical direction as a function of time. The video from the latex's top view shows the drying boundary and "grooves" developing along the horizontal direction. The drying curve measured by gravimetry reflects drying inhomogeneities in both horizontal and vertical directions that are observed in both OCT profile and video. Based on these results, a theoretical model is developed to describe the thickening process of coalesced layer until the entire latex film becomes dried and transparent. This chapter also includes the effects of latex's initial solids content (k_{s0}), polymer T_g and particle size on drying of latex films by using the series of PBM latexes (with different BA/MMA ratios and particle sizes, listed in Table 2.5) in addition to the PEM latex.

4.2 Materials and methods

4.2.1 Latex systems

All latexes used in this chapter have polymer T_g's near or lower than room temperature, so that a transparent continuous polymer film can be formed after all water evaporates by drying under room conditions. They are PEM (poly(64EHA/35MMA/1MAA)), PBM1 (poly(77BA/22MMA/1MAA)), PBM2 (poly(60BA/39MMA/1MAA)), PBM3 (poly(45BA/54MMA/1MAA)), and D-PBM2 (D-poly(60BA/39MMA/1MAA) with larger particle size). The properties of these latexes can be found in Table 2.4 (for particles sizes) and Table 2.5 (for other properties). According to Table 2.5 (Chapter 2), they have measured T_g's as -19 °C, -25 °C, -3 °C, 23 °C and 0 °C, respectively; initial % solids contents (k_{s0}) as 49.94, 52.27, 50.61, 51.07 and 57.89, respectively; and DLS average particle diameters (D_p, measured by DLS) as 176 nm, 189 nm, 175 nm, 187 nm and 360 nm, respectively. It should be noted that k_{s0} of PEM latex in this chapter is 49.94% due to the different synthesis batch, instead of 50.37% listed in Table 2.5 (Chapter 2). Their densities of solids (mostly polymers) are 1.03 g/cm^3, 1.02 g/cm^3, 1.06 g/cm^3 1.09 g/cm^3 and 1.06 g/cm^3, respectively, which are close to and slightly heavier than water; in future calculations, they are set about the same as water ($\rho = \rho_s = \rho_w = 1\ \mathrm{g/cm^3}$) (see Section 2.3.1.2 in Chapter 2). The details of the recipes and synthesis procedures of those latexes are shown in Tables 2.1 and 2.2 (Chapter 2), from which the major compositions of latexes can be inferred.

4.2.2 OCT-Gravimetry-Video method

The OCT-Gravimetry-Video method (see Figure 3.1 in Chapter 3 for experimental system set-up) was used to characterize the drying process of latex film. For OCT imaging, the light beam scanned in a two-dimensional fashion along the horizontal surface – N_x points on x-axis and N_y points on y-axis. At each point, the scattered light intensities at N_z points along z-axis in the vertical direction were decoded from the spectrum of interfered light. "3D OCT structural images" of scattered light intensity were acquired with $N_x = 100$, $N_y = 100$ and $N_z = 512$. The pixel sizes on x-axis and y-axis were 10 μm and 8.7 μm, respectively. By using the poly(methyl methacrylate)'s refractive index (1.48), the pixel size (resolution) on z-axis was 6.7/1.48 = 4.5 μm. The image was also rotated by vertically shifting each column of pixels by Matlab, so as to make sure the Petri dish surface was leveled in the image. By averaging each 3D OCT structural image along the horizontal direction, the "time-lapse OCT intensity profile" ("OCT profile" for short) was obtained to show the time-evolution of backscattered light intensity distribution in the vertical direction.

In this chapter, the OCT profile not only shows the film top and film bottom, but also distinguishes the packing/suspension boundary, and the skin (and coalesced layer)/wet domain boundary in the vertical direction (shown as Figure 4.1d1). During the process of particles' packing, the upper packed layer (where particles contact each other) and the lower suspension layer (where particles are separately suspended) show different reflectivity (see Section 3.3.1.3 in Chapter 3). During the processes of skin layer formation and further film formation, since the upper skin and coalesced layer is a dried transparent polymer film and the lower wet domain has significant amount of water, the reflectivity of skin layer and coalesced layer is much weaker than that of the wet domain. Thus, by

determining the half increment of scattered light intensity along the vertical direction, both the packing/suspension boundary and the skin (and coalesced layer)/wet domain boundary can be drawn. Then, the "film thickness", the "packed layer thickness", the "skin layer thickness" and the "coalesced layer thickness" (which from the point in time >1050 min in Fig. 4(d1) includes the skin layer thickness) are determined as the vertical distances between film top and film bottom, between film top and packing/suspension boundary, and between film top and skin (and coalesced layer)/wet domain boundary, respectively. Those thicknesses are tracked as a function of time (shown in Figure 4.1e). Among them, the packed layer thickness is recorded from the start of drying until all particles become packed (~270 min in Figure 4.1e), which is the period of "packing process" (in Figure 4.1f). After the packing process, the particles remain packed and get consolidated, deformed and coalesced.

For gravimetry, the initial weight of latex film in the Petri dish (~11.4 g of PEM with 49.94% solids) was set so that the thickness of dried latex film (with no water) is expected to be 1 mm. The drying curve ($w(t)$), the drying rate curve ($dw(t)/dt$), the drying extent curve ($\phi_w(t)$) and the film water content curve ($k_w(t)$) were measured and defined the same as in Section 3.2.3.4 in Chapter 3. For video, the camera took time-lapse photos from top view. All measurements were synchronized and took data every 2 minutes.

4.2.3 Drying curve measurement in controlled environment

The drying curve measurements were conducted on the 0.0001g-precision digital balance (AGN200, Torbal, USA) which was placed in the environmental chamber (KBF 720, BINDER, Germany) controlled at 23 °C and 50% RH. The balance's door was closed to

limit air flow, but the water vapor still diffused freely through spacing between the balance's door and the chamber's environment. The measurements followed the same procedure as the gravimetric analysis in the OCT-Gravimetry-Video method. The initial weight of latex film in the Petri dish was set so that the thickness of dried latex film (with no water) is expected to be 1 mm. Data were taken every 2 minutes.

4.3 Results and discussions

4.3.1 OCT-Gravimetry-Video characterizations on the drying process of PEM latex – "vertical packing", "consolidation", "grooves", "drying boundary", "skin layer" and "coalesced latex polymer layer"

Figure 4.1 presents the time-lapse OCT-Gravimetry-Video measurements on the drying process of PEM latex. The local internal microstructure at the OCT scanning spot (1 mm in length), the global drying curves and the top-view visual appearance of the whole latex (8.52 cm for Petri dish's diameter) were characterized simultaneously. The room temperature and humidity were tracked as about 25 °C and 46% RH, respectively. In the experiment, 11.4 g PEM latex (with 49.94 % solids) was spread on the Petri dish, so that the initial latex thickness was 2 mm and the fully dried film thickness was 1 mm. With the polymer T_g (-19 °C), the particle diameter (176 nm) and the initial drying rate ($1.6 \times 10^{-4}\,\mathrm{g/(cm^2 \cdot min)}$ in Figure 4.1a), calculations[1] show that the Peclet number $Pe = 19.1 > 1$ and the dimensionless parameter $\bar{\lambda} = 1.8 \times 10^{-4} < 1$. Thus, PEM latex is a good candidate to study the skin layer formation process.

For the PEM latex, from 0 min to ~270 min, the video shows that the top surface of the latex film was smooth, and its color changed from opaque white to more transparent blue (Figures 4.1b1-b2), referred to as the "initial drying" state in Figure 4.1c. During the same period, the OCT profile shows a linear packing/suspension boundary inside the film (red dashed line in Figure 4.1d2). This boundary indicates the vertical packing process of particles with the packed layer thickness increasing linearly with time. It corresponds well with the calculated large Pe (= 19.1). The film thickness decreased linearly with time

mostly (Figures 4.1d2 and e), corresponding to the constant drying rate close to that of DI water (Figure 4.1a). At 270 min when all particles became packed, k_w = 36.3% (Figure 4.1b2 or Figure 4.1a), which is close to the 36% void fraction of closely random packing. The time from 0 min to ~270 min is referred to as the "packing process" state in Figure 4.1f.

After ~270 min, the video shows uneven film thicknesses near the edge of Petri dish (black arrows in Figures b2-b4). They were areas with film thicknesses much thinner than surroundings, named "grooves", caused by the volume shrinkage of latex. The grooves propagated along the dish edge until 400 min. The period of ~270 min to ~400 min is named "grooves formation and propagation" state in Figure 4.1c. Although the drying rate from 0 min to ~400 min was fast and constant (Figure 4.1a), the film thickness curve (measured by OCT profile) shows a "kink point" at 270 min, near which the film thickness profile changed slightly but continued to decrease past this kink (Figures 4.1d1 and e). This happened concomitantly to the formation of grooves. The reason can be that, the horizontal compressive stresses dragged latex particles from the grooves to the middle of the latex film to compensate for the water loss at the OCT scanning spot. Thus, 270 min was called "stress relaxation" point in Figure 4.1f. From 270 min to 550 min, the film thickness continued dropping fast (Figures 4.1d1 and e) and k_w decreased from 36.3% to 15.2% (Figure 4.1a). During this period, the particles packed further and became partially deformed, referred to as the "consolidation" state in Figure 4.1f. The film's structure was still so permeable that the free water evaporation was still as fast as that of the "packing process" state (close to DI water).

From ~380 min to ~540 min, which took ~160 min, the video shows that a clear drying boundary appeared on the left of the Petri dish and propagated to the dish wall (Figures 4.1b3-b6), referred to as the "drying boundary propagation" state in Figure 4.1c. Meanwhile, from ~490 min to ~610 min, which took ~120 min, the drying rate decreased from $1.3 \times 10^{-4}\,\mathrm{g/(cm^2 \cdot min)}$ to$1.7 \times 10^{-5}\,\mathrm{g/(cm^2 \cdot min)}$, referred to as the "drying rate decrease" state in Figure 4.1c. Both states indicate the horizontal drying inhomogeneity. The "drying rate decrease" state actually corresponds to the formation and propagation of low-permeable skin layer along the horizontal direction, during which the fast-drying area without skin's coverage kept shrinking from ~490 min until ~610 min. After ~610 min, the whole latex film was covered by the skin with low permeability, and the drying rate became close to 0 (Figure 4.1a). During this period (referred to as "drying through low-permeable skin" state in Figure 4.1c), the skin became no longer fragile but with enough strength that it could be peeled off without breaking, indicating that the particles in the skin layer at the film top become coalesced. Since there was still a relatively significant amount of water trapped under the skin (k_w = 12.6% at 610 min and k_w = 6.0% at 2000 min), the latex film still looked opaque and white (shown in Figures 4.1b7-b10) due to light scatterings in the wet domain below the skin. The period after ~610 min is thus referred to as the "slow drying process" in Figure 4.1c. The "drying rate decrease" state (from ~490 min to ~610 min) happened later than the "drying boundary propagation" state (from ~380 min to ~540 min), indicating that at a specific location on the film, the coalescence of particles in the skin became developed after the drying boundary passed that location.

In the OCT profile, at ~550 min, a thin transparent layer with low scattered light intensity appeared on film top (see Figure 4.1d1), while the wet domain below it shows higher light intensity. At the same time, the film thickness began decreasing much slower with time due to the significant reduction of drying rate (see Figure 4.1e). This indicates that the particles on film top coalesced into a low-permeable and apparent skin layer, which is referred to as the "appearance of apparent skin layer" in Figure 4.1f. It happened ~70 min after the drying boundary passed by the OCT scanning spot (Figures 4.1b4-b6). Between ~550 min and ~1050 min, the apparent skin shows a relatively constant thickness of ~30 μm (see Figure 4.1e), which was made of ~170 layers of latex particles (considering the particle diameter of 176 nm) which amounts to ~3 wt% of total polymer in the latex used in the experiment (considering the dried film thickness of 1 mm). It should be reasonable to assume that even before ~550 min, several or tens of layers of latex particles had been aggregated on the film top to form an incipient skin layer, although such incipient skin layer could be made of open structure with relatively high permeability and re-dispersible in water. Such incipient skin layer would not be observable by the OCT imaging due to its 4.5 μm (equivalent to ~26 layers of particles) resolution along vertical direction. With the capillary force applied on the first layer of particles and the polymer/water interfacial tension applied on particles below, the resulting pressure should be large enough to overcome the repulsive forces between particles and to break up the contact area between adjacent particles to initiate their coalescence[14].

Based on the measured drying rates near 630 min and 1000 min ($1.7 \times 10^{-5}\,\mathrm{g/(cm^2 \cdot min)}$ and $9.1 \times 10^{-6}\,\mathrm{g/(cm^2 \cdot min)}$, respectively, derived from the drying

curve in Figure 4.1a), the change of WVP of the ~30 μm-thick apparent skin layer can be calculated by Equation 2.18 (Chapter 2):

$$\text{WVP} = \frac{J \cdot h_{skin}}{p_0 \cdot \Delta RH} \qquad (4.1)$$

with the skin thickness (h_{skin}) at 30 μm, the equilibrium vapor pressure at 25 °C (p_0 = 3169 Pa), the room humidity at 46% RH and the unit humidity of wet domain. Results show skin's WVPs at 630 min and 1000 min are 3.0×10^{-11} g/(cm · min · Pa) and 1.6×10^{-11} g/(cm · min · Pa), respectively, which are close to the WVP of PEM's fully dried coalesced latex film ($(4.0 \pm 0.3) \times 10^{-11}$ g/(cm · min · Pa), in Section 2.3.4 or Table 2.5 in Chapter 2). This indicates that the particles in the apparent skin layer were coalesced to a similar extent of the fully coalesced latex film. The continuous decrease of skin's WVP also indicates that, even after ~550 min, the particles in the apparent skin continued to undergo "further gradual coalescence"[15] which lowered the skin's WVP. Thus, the period from ~550 min to ~1050 min in the OCT profile is defined as the "maturation of incipient skin" state (see Figure 4.1f).

After ~1050 min, the drying process of latex film continued, even though it was very slow due to the low-permeable skin layer. In the OCT profile, the transparent layer on film top expanded and the wet domain shrank with time. This indicates that the particles below the skin become dried, coalesced and added to the transparent layer. This layer is named as "the coalesced latex polymer layer" or (referred to as "coalesced layer" for short), which as mentioned earlier also includes the skin layer. The thickness of coalesced layer (h_{coal}) increased slowly with time, corresponding to the drying rate decrease from

$1.9 \times 10^{-6}\,\mathrm{g/(cm^2 \cdot min)}$ at 1500 min to $7.0 \times 10^{-7}\,\mathrm{g/(cm^2 \cdot min)}$ at 3000 min, because the drying rate is inversely proportional to the thickness of dried film. By profiling the coalesced layer/wet domain boundary within the film, the coalesced layer's thickness was found to increase with the square root of time (shown as the good fitting between the blacked dotted curve and the yellow curve in Figure 4.1e), which is expressed as:

$$h_{coal} = 12.1\ \frac{\mu\mathrm{m}}{\mathrm{min}^{1/2}} \times (t - 1016\ \mathrm{min})^{1/2} \qquad (4.2)$$

Such thickening process can be explained by the fact that, with the slow drying through skin, the particles below the initial ~30 μm-thick low-permeable skin layer continued to coalesce as part of the film formation process, leading to the noticed increase in h_{coal}. This film formation drying process continued until the entire film becomes dried and transparent. A mathematical model based on this explanation will be developed in the next section. Therefore, the period after 1050 min is denoted as the "thickening of coalesced layer" state in Figure 4.1f. Furthermore, since the particles in the wet domain continued with the film formation process (including packing, consolidation, deformation and coalescence) after the ~30 μm thick skin layer was formed at ~550 min, the entire period after ~550 min is referred to as the "completion of latex film drying process below skin" state in Figure 4.1f, which includes both the "maturation of incipient skin" state and the "thickening of coalesced layer" state.

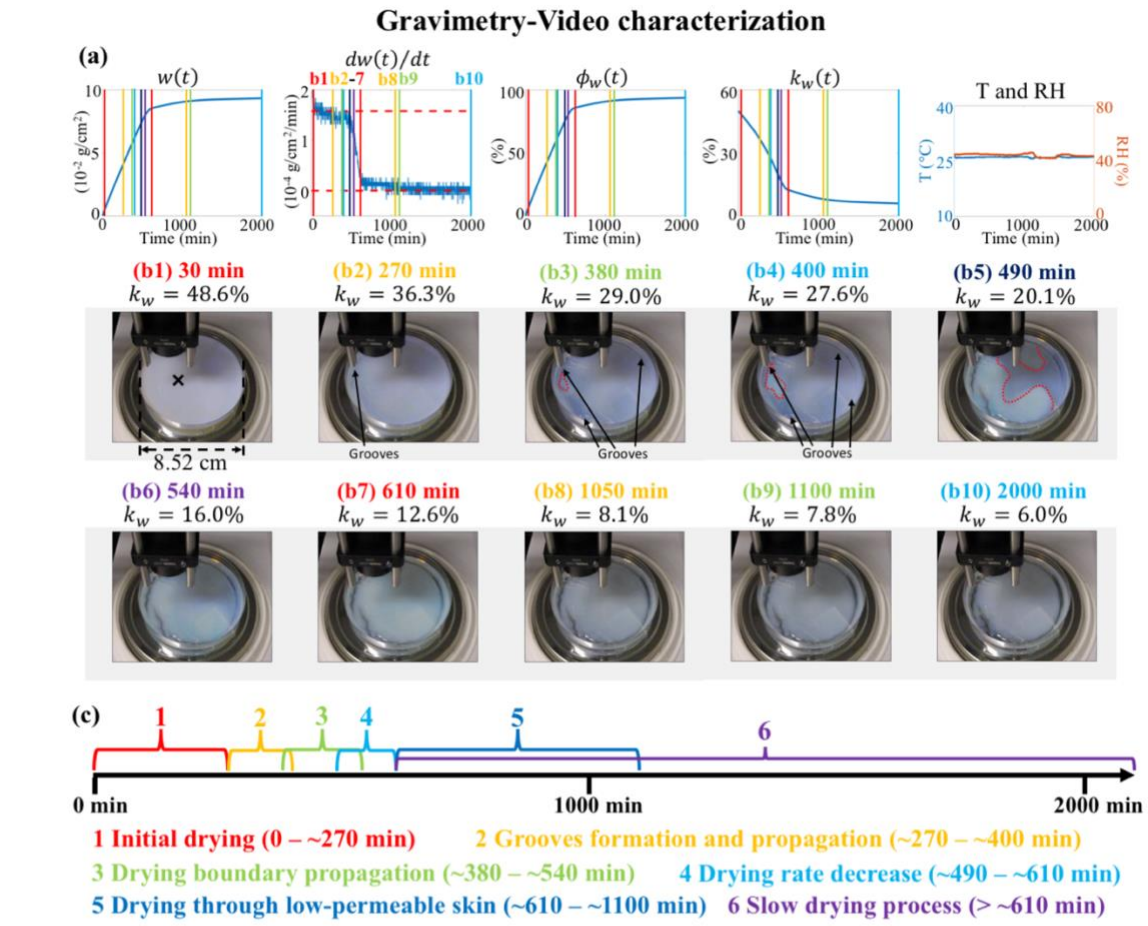
Gravimetry-Video characterization
(a)
w(t)
dw(t)/dt
b1 b2-7 b8 b9 b10
φw(t)
kw(t)
T and RH
Time (min)
T (°C)
RH (%)
(b1) 30 min
kw = 48.6%
(b2) 270 min
kw = 36.3%
(b3) 380 min
kw = 29.0%
(b4) 400 min
kw = 27.6%
(b5) 490 min
kw = 20.1%
8.52 cm
Grooves
(b6) 540 min
kw = 16.0%
(b7) 610 min
kw = 12.6%
(b8) 1050 min
kw = 8.1%
(b9) 1100 min
kw = 7.8%
(b10) 2000 min
kw = 6.0%
(c)
0 min
1000 min
2000 min
1 Initial drying (0 – ~270 min)
2 Grooves formation and propagation (~270 – ~400 min)
3 Drying boundary propagation (~380 – ~540 min)
4 Drying rate decrease (~490 – ~610 min)
5 Drying through low-permeable skin (~610 – ~1100 min)
6 Slow drying process (> ~610 min)

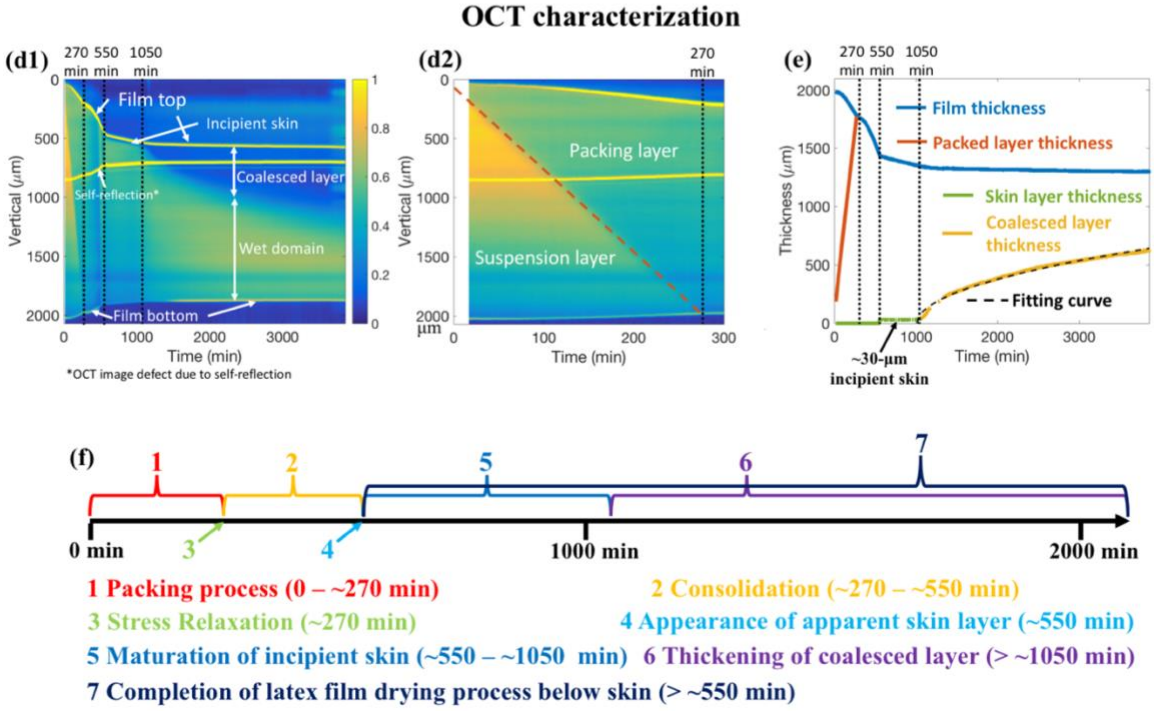
OCT characterization
(d1)
270 min
550 min
1050 min
Film top
Incipient skin
Coalesced layer
Self-reflection*
Wet domain
Film bottom
Vertical (μm)
Time (min)
*OCT image defect due to self-reflection
(d2)
Packing layer
Suspension layer
(e)
Film thickness
Packed layer thickness
Skin layer thickness
Coalesced layer thickness
Fitting curve
Thickness (μm)
~30-μm incipient skin
(f)
0 min
1000 min
2000 min
1 Packing process (0 – ~270 min)
2 Consolidation (~270 – ~550 min)
3 Stress Relaxation (~270 min)
4 Appearance of apparent skin layer (~550 min)
5 Maturation of incipient skin (~550 – ~1050 min)
6 Thickening of coalesced layer (> ~1050 min)
7 Completion of latex film drying process below skin (> ~550 min)

Figure 4.1: **OCT-Gravimetry-Video characterizations on PEM latex**. (a) drying curve ($w(t)$), drying rate curve ($dw(t)/dt$), drying extent curve ($\phi_w(t)$) and film water content curve ($k_w(t)$), with the monitored temperature and relative humidity. (b1-b10) video photos at 30, 270, 380, 400, 490, 540, 610, 1050, 1100 and 2000 min. (c) Drying states from the drying start to the skin layer formation, defined by Gravimetry-Video characterization. (d1) Time-lapse OCT intensity profile, from 0 min to 3856 min. (d2) Time-lapse OCT intensity profile, from 0 min to 300 min. (e) the film thickness (blue line), the packed layer thickness (red line), the initial skin layer thickness (green line), and the coalesced layer's thickness (yellow line) as a function of drying time. (f) Drying states, defined by OCT characterization. Black cross in (b1): OCT scanning spot. Red dotted curves in (b3-b5): horizontal drying boundary. Red dotted line in (d2): packing/suspension boundary. Black dash curve in (e): fitting curve on the thickening process of coalesced layer, due to the coalescence of latex particles below the skin layer during the slow drying process, with the expression of Equation 4.2.

4.3.2 Coalesced layer thickening model

As shown above, the drying process of a thick low-T_g latex film encounters the formation of skin layer. With the particles in skin being coalesced, the particles below the skin continue the film formation process and coalesce into the coalesced layer. It should be noted that the coalesced layer's thickness (h_{coal}) includes the skin thickness (h_{skin}), since both are made of coalesced latex particles. As observed in the OCT profile (Figure 4.1d1), h_{skin} remained almost constant at ~30 μm from 550 min to 1050 min with a simultaneous decrease of drying rate during the same period. As mentioned earlier it should be noted that the skin layer could already exist before 550 min perhaps with a h_{skin} smaller than the OCT resolution (4.5 μm). Beyond 1050 minutes, h_{coal} increased slowly with time, due to the continuous film formation process of latex particles below the skin. At the end of the drying process which takes ~4 days, the entire latex film becomes dried and transparent (not shown in Figure 4.1b). In order to describe or predict the increase of h_{coal} with time, a theoretical model is established using the definition of WVP (Equation 2.18 in Chapter 2) for which the drying rate is inversely proportional to the thickness of dried latex polymer film. For simplicity (as shown in Figure 4.2), the model assumes: 1) the water content in the wet domain (k_w^*) is uniform and constant during the entire coalesced layer thickening process; 2) the coalesced layer has no water and it thickens because of the transformation from wet domain to polymer film near the coalesced layer/wet domain boundary; 3) WVP of coalesced layer do not change with time; 4) h_{coal} starts from 0 when the coalesced layer begins to increase, although before which there could be a thin skin that already exists whose thickness could be ignored relative to the total film thickness (i.e., ~30 μm thick skin layer relative to 1 mm dried film thickness for PEM latex).

First, the drying rate at a specific spot on the latex film is determined by Equation 2.18 (Chapter 2) as:

$$\frac{\partial w}{\partial t} = \frac{\mathrm{WVP} \cdot p_0 \cdot \Delta RH}{h_{coal}(t)} \qquad (4.3)$$

Second, the loss of water mass per unit area (∂w) converts the wet domain to the coalesced layer by:

$$\partial w \cdot \frac{1 - k_w^*}{k_w^*} = \partial h_{coal} \cdot \rho_s \qquad (4.4)$$

Combining Equation 4.3 and 4.4 gives:

$$\frac{h_{coal} \cdot \partial h_{coal}}{\partial t} = \frac{\mathrm{WVP} \cdot p_0 \cdot \Delta RH}{\rho_s k_w^* / (1 - k_w^*)} \qquad (4.5)$$

With the differential equation's boundary condition as $h_{coal}(t_{coal}) = 0$ in which t_{coal} is the point in time at which the coalesced layer just began thickening, Equation 4.5 can be solved as:

$$h_{coal}(t) = A_{coal}(t - t_{coal})^{1/2} = \sqrt{\frac{2\mathrm{WVP} \cdot p_0 \cdot \Delta RH}{\rho_s k_w^* / (1 - k_w^*)}} \cdot (t - t_{coal})^{1/2} \qquad (4.6)$$

with $t \geq t_{coal}$, where A_{coal} is called the "coalesced layer thickening prefactor".

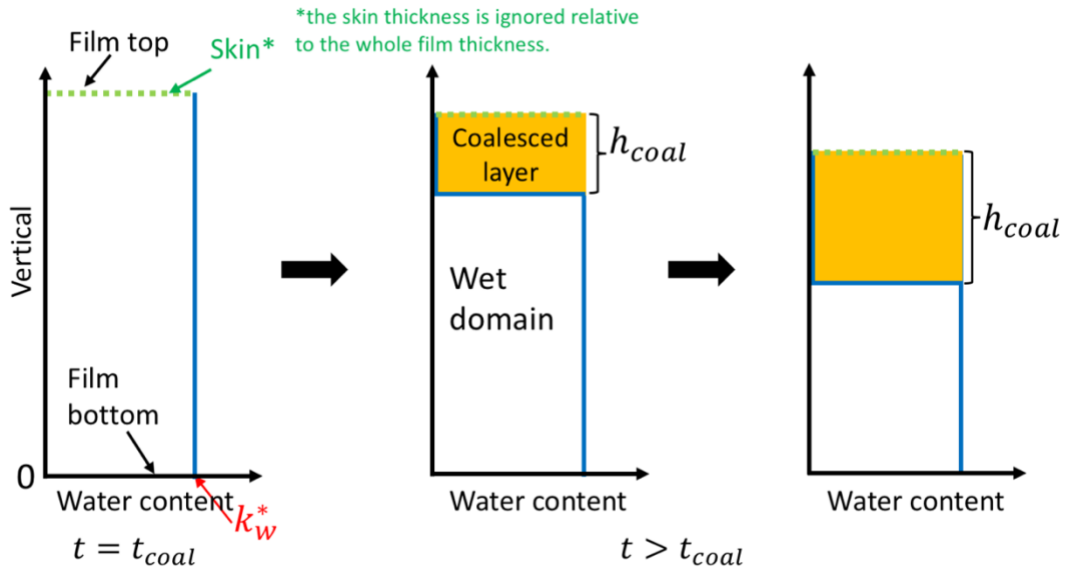

Figure 4.2: Schematic illustration of the coalesced layer thickening model. k_w^* in the figure denotes the value of water content in wet domain below the skin or coalesced layer. In this model, the skin thickness is ignored relative to the whole film thickness (i.e., ~30 μm thick skin relative to 1 mm dried film thickness for PEM latex).

In the case of PEM latex film, Figure 4.1e shows that the coalesced layer thickening model (based on Equation 4.6) can be applied to explain the curve showing the measured coalesced layer thickness (based on Equation 4.2), where the ~30 μm thick skin can be ignored relative to the 1 mm dried film thickness. Based on the curve fitting, $A_{coal} = 12.1\ \mu m/min^{1/2}$, which gives:

$$\frac{\mathrm{WVP} \cdot p_0 \cdot \Delta RH}{\rho_s k_w^* / (1 - k_w^*)} = \frac{A_{coal}^2}{2} = 73\ \frac{\mu m^2}{min} \qquad (4.7)$$

With k_w^* = 7.3% (k_w at 1050 min in Figure 4.1b8), $\rho_s = 1\ g/cm^3$, p_0 and ΔRH (in Equation 4.1) substituted into Equation 4.7, the WVP of coalesced layer can be derived as:

$$\mathrm{WVP} = 73\ \frac{\mu\mathrm{m}^2}{\mathrm{min}} \cdot \frac{\rho_s k_w^* / (1 - k_w^*)}{p_0 \cdot \Delta RH} = 3.4 \times 10^{-11}\ \mathrm{g/(cm \cdot min \cdot Pa)} \qquad (4.8)$$

The derived WVP of coalesced layer is close to both that of the ~30 μm thick skin layer and that of the PEM's dried coalesced latex film.

This coalesced layer thickening model has successfully fitted the increment of PEM's coalesced polymer layer (beyond the 30 μm incipient skin) thickness with time. However, since the water content in the wet domain may not be uniform[1], this model can further be improved with considerations of water distribution and water flux within the wet domain. Equation 4.6 provides some valuable guidance in order to control the increment of coalesced layer's thickness and the film drying time. For instance, in order to shorten the drying time of a latex film, h_{coal} needs to increase faster with time so that the wet domain or the entire film can become dried and transparent earlier. The followings are some approaches that may be considered to achieve the goal based on the parameters included in Equation 4.6.

First, WVP of coalesced layer can be higher. In this way, the drying rate through the skin or coalesced layer becomes faster, so that less time is needed for drying and film formation of the wet domain. Addition of long water-soluble polymer chains or hollow particles may create micro-channels in the polymer matrix to increase the coalesced layer's WVP permanently. Moreover, by increasing the room temperature, the coalesced layer's WVP can be also increased due to the faster mobility of water molecules and the larger free volume of polymer matrix. Second, ΔRH can be higher. After the skin or coalesced layer is formed, the latex film can be placed in an environment with lower humidity, so that the higher vapor gradient from the wet domain to the environment can accelerate water

diffusion through coalesced layer, thus to increase the drying rate. Third, water content in wet domain (k_w^*) can be lower. The less the water is contained in the wet domain, the shorter the time for drying and film formation of the wet domain. This way is more effective, because with a k_w^* close to 0, A_{coal} can be infinitely large (according to Equation 4.6), so that h_{coal} can increase very fast, and thus the entire film can become dried and transparent in a short time. This can be achieved by impeding the coalescence of particles, such as using high-T_g latex and large particle size (which will be discussed in the next section), or using surfactant molecules (which will be studied in Chapter 5). In this way, the maturation of the incipient skin (due to particles' coalescence) can be delayed, so that more water can evaporate freely before the incipient skin becomes a layer with low permeability, leading to lower k_w^*, faster increment of h_{coal} and shorter film drying time.

4.3.3 The effects of latex solids content, polymer T_g and particle size on film drying

Drying curves of PBM1, PBM2, PBM3 and D-PBM2 with different polymer T_g's and particle sizes were measured under the same controlled environment (23 °C and 50% RH in the environmental chamber, see Section 4.2.3). Among them, two samples were made by diluting PBM1 latex with DI water by two and three times, whose drying curves were also measured. The masses of initial latexes in Petri dish were set so that the thicknesses of fully dried latex films (dried film thicknesses) would be 1 mm. With an initial latex thickness of 2 mm and the initial drying rate under this environment, the calculated Pe and $\bar{\lambda}$ of these PBM latexes are listed in Table 4.1. All Pe's are larger than one, so that the vertical packing process occurs for all PBM latexes. $\bar{\lambda}$'s of PBM1 and PBM2 (with T_g more than 20 °C lower than room temperature) are less than one, so that

skin can form readily. $\bar{\lambda}$ of PBM3 (with T_g around room temperature) is higher than one, indicating that particles are so hard that most water evaporates before particles become fully deformed and coalesced; thus, the skin formation is not obvious.

Figure 4.3 shows the film water content curves ($k_w(t)$) of all PBM latexes. In Figure 4.3a, PBM1 latexes with different initial solids contents (k_{s0}) show the same k_w (8%) when the drying rate slowed down with the formation of low-permeable skin. Figures 4.1d1 and f show that the maturation of incipient skin occurs after the "packing process" and "consolidation" states. Since k_{s0} is not related to the water content when all particles become packed, it should not affect the maturation of incipient skin afterwards. In Figure 4.3b, PBM1 and PBM2 show k_w = 8% while PBM3 shows k_w = 4% when the drying rates slowed down. This indicates that, when T_g is more than 20 °C lower than room temperature (for PBM1 and PBM2), the particles on the film top are soft enough to deform and coalesce fast to form a low-permeable skin early, thus T_g in this low T_g range is not affecting the maturation of incipient skin much. On the other hand, when T_g is higher (for PBM3 with T_g near room temperature), the particles on the film top deform and coalesce slower (due to the low mobility of polymer chains), so that a higher T_g causes less water to be contained under the matured skin (or lower k_w^*). The same reason also explains the effect of particle size, shown in Figure 4.3c where D-PBM2 shows k_w = 5% which is less than that of PBM2. The larger the particle size is, the less the compressive stresses are applied on particles, thus the slower the particles' deformation will be, and the less water will be trapped after the skin is matured. Therefore, by using latexes with higher T_g or larger particle size to impede the particles' deformation and coalescence, the maturation of incipient skin can be

delayed, so that k_w^* in the skin thickening model (Equation 4.6) can be lowered, and thus the film drying time can be shortened.

Table 4.1: Initial solids contents (k_{s0}), T_g, particle size, calculated Pe and $\bar{\lambda}$ of PBM1, PBM2, PBM3 and D-PBM2 latexes.

Latex	k_{s0} [a] (%)	T_g [a] (°C)	Particle diameter [a] (nm)	Pe [b]	$\bar{\lambda}$ [b]
PBM1	52.27	-25	189	9.0	4.3×10^{-5}
PBM2	50.61	-3	175	8.4	0.0033
PBM3	51.07	23	187	8.9	14.8
D-PBM2	57.89	0	360	17.2	0.014

[a] measured data abstracted from Figure 2.5 in Chapter 2; the particle diameter is measured by DLS.
[b] calculated based on T_g and particle size[1], using an initial latex thickness of 2 mm and the initial drying rate (7.0×10^{-5} g/(cm^2 · min)) in the environmental chamber (23 °C and 50% RH).

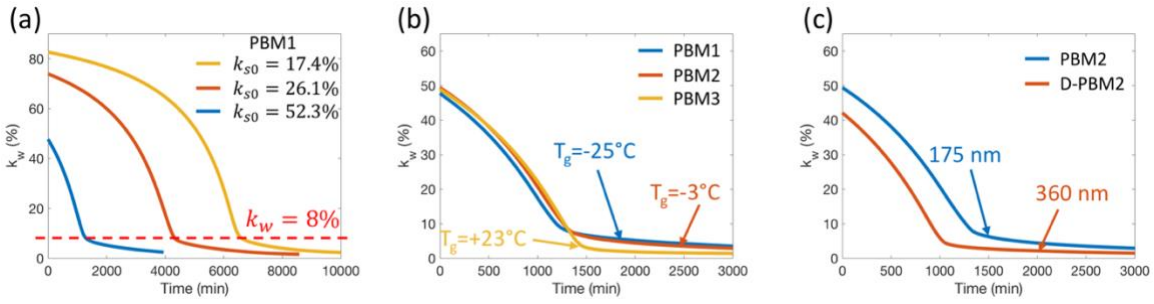

Figure 4.3: Film water content curves ($k_w(t)$) of latexes with 1-mm dried film thicknesses, measured in the environmental chamber (23 °C and 50% RH). (a) PBM1 latexes with varied % solids contents (k_{s0}). (b) PBM1, PBM2, PBM3 with varied T_g's. (c) PBM2 and D-PBM2 with varied particle diameters.

4.4 Conclusions

The drying process and skin layer formation of low-T_g latex system (PEM latex herein) is studied by the OCT-Gravimetry-Video method. OCT, based on the back-scattered light image, shows the particles' packing, the particles' consolidation, the formation of apparent skin layer and the thickening of coalesced latex polymer layer (coalesced layer) in the vertical direction. Gravimetry and video show the formation of grooves, and the propagations of drying boundary and skin layer along the horizontal direction. As demonstrated in Figure 4.4, the whole drying process of low-T_g latex film is generalized into four consecutive stages: Stage I, the latex particles become packed from film top to film bottom (referred to as the "packing" stage); Stage II, the packed particles become further consolidated, by being more densely packed or being distorted (referred to as the "consolidation" stage); Stage III, the particles on the film top form an incipient skin and then coalesce into a low-permeable skin, while the wet domain below the skin layer remains opaque and wet (referred to as the "formation and maturation of incipient skin layer" stage); Stage IV, with further slow drying, more particles in the wet domain become coalesced, and the coalesced layer thickness increases with time until the entire film becomes dried and transparent (referred to as the "thickening of coalesced layer" stage). During Stages I and II, the water evaporates freely through interstices between particles, with the drying rate close to that of DI water. During Stage III, the particles on film top form an incipient skin; with the pressure exerted on particles initially due to the water/air and then due to water/polymer interfacial tensions, the particles begin to coalescence and evolve with time, until the skin becomes matured with low-permeability to water and the drying rate decreases significantly. During Stage IV, the particles below the skin continue

with the film formation process (including consolidation, deformation and coalescence) and add to the thickness of coalesced layer (h_{coal}); h_{coal} increases slowly with the square root of time with further reduction of drying rate, until the entire film becomes dried and transparent.

The "coalesced layer thickening model" (Equation 4.6) is established to describe and predict the increment of h_{coal} with square root of time, as a function of several factors such as the coalesced layer's water vapor permeability (WVP), the environmental humidity and the wet domain's water content (k_w^*). A shorter film drying time can be achieved if the particles in wet domain can finish the film formation process earlier. According to this model, the faster the increment of h_{coal} with time, the earlier the wet domain or the entire film will become dried and transparent. This may be achieved by increasing the coalesced layer's WVP or lowering the environmental humidity, so that faster drying rate through skin makes the drying time of the wet domain shorter. Another approach, which is more effective, is to lower k_w^* when a low-permeable skin is formed, so that it takes less time to dry and to finish the film formation of the wet domain. Drying curves of different latexes show that higher T_g and larger particle size can decrease k_w^*. This indicates that low k_w^* can be realized by impeding the coalescence between particles and thus delaying the maturation of incipient skin, so that more water can evaporate before the particles on film top coalesce into a low-permeable skin. In the next chapter, the effects of surfactants on the drying process of thick low-T_g latex film will be investigated. Presumably, with more surfactant molecules adsorbed on particles' surface (and/or residing at the interstices between particles), the coalescence between particles can be impeded, so that a low k_w^*, a fast increment of h_{coal} and a shorter film drying time would be attained.

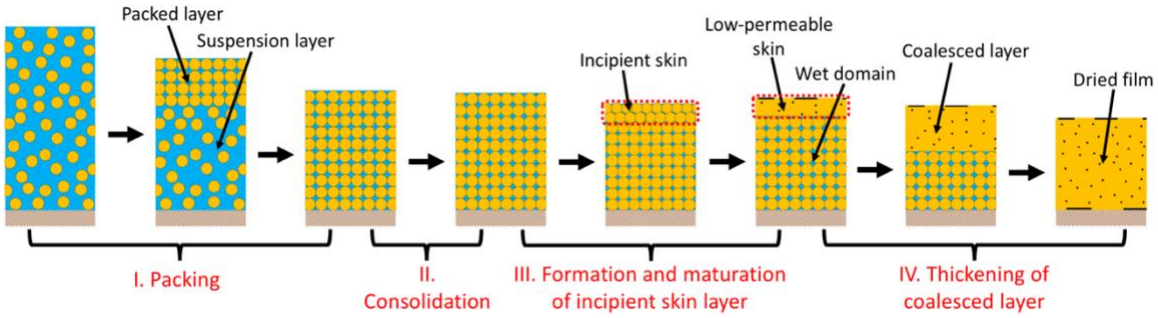

Figure 4.4: Schematic illustration of the drying process of a low-T_g latex film. The black dots and short lines in skin and fully dried film represent surfactant and water-soluble molecules that are trapped in polymer matrix and segregated at film interfaces, the same as shown in Figure 1.1 in Chapter 1.

4.5 References

1. Carter, F. T., Kowalczyk, R. M., Millichamp, I., Chainey, M. & Keddie, J. L. Correlating Particle Deformation with Water Concentration Profiles during Latex Film Formation: Reasons That Softer Latex Films Take Longer to Dry. *Langmuir* **30,** 9672–9681 (2014).
2. Routh, A. F. & Russel, W. B. A Process Model for Latex Film Formation: Limiting Regimes for Individual Driving Forces. *Langmuir* **15,** 7762–7773 (1999).
3. Routh, A. F. & Russel, W. B. A Process Model for Latex Film Formation: Limiting Regimes for Individual Driving Forces. *Langmuir* **17,** 7446–7447 (2001).
4. Okuzono, T., Ozawa, K. & Doi, M. Simple Model of Skin Formation Caused by Solvent Evaporation in Polymer Solutions. *Phys. Rev. Lett.* **97,** (2006).
5. Sheetz, D. P. Formation of films by drying of latex. *J. Appl. Polym. Sci.* **9,** 3759–3773 (1965).
6. Vanderhoff, J. W., Bradford, E. B. & Carrington, W. K. The transport of water through latex films. *J. Polym. Sci. Polym. Symp.* **41,** 155–174 (1973).
7. Routh, A. F. & Russel, W. B. Deformation Mechanisms during Latex Film Formation: Experimental Evidence. *Ind. Eng. Chem. Res.* **40,** 4302–4308 (2001).
8. Simon F., Kunkel S., Oehler H., Lellinger D., Spahn P. & Alig I. Investigation of deformation mechanisms during latex film formation by combination of unilateral NMR and near infrared measurements. *Prog. Org. Coat.* **70,** 230–239 (2011).
9. Erkselius, S., Wadsö, L. & Karlsson, O. J. Drying rate variations of latex dispersions due to salt induced skin formation. *J. Colloid Interface Sci.* **317,** 83–95 (2008).

10. Divry V., Gromer A., Nassar M., Lambour C., Collin D. & Holl Y. Drying Mechanisms in Plasticized Latex Films: Role of Horizontal Drying Fronts. *J. Phys. Chem. B* **120,** 6791–6802 (2016).

11. Saccon FAM, Oliveira FMDR de, Ribas MO, Jr PZ, Muller M & Fabris JL. Kinetics of varnish long-term drying process monitored by a heterogeneous optical sensor system. *Meas. Sci. Technol.* **24,** 094013 (2013).

12. König, A. M., Weerakkody, T. G., Keddie, J. L. & Johannsmann, D. Heterogeneous Drying of Colloidal Polymer Films: Dependence on Added Salt. *Langmuir* **24,** 7580–7589 (2008).

13. Narita, T., Hébraud, P. & Lequeux, F. Effects of the rate of evaporation and film thickness on nonuniform drying of film-forming concentrated colloidal suspensions. *Eur. Phys. J. E* **17,** 69–76 (2005).

14. El-Aasser, M. S. & Robertson, A. A. An ultracentrifugation technique for the study of latex coalescence. *J. Colloid Interface Sci*. **36**, 86–93 (1971).

15. El-Aasser, M. S. & Robertson, A. A. Film formation of latexes. *J. Paint Technol.* **47,** 50–53 (1975).

5 Chapter 5 Effects of Post-Polymerization Added Surfactants on Drying of Thick Films of Model Poly(64EHA/35MMA/1MAA) Latex System

5.1 Introduction

Skin layer formation is one type of drying inhomogeneity in the vertical direction during drying of latex films. In this case, particles on the film top become packed, deformed and coalesced early due to their vicinity of air, thus forming a dried coalesced polymer skin that traps remaining water beneath (in the wet domain). It happens when two conditions are satisfied[1,2]: particles are more densely populated on the film top than those below (Peclet number $Pe > 1$); particles are soft enough so that they deform and coalesce early before all water evaporates ($\bar{\lambda} < 1$). Expressions of Pe and $\bar{\lambda}$ can be found as Equation 1.1 and 1.2 in Chapter 1 (or in Section 4.1 in Chapter 4), lumping together major factors of particle size (diameter, D_p), drying rate (water receding rate, $\dot{E}$), polymer viscosity (η), interfacial tension (γ) and film thickness (the distance between film top and film bottom, H). In addition, the previous chapter (Chapter 4) investigated the kinetic processes of skin layer formation and latex film formation, answering the following three questions: (i) when does the incipient skin becomes matured (or latex particles on the film top become coalesced into a low-permeable skin)? (ii) how does the thickness of coalesced latex polymer layer (coalesced layer) evolve with time? And (iii) to what extent can the drying rate be inhibited by skin and coalesced layer? The OCT-Gravimetry-Video characterizations of the model Poly(64EHA/35MMA/1MAA) latex (PEM latex), which is dried under room condition, demonstrate that: 1) the formation and maturation of incipient

skin layer (Stage III) occurs after latex particles experience the stages of packing (Stage I, where particles' Brownian motions are restricted due to mutual contact) and consolidation (Stage II, where particles become more densely packed or distorted); 2) while drying through skin goes on, latex particles in the wet domain continue the film formation process and add to the coalesced layer's thickness (h_{coal}, which includes the skin layer thickness), until the entire film becomes transparent and dried (Stage IV); 3) the drying rates during Stages I and II are fast and close to free water evaporation, while those during Stages III and IV are slow and limited by the water vapor permeability (WVP) and the thickness of skin and coalesced layer. The WVP of skin and coalesced layer was found to be similar to that of the fully dried coalesced latex film, and the layer was elastic and in-disintegrable, confirming that the skin and coalesced layer was actually a coalesced polymer film. The "coalesced layer thickening model" was developed to describe the h_{coal} increment as a function of time, given as Equation 4.6 (Chapter 4):

$$h_{coal}(t) = A_{coal}(t - t_{coal})^{1/2} = \sqrt{\frac{2\mathrm{WVP} \cdot p_0 \cdot \Delta RH}{\rho_s k_w^* / (1 - k_w^*)}} \cdot (t - t_{coal})^{1/2} \qquad (5.1)$$

where A_{coal} is the "coalesced layer thickening prefactor", t_{coal} is the point in time when the coalesced layer begins to increase, t is the time from the start of drying (in this model, $t \geq t_{coal}$), p_0 is the equilibrium vapor pressure at room temperature, ΔRH is the difference of relative humidity between the wet domain and air, ρ_s is the density of solid (mainly polymer) and approximately equal to water (1 g/cm^3), and k_w^* is the water content (weight percentage of water) in the wet domain. The film is presumably totally dried when h_{coal}

increases until latex particles in the wet domain complete the film formation process with the entire film becoming transparent.

In Chapter 4, the drying time of latex film with relatively low T_g (more than 20 °C below room temperature) has been shown to be much longer than that with relatively high T_g (near or slightly higher than room temperature), due to skin layer formation. The long drying time is usually not acceptable in coating applications, especially for thick latex films (with film thickness in millimeter range) for which more than 10% of water can be trapped below the skin and coalesced layer. As mentioned in Section 4.1 in Chapter 4, the model PEM latex (discussed in this chapter) and the commercial PLB latex (to be discussed in Chapter 6) with an initial wet thickness of 2 mm take >4 days and >12 days to get 95% of water evaporated, respectively. One reason is that, with a larger film thickness, Pe becomes larger and $\bar{\lambda}$ becomes smaller, which promote the formation of skin. Another reason, more importantly, is that a thicker film contains more water per drying area, leading to more water trapped in the wet domain after the skin becomes matured and low-permeable (or higher k_w^*). According to the coalesced layer thickening model (Equation 5.1 or Equation 4.6 in Chapter 4), a higher k_w^* makes A_{coal} smaller, thus h_{coal} increases slower with time, which takes longer time for the entire film to become transparent and dried. Therefore, in order to shorten the drying time of thick latex film, one effective way is to make k_w^* lower, so that h_{coal} increases faster with time and less time is needed for the drying and film formation of latex particles in the wet domain.

As proposed in Section 4.3.2 (Chapter 4), by impeding the coalescence between particles, more water can evaporate freely through the boundaries between non-coalesced particles in the incipient skin before they coalesce into a low-permeable matured skin, so

that k_w^* becomes lower and h_{coal} increases faster. Gravimetric measurements[3,4] showed that extra surfactant added in the latex after emulsion polymerization (post-added surfactant) shortened the film drying time, which was supposedly related to the more coverage of the latex particles' surface by surfactant molecules leading to higher colloidal stability of the latex. However, their explanations were rather qualitative and inadequate. Other studies using AFM profiling[5] and Förster resonance energy transfer (FRET)[6] showed that the extra surfactant adsorbed on particles' surface could act as a "barrier" in impeding the coalescence of latex particles. Such "barrier" should be related to the repulsive potential energy or force between particles that has to be overridden in order to initiate the particles' coalescence[7]. Therefore, as proposed in this dissertation, there should be a strong correlation between the surfactant coverage on the particles' surface, and the delay of particles' coalescence and film drying time.

This chapter mainly studies the effects of post-added surfactants on the drying process of the model PEM (poly(64EHA/35MMA/1MAA)) latex system. The surfactants used are sodium lauryl sulfate (SLS) and Triton X-100 (TTX), which represent an ionic and a non-ionic surfactants, respectively. First, the OCT-Gravimetry-Video method is used to monitor the drying process of latex films under room condition. The increment of h_{coal} with time (measured by OCT profile) is correlated with the water content in wet domain (k_w^*, measured by gravimetry) via Equation 5.1, which can be affected by the amount of post-added surfactant. Second, drying curves of PEM latex films with and without post-added surfactants are measured in a controlled environment (23 ℃ and 50% RH without wind). The same drying environment ensures that the difference between different drying curves are solely caused by the post-added surfactant, excluding the variations caused by

temperature or humidity. The coalescence delay time (Δt_{del}) is then defined based on the difference of film water contents when drying rates become close to zero (i.e. when skin is matured). Third, the distributions of surfactant molecules in the latex (either adsorbed on particles' surface or soluble in water) are modeled based on the measured surfactant adsorption isotherm curves. It would be valuable to correlate the percentage of particles' surface coverage by surfactant molecules (SC_{sur}) with Δt_{del}. Finally, concerning the water resistance of dried film for coating applications, the water absorptions of dried films with and without post-added surfactants are measured and compared.

5.2 Materials and experimental methods

5.2.1 Model PEM latex system, calculations of % of particles' surface coverages by chemically bound carboxyl groups (SC_{carb}) and sulfate groups (SC_{sulf}), and an estimate of MAA-based oligomers in the aqueous phase.

This chapter uses the model PEM (poly(64EHA/35MMA/1MAA)) latex to investigate the effects of surfactants on the drying process and the skin layer formation of low-T_g latex. According to Tables 2.4 and 2.5 in Chapter 2, PEM latex has T_g as -19 °C, particle diameter (D_p, measured by DLS) as 176 nm and the WVP of dried latex film as $(4.0 \pm 0.3) \times 10^{-11}$ g/(cm · min · Pa). The initial % solids content (k_{s0}) of PEM latex used in this chapter can be 49.94% or 50.37% due to the different synthesis batch. The density of solid (mostly polymer) is 1.03 g/cm^3, which is close to but slightly heavier than water; in the calculations, it is set about the same as water ($\rho = \rho_s = \rho_w = 1$ g/cm^3) (see Section 2.3.1.2 in Chapter 2). The carboxyl groups and the sulfate groups that are

chemically bound to particles' surface have the number densities of 0.942/nm^2 (φ_{carb}) and 0.181/nm^2 (φ_{sulf}), respectively. Considering their molecular areas (0.017 nm^2 for -COOH and 0.032 nm^2 for -SO_4^-, calculated based on the interatomic bond lengths[15]), the % of particles' surface coverages (SC) by carboxyl groups and sulfate groups are calculated as:

$$SC_{carb} = \varphi_{carb} \cdot 0.017\ \text{nm}^2 = 1.6\% \quad (5.2)$$

$$SC_{sulf} = \varphi_{sulf} \cdot 0.032\ \text{nm}^2 = 0.6\% \quad (5.3)$$

According to the synthesis recipe of PEM latex (Table 2.1 in Chapter 2), the major compositions include the polymer particles (~49 wt%), the water (~50 wt%), the SLS surfactant (~0.25 wt%) and the Na_2CO_3 salt (~0.20 wt%). In the latex system of poly(EHA/MAA) with SLS surfactant, it was found that only 2% of all carboxyl groups (coming from MAA) were in the form of low molecular weight water-soluble oligomers in the aqueous phase, while 98% were either bound on particles' surface or buried inside the particles[21]. Thus, in the PEM latex of poly(64EHA/35MMA/1MAA) with 0.50 wt% MAA composition in the latex (see Table 2.1 in Chapter 2), it can be estimated that 2% of MAA resides in the aqueous phase in the form of water-soluble oligomers; 46% of MAA is bound on particles' surface (according to the conductometric titration measurement in Section 2.3.2 in Chapter 2); the remaining 52% of MAA is buried inside particles. Therefore, it is estimated that in the PEM latex, 38.7 mM Na_2CO_3 and 2.4 mM MAA-based oligomers (corresponding to 2% of MAA) are dissolved in the aqueous phase.

5.2.2 Surfactant adsorption isotherms of SLS and TTX in the PEM latex system

The ionic and non-ionic surfactants used in this chapter are sodium lauryl sulfate (SLS) from Alfa Aesar and Triton X-100 (TTX) from Sigma-Aldrich, respectively. SLS is a sulfuric acid n-dodecyl ester salt, with a surfactant molecular weight (M_{sur}) of 288 g/mol. Triton X-100 is a t-octylphenoxy polyethoxy ethanol, with a molecular structure of $(CH_3)_3C\text{-}CH_2\text{-}(CH_3)_2C\text{-}C_6H_4\text{-}(OCH_2CH_2)_{9\text{-}10}\text{-}OH$ and M_{sur} = 625 g/mol. Both SLS and TTX molecules have aliphatic tails which are hydrophobic. However, their hydrophilic heads are different – ionic sulfate group ($-SO_4^-$) for SLS and non-ionic ethoxylate group ($-(OCH_2CH_2)_{9-10}-OH$) for TTX. Each one of these surfactants will have its own equilibrium distributions between surfactant molecules adsorbed on the latex particles' surface and surfactant molecules soluble in the aqueous phase (serum).

The surfactant adsorption isotherm curves of SLS and TTX surfactant on the PEM latex particles, i.e. the equilibrium distribution of surfactant number density on the particles' surface ($\varphi_{sur,p}$) as a function of surfactant concentration in the aqueous phase or serum ($c_{sur,aq}$), are determined by measuring the surface tensions of the 5x diluted PEM latex and its serum with different amounts of added surfactant, following the same procedures as documented in Section 2.3.3 in Chapter 2, and Figure 2.4 for the SLS adsorption isotherms on PEM. Figure 5.1 shows similar data processes used to derive the isotherm curves of TTX surfactant.

First, the surface tensions of both latex and serum were measured with the added concentrations of non-ionic surfactant TTX (Figure 5.1A); second, the surface tension curves were adjusted to start and end at the same respective tension values (Figure 5.1B); third, the surfactant adsorption isotherm curve (Figure 5.1C) was determined following

Equations 2.11 – 17 (Chapter 2). Note that the SLS isotherm curve (Figure 2.4C) includes both the post-added SLS and the original SLS in the PEM latex; the TTX isotherm curve (Figure 5.1C) includes only the post-added TTX, since there was no TTX in the PEM latex. Both adsorption isotherm curves have the same expression as (see Equation 2.17 in Chapter 2):

$$\varphi_{sur,p}\left(c_{sur,aq}\right) = \begin{cases} \tilde{\varphi}_{sur} c_{sur,aq}, & 0 < c_{sur,aq} \leq CMC_{serum} \\ \varphi_{sur,p,max}, & c_{sur,aq} > CMC_{serum} \end{cases} \quad (5.4)$$

where $\tilde{\varphi}_{sur}$ is the slope of $\varphi_{sur,p}$ vs. $c_{sur,aq}$ (see Figure 5.1C – the increment of $\varphi_{sur,p}$ for every mM increment of $c_{sur,aq}$), CMC_{serum} is the critical micelle concentration of surfactant in the serum, and $\varphi_{sur,p,max}$ is the maximum number density of surfactant molecules adsorbed on the latex particles' surface (100% surface coverage for the PEM latex particles 5x diluted relative to the original PEM latex as prepared) . The subscripts of "sur" can be "SLS" or "TTX" to represent the SLS or TTX surfactants, respectively. For SLS in the PEM latex, $\tilde{\varphi}_{SLS} = 0.401\ \mathrm{nm^{-2}/mM}$, $CMC_{serum} = 2.93\ \mathrm{mM}$, and $\varphi_{SLS,p,max} = 1.175\ \mathrm{nm^{-2}}$; for TTX in the PEM latex, $\tilde{\varphi}_{TTX} = 14.1\ \mathrm{nm^{-2}/mM}$, $CMC_{serum} = 0.0436\ \mathrm{mM}$, and $\varphi_{TTX,p,max} = 0.614\ \mathrm{nm^{-2}}$. It should be noted that, for the PEM latex with post-added TTX, TTX molecules with a higher adsorption energy could displace the existent SLS molecules on particles' surface[16]; moreover, TTX molecules may also form surfactant complexes with SLS molecules that alter the adsorption isotherm of surfactant mixture[17]. However, when calculating the % particles' surface coverage by the surfactant molecules and the surfactant distributions, such two effects are not taken into

account and it assumes that SLS and TTX get adsorbed on the particles' surface independently.

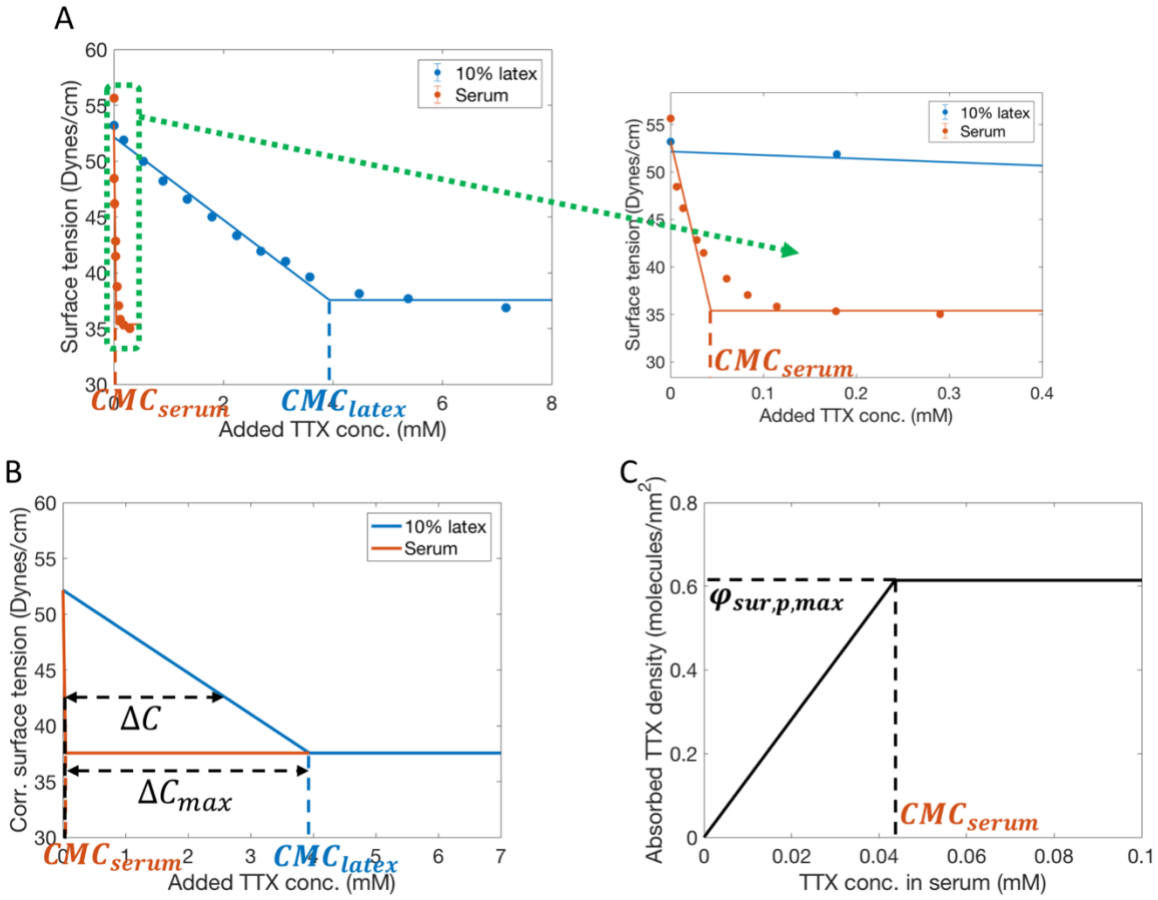

Figure 5.1: (A) measured surface tension curves of 5x diluted PEM latex and its serum – surface tensions as a function of added TTX concentrations (based on the aqueous phase). Since the TTX concentration in serum is very low (CMC < 0.1 mM), the horizontal axis is expanded so that the change of serum's surface tension versus the added TTX concentration can be clearly shown in the figure next to (A). (B) modified surface tension curves of 5x diluted PEM latex and its serum. (C) TTX adsorption isotherm curve of the PEM latex system, given as $\varphi_{sur,p}$ (molecules/nm^2) vs. $c_{sur,aq}$ (TTX concentration in the aqueous phase or serum).

5.2.3 PEM latex systems with post-added anionic and nonionic surfactants (SLS and TTX)

This chapter investigates the drying processes of latexes with different concentrations of SLS and TTX that impart different % surfactant coverages on the PEM latex particles' surface. The series of latex systems with post-added SLS (denoted as "PEM+SLS" latexes) and post-added TTX (denoted as "PEM+TTX" latexes) were prepared as follows. First, 20 wt% surfactant aqueous solutions were prepared. Second, based on the solid weight in the PEM latex, different amounts of surfactant solutions were mixed with the PEM latex to obtain different weight ratios of surfactant versus PEM solids ($k_{sur/s}$); at the same time, the latex solids contents (k_{s0}) decreased slightly due to water from the added surfactant solution. The subscripts of "sur" of $k_{sur/s}$ can be "SLS" or "TTX" to represent the SLS or TTX surfactants, respectively.

By adding SLS (or TTX) with 1 wt% relative to the PEM's solids, the obtained latex is named as "PEM+1%SLS (or TTX)". Thus, the PEM+SLS latex series used in this chapter are PEM+0.1%SLS, PEM+0.3%SLS, PEM+0.5%SLS, PEM+1%SLS and PEM+2%SLS; the PEM+TTX latex series include PEM+0.5%TTX, PEM+1%TTX and PEM+2%TTX. It should be noted that the original PEM latex has SLS with $k_{SLS/s}$ = 0.5% (see the synthesis recipe given by Table 2.1 in Chapter 2), while with $k_{TTX/s}$ = 0. For a particular latex with known k_{s0} and $k_{sur/s}$ as well as known water density (ρ_w) and surfactant molecular weight (M_{sur}), the weight percentage (based on latex) and concentration (in mM based on aqueous phase) of surfactant are calculated as:

$$Surfactant\ weight\ percentage\ (based\ on\ latex) = k_{sur/s} \cdot k_{s0} \qquad (5.5)$$

$$Surfactant\ concentration\ (based\ on\ aqueous\ phase) = \frac{k_{sur/s} \cdot k_{s0} \cdot \rho_w}{M_{sur}(1 - k_{s0})} \qquad (5.6)$$

In Table 5.1, k_{s0} 's, $k_{sur/s}$'s (including both $k_{SLS/s}$ and $k_{TTX/s}$), surfactant weight percentages and surfactant concentrations (including both SLS and TTX) of all PEM, PEM+SLS and PEM+TTX latexes are listed.

Table 5.1: PEM latex systems with post-added anionic (SLS) and non-ionic (TTX) surfactants

Latex	k_{s0} (%)	$k_{SLS/s}$ (%)	SLS weight perc. (%)[b]	SLS conc. (mM)[c]	$k_{TTX/s}$ (%)	TTX weight perc. (%)	TTX conc. (mM)[c]
PEM	49.94[a]	0.5[d]	0.25	17.3	0	0	0
PEM+0.1%SLS	49.87	0.6	0.30	20.7	0	0	0
PEM+0.3%SLS	49.72	0.8	0.40	27.4	0	0	0
PEM+0.5%SLS	49.58	1	0.50	34.1	0	0	0
PEM+1%SLS	49.22	1.5	0.74	50.4	0	0	0
PEM+2%SLS	48.52	2.5	1.21	81.7	0	0	0
PEM	50.37[a]	0.5[d]	0.25	17.6	0	0	0
PEM+0.5%TTX	50.00	0.5	0.25	17.6	0.5	0.25	8.0
PEM+1%TTX	49.63	0.5	0.25	17.6	1	0.50	15.8
PEM+2%TTX	48.92	0.5	0.25	17.6	2	0.98	30.6

[a] These two batches of PEM latexes differ by about 0.4% in their original solids (k_{s0}), even though they were synthesized by the same recipe (Table 2.1 in Chapter 2).
[b] Weight percentage based on the original PEM latex.
[c] Concentrations are given in mM based on the aqueous phase.
[d] The weight ratio of the surfactant versus the solids in the original PEM latex is $k_{SLS/s}$ = 0.5% (see the synthesis recipe given by Table 2.1 in Chapter 2).

5.2.4 Prediction of surfactant distributions between particles' surface and aqueous phase, and calculation of % surfactant surface coverages (SC_{sur}) at the start and in the middle of drying of PEM latex film

For a latex with known particle diameter (D_p), densities of polymer, water and latex (ρ_s, ρ_w and ρ, respectively), and the surfactant molecular weight (M_{sur}), then the surfactant number density adsorbed on latex particles' surface ($\varphi_{sur,p}$, number of surfactant molecules per nm^2 on particles' surface), the % surfactant surface coverage (SC_{sur} , percentage of particles' surface covered by surfactant molecules), the surfactant concentration in aqueous phase ($c_{sur,aq}$) and the partition coefficient (K_D, the molar amount ratio of surfactant molecules on particles' surface versus those in aqueous phase) can be determined as a function of latex % solids (k_{s0}) and wt% ratio of surfactant versus latex solids ($k_{sur/s}$), based on the surfactant adsorption isotherm curve (Equation 5.4). The subscripts of "sur" of φ_{sur}, c_{sur} and $k_{sur/s}$ can be "SLS" or "TTX" to represent the SLS or TTX surfactants, respectively.

With an aqueous volume of V_w in latex, the total surface area of latex particles is calculated as (according to Equation 2.13 in Chapter 2):

$$A_p = \frac{6\rho_w V_w k_{s0}}{\rho_s D_p (1 - k_{s0})} \qquad (5.7)$$

The total mole amount of surfactant in the latex is:

$$n_{sur} = \frac{\rho_w V_w k_{s0} k_{sur/s}}{(1 - k_{s0}) M_{sur}} \quad (5.8)$$

In order to derive $\varphi_{sur,p}$ and $c_{sur,aq}$ for the specific latex system with k_{s0} and $k_{sur/s}$, two cases are considered: I) $0 < c_{sur,aq} \leq CMC_{serum}$ and 2) $c_{sur,aq} > CMC_{serum}$.

I) $0 < c_{sur,aq} \leq CMC_{serum}$

In this case, the mole amount of surfactant adsorbed on particles' surface is $n_{sur,p} = \tilde{\varphi}_{sur} c_{sur,aq} A_p / N_A$ and that of surfactant soluble in aqueous phase is $n_{sur,aq} = c_{sur,aq} V_w$. Then, the partition coefficient (K_D) is given as:

$$K_D = \frac{n_{sur,p}}{n_{sur,aq}} = \frac{\tilde{\varphi}_{sur} A_p}{N_A V_w} \quad (5.9)$$

With the total amount of surfactant (Equation 5.8), $c_{sur,aq}$ can be derived as:

$$c_{sur,aq} = \frac{n_{sur}}{V_w (K_D + 1)} \quad (5.10)$$

And $\varphi_{sur,p}$ becomes:

$$\varphi_{sur,p} = \tilde{\varphi}_{sur} c_{sur,aq} = \frac{\tilde{\varphi}_{sur} n_{sur}}{V_w (K_D + 1)} \quad (5.11)$$

Combining Equation 5.4 and Equations 5.7 – 11 gives:

$$c_{sur,aq}\left(k_{s0}, k_{sur/s}\right) = \frac{\rho_s \rho_w N_A D_p}{M_{sur}} \cdot \frac{k_{s0} k_{sur/s}}{6\rho_w \tilde{\varphi}_{sur} k_{s0} + \rho_s N_A D_p (1 - k_{s0})} \quad (5.12)$$

and

$$\varphi_{sur,p}\left(k_{s0}, k_{sur/s}\right) = \tilde{\varphi}_{sur} \cdot c_{sur,aq}\left(k_{s0}, k_{sur/s}\right) \quad (5.13)$$

II) $c_{sur,aq} > CMC_{serum}$

In this case, the amount of surfactant adsorbed on particles' surface reaches the maximum coverage with $n_{sur,p} = \varphi_{sur,p,max} A_p / N_A$, while the remaining surfactant is in aqueous phase which exceeds CMC. With the total amount of surfactant (Equation 5.8), $c_{sur,aq}$ can be derived as:

$$c_{sur,aq} = \frac{n_{sur} - \varphi_{sur,p,max} A_p / N_A}{V_w} \quad (5.14)$$

Substituting Equations 5.7 and 5.8 into Equation 5.14 gives:

$$c_{sur,aq}\left(k_{s0}, k_{sur/s}\right) = \frac{\rho_w k_{s0}}{1 - k_{s0}} \cdot \left(\frac{k_{sur/s}}{M_{sur}} - \frac{6\varphi_{sur,p,max}}{\rho_s D_p N_A} \right) \quad (5.15)$$

and

$$\varphi_{sur,p}(k_{s0}, k_{sur/s}) = \varphi_{sur,p,max} \quad (5.16)$$

Finally, based on the $c_{sur,aq}$ and $\varphi_{sur,p}$ determined in these two cases, the partition coefficient (K_D) is derived as:

$$K_D(k_{s0}, k_{sur/s}) = \frac{\varphi_{sur,p} A_p}{N_A c_{sur,aq} V_w} = \frac{\varphi_{sur,p}}{c_{sur,aq}} \cdot \frac{6\rho_w k_{s0}}{\rho_s D_p (1 - k_{s0}) N_A} \quad (5.17)$$

In the calculations, the first step is to use Equation 5.12 to get a temporary value as $c_{sur,aq,temp}$. If $c_{sur,aq,temp} \leq CMC_{serum}$, then $c_{sur,aq} = c_{sur,aq,temp}$ and $\varphi_{sur,p} = \tilde{\varphi}_{sur} c_{sur,aq}$; if $c_{sur,aq,temp} > CMC_{serum}$, then $c_{sur,aq}$ is calculated by Equation 5.15, and $\varphi_{sur,p} = \varphi_{sur,p,max}$. After $c_{sur,aq}$ and $\varphi_{sur,p}$ are determined, K_D is calculated by Equation 5.17. The % of particles' surface coverage by surfactant molecules (SC_{sur}) is given as:

$$SC_{sur}(k_{s0}, k_{sur/s}) = \frac{\varphi_{sur,p}(k_{s0}, k_{sur/s})}{\varphi_{sur,p,max}} \quad (5.18)$$

where the subscripts of "sur" can be "SLS" or "TTX" to represent the SLS or TTX surfactant, respectively. Examples of sample calculations of the % surfactant surface coverages (SC) of PEM, PEM+1%SLS and PEM+1%TTX latexes are demonstrated in Appendix I.

Equations 5.12, 5.13, 5.15, 5.16, 5.17 and 5.18 show the determinations of $c_{sur,aq}$, $\varphi_{sur,p}$, K_D and SC_{sur} as a function of k_{s0} and $k_{sur/s}$ regarding a specific latex system. In

the middle of drying before latex particles contact each other (or before the % solids content k_s reaches 64% corresponding to closely random packing), $c_{sur,aq}$, $\varphi_{sur,p}$, K_D and SC_{sur} can be also obtained simply by replacing k_{s0} with the solids content at a time during drying (k_s) in the above equations, given the fact that surfactant molecules redistribute much faster (in seconds[8]) than the water volume change due to evaporation (in hundreds of minutes herein). It should be noted that, after the latex particles become packed, the pressure applied on particles compresses the contact area between adjacent particles and some of the surfactant molecules begin to desorb from particles' surface and migrate to the interstices between the packed particles, or to the surface and/or the bottom of the drying latex film. Thus, this model prediction only applies before the packing of particles takes place. The results of $c_{sur,aq}$, $\varphi_{sur,p}$, K_D and SC_{sur} at the start of drying with the initial % solids in the latex film (k_{s0}) and those at a time when k_s = 64% are reported in Table 5.2.

Interestingly, in Table 5.2, except for the PEM+2%SLS latex with SLS reaching $\varphi_{sur,max}$, all the other latex systems with surfactants not reaching $\varphi_{sur,p,max}$ show almost constant $c_{sur,aq}$'s and $\varphi_{sur,p}$'s (as well as constant SC_{sur}'s) during drying from the start of drying with k_{s0} = 50% to the time when k_s = 64% (closely random packing), as given in Table 5.2. The reason is that: in the initial latex containing either SLS or TTX, almost all of the surfactant molecules are adsorbed on particles' surface (K_D = ~22 for SLS and ~780 for TTX at the start of drying). With the decrease in the water volume during drying before latex particles are packed, the surfactant molecules redistribute very fast (in seconds[8]), so that the surfactant molecules in aqueous phase continue to adsorb onto the particles' surface. Since almost all of the surfactant molecules in the latex are adsorbed on particles' surface (K_D = ~22 for SLS and ~780 for TTX at the start of drying), $\varphi_{sur,p}$ or SC_{sur} should not

change much, even with the continuous adsorption of molecules from aqueous phase to particles' surface; and $c_{sur,aq}$ is also almost constant according to the surfactant adsorption isotherm (Equation 5.4). As for the PEM+2%SLS latex with the SLS reaching $\varphi_{sur,p,max}$, the $c_{sur,aq}$ increases with time while $\varphi_{sur,p}$ remain constant at $\varphi_{sur,p,max}$, since the surfactant molecules in aqueous phase cannot adsorb on particles' surface (which are already saturated) during drying. In Section 5.3.2, the % of particles' surface coverage by surfactant molecules SC_{sur}'s in the initial latex will be used to correlate with the measured coalescence delay time (Δt_{del}).

Table 5.2: Surfactant distributions of both SLS and TTX at the start of drying or initial latex (A) and at the time when the film's solids content reaches 64% at closely random packing (B). Results include the number density of surfactant adsorbed on particles' surface ($\varphi_{sur,p}$), the concentration of surfactant in aqueous phase ($c_{sur,aq}$), the partition coefficients (K_D) and the % surface coverage of surfactant (SC_{sur}, including SC_{SLS} and SC_{TTX}) for PEM, PEM+SLS and PEM+TTX latexes.

A. At the start of drying (initial latex with k_{s0})

Latex[a]	SLS surfactant				TTX surfactant			
	$\varphi_{SLS,p}$ (1/nm^2)	$c_{SLS,aq}$ (mM)	K_D	SC_{SLS} (%)	$\varphi_{TTX,p}$ (1/nm^2)	$c_{TTX,aq}$ (mM)	K_D	SC_{TTX} (%)
PEM	0.29	0.73	23.0	25.0	0	0	/	0
PEM+0.1%SLS	0.35	0.88	22.6	30.0	0	0	/	0
PEM+0.3%SLS	0.47	1.17	22.4	39.9	0	0	/	0
PEM+0.5%SLS	0.59	1.46	22.3	49.9	0	0	/	0
PEM+1%SLS	0.88	2.19	22.0	74.8	0	0	/	0
PEM+2%SLS[b]	1.17	19.0	3.3	100.0	0	0	/	0
PEM	0.29	0.73	23.0	25.0	0	0	/	0
PEM+0.5%TTX	0.29	0.73	23.0	25.0	0.14	0.01	796.8	23.0
PEM+1%STTX	0.29	0.73	23.0	25.0	0.28	0.02	785.1	46.0
PEM+2%TTX[c]	0.29	0.73	23.0	25.0	0.56	0.04	763.1	91.9

B. In the middle of drying when k_s = 64% (closely random packing)

Latex[a]	SLS surfactant				TTX surfactant			
	$\varphi_{SLS,p}$ (1/nm^2)	$c_{SLS,aq}$ (mM)	K_D	SC_{SLS} (%)	$\varphi_{TTX,p}$ (1/nm^2)	$c_{TTX,aq}$ (mM)	K_D	SC_{TTX} (%)
PEM	0.30	0.75	40.4	25.4	0	0	/	0
PEM+0.1%SLS	0.36	0.89	40.4	30.5	0	0	/	0
PEM+0.3%SLS	0.48	1.19	40.4	40.7	0	0	/	0
PEM+0.5%SLS	0.60	1.49	40.4	50.9	0	0	/	0
PEM+1%SLS	0.90	2.24	40.4	76.3	0	0	/	0
PEM+2%SLS[b]	1.17	35.9	3.3	100	0	0	/	0
PEM	0.30	0.75	40.4	25.4	0	0	/	0
PEM+0.5%TTX	0.30	0.75	40.4	25.4	0.14	0.01	1417	23.0
PEM+1%STTX	0.30	0.75	40.4	25.4	0.28	0.02	1417	46.0
PEM+2%TTX[c]	0.30	0.75	40.4	25.4	0.56	0.04	1417	92.0

[a] The weight percentages and concentrations of SLS and TTX surfactants in these latexes can be found in Table 5.1.

[b] The amount of total SLS in PEM+2%SLS latex is already more than that is needed to reach the maximum surface coverage (SC_{SLS} = 100%); the extra surfactant molecules remain in the aqueous phase in the form of micelles.

[c] The total surface coverage of both SLS and TTX ($SC_{SLS} + SC_{TTX}$) is 117% which exceeds 100%, due to the formation of surfactant complexes caused by the interactions between SLS and TTX molecules[17].

5.2.5 Calculations of average inter-distance of separation between particles (d_{in}) in the initial PEM latex system and during drying of PEM latex film

The inter-distance between particle's surfaces is defined as the gap between the surfaces of two adjacent latex particles. To calculate the average inter-distance (d_{in}), particles with diameter of D_p are assumed regularly arranged in the face-centered cubic (FCC) lattices[18], although in reality particles are arranged randomly in space. On average, one cubic unit of FCC lattice is comprised of four particles with a cubic length of $\sqrt{2}(D_p + d_{in})$. With known densities of polymer and latex (ρ_s and ρ, respectively), the solids content of one unit of FCC lattice is given as:

$$k_{FCC} = \frac{4 \cdot \frac{\pi D_p^3}{6} \cdot \rho_s}{\left(\sqrt{2}(D_p + d_{in})\right)^3 \cdot \rho} = \frac{\pi D_p^3 \rho_s}{3\sqrt{2}(D_p + d_{in})^3 \rho} \qquad (5.19)$$

The ratio of the average inter-distance versus the particle diameter (d_{in}/D_p) is then derived as:

$$d_{in}/D_p = \left(\frac{\pi \rho_s}{3\sqrt{2} k_{FCC} \rho}\right)^{1/3} - 1 \qquad (5.20)$$

Table 5.3 shows the calculated d_{in} and d_{in}/D_p of the PEM latex at the start of drying with the initial % solids in the latex film ($k_{FCC} = k_{s0}$) and those at a time when $k_{FCC} = k_s$ = 64%. Moreover, d_{in} is compared with the molecular length of SLS (l_{SLS} = ~1.5 nm)[19] with the values of d_{in}/l_{SLS} listed in Table 5.3. It should be noted that, at the time when k_s = 64%,

although d_{in} = 8.8 nm based on the FCC lattice, the reality is that particles contact each other by closely random packing.

Table 5.3: Average inter-distances (d_{in}) of separation between PEM latex particles' surface at the start of drying when the % solids content (k_s) is k_{s0} = 50% and at a time when k_s = 64% (closely random packing). The ratios of d_{in} versus particle diameter (D_p) and those of d_{in} versus SLS molecule length (l_{SLS}) are also included.

Latex	D_p (nm)	$k_{FCC} = k_{s0}$ = 50% (initial latex)			$k_{FCC} = k_s$ = 64% (closely random packing)		
		d_{in}/D_p	d_{in} (nm)	d_{in}/l_{SLS} [a]	d_{in}/D_p	d_{in} (nm)	d_{in}/l_{SLS} [a]
PEM	176	0.140	24.6	16.4	0.050	8.8 [b]	5.8

[a] The molecular length of SLS surfactant[19] is about 1.5 nm.
[b] At the time when k_s = 64%, although d_{in} = 8.8 nm based on the FCC lattice, particles (which are closely randomly packed) should be in close contact with each other.

5.2.6 OCT-Gravimetry-Video method

The OCT-Gravimetry-Video method was used to monitor and characterize the drying processes of PEM latex films with post-added surfactants. The same procedure documented in Section 4.2.2 (Chapter 4) was followed, which was also used to investigate the drying process of PEM latex in Chapter 4. In the OCT profile, the processes of particles' packing, consolidation, skin layer formation and coalesced layer thickening are visualized. The "film thickness", the "packed layer thickness", the "skin layer thickness" (h_{skin}) and the "coalesced layer thickness" (h_{coal}) as a function of drying time are also measured based on the OCT profile. The gravimetry tracks the weight change of film with time and gives the film water content curve ($k_w(t)$). The initial weight of latex film in the Petri dish was set at ~2 mm so that the thickness of dried latex film (with no water) is expected to be 1

mm. The video takes time-lapse photos of film's appearance. All characterizations were synchronized and took data every 2 minutes.

5.2.7 Drying curve in controlled environment and determination of "inflection point"

The drying curves in controlled environment (23 °C and 50% RH without wind) of latex films were measured in the environmental chamber. The measurements followed the same procedures as documented in Section 4.2.3 (Chapter 4). Data were taken every 2 minutes. The initial weight of latex film in the Petri dish was set at ~2 mm so that the thickness of dried latex film (with no water) is expected to be 1 mm. The results given in Figure 5.2 include the drying curves ($w(t)$), the drying rate curves ($dw(t)/dt$) and the film water content curves ($k_w(t)$), as a function of time up to 3000 minutes (2.1 days). Since the dryings started at slightly different initial solids contents for different latexes (see k_{s0}'s in Table 5.1), the drying curves were intentionally shifted along the time axis so that all started at the same solids content of 50% (or k_w = 50%). Ideally, the initial drying rates of free water evaporation in the controlled environment should be exactly the same for all latex films. However, real measurements (given in Figures 5.2 A and B) show that the initial drying rates varied a bit ($(7.0 \pm 0.5) \times 10^{-5}\,\mathrm{g/(cm^2 \cdot min)}$), which could be the results of slight disturbance by minor non-uniform distribution of humidity in the environmental chamber affected by other samples in the chamber.

As discussed in Chapter 4 (especially Section 4.3.1), the initial drying rate (similar to the drying of DI water) started dropping when the lower-permeable skin appeared near the grooves; then the skin propagated along the horizontal surface with the drying rate decreasing; when the skin covered the entire film area, the drying rate became near zero

and limited by the matured skin layer and the developing layer of coalesced latex particles below the skin layer (or coalesced layer). In this chapter, the "inflection point" (t_{infl}) is defined as the point in time at which the drying rate drops to 1/10th of the initial drying rate of free water. The inflection point is close to the time when the low-permeable skin covers the entire film area. The corresponding film water content at the inflection point is named as $k_{w,infl}$.

Figures 5.2A and B show the drying curves ($w(t)$), the drying rate curves ($dw(t)/dt$) and the film water content curves ($k_w(t)$) of PEM latex, PEM+SLS latexes and PEM+TTX latexes with an initial wet film thickness of 2 mm (with latex solids of about 50% and a final dried film thickness expected to be 1 mm), which were measured in the controlled environment. The t_{infl}'s and $k_{w,infl}$'s derived from their drying curves are listed in Table 5.4 (see in Section 5.2.8). The inflection points of some latex samples are labelled with colored circles on the $k_w(t)$ curves in Figure 5.2.

For both SLS and TTX, a higher post-added surfactant concentration gives more water loss (see $w(t)$ in Figure 5.2) and less water trapped in the film (see $k_w(t)$ in Figure 5.2) after the inflection point (t_{infl}). The only exception is PEM+2%SLS film, which has a $k_{w,infl}$ between PEM+0.5%SLS and PEM+1%SLS (see $k_w(t)$ in Figure 5.2A or Table 5.4). The PEM+2%SLS latex became transparent after its t_{infl} = 1500 min (1.0 day); however, at that time and even after being dried for 3000 min (2.1 days), the film was easily disintegrated and re-dispersible in water, indicating poor coalescence between particles. Then with further increase in the drying time, the film became a bit opaque gradually (probably because of migration and clustering of the excess surfactant molecules within the latex polymer matrix); after 5 days, the film became coherent and no longer re-

dispersible, but still a bit opaque. This agrees with the surfactant distribution's prediction that the SLS concentration in aqueous phase continues to increase with drying time for the PEM+2%SLS latex film (see Table 5.2), so that a large amount of surfactant molecules reside within the interstices between particles leading to retarding particles' coalescence. Thus, the PEM+2%SLS latex cannot form a coherent film within 3000 min of drying time, while other latexes do. The higher $k_{w,infl}$ of PEM+2%SLS film than that of PEM+1%SLS film indicates more water is retained within the higher amount of surfactant molecules. The drying rate curves (see $dw(t)/dt$ in Figure 5.2) show that the region of the drop in the drying rate shifts rightwards with post-added surfactant (see red arrows in Figure 5.2), indicating the time delay of particles' coalescence in the incipient skin layer.

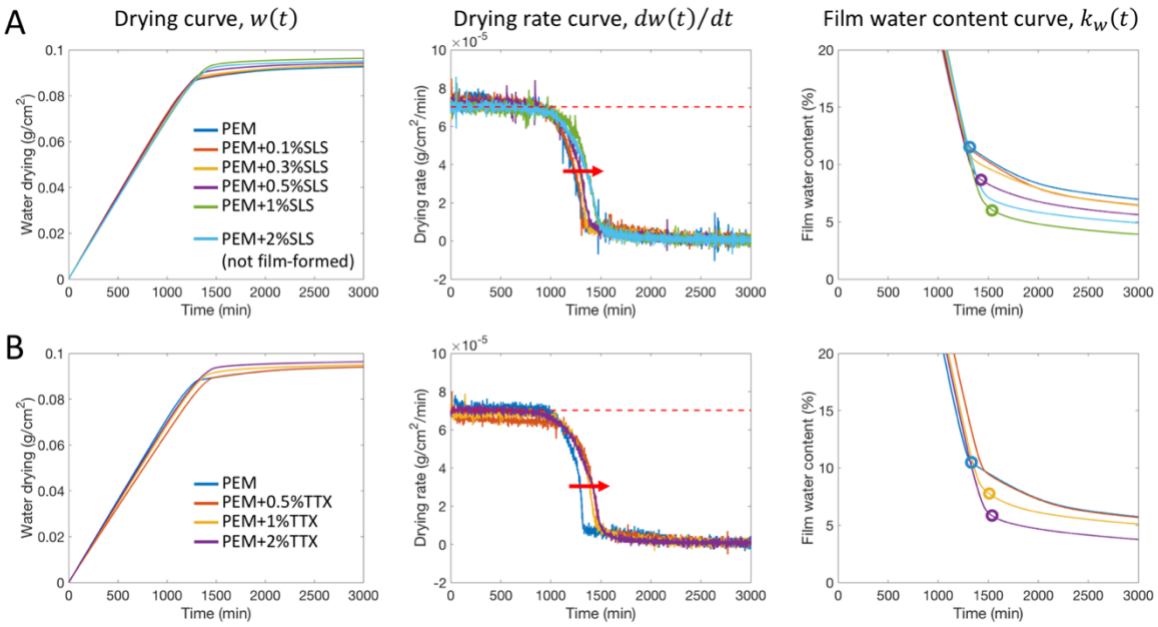

Figure 5.2: The drying curves ($w(t)$), the drying rate curves ($dw(t)/dt$) and the film water content curves ($k_w(t)$) of PEM latex, PEM+SLS latexes (A) and PEM+TTX latexes (B). The red arrows denote the rightward shifts of the $dw(t)/dt$ curves in the regions where the drying rates drop. The circles on the $k_w(t)$ curves denote the inflection points (t_{infl}'s) of the PEM, PEM+0.5%SLS, PEM+1%SLS, PEM+1%TTX and PEM+2%TTX latexes.

5.2.8 Determination of coalescence delay time (Δt_{del}) based on inflection points

With the coalescence of latex particles impeded by surfactant[5], the water in the wet domain can be siphoned upward through boundaries between the deformed particles within the incipient skin and freely evaporates into air, before those particles coalesce into a low-permeable matured skin. Thereby, the longer the coalescence delay time (time difference between particles' deformation and coalescence) is, the more water evaporates freely before the incipient skin becomes matured into a low-permeable skin, thus the less water will be contained in the wet domain, and the shorter the film drying time will be. According to the Förster resonance energy transfer (FRET)'s measurement[6], the coalescence delay time ranges from several minutes to tens of minutes depending on the amount of surfactant added to the latex.

Ideally, if the drying curves of all samples were measured exactly under the same condition with the same initial drying rate, the coalescence delay time can be derived as the time difference between the inflection point of the latex film with delayed coalescence and that of the latex film without delayed coalescence (Δt_{infl}). However, the variation of initial drying rate in the environmental chamber ($(7.0 \pm 0.5) \times 10^{-5}\,\mathrm{g/(cm^2 \cdot min)}$) can cause large errors in Δt_{infl}.

In this chapter, $k_{w,infl}$'s of latex films are used to determine the coalescence delay times. In order to do that, three reasonable assumptions are made: 1) $k_{w,infl}$ is insensitive to minor variation of the drying condition in the environmental chamber; 2) the drying rate through the permeable incipient skin is similar to the initial drying rate of free water ($v_0 = 7.0 \times 10^{-5}\,\mathrm{g/(cm^2 \cdot min)}$); 3) the coalescence delay time of the original latex without post-added surfactant is very short and assumed to be zero; the Förster resonance energy

transfer (FRET) study also showed that deformation and coalescence occurred almost simultaneously for the latex with a similar synthesis recipe as for PEM[6]). The approach used to determine the coalescence delay time is as follows. First, $k_{w,infl}$ of the original latex film is measured and denoted as $k_{w,infl0}$; then, $k_{w,infl}$ of the latex film with post-added surfactant is measured and denoted as $k_{w,infl1}$. Both films have the same dried thickness or the same solid mass per unit area (m_s), which is 0.1 g/cm^2 with 1 mm dried film thickness herein. Thus, the water masses per unit area of these two films at inflection points ($m_{w,infl0}$ and $m_{w,infl1}$) are:

$$m_{w,infl0} = \frac{m_s k_{w,infl0}}{1 - k_{w,infl0}} \qquad (5.21)$$

$$m_{w,infl1} = \frac{m_s k_{w,infl1}}{1 - k_{w,infl1}} \qquad (5.22)$$

Since $k_{w,infl1} < k_{w,infl0}$, $m_{w,infl1} < m_{w,infl0}$, then with the initial drying rate of free water ($v_0 = 7.0 \times 10^{-5}\,\mathrm{g/(cm^2 \cdot min)}$), the coalescence delay time (Δt_{del}) is derived as:

$$\Delta t_{del} = \frac{m_{w,infl0} - m_{w,infl1}}{v_0} = \frac{m_s}{v_0} \cdot \frac{k_{w,infl0} - k_{w,infl1}}{\left(1 - k_{w,infl0}\right)\left(1 - k_{w,infl1}\right)} \qquad (5.23)$$

Table 5.4 shows the measured $k_{w,infl}$'s and Δt_{del}'s of PEM, PEM+SLS and PEM+TTX latex films with an initial wet film thickness of 2 mm (with latex solids of about 50% and a final dried film thickness expected to be 1 mm). It should be noted that Δt_{del} of

the PEM+2%SLS latex was not calculated in Table 5.4, because the latex did not form a coherent film due to the lack of particles' coalescence even after being dried for 3000 min (as discussed in Section 5.2.7). The results in Table 5.4 clearly show that Δt_{del} increases with more post-added surfactants.

Table 5.4: Solids content of the original latex (k_{s0}), surfactant % of particles' surface coverage by surfactants (SC_{SLS} and SC_{TTX}), inflection points (t_{infl}), film water contents at t_{infl} ($k_{w,infl}$) and their derived coalescence delay times (Δt_{del}) for PEM, PEM+SLS and PEM+TTX latex films.

Latex	k_{s0} (%)	SC_{SLS} [a] (%)	SC_{TTX} [a] (%)	t_{infl} [b] (min)	$k_{w,infl}$ [b] (%)	Δt_{del} (min)
PEM	49.94	25.0 [c]	0	1340	11.36	0
PEM+0.1%SLS	49.87	30.0	0	1320	11.31	0.9
PEM+0.3%SLS	49.72	39.9	0	1370	10.33	18.5
PEM+0.5%SLS	49.58	49.9	0	1440	8.62	48.3
PEM+1%SLS	49.22	74.8	0	1520	6.17	89.1
PEM+2%SLS [d]	48.52	100.0	0	1500	7.14	/
PEM	50.37	25.0 [c]	0	1340	10.43	0
PEM+0.5%TTX	50.00	25.0	23.0	1520	9.35	19.0
PEM+1%TTX	49.63	25.0	46.0	1510	7.75	46.3
PEM+2%TTX [e]	48.92	25.0	92.0	1520	5.95	76.0

[a] SC_{SLS} and SC_{TTX} are the data at the start of drying of PEM latex in Table 5.2A.
[b] t_{infl} and $k_{w,infl}$ are determined in Section 5.2.7 according to the drying curves. It should be noted that Δt_{del} is determined by the difference of $k_{w,infl}$ (using Equation 5.23), not the difference of t_{infl} (which can produce large errors).
[c] There exists $k_{SLS/s}$ = 0.5% SLS (corresponding to SC_{SLS} = 25.0%) in the original PEM latex.
[d] PEM+2%SLS latex was unable to form a coherent film after drying for 3000 min, due to the lack of coalescence (where the particles in the dried film were re-dispersible in water) (see more explanation in Section 5.2.7). Thus its Δt_{del} was not calculated.
[e] $SC_{SLS} + SC_{TTX}$ = 117% > 100%, due to the formation of surfactant complexes (see more details below Table 5.2B in Section 5.2.4).

5.2.9 Water vapor permeability (WVP) and water absorption of dried latex film

The WVP of dried latex film correlates with that of the skin and coalesced layer, since the layer on film top is also made up of the same coalesced latex particles as those in the dried latex film. The measurement of WVP of dried latex film follows the same procedure documented in Section 2.3.4 in Chapter 2. The dried 1 mm-thick films of PEM latex and PEM+1%SLS were examined in order to see whether surfactant can affect WVP or not.

The water absorption measures the ability of dried latex film to imbibe water in a milieu of water-saturated environment. The experiment was conducted by immersing the dried latex film (dried in Petri dish until k_w < 2%) into DI water. The film had a mass (W_s) of ~5.7 g with 1 mm dried film thickness, which was accurately weighed. The DI water was renewed every day. At varied immersing times, the film was taken out of water and blown by air to strip off water droplets on the film surface. The film with absorbed water was weighed quickly before being placed back into water, whose mass was recorded as $W_{s,abs}$. Then the relative absorbed water mass (R_{abs}) is derived as:

$$R_{abs} = \frac{W_{s,abs} - W_s}{W_s} \qquad (5.24)$$

As expected, R_{abs} increases with immersion time in water, due to the ongoing intrusion of water into the coalesced latex polymer matrix. In this chapter, the relative absorbed water mass as a function of immersing time ($R_{abs}(t)$) are reported and given in Figure 5.5 in Section 5.3.3.

Both the WVP and the water absorption of dried latex film characterize the water resistance of dried latex film and correlate with each other. Normally, the higher the water absorption is, the higher the WVP is, and thus the lesser water-resistant film[9].

5.3 Results and discussions

5.3.1 OCT-Gravimetry-Video characterizations

Figure 5.3 presents the experimental results of PEM, PEM+0.5%SLS and PEM+1%SLS latex films with an initial wet film thickness of 2 mm (with latex solids of about 50% and a final dried film thickness expected to be 1 mm), characterized by the OCT-Gravimetry-Video method. The room condition was monitored with temperature as 24 – 26 °C and humidity as 35 – 45% RH. Due to the small $\bar{\lambda}$ and large Pe by drying these three latex films under room condition ($\bar{\lambda} = 1.8 \times 10^{-4} < 1$ and $Pe = 19.1 > 1$ calculated for 2 mm-thick PEM latex in Section 4.3.1 in Chapter 4), skin layers should always form during their drying processes. However, this section shows how profoundly the post-added surfactant can affect the formation of skin layer and the whole course of latex film formation.

The video photos in Figure 5.3 already show the dramatic differences in appearance of the latex films with and without post-added SLS surfactant after being dried for 2500 min (1.7 days): PEM+1%SLS film is transparent (in Figure 5.3C) , PEM+0.5%SLS film is close to being transparent with a bit opacity (Figure 5.3B), and PEM film with no extra surfactant is still white and opaque (Figure 5.3A). Grooves (area with film thickness much thinner than surroundings) were observed near the Petri dish wall for all films. The difference of opacities agrees with the gravimetric measurements, showing that PEM film

contains more water than PEM+SLS does after low-permeable skins are formed ($k_{w,infl}$ = 12.55% for PEM, 9.47% for PEM+0.5%, 6.89% for PEM+1%, see red circles in the corresponding drying curves given in Figures 5.3 A, B and C, respectively).

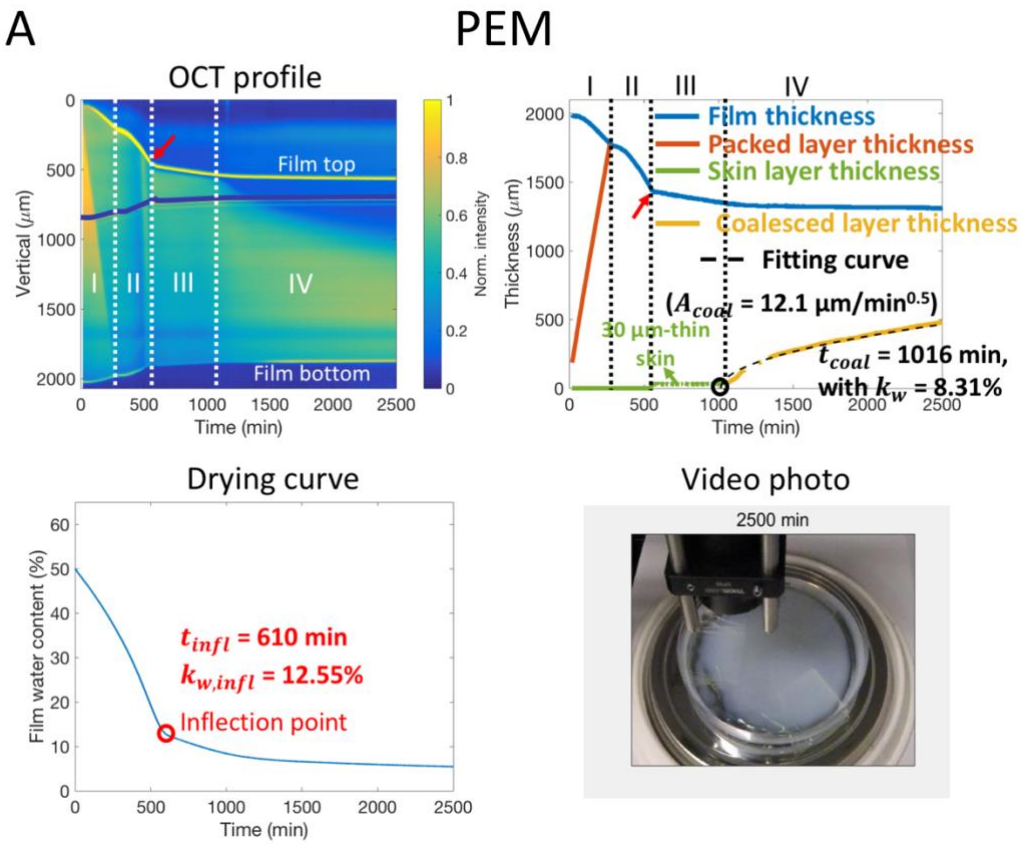
A
PEM
OCT profile
Film top
Film bottom
I
II
III
IV
Vertical (μm)
Time (min)
Norm. intensity
Thickness (μm)
Film thickness
Packed layer thickness
Skin layer thickness
Coalesced layer thickness
Fitting curve
(A_{coal} = 12.1 μm/min$^{0.5}$)
50 μm-thin skin
t_{coal} = 1016 min,
with k_w = 8.31%
Drying curve
Film water content (%)
t_{infl} = 610 min
$k_{w,infl}$ = 12.55%
Inflection point
Video photo
2500 min

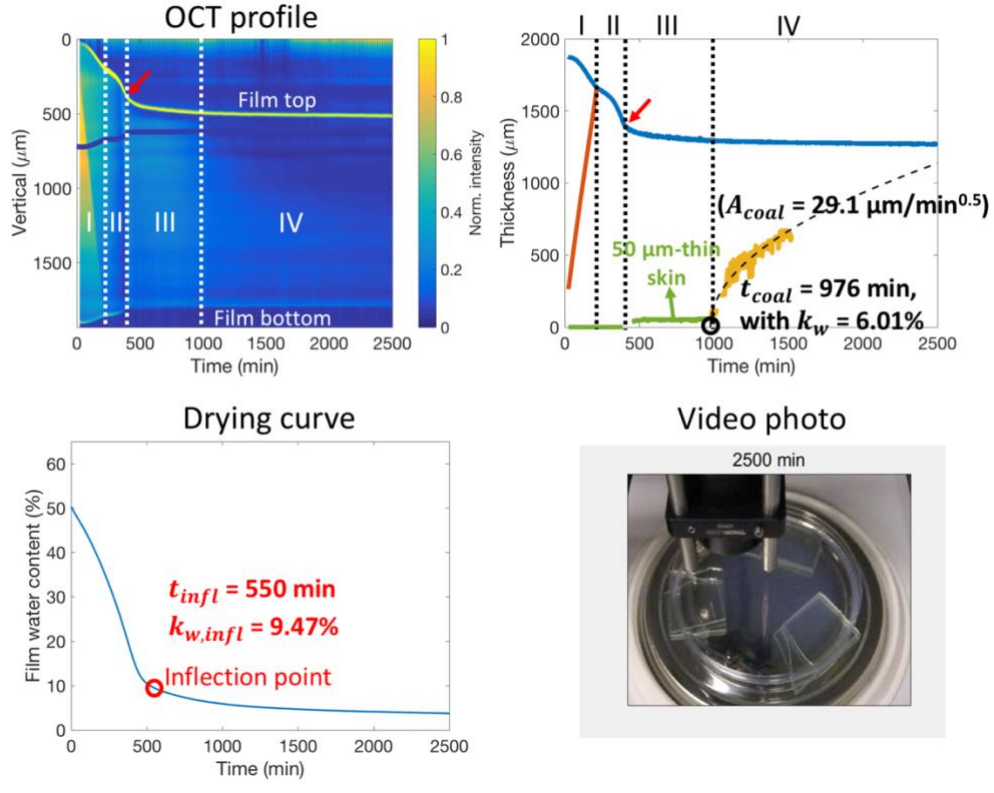
B
PEM+0.5%SLS
OCT profile
Film top
Film bottom
I
II
III
IV
Vertical (μm)
Time (min)
Norm. intensity
Thickness (μm)
(A_{coal} = 29.1 μm/min$^{0.5}$)
50 μm-thin skin
t_{coal} = 976 min,
with k_w = 6.01%
Drying curve
Film water content (%)
t_{infl} = 550 min
$k_{w,infl}$ = 9.47%
Inflection point
Video photo
2500 min

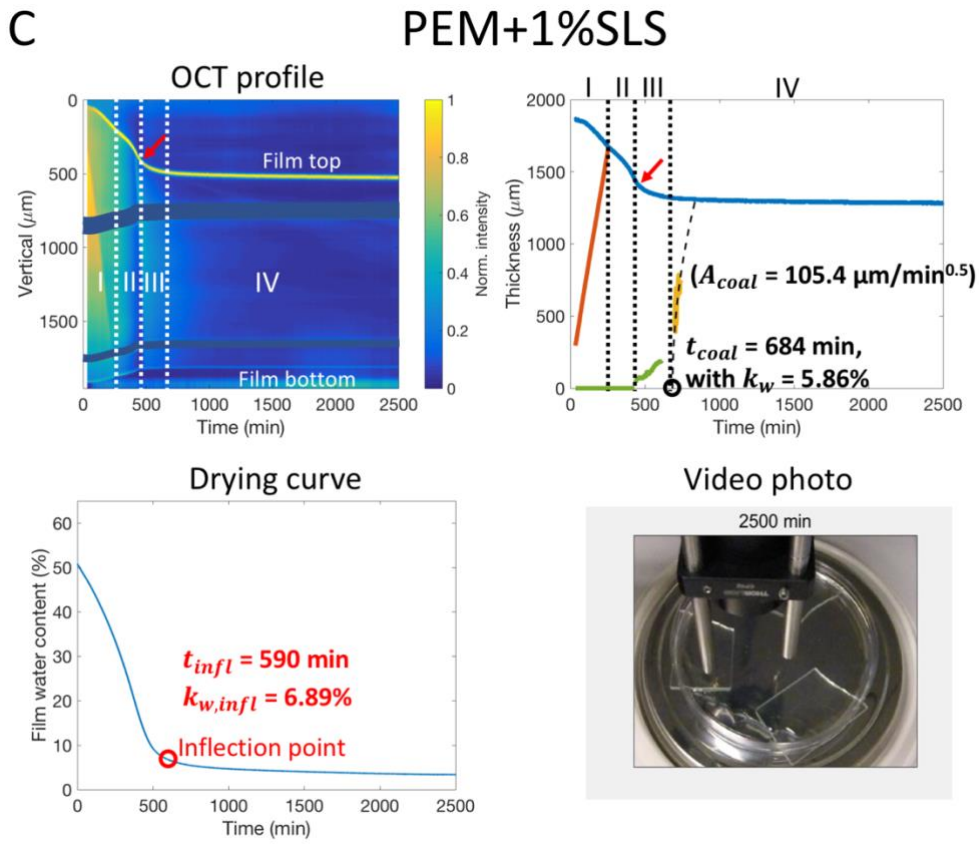

Figure 5.3: Results of OCT-Gravimetry-Video characterizations of PEM (A), PEM+0.5%SLS (B) and PEM+1%SLS (C) films with an initial wet film thickness of 2 mm (with latex solids of about 50%) and a final dried film thickness of 1 mm. In each set of figures, the first figure (top left) is the OCT profile; the second (top right) are the time-evolved curves of the film thickness (blue line), the packed layer thickness (red line), the initial apparent skin layer thickness (green line), and the coalesced layer thickness (yellow line), as well as the fitting curve of coalesced layer thickening model (black dashed line); the third (bottom left) is the film water content curve ($k_w(t)$) measured by gravimetry; the fourth (bottom right) is the video photo at the drying time of 2500 min. Notes: the red arrows in the OCT profiles and film thickness curves denote the points in time when the apparent incipient skin layer appears; the dark blue lines in the OCT profiles are used to cover the self-reflections of OCT image's artifacts.

The OCT profiles of PEM, PEM+0.5%SLS and PEM+1%SLS latex films in Figure 5.3A, B and C, respectively, show microscopic details on how the post-added surfactant affects the film formation process. From these profiles, the curves of film thickness, packed layer thickness, skin layer thickness (h_{skin}) and coalesced layer thickness (h_{coal}) as a function of drying time are derived (shown in the top right side in each set of figures given in Figure 5.3). All these thick latex films (starting with a 2 mm wet film thickness and ending with a 1 mm dried film thickness) experienced four drying stages: I) packing of particles, II) consolidation of particles, III) formation and maturation of incipient skin layer, IV) thickening of coalesced layer, which have been described in the Introduction (Section 5.1) and also in more details in Figure 4.4 and related text in Chapter 4. According to the OCT profiles, the most pronounced differences between these samples' drying profiles are the increasing rate of h_{coal} in Stage IV. Details about the effects of post-added SLS on the film formation process are discussed as follows.

First, within the first 300 min, the vertical packing processes (Stage I) for all samples were linear. Although the packing stages ended at different times (270 min for PEM, 212 min for PEM+0.5%SLS, 254 min for PEM+1%SLS) which was caused by differences of the initial drying rate due to variations of room condition, the films' water contents (k_w's) when all particles become packed (in Stage I) are quite similar and the void fraction is close to 36% for closely random packing (36.3% for PEM, 36.0% for PEM+0.5%SLS, 33.1% for PEM+1%SLS). During the packing process, the average inter-distance between particles (d_{in}, based on the face-centered cubic arrangement) decreased from 24.6 nm (equivalent to 16.4 lengths of SLS molecule which is 1.5 nm) at the start of drying to 8.8 nm (equivalent to 5.8 lengths of SLS molecule) when the particles became

packed (see Table 5.3). Although more SLS imparts more surface charges on each particle due to the higher coverage by surfactant molecules on the particles' surface (Table 5.2), the particles' packing process does not seem to be affected by the amount of post-added SLS to the PEM latex. This may be because of the weak interactions between particles at such particles' inter-distances (from 8.8 nm to 24.6 nm), so that the Peclet numbers (Pe, which determines the profile of particles' packing) of these three latex films with an initial 2 mm thickness should be similar[11]. Considering the high salt concentration (38.7 mM Na_2CO_3) in PEM latex (see Table 2.1 in Chapter 2), the thickness of electrical double layer around particles (Debye length)[10] is calculated as about 0.89 nm, equivalent to 0.6 length of SLS molecule. Since during the packing process, d_{in} decreases from 24.6 nm to 8.8 nm, which is more than 4 times of the Debye length, the interactions between particles can be ignored according to the particle surface potential calculation[10]. After the packing stage, all film thickness curves showed a "kink point" (due to stress relaxation and formation of grooves, see Section 4.3.1 in Chapter 4), followed by a continuous decrease in film thickness due to particles' consolidation (Stage II).

Second, with the incipient skin layer being formed (during Stages I & II) and matured (Stage III) and the thickening of coalesced layer (Stage IV), the behaviors of film formation process in these three systems (PEM, PEM+0.5%SLS and PEM+1%SLS) are significantly different. For the PEM film (Figure 5.3A), the apparent thin skin layer with h_{skin} = ~30 μm formed, matured and maintained for ~500 min (during Stage III); after that, h_{coal} increased slowly with square root of time (Stage IV). It took more than 4 days for h_{coal} to increase until the entire film became transparent. For the PEM+0.5%SLS film (Figure 5.3B), an apparent thin skin layer also appeared and lasted for ~510 min with a

thickness h_{skin} = ~50 μm (during Stage III); then h_{coal} increased faster with time (Stage IV). Since there was less water retained in the wet domain, the scattered light intensity contrast was so weak that h_{coal} (or the coalesced layer/wet domain boundary) could not be clearly defined after ~1500 min. It took about 2 days for the entire film to become transparent. For the PEM+1%SLS film (Figure 5.3C), during Stage III, h_{skin} increased from ~40 μm to ~250 μm within ~250 min; afterwards, h_{coal} increased so rapidly (which could not be clearly defined after ~740 min due to weak light scattering in the wet domain) such that the entire film became transparent in about 0.7 day (~1000 min). Based on Equation 4.1 (Chapter 4), the apparent thin skin layers of PEM and PEM+0.5%SLS films with their corresponding drying rates show that, their mean WVP's during Stage III are 2.3×10^{-11} g/(cm · min · Pa) and 2.0×10^{-11} g/(cm · min · Pa), respectively. Separate measurements of the dried latex film's WVP showed that the WVP of the PEM+1%SLS dried film is 3.7×10^{-11} g/(cm · min · Pa), which is close to the measured value of 4.0×10^{-11} g/(cm · min · Pa) for the PEM dried film. All these WVP's of skin layers and dried films are similar, meaning that the extra amount of SLS (with $k_{sur/s} \leq$ 1%) trapped in the polymer film does not affect the WVP of the coalesced polymer film that much.

Since the SLS does not give a more permeable skin and coalesced layer, the surfactant's role in shortening the film drying time should be making the water content in wet domain (k_w^*) lower. The reason, which will be described more in the next section, can be that: the extra surfactant molecules on the particles' surface and/or in the interstices between the closely packed particles (due to post-added surfactant into the latex) act as a barrier to impede or delay the coalescence of particles. Since water still evaporates freely

through the boundaries between non-coalesced particles in the incipient skin, less water will be trapped in the wet domain after the particles inside the incipient skin coalesce into a matured skin with low permeability, in which case k_w^* is lower, h_{coal} increases faster with time (according to Equation 5.1) and the film drying time becomes shorter. By fitting the measured h_{coal} curves in Figure 5.3 using the coalesced layer thickening model (Equation 5.1), the A_{coal}'s of PEM, PEM+0.5%SLS and PEM+1%SLS are derived as 12.1, 29.1 and 105.4 μm/min$^{0.5}$, respectively, with their t_{coal}'s (the point in time at which h_{coal} begins to increase) as 1016 min, 976 min and 684 min. By substituting these A_{coal}'s into Equation 5.1, the effective k_w^* ($k_{w,eff}^*$) can be derived as:

$$\frac{k_{w,eff}^*}{1-k_{w,eff}^*} = \frac{2\text{WVP}\cdot p_0 \cdot \Delta RH}{\rho_s A_{coal}^2} \qquad (5.25)$$

Using WVP = 4.0×10^{-11} g/(cm · min · Pa) for all coalesced layers, p_0 = 3169 Pa at 25 °C and ΔRH = 1 - 45% = 55%, the effective water content in the wet domain $k_{w,eff}^*$ can be obtained as 8.70% for PEM, 1.62% for PEM+0.5%SLS and 0.13% for PEM+1%SLS. While $k_{w,eff}^*$ for PEM (8.70%) is close to the measured film water content k_w at its t_{coal} (8.31% at 1016 min, see Figure 5.3A – top right), $k_{w,eff}^*$'s for PEM+0.5%SLS (1.62%) and PEM+1%SLS (0.13%) are much smaller than the measured k_w's at their t_{coal}'s (6.01% at 976 min and 5.86% at 684 min, respectively, see Figures 5.3B and C – top right). This is because, besides the water trapped in the wet domain, there is residual strong-bonded water molecules trapped within the coalesced layer, possibly due to the chemically bound carboxyl groups on the particles' surface and the water-soluble molecules (such as

surfactants, oligomers and salts) trapped within the layer. Since the coalesced layer thickening model assumes no water exists in the coalesced layer, $k^*_{w,eff}$ derived by model fitting should underestimate the real water content of the entire film. Furthermore, the water concentration gradient along the vertical direction in the wet domain, which was not considered in this model, can also cause deviations. Another notable detail in the OCT profile is the sharpness of the film thickness curve at the point in time at which the apparent skin layer appears (see red arrows in Figure 5.3). The point was very sharp for the PEM film (Figure 5.3A), while those for PEM+0.5%SLS and PEM+1%SLS films became smoothed and curved (Figures 5.3B and C). The sharpness of these points in the OCT profiles (red arrows in Figure 5.3) also correspond well with the sharpness of the inflection points in drying curves (red circles in Figure 5.3). These observations indicate that for the PEM latex, the particles' coalescence happened instantly when the apparent skin layer was formed; while for the PEM latexes with post-added surfactants, the coalescence could develop more gradually. Although the sulfate and carboxyl groups chemically bound on the particles' surface ($SC_{carb} = 1.6\%$ and $SC_{sulf} = 0.6\%$) as well as the salt (38.7 mM Na_2CO_3) and the oligomers with carboxyl group (2.4 mM) in the aqueous phase could also act as a barrier to impede coalescence, the work discussed in this chapter ignores their effects and only investigates the effects of post-added surfactants. Further research work is needed to investigate the influences of such chemically bound groups and water-soluble species, as will be mentioned in the recommendations for future work in Chapter 7.

5.3.2 Coalescence delay time (Δt_{del}) versus % of particles' surface coverage by surfactant molecules (SC_{sur})

After the latex particles become packed and in contact with each other, continuous water evaporation begins to compress and distort the particles due to the water/air and polymer/water interfacial tensions; at the same time, the high compression force (in the range of MPa) can break up the contact area between adjacent particles to initiate particles' coalescence[12], and the surfactant molecules are forced to desorb from particles' surface and reside within the interstices between particles (or migrate further to the top or bottom of the drying film). When the concentration of surfactant (either ionic or non-ionic) in latex or the surfactant coverage on the particles' surface is high, two effects can take place to retard the coalescence between particles: 1) the repulsive forces or potential energies between particles are increased, so that more water evaporation is needed to force particles to a closer contact and to make the van der Waals attractions between particles predominate in order to initiate coalescence[12], during which the surfactant acts as a "potential energy barrier"; 2) just after coalescence, more surfactant molecules desorb from the particles with a higher surfactant surface coverage and become trapped within the interstices between particles' boundaries, so that more time is needed for surfactant molecules to migrate and for particles to get further coalesced, during which the surfactant acts as a "physical barrier". Thus, the more the surfactant molecules are adsorbed on latex particles' surface (with post-added surfactant), the longer the time is needed for particles to develop coalescence, thus the longer coalescence delay time (Δt_{del}). In this way, the time duration of the high-permeable incipient skin can be extended, so that more water evaporates fast before the particles in the incipient skin begin to coalesce into a low-permeable matured

skin, leading to a lower water content in the wet domain (k_w^*) and afterwards a faster increase of the coalesced layer thickness (h_{coal}) with time and thus a shorter film drying time. Although chemically bound functional groups on the particles' surface and other water-soluble species (such as salt and oligomers) can also delay coalescence due to either the "potential energy barrier" effect or the "physical barrier" effect, this chapter only studies the effects of post-added surfactants on the drying process of latex film, especially the correlation between Δt_{del} and the % of particles' surface coverage by surfactant molecules (SC_{sur}).

In this chapter, Δt_{del} is determined as the drying time responsible for lowering the water content in the wet domain (k_w^*) due to the post-added surfactant (see Section 5.2.8). The % of particles' surface coverage by surfactant molecules is characterized by $SC_{SLS} + SC_{TTX}$ (sum of the surface coverages by the SLS and TTX surfactants which are determined in Section 5.2.4). The Δt_{del}'s, SC_{SLS}'s and SC_{TTX}'s of PEM, PEM+SLS series and PEM+TTX series are listed in Table 5.4. The only exception is the PEM+2% SLS latex film whose Δt_{del} was not calculated, due to the lack of particles' coalescence even after being dried for 3000 min (see Section 5.2.7), probably because too much surfactant was trapped within the interstices between particles acting as a "physical barrier" to retard coalescence.

The relationship between Δt_{del} and the sum of the percentages of particles' surface coverage by the two surfactants ($SC_{SLS} + SC_{TTX}$) is plotted in Figure 5.4, using the data given in Table 5.2A. It should be noted that $SC_{SLS} + SC_{TTX}$ = 117% > 100% for the PEM+2%TTX latex, because SLS and TTX molecules can bind together and form surfactant complexes. The results show that Δt_{del} increases almost linearly with ($SC_{SLS} +$

SC_{TTX}) for both PEM+SLS latex series and PEM+TTX latex series. However, the linear fitting slopes of Δt_{del} versus ($SC_{SLS} + SC_{TTX}$), defined as the "coalescence delay efficiency" ($\widetilde{\Delta t}_{del}$), are different. The $\widetilde{\Delta t}_{del}$ represents the average increase of Δt_{del} for every 1% increase of SC_{SLS} for PEM+SLS series or SC_{TTX} for PEM+TTX series. The calculated $\widetilde{\Delta t}_{del}$'s are 1.90 min/(1%) for SLS surfactant and 0.84 min/(1%) for TTX surfactant. Therefore, at the same % of particles' surface coverage by surfactant molecules, SLS (with a higher $\widetilde{\Delta t}_{del}$) is more effective than TTX (with a lower $\widetilde{\Delta t}_{del}$) to extend the coalescence delay time. On one hand, the ionic SLS molecules adsorbed on particles may impart stronger repulsive interactions between particles than the non-ionic TTX molecules do in the PEM latex system, leading to a higher potential energy barrier and a longer coalescence delay time. On the other hand, the $\widetilde{\Delta t}_{del}$ difference may be qualitatively related to the hydrophile-lipophile balance (HLB) values of the two surfactants – HLB = 40 for SLS and HLB = 13.5 for TTX[20]: the more hydrophilic surfactant (with higher HLB), the more hydrophilic "physical barrier" (surfactant molecules trapped in the interstices between particles), the harder for the hydrophobic polymer chains from latex particles to penetrate that barrier, thus the longer coalescence delay time.

Besides surfactants, the carboxyl and sulfate groups on the particles' surface were found to be able to retard the coalescence between particles[22]. Moreover, the salts and oligomers in the aqueous phase may be trapped between particles and affect their coalescence. The molecular interactions between SLS and TTX (to form surfactant complexes) that influence their adsorption on particles' surface (and perhaps their desorption and redistribution) and change the rheological property of the aqueous fluid at the interstices between particles[17] may also impact the coalescence delay time.

Nevertheless, this chapter only investigates the effects of surfactants, without considering the carboxyl and sulfate groups on the particles' surface or the salts or the oligomers in the aqueous phase, as well as assuming that SLS and TTX get adsorbed on particles' surface independently. As proposed above, the surfactants adsorbed on latex particles' surface can delay the coalescence between particles by both the potential energy barrier (due to the particles' interactions) and the physical barrier (due to the desorbed surfactant molecules trapped between particles), which provides a longer time (Δt_{del}) for water to evaporate freely through non-coalesced particles within the incipient skin, so that less water will be trapped under the matured low-permeable skin and less time is needed for the entire film to become dried.

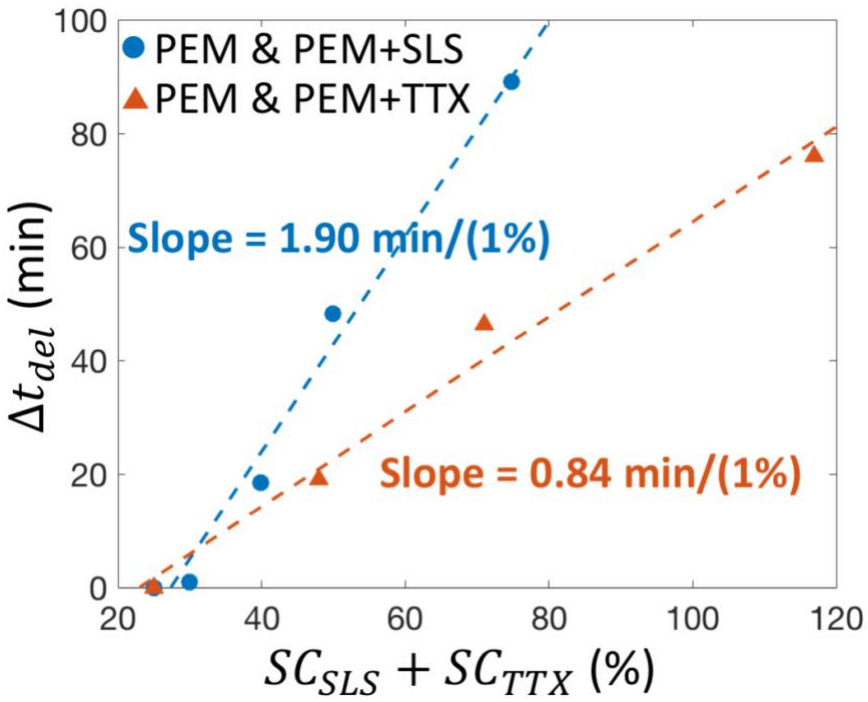

Figure 5.4: Relationships between Δt_{del} and $(SC_{SLS} + SC_{TTX})$ of PEM, PEM+SLS and PEM+TTX latexes, according to the data given in Table 5.4. The blue circles are the results of PEM, PEM+0.1%SLS, PEM+0.3%SLS, PEM+0.5%SLS and PEM+1%SLS latex films. The red triangles are the results of PEM, PEM+0.5%TTX, PEM+1%TTX and PEM+2%TTX latex films. The two dashed lines are linear fittings on data points regarding PEM+SLS latexes and PEM+TTX latexes, respectively.

5.3.3 Water absorption of dried latex film

As shown above, with the post-added surfactant in latex, the film formation process can be promoted by delaying the coalescence of particles so that more water evaporates freely through the incipient skin and less water is trapped in the wet domain after the skin becomes matured with low permeability. However, a major concern about coating applications is the water resistance of the dried latex film, because high water absorption can make the film white and opaque with poor mechanical strength[13]. In order to determine the extent to which the added surfactant can affect the water absorption of dried film, the relative absorbed water masses (R_{abs}) in the dried latex films of PEM, PEM+1%SLS, PEM+1%TTX and PEM+2%TTX (with 1 mm dried film thickness) were measured as a

function of immersing time (t). The results are given in Figure 5.5, which shows that for all films, R_{abs}'s increase with time. While $R_{abs}(t)$ curves of PEM+1%SLS and PEM+1%TTX films are close to that of PEM film, the curve of PEM+2%TTX film is much higher than that of PEM film (see Figure 5.5A). This is probably due to the large amount of TTX molecules trapped within the latex film that can absorb and retain more water by the ethoxylate groups of TTX. In addition, the surfactant complexes formed by SLS and TTX that contribute to the retardation of coalescence may also increase the film's water absorption. By plotting R_{abs}'s against the square root of time (in Figure 5.5B), the data points are found to mostly follow the proportional relationship, corresponding to the Fickian absorption kinetics[14]. Their linear fitting slopes of R_{abs} versus $t^{0.5}$, defined as the water absorption efficiency ($\tilde{R}_{abs}$), are derived as 0.017 day$^{-0.5}$ for PEM film, 0.022 day$^{-0.5}$ for PEM+1%SLS film, 0.021 day$^{-0.5}$ for PEM+1%TTX film and 0.039 day$^{-0.5}$ for PEM+2%TTX film. While $\tilde{R}_{abs}$ of PEM+2%TTX is more than twice as large as that of PEM, $\tilde{R}_{abs}$'s of PEM+1%SLS and PEM+1%TTX are only about 20% higher than $\tilde{R}_{abs}$ of PEM. The smaller difference of $\tilde{R}_{abs}$ between PEM film and PEM+1%SLS film corresponds to their similar WVPs, which means both films are similarly hydrophobic. Therefore, in order to get a film with good water resistance and short film drying time, the amount and type of post-added surfactants in the latex need to be optimized. Too much surfactant can cause either poor film formation (the fate of PEM+2%SLS) or high water absorption (the fate of PEM+2%TTX).

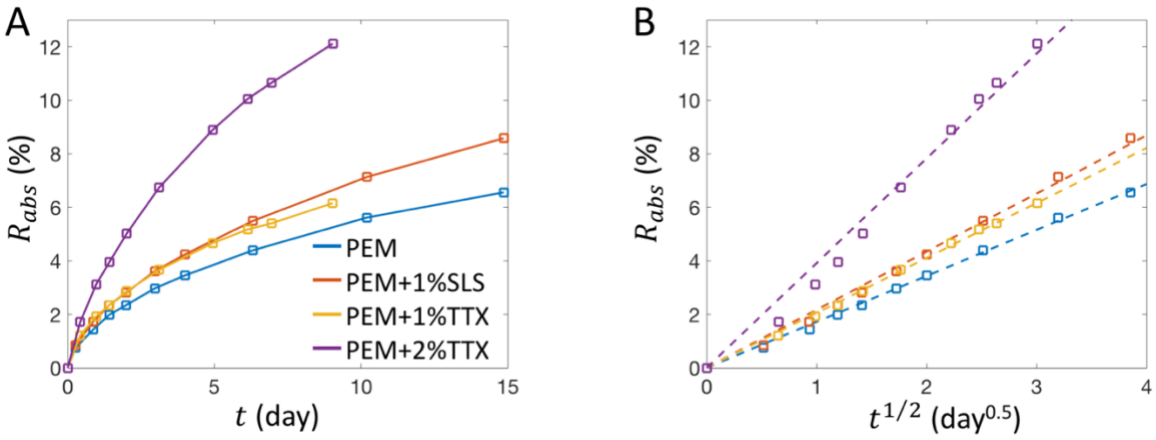

Figure 5.5: the relative absorbed water masses (R_{abs}) in dried latex films of PEM, PEM+1%SLS, PEM+1%TTX and PEM+2%TTX (with 1 mm dried film thickness), as a function of time (A) and square root of time (B).

5.4 Conclusions

This chapter mainly investigates the effects of surfactants on the skin layer formation and the drying process of latex film with a wet film thickness in the millimeter range. Figure 5.6 gives a schematic illustration with a global summary of the various stages in drying a low-T_g latex film with the demonstration of the effects of post-added surfactants. The OCT-Gravimetry-Video characterizations monitored the microscopic OCT profile, the global drying curve and the appearance of the film simultaneously. With post-added surfactant in the latex, the film shows a lower water content in the wet domain (k_w^*) at the inflection point when the drying rate was slowed down by the maturation of skin layer, with the results of a noticeable faster increment of coalesced layer thickness (h_{coal}) with time and a shorter film drying time. Such results are explained by the time delay of particles' coalescence (see the schematic illustration in Figure 5.6). With more post-added surfactant in the latex, more surfactant molecules are adsorbed on the particles' surface. During the drying process, they can act as a "potential energy barrier" (due to the particles' repulsive

interactions) and a "physical barrier" (due to the desorbed surfactant molecules trapped between particles) in impeding the coalescence between deformed particles. During the coalescence delay time (Δt_{del}), water still evaporates fast through the boundaries between non-coalesced particles in the incipient skin layer. In this way, more water evaporates before the incipient skin matures into a low-permeable skin, so that k_w^* can be lower, and less time is needed for drying and film formation of the wet domain. According to the coalesced layer thickening model (Equation 5.1), less k_w^* makes h_{coal} to increase faster, agreeing with the results of OCT profiles.

Based on such concept, Δt_{del} can be defined as the time required for k_w^* to decrease from the value of the original latex film without post-added surfactant to the value of latex+surfactant film at the inflection point. The Δt_{del} is correlated with the surfactant surface coverage (SC_{sur}) which is a function of the amount of post-added surfactant. For both ionic surfactant (SLS) and non-ionic surfactant (TTX) in PEM latex, Δt_{del} increases about linearly with SC_{sur}. Moreover, SLS is more effective than TTX in increasing Δt_{del}, as shown by its larger linear slope of Δt_{del} versus SC_{sur} (i.e. coalescence delay efficiency, $\widetilde{\Delta t}_{del}$). This may be related to the larger repulsive forces between latex particles with higher amount of adsorbed SLS molecules, giving a higher potential energy barrier; or the higher hydrophile-lipophile balance (HLB) value of SLS surfactant, giving a more hydrophilic physical barrier which is harder for the hydrophobic polymer chains from the latex particles to penetrate through. With an appropriate amount of surfactant post-added to the latex, not only the film drying time becomes much shorter, but also the water resistance of the dried film is not compromised. Nevertheless, too much surfactant in the latex either causes incomplete film formation with poor coalescence, or a high water absorption of dried film.

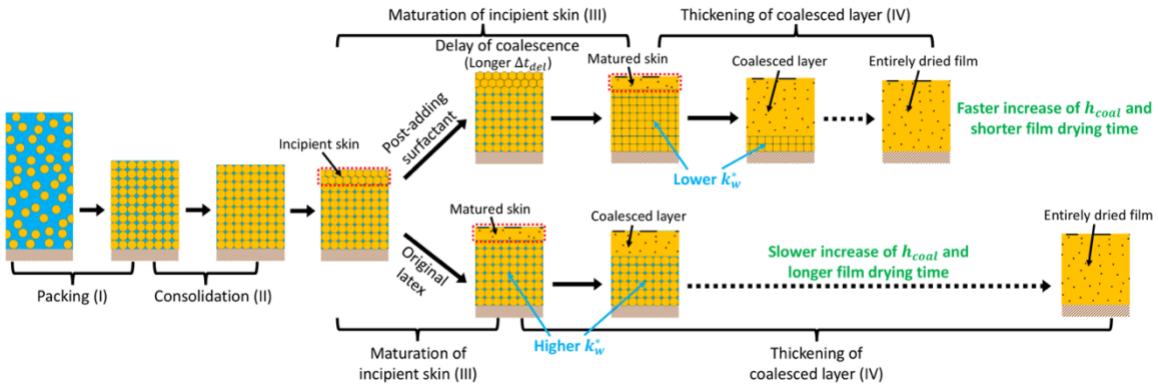

Figure 5.6: Schematic illustration of the effect of post-added surfactant on the drying process of a low-T_g latex film. The extra surfactant adsorbed on particles' surface can delay coalescence so that more water evaporates freely before the particles on film top coalesce into a low-permeable matured skin. Note that k_w^* represents the water content in the wet domain below the matured skin; h_{coal} represents the thickness of the coalesced layer.

5.5 References

1. Routh, A. F. & Russel, W. B. Deformation Mechanisms during Latex Film Formation: Experimental Evidence. *Ind. Eng. Chem. Res.* **40,** 4302–4308 (2001).
2. Carter, F. T., Kowalczyk, R. M., Millichamp, I., Chainey, M. & Keddie, J. L. Correlating Particle Deformation with Water Concentration Profiles during Latex Film Formation: Reasons That Softer Latex Films Take Longer to Dry. *Langmuir* **30,** 9672–9681 (2014).
3. Winnik, M. & Feng, J. Latex blends: an approach to zero VOC coatings. *JCT J. Coat. Technol.* **68,** 39–50 (1996).
4. Erkselius, S., Wadsö, L. & Karlsson, O. J. Drying rate variations of latex dispersions due to salt induced skin formation. *J. Colloid Interface Sci.* **317,** 83–95 (2008).
5. Mallégol, J.; Bennett, G.; McDonald, P. J.; Keddie, J. L. & Dupont, O. J. Origins and Effects of a Surfactant Excess near the Surface of Waterborne Acrylic Pressure-Sensitive Adhesives. *Langmuir* **18,** 4478–4487 (2002).
6. Pohl, K., Adams, J. & Johannsmann, D. Correlation between Particle Deformation Kinetics and Polymer Interdiffusion Kinetics in Drying Latex Films. *Langmuir* **29,** 11317–11321 (2013).
7. El-Aasser, M. S. & Robertson, A. A. A study of interparticle forces in latexes by ultracentrifugation. *Kolloid-Z. Z. Für Polym.* **251,** 241–250 (1973).
8. Kalekar, M. S. & Bhagwat, S. S. Dynamic Behavior of Surfactants in Solution. *J. Dispers. Sci. Technol.* **27,** 1027–1034 (2006).
9. Richard, J., Mignaud, C. & Wong, K. Water vapour permeability, diffusion and solubility in latex films. *Polym. Int.* **30,** 431–439 (1993).

10. Ottewill, R. H. Stabilization of Polymer Colloid Dispersions. in *Emulsion Polymerization and Emulsion Polymers* (eds. Lovell, P. A. & El-Aasser, M. S.) 59–121 (Wiley, 1997).

11. König, A. M., Weerakkody, T. G., Keddie, J. L. & Johannsmann, D. Heterogeneous Drying of Colloidal Polymer Films: Dependence on Added Salt. *Langmuir* **24,** 7580–7589 (2008).

12. El-Aasser, M. S. & Robertson, A. A. An ultracentrifugation technique for the study of latex coalescence. *J. Colloid Interface Sci.* **36,** 86–93 (1971).

13. Agarwal, N. & Farris, R. J. Water absorption by acrylic-based latex blend films and its effect on their properties. *J. Appl. Polym. Sci.* **72,** 1407–1419 (1999).

14. van der Wel, G. K. & Adan, O. C. G. Moisture in organic coatings — a review. *Prog. Org. Coat.* **37,** 1–14 (1999).

15. Haynes, W. M. CRC Handbook of Chemistry and Physics, 95th Edition. (CRC Press, 2014).

16. Porcel, R., Jódar, A. B., Cabrerizo, M. A., Hidalgo-Álvarez, R. & Martín-Rodríguez, A. Sequential Adsorption of Triton X-100 and Sodium Dodecyl Sulfate onto Positively and Negatively Charged Polystyrene Latexes. *J. Colloid Interface Sci.* **239**, 568–576 (2001).

17. Colombié, D., Landfester, K., Sudol, E. D. & El-Aasser, M. S. Competitive Adsorption of the Anionic Surfactant SLS and the Nonionic Surfactant Triton X-405 on Polystyrene Latex Particles. *Langmuir* **16**, 7905–7913 (2000).

18. Conway, J. H. & Sloane, N. J. A. Sphere Packings, Lattices and Groups. (Springer New York, 1999).

19. Bruce, C. D., Berkowitz, M. L., Perera, L. & Forbes, M. D. E. Molecular Dynamics Simulation of Sodium Dodecyl Sulfate Micelle in Water: Micellar Structural Characteristics and Counterion Distribution. *J. Phys. Chem. B* **106**, 3788–3793 (2002).

20. Neugebauer, J. M. Detergents: An overview. in Methods in Enzymology 182, 239–253 (Elsevier, 1990).

21. Loncar, F. Analysis, Kinetics and Alkali-swellability of Carboxylated Latexes. (Lehigh University, 1985).

22. Kim, H.-B. & Winnik, M. A. Factors Affecting Interdiffusion Rates in Films Prepared from Latex Particles with a Surface Rich in Acid Groups and Their Salts. *Macromolecules* **28**, 2033–2041 (1995).

6 Chapter 6 Study of Film Formation and Skin Layer during Drying of a Commercial Latex

6.1 Introduction

Skin layer formation is the process that takes place during drying of a latex film, in which the latex particles on the film top (film/air interface) become dried early on and coalesce into a polymer skin that traps water beneath it (in the wet domain). It is usually encountered by drying a low- T_g thick latex film when the Peclet number $Pe > 1$ and the dimensionless number $\bar{\lambda} < 1$ (defined as Equations 1.1 and 1.2 in Chapter 1, respectively). The drying process of a low-T_g latex film with a thickness in the millimeter range experiences four stages (see Figure 4.4 in Chapter 4): I) packing of particles (where particles become in contact with each other which cause their Brownian motions to be restricted), II) consolidation of particles (where particles become more densely packed or distorted), III) formation and maturation of an incipient skin layer (where deformed particles on the film top become coalesced into a transparent and coherent polymer skin), IV) thickening of coalesced latex polymer layer (coalesced layer) (where the particles in the wet domain below the skin continue to coalesce until the entire film becomes dried and transparent). The matured skin layer and the coalesced layer are both made of coalesced latex particles with a similar water vapor permeability (WVP) which is usually low due to polymer's hydrophobicity. Although the drying rate during Stages I and II is fast and close to that of DI water, the water evaporation during Stages III and IV becomes very slow and limited by the thickness and WVP of the skin and coalesced layer. Thus, the entire film drying time largely depends on how long it takes for the water in the wet domain to evaporate

through the skin and coalesced layer or how long it takes for the thickness of coalesced layer (h_{coal}, which includes the skin layer thickness) to increase until the entire film becomes transparent. An equation, called "the coalesced layer thickening model", was developed as Equation 4.6 in Chapter 4 to describe and predict the increment of h_{coal} with time:

$$h_{coal}(t) = A_{coal}(t - t_{coal})^{1/2} = \sqrt{\frac{2\mathrm{WVP} \cdot p_0 \cdot \Delta RH}{\rho_s k_w^* / (1 - k_w^*)}} \cdot (t - t_{coal})^{1/2} \qquad (6.1)$$

where A_{coal} is the "coalesced layer thickening prefactor", t_{coal} is the point in time when the coalesced layer begins to increase, t is the time from the start of drying ($t \geq t_{coal}$), p_0 is the equilibrium vapor pressure at room temperature, ΔRH is the difference of relative humidity between the wet domain and the air, ρ_s is the density of solid (mainly polymer) and approximately equal to water (1 g/cm^3) herein, and k_w^* is the water content (or water's weight percentage) in the wet domain below the skin or coalesced layer.

One effective way to shorten the film drying time is to make k_w^* smaller so that h_{coal} increases faster with time and thus less time is needed for the remaining water in the wet domain to evaporate through the skin and coalesced layer. As investigated in Chapter 5, this can be achieved by post-adding surfactants into the latex after the emulsion polymerization while prior to the drying process. With more surfactant molecules adsorbed on latex particles' surface, the effects of "potential energy barrier" (due to the increased repulsive interactions between particles) and "physical barrier" (due to the desorbed surfactant molecules and water-soluble oligomers as well as other molecules trapped within

interstices between particles) can delay the coalescence of particles and extend the time duration of Stage III. In this way, more water can evaporate freely through boundaries between non-coalesced particles within the incipient skin before a matured skin is formed, leading to a lower k_w^*. According to Equation 6.1, A_{coal} becomes larger and the coalesced layer thickens faster with time. In Chapter 5, it was reported that the coalescence delay time (Δt_{del}) increases linearly with the percentage of particles' surface coverage by surfactant molecules (SC_{sur}). At the same level of SC_{sur}, sodium lauryl sulfate (SLS) was found to give a longer Δt_{del} than Triton X-100 (TTX) does, possibly due to the higher "potential energy barrier" (larger repulsive forces) between particles imparted by SLS or the more hydrophilic "physical barrier" made of SLS molecules due to the SLS's higher hydrophile-lipophile balance (HLB) value.

This chapter covers the studies conducted on the processes of skin layer formation and film formation of a commercial latex (called "PLB" latex, as will be introduced in the next section). This PLB latex, with four copolymer's compositions (lauryl methacrylate, n-butyl acrylate, methyl methacrylate units, and a minor amount of methacrylic acid units), is widely used as the architectural waterproof coatings with dry film thicknesses in the millimeters' range. This latex film has a serious drying problem, trapping near 15 wt% water in the film when the skin and coalesced layer is formed. The large amount of water in the wet domain of the film causes a poor adhesion to the substrate and can form water vapor bubbles within the film when heated by the sun. The drying of the PLB latex with an initial wet film thickness of 2 mm under room condition takes >12 days to get 95% of water evaporated. The effects of post-added SLS surfactant and other water-soluble additives on the drying process of PLB latex film are also investigated in this chapter. The

set of experimental protocols that have been documented in Chapters 2 – 5 are followed in the studies reported in this chapter. The studies include four parts: I) the characterizations of the PLB latex (see experimental procedures in Chapter 2), II) the use of OCT-Gravimetry-Video characterizations (see experimental procedures in Chapters 3 – 5) to follow the drying process of the PLB latex films, III) the drying curves' measurement under the controlled environment at 23 ℃ and 50% RH (see experimental procedures in Chapter 5), and IV) the water absorptions' measurement of the dried PLB latex films (see experimental procedures in Chapter 5). In Part I, the latex solids content (k_{s0}), the polymer T_g, the particle size and size distribution, the adsorption isotherm of SLS surfactant on particles' surface, and the dried film's water vapor permeability (WVP) of the commercial PLB latex were measured. In Part II, the microscopic internal structure (by OCT), the global drying curve (by gravimetry) and the macroscopic appearance (by video) of the commercial latex films without and with post-added SLS into the PLB latex were characterized simultaneously as a function of drying time. In Part III, the coalescence delay times (Δt_{del}) that postpone the formation of matured skin layer were derived based on the measured drying curves (at constant temperature at 23 ℃ and humidity at 50% RH without wind) of the PLB latex films without and with post-added SLS or other water-soluble additives in the latex. In Part IV, the effects of post-added SLS and other additives on the water absorptions of the dried PLB latex films were investigated, in order to select the appropriate additives that can shorten the film drying time while not compromising the water resistance property of the dried coating.

6.2 Materials and methods

6.2.1 Commercial PLB latex system and its characterizations

The polymer particles in the commercial latex, which are stabilized by a mixture of ionic and non-ionic ethoxylated surfactants, have the copolymer compositions of 40 wt% lauryl methacrylate (LMA) units, 35 wt% n-butyl acrylate (BA) units, 24 wt% methyl methacrylate (MMA) units and 1 wt% methacrylic acid (MAA) units[1]. The latex is designated as "poly(40LMA/35BA/24MMA/1MAA) latex" or "PLB latex" for short.

The % solids content (k_{s0}, which is mostly polymers) of the PLB latex was measured as 53.07 or 55.30, due to the different synthesis batches.

According to the densities of the homopolymers[2], the copolymer density of poly(40LMA/35BA/24MMA/1MAA) is calculated to be 1.02 g/cm^3. In the calculation of film thickness and latex particles' volume fraction, the density of polymer (or solid, ρ_s) and the density of latex (ρ) are set to be about the same as that of water ($\rho = \rho_s = \rho_w = 1\ \mathrm{g/cm^3}$).

The T_g of PLB's polymer was measured as -10 ℃.

The latex particle size (diameter, D_p) and size distribution were measured by transmission electron microscopy (TEM) and dynamic light scattering (DLS). By measuring the sizes of 1000 particles under TEM, the size distributions based on both number percentage and weight percentage are derived and shown in Figure 6.1 which also shows a TEM micrograph. The number average diameter (d_n), the surface-area average diameter (d_s), the weight average diameter (d_w), the volume average diameter (d_v), the diameter standard deviation (SD) and the polydispersity index (PDI) are calculated as 402

nm, 463 nm, 497 nm, 431 nm, 108 nm and 1.24, respectively. The D_p measured by dynamic light scattering (d_{LS}) is found to be 333 nm with 100 nm standard deviation. It should be noted that the particle sizes measured by TEM are larger by 69 nm (for d_n), and by 164 nm (for d_w) than that measured by DLS. The reason might be the broad size distribution of PLB latex particles (PDI = 1.24), leading to large errors in size measurements. All the particle sizes of both PLB and PEM measured by DLS and TEM are summarized in Table 6.1. To be consistent with previous chapters, the D_p measured by DLS (d_{LS} = 333 nm of PLB latex) will be used to calculate the particle's surface area of PLB latexes in this chapter.

Table 6.1: DLS and TEM measurements of particle sizes of all model latex systems, given as particle diameters (D_p)

Latex	D_p by DLS		D_p by TEM					
	d_{LS} (nm)	SD (nm)	d_n (nm)	SD (nm)	d_w (nm)	PDI	d_s (nm)	d_v (nm)
PLB	333[b]	100	402	108	497	1.24	463	431
PEM[a]	176[b]	18	182	28	194	1.07	190	186

[a] The particle sizes of PEM latex measured by DLS and TEM are abstracted from Table 2.4 in Chapter 2.

[b] It should be noted that D_p measured by DLS is smaller than those measured by TEM for both PLB and PEM latexes. The latex particles after being dried on the TEM's carbon grid became a bit flattened and appeared larger due to the deformation of particles despite the treatment with phosphotungestic acid. (see the partially deformed particles of PLB latex in the TEM micrograph in Figure 6.1 and those of PEM latex in Figure 2.2A in Chapter 2).

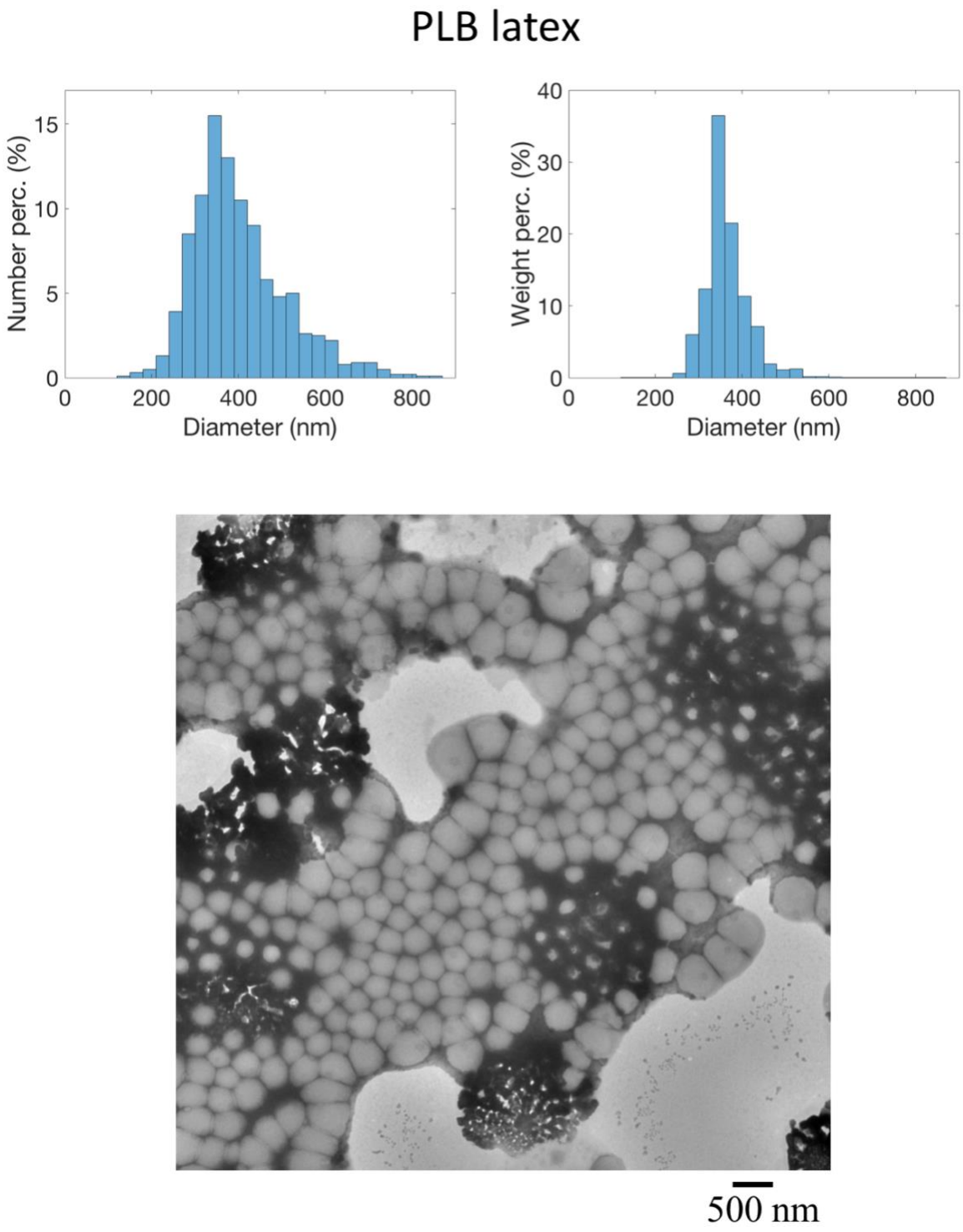

Figure 6.1: Particle size distributions (based on both number percentage and weight percentage) and a TEM micrograph of PLB latex. The scale bar at the bottom right corner of TEM micrograph denotes 500 nm.

The water vapor permeability (WVP) of the PLB dried latex film was measured as $(6.0 \pm 0.2) \times 10^{-11}$ g/(cm · min · Pa) (also mentioned in Section 6.2.5).

The SLS surfactant adsorption isotherm curve was derived by measuring the surface tensions of the 5x diluted PLB latex and its serum with different amounts of post-added SLS surfactant, following the same procedures as documented in Section 2.3.3 in Chapter 2. Figure 6.2 shows the surface tension vs. SLS concentration graphs, and the SLS adsorption isotherm curve which can be described by the following equation:

$$\varphi_{SLS,p}(c_{SLS,aq}) = \begin{cases} \tilde{\varphi}_{SLS} c_{SLS,aq}, & 0 < c_{SLS,aq} \leq CMC_{serum} \\ \varphi_{SLS,p,max}, & c_{SLS,aq} > CMC_{serum} \end{cases} \quad (6.2)$$

where $\varphi_{SLS,p}$ is the SLS number density adsorbed on latex particles' surface (number of molecules per nm^2 on particle surface), $c_{SLS,aq}$ is the surfactant concentration (in mM) in aqueous phase, CMC_{serum} is the critical micelle concentration of SLS in aqueous phase (or serum), $\varphi_{SLS,p,max}$ is the maximum SLS number density adsorbed on latex particles' surface, and $\tilde{\varphi}_{SLS}$ is the linear slope of $\varphi_{SLS,p}$ vs. $c_{SLS,aq}$ before $\varphi_{SLS,p}$ reaches its maximum. For the PLB system, $\tilde{\varphi}_{SLS} = 0.558$ nm^{-2}/mM, $CMC_{serum} = 2.20$ mM, and $\varphi_{SLS,p,max} = 1.22$ nm^{-2}. All the characterizations of the PLB latex above follow the same procedures as documented in Chapter 2. The results are summarized in Table 6.2.

Table 6.2: Characterization results of the PLB latex system

Latex	Polymer composition (weight ratios of polymerized monomers)	Solids content k_{s0} (%)	Poly-mer Tg (°C)	Particle diameter, D_p	
				by DLS (nm)	d_s by TEM (nm)
PLB	40LMA/35BA/24MMA/1MAA	53.07 or 55.30	-10	333 (SD=100)	463 (SD=108)

Latex	SLS adsorption isotherm			WVP of dried latex film [a] ($g/(cm \cdot min \cdot Pa)$)
	$\tilde{\varphi}_{SLS}$ (nm^{-2}/mM)	CMC_{serum} (mM)	$\varphi_{SLS,max}$ (nm^{-2})	
PLB	0.558	2.20	1.22	$(6.0 \pm 0.2) \times 10^{-11}$

[a] The water vapor permeability (WVP) of the dried latex film is determined in Section 6.2.5.

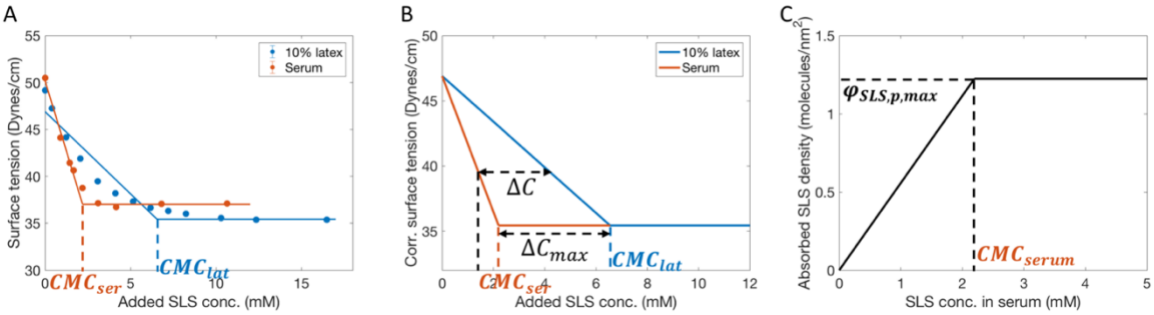

Figure 6.2: (A) measured surface tension curves of 5x diluted PLB latex and its serum – surface tensions as a function of added SLS concentrations (based on the aqueous phase). (B) modified surface tension curves of 5x diluted PLB latex and its serum. (C) SLS adsorption isotherm curve of the PLB latex system.

6.2.2 PLB latex systems with post-added SLS surfactant and other water-soluble additives

The water-soluble additives used in this chapter include: sodium lauryl sulfate (SLS) from Alfa Aesar, Triton X-100 (TTX) from Sigma-Aldrich, ammonium polyacrylate (APA) from Dow Chemical, and polyethylene glycol (PEG) from Sigma-Aldrich. The average molecular weights of SLS, TTX, APA and PEG are 288 g/mol, 625 g/mol, 2500 g/mol and 1000 g/mol, respectively. The anionic (SLS) and non-ionic surfactants (TTX) adsorb on the latex particles' surface which provide colloidal stability to latex system. The APA is usually used as dispersant molecules to stabilize the inorganic pigment and/or filler particles that are dispersed into the latex for coatings applications[3]. The PEG is a typical antifreeze to offer the freeze-thaw stability to a latex coating[4].

The preparation of the PLB latex systems with these post-added additives (denoted as "PLB+additive") is as follows. The aqueous solutions of additives were first prepared and then mixed with the PLB latexes to obtain different weight ratios of additive versus PLB's solids ($k_{add/s}$, where the subscript of "add" can be SLS, TTX, APA or PEG). For example, with $k_{SLS/s}$ = 0.1% added into the PLB latex, the resulting latex is named as "PLB+0.1%SLS". Several combinations of PLB with various concentrations of above additives were prepared; these are listed in Table 6.3. The weight percentages (based on latex) and the concentrations (in mM based on aqueous phase) of the additives in the PLB+additive latexes are calculated by Equations 5.5 and 5.6 (in Chapter 5) and given in Table 6.3. It should be noted that a mixture of ionic and non-ionic surfactants also exists in the original PLB latex, which may have molecular interactions with these post-added additives.

For the "PLB+SLS" series, there are equilibrium distributions between the SLS surfactant molecules adsorbed on the latex particles' surface and those soluble in the aqueous phase. Table 6.3 lists the related following data. The surfactant number density adsorbed on latex particles' surface ($\varphi_{SLS,p}$, number of surfactant molecules per nm^2 on particle surface), the surfactant concentration in aqueous phase ($c_{SLS,aq}$) and the partition coefficient (K_D, the mole amount ratio of surfactant molecules on particle surface versus those in aqueous phase), and the SLS surfactant surface coverage (SC_{SLS}, % of particle surface covered by SLS molecules) are derived by Equations 5.12, 5.13, 5.15, 5.16, 5.17 and 5.18 (in Chapter 5), based on the measured SLS adsorption isotherm curve (Equation 6.2). Although there may exist molecular interactions between the post-added SLS and the ethoxylated surfactant in the original latex or the oligomers soluble in water that influence the SLS's adsorption property, in this chapter it is assumed that the SLS molecules adsorb independent of other species on the particles' surface.

The $\varphi_{SLS,p}$'s, $c_{SLS,aq}$'s, K_D's and SC_{SLS}'s of the PLB+SLS series are also listed in Table 6.3. As discussed in Section 5.2.4 (Chapter 5), due to the large K_D's (~20, see Table 6.3) of PLB+0.1%SLS, PLB+0.3%SLS, PLB+0.5%SLS and PLB+1%SLS, $\varphi_{SLS,p}$, $c_{SLS,aq}$ and SC_{SLS} should almost remain constant during the drying process from the start of drying with k_{s0} = 55% to the time when the latex solids content k_s becomes 64% (closely random packing).

As for the PLB+2%SLS latex with SLS reaching $\varphi_{SLS,p,max}$, the concentration of SLS in the aqueous phase $c_{SLS,aq}$ increases with time while $\varphi_{SLS,p}$ remains constant at $\varphi_{sur,p,max}$, since the surfactant molecules in aqueous phase cannot continue to adsorb on particles' surface during drying. In Section 6.3.2, the particle surface coverage by SLS

surfactant molecules SC_{SLS}'s in the initial latex will be used to correlate with the measured coalescence delay time (Δt_{del}).

Table 6.3: PLB latex systems with post-added SLS surfactant and other water-soluble additives

Latex	k_{s0} (%)	$k_{add/s}$ (%)	Added additive weight perc. (%)[b]	Added additive conc. (mM)[c]	$\varphi_{SLS,p}$ (1/nm^2)	$c_{SLS,aq}$ (mM)	K_D	SC_{SLS} (%)	Δt_{del} (min)[e]
PLB [a]	55.3	0	0	0	0	0	/	0	0
PLB+0.1%SLS	55.25	0.1	0.06	4.3	0.11	0.20	20.6	9.0	14.8
PLB+0.3%SLS	55.14	0.3	0.17	12.8	0.33	0.59	20.5	27.1	60.9
PLB+0.5%SLS	55.04	0.5	0.28	21.2	0.55	0.99	20.4	45.1	98.7
PLB+1%SLS	54.78	1	0.55	42.0	1.10	1.98	20.2	90.2	134.1
PLB+2%SLS [d]	54.27	2	1.09	82.3	1.22	38.8	1.12	100 [d]	141.3
PLB [a]	55.30	0	0	0	/	/	/	/	0
PLB+2%APA	53.45	2	1.07	9.2	/	/	/	/	-55.8
PLB+2%PEG	53.45	2	1.07	23.0	/	/	/	/	33.3
PLB+2%TTX	53.45	2	1.07	36.7	/	/	/	/	82.3
PLB+2%SLS	53.45	2	1.07	79.7	/	/	/	/	146.3

[a] It should be noted that a mixture of ionic and non-ionic surfactants exists in the original PLB latex, which may have molecular interactions with the post-added additives listed in this table.

[b] Weight percentages of additives are based on the original PLB latex.

[c] Concentrations of additives, given in mM, are based on the aqueous phase.

[d] The amount of total SLS in PLB+2%SLS latex is already more than that is needed to reach the maximum surface coverage (SC_{SLS} = 100%); the extra surfactant molecules remain in the aqueous phase in the form of micelles.

[e] The coalescence delay times (Δt_{del}'s) are determined in Section 6.2.4, based on the measured drying curves under a controlled environment (23 °C and 50% RH without wind).

6.2.3 OCT-Gravimetry-Video method

The OCT-Gravimetry-Video method was used to monitor the internal microstructure, the global drying curve and the macroscopic appearance of a latex film during its entire drying process, following the same procedures documented in Section 4.2.2 (Chapter 4).

The initial weight of the latex film in the Petri dish was set at ~1.8 mm-thickness (with ~55% solids content) so that the thickness of dried latex film (with no water) is expected to be 1 mm. All characterizations were synchronized and data taken every 2 minutes. In the OCT profile, the processes of particles' packing, consolidation, skin layer formation and coalesced layer thickening were visualized. The "film thickness", the "packed layer thickness", the "skin layer thickness" (h_{skin}) and the "coalesced layer thickness" (h_{coal}, which includes the skin layer thickness) as a function of drying time were also measured based on the OCT profile.

The OCT-Gravimetry-Video characterizations results of PLB, and PLB+SLS latex films are reported and discussed in Section 6.3.1.

6.2.4 Measurement of drying curves under controlled environment

Two types of drying curves were measured under controlled environment (23 ℃ and 50% RH without wind) of latex films with an initial wet thickness at ~1.8 mm (so that the thickness of dried latex film (with no water) was expected to be 1 mm). One type is the "continuous drying curve" where the drying data were taken every 2 min's, following the procedures documented in Section 4.2.3 (Chapter 4). Figure 6.5A in Section 6.3.2 shows the continuous drying curves ($w(t)$), the drying rate curves ($dw(t)/dt$) and the film water

content curves ($k_w(t)$) of PLB and PLB+SLS latex films as a function of time up to 3000 minutes (2.1 days).

The second type is the "discrete drying curve" where the drying data were taken once per day. This is a more effective way to glean the drying data of multiple latex films all together at different times, although the time resolutions are sacrificed. Figure 6.5B in Section 6.3.2 shows the discrete drying curves (or data points) of $w(t)$ and $k_w(t)$ of PLB, PLB+2%APA, PLB+2%PEG, PLB+2%TTX and PLB+2%SLS latex films as a function of time up to 8600 minutes (6.0 days). The $dw(t)/dt$ curves were not obtained, because the time interval between two adjacent $w(t)$ points was too long to get an accurate derivative of w versus t.

Since the dryings started at slightly different initial solids contents (see k_{s0}'s in Table 6.3), both of the two types of drying curves were intentionally shifted along the time axis so that all started at the same solids content of 55% (or k_w = 45%).

6.2.5 Water vapor permeability (WVP) and water absorption of dried latex film

The water vapor permeability (WVP) of the dried latex film with a 1 mm film thickness was measured following the same procedure documented in Section 2.3.4 in Chapter 2. WVP has the expression (see Equation 2.18 in Chapter 2) as:

$$\text{WVP} = \frac{JH_{dry}}{p_0 \cdot \Delta RH} \qquad (6.3)$$

where J is the water flux through the dried film (water mass loss per unit film area per unit time), H_{dry} is the dried film thickness, p_0 is the equilibrium vapor pressure at room

temperature, and ΔRH is the difference of relative humidities on two sides of film. The WVP's of the PLB dried film and the PLB+2%SLS dried film were measured and given in Table 6.4 in Section 6.3.3.

The water absorption curve, i.e. the relative absorbed water mass (R_{abs}, the mass ratio of the absorbed water versus the dried film) as a function of immersion time (t) in DI water, was measured on the dried latex film with a 1 mm film thickness in the Petri dish, following the same procedure documented in Section 5.2.9 in Chapter 5. R_{abs} of a dried latex film is usually proportional to $t^{1/2}$ (see Figure 5.5B for PEM+additive films, and Figure 6.7B for PLB+additive films), corresponding to the Fickian absorption kinetics[5]. The water absorption efficiencies ($\tilde{R}_{abs}$'s, the linear fitting slopes of R_{abs} versus $t^{1/2}$) are derived and given in Table 6.4 in Section 6.3.3.

6.3 Results and discussions

6.3.1 OCT-Gravimetry-Video characterizations and the effects of SLS surfactant

Figure 6.3 presents the characterization results by the OCT-Gravimetry-Video method on the PLB, PLB+0.5%SLS and PLB+1%SLS latex films with an initial wet film thickness of 1.8 mm (with latex solids of about 55% and a final dried film thickness expected to be 1 mm). While the room temperature was relatively constant (24 – 26 °C), the relative humidity was not controlled in the lab, which varied from 7% RH (in Figure 6.3A) to 43% RH (in Figure 6.3B). With the polymer T_g (-10 °C), the average particle diameter (333 nm as measure by DLS) and the initial drying rate (3.3×10^{-4} g/(cm^2 · min) at 26 °C and 7% RH), calculations[1] show that the Peclet number $Pe = 74.6 > 1$ and the dimensionless

parameter $\bar{\lambda} = 4.0 \times 10^{-3} < 1$, meaning that skin layers should form during the drying processes of PLB latex films.

Similar to the PEM latex film (see Figure 5.3A), the OCT profile in Figure 6.3A (top left) also shows that the drying process of the PLB latex film experienced four stages: I) packing of particles, II) consolidation of particles, III) formation and maturation of incipient skin layer and IV) thickening of coalesced layer. However, Stage III for the PLB film was not evident, since there was no apparent thin incipient skin with a constant skin thickness before the point in time when the coalesced layer's thickness began increasing with time (t_{coal} = 180 min, see the red arrows in Figure 6.3A (top left & top right)). This is either because the incipient skin was too thin to be detectable by the OCT profile (with a resolution of 4.5 μm which is equivalent to ~14 layers of packed PLB latex particles) before t_{coal}, or Stage III happened so fast near t_{coal} that it was not captured by the 2 min's time resolution. Thus, in the OCT profile in Figure 6.3A, Stages III and IV were combined after t_{coal}. The corresponding film thickness curve, the packed layer thickness curve and the coalesced layer thickness (h_{coal}) curve as a function of drying time are shown in Figure 6.3 A (top right). The film thickness decreased linearly with time before t_{coal} due to the free water evaporation, then became almost constant abruptly after t_{coal} due to the impeded drying by the skin and coalesced layer. The global drying curve (film water content curve, $k_w(t)$) in Figure 6.3A (bottom left) shows the inflection point at t_{infl} = 250 min when the low-permeable skin layer covered the entire drying area of the film. The time difference between t_{infl} and t_{coal} indicates the drying inhomogeneity along the horizontal direction during which the drying boundary propagated along the film surface. The film water content at the inflection point ($k_{w,infl}$ = 17.07%) can be used to represent the water

content in the wet domain below the skin/coalesced layer. The video photo at 1500 min in Figure 6.3A (bottom right) shows a white and opaque film after the inflection point, indicating a significant amount of water trapped in the film. Grooves (area with film thickness much thinner than surroundings) were also observed near the Petri dish wall.

In Figures 6.3B and C, the drying processes of PLB+0.5%SLS and PLB+1%SLS films were also found to experience Stages I – IV. The effects of the post-added SLS surfactant on the film formation process of PLB latex are manifested and discussed in three respects as follows.

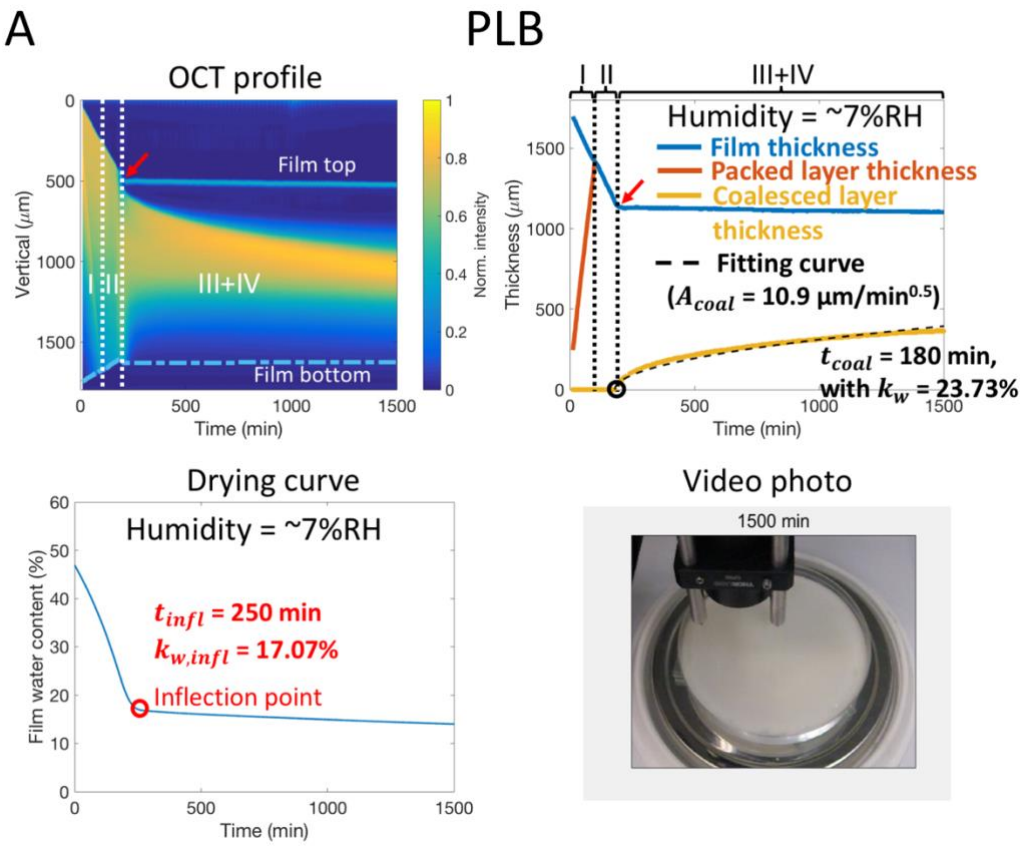
A
PLB
OCT profile
Film top
Film bottom
I
II
III+IV
Vertical (μm)
Time (min)
Norm. intensity
Humidity = ~7%RH
Film thickness
Packed layer thickness
Coalesced layer thickness
Fitting curve
(A_{coal} = 10.9 μm/min$^{0.5}$)
t_{coal} = 180 min,
with k_w = 23.73%
Thickness (μm)
Drying curve
Humidity = ~7%RH
t_{infl} = 250 min
$k_{w,infl}$ = 17.07%
Inflection point
Film water content (%)
Video photo
1500 min

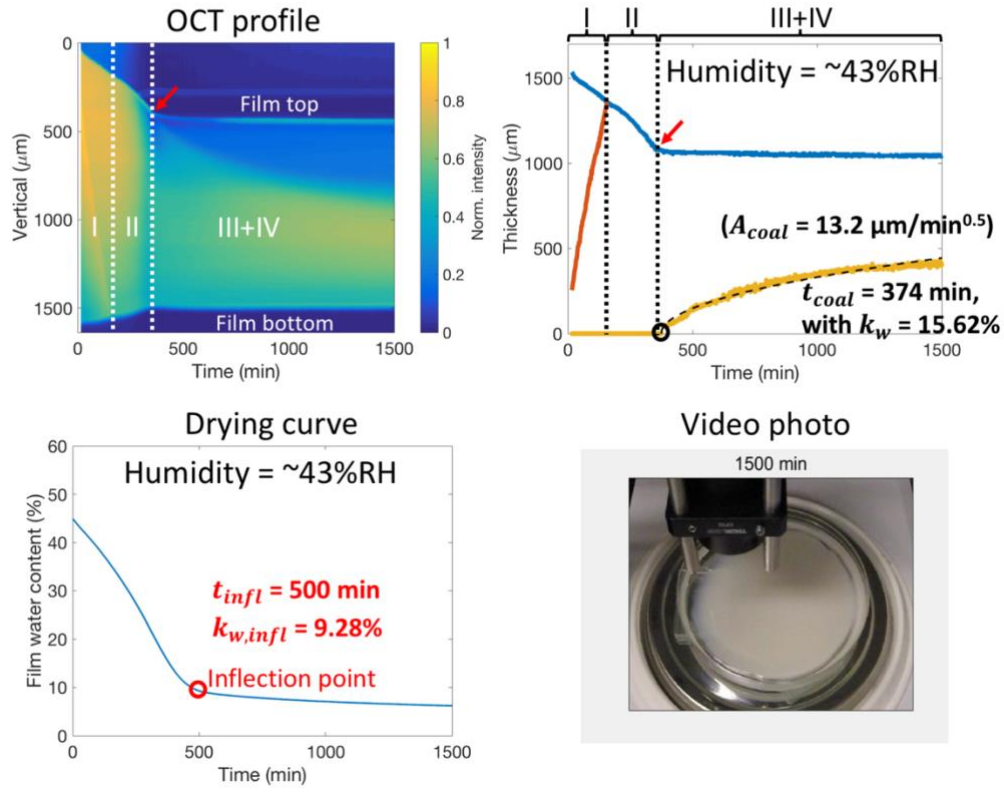
B
PLB+0.5%SLS
OCT profile
Film top
Film bottom
I
II
III+IV
Vertical (μm)
Time (min)
Norm. intensity
Humidity = ~43%RH
(A_{coal} = 13.2 μm/min$^{0.5}$)
t_{coal} = 374 min,
with k_w = 15.62%
Thickness (μm)
Drying curve
Humidity = ~43%RH
t_{infl} = 500 min
$k_{w,infl}$ = 9.28%
Inflection point
Film water content (%)
Video photo
1500 min

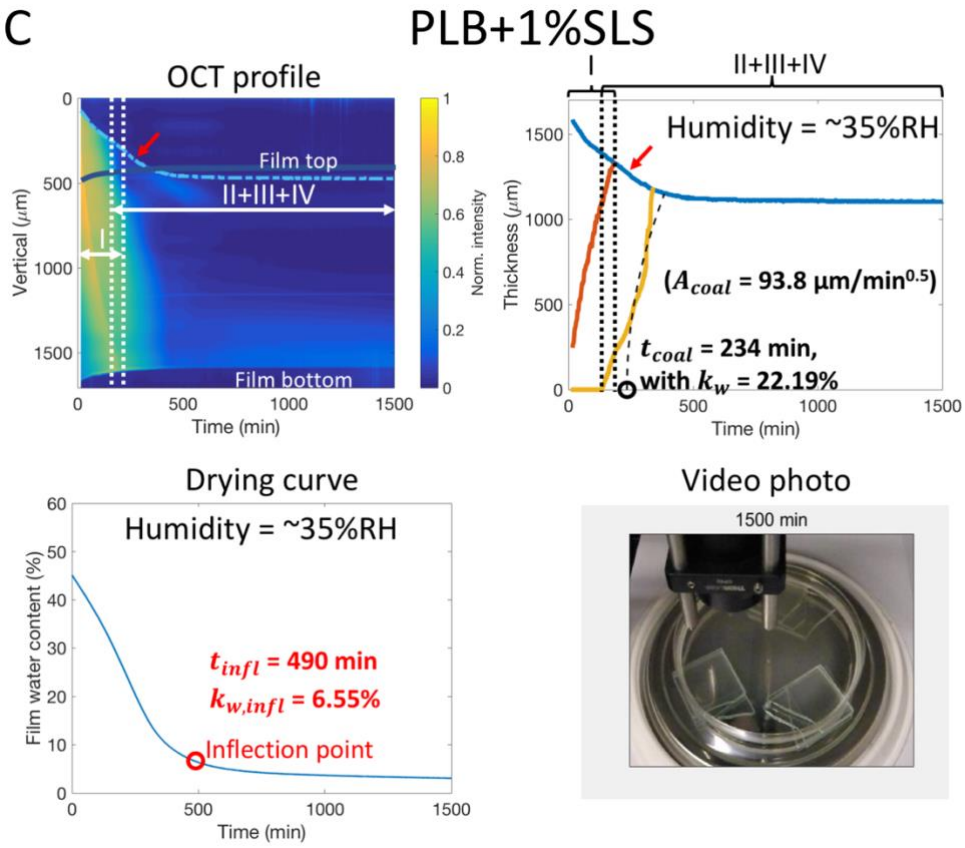

Figure 6.3: Results of OCT-Gravimetry-Video characterizations of PLB (A), PLB+0.5%SLS (B) and PLB+1%SLS (C) films with an initial wet film thickness of ~1.8 mm (with latex solids of about 55%) and a final dried film thickness of 1 mm. In each set of figures, the first (top left) figure is the OCT profile; the second (top right) are the time-evolved curves of the film thickness (blue line), the packed layer thickness (red line) and the coalesced layer thickness (yellow line, which includes the skin layer thickness), as well as the fitting curve of the coalesced layer thickening model (black dashed line); the third (bottom left) is the film water content curve ($k_w(t)$) measured by gravimetry; the fourth (bottom right) is the video photo at the drying time of 1500 min. Notes: the red arrows in the OCT profiles and the film thickness curves denote the points in time when the apparent coalesced layers begin thickening; the dark blue lines in the OCT profiles are used to cover the self-reflections of OCT image's artifacts.

1) SLS's effects on the particles' packing profile

At the end of Stage I, all latex particles in the OCT profile become packed and restricted in motions. As shown in Figure 6.4, Stage I of the PLB latex film ended at 100 min with the film water content k_w = 35.81%; that of the PLB+0.5%SLS latex film ended at 158 min with k_w = 34.76%; that of the PLB+1%SLS latex film ended at 188 min with k_w = 27.49%. For both PLB latex and PLB+0.5%SLS latex (see Figures 6.4A and B), k_w's at the end of Stage I were close to the 36% void volume fraction of closely random packing. The packed layer thicknesses increased quite linearly with time (although the packed layer thickness curve of PLB+0.5%SLS was slightly curved in Figure 6.4B), corresponding to the large Pe = 74.6 > 1. The difference of the ending times (100 min for PLB and 158 min for PLB+0.5%SLS) was due to the different initial drying rates at different environmental humidity (~7% RH for PLB and ~43% RH for PLB+0.5%SLS). Similar results were found for the drying of PEM and PEM+SLS latex films in Section 5.3.1 in Chapter 5, where the post-added SLS surfactant in the same range of concentration did not affect the packing process. Nevertheless, the packing profile of PLB+1%SLS is a bit peculiar (see Figure 6.4C). First, the increment of packed layer thickness became curved, which is faster at the beginning but slower near the end. Second, when the packing process ended at 188 min, k_w (= 27.49%), the void volume fraction was 8.5% less than the 36% of closely random packing, indicating that the particles within the packed layer already began their consolidation (Stage II) before 188 min. Moreover, after 136 min, the region near the film top became transparent (see Figure 6.3C top left) and the coalesced layer began increasing with time (see Figure 6.3C top right), indicating that the particles near the film top became fully deformed and partially coalesced even before the end of Stage I at 188 min. Thus,

there was some time overlapping between Stage I and Stages II, III & IV for the PLB+1%SLS film, as shown in Figure 6.3C. The reason for the obvious change in the packing profile with the post-added amount of SLS from 0.5% to 1% (relative to the latex solids weight) is not fully understood yet. It may be related to the constrained aqueous medium between particles, which contains water-soluble species of mixed surfactants, salts and oligomers. During the packing process where the average inter-distance (d_{in}) of separation between the PLB latex particles decreases from 46.6 nm at the start of drying to 16.7 nm when k_w = 36% (calculated by Equation 5.20 in Chapter 5), the constrained aqueous medium in the void fraction between particles, which continues to shrink with drying time, can affect the surfactant adsorption/desorption at the particles' surface as well as the particle-particle interaction that determines the Peclet number Pe.

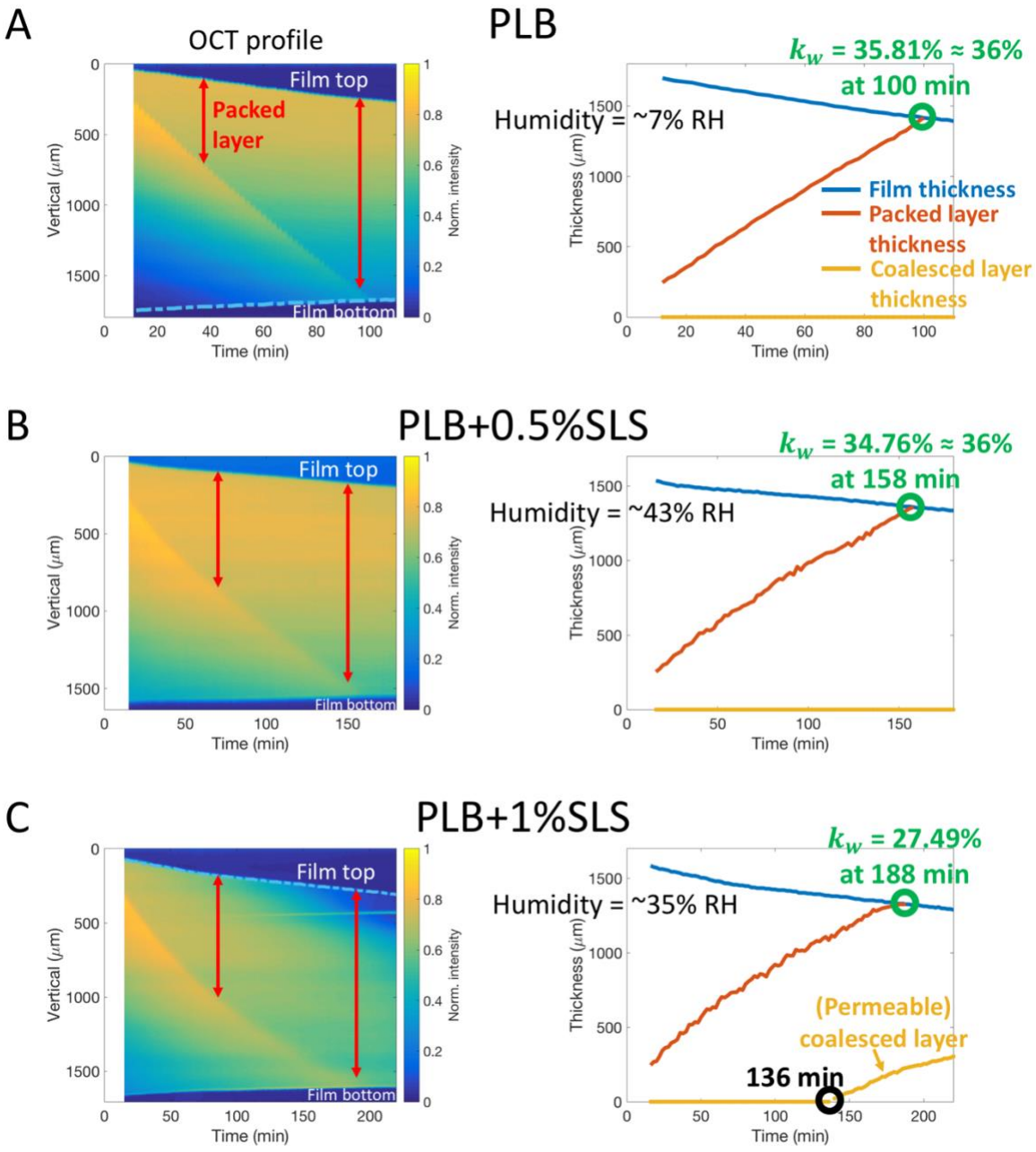

Figure 6.4: OCT profile and curves of film thickness, packed layer thickness and coalesced layer thickness during the packing process (Stage I), (A) for PLB, (B) for PLB+0.5%SLS and (C) for PLB+1%SLS films. The data were abstracted from Figure 6.3. The double headed arrows in the OCT profiles denote the packed layer where the particles' motions are restricted.

2) SLS's effects on the appearance of skin and coalesced layers

For both the PLB and the PLB+0.5%SLS latex films, the linear decrement of the film thickness was impeded abruptly at the point in time when the skin and coalesced layer appeared on the film top (see the red arrows in Figures 6.3A and B at which the film thickness curves were sharp). The appearance of skin and coalesced layer occurred after all the particles in the OCT profile became packed (Stage I) and consolidated (Stage II); the thickness of that layer could be determined by the OCT with its limited resolution of 4.5 μm. However, as discussed above for the PLB+1%SLS latex film, the skin and coalesced layer on the film top appeared even before the end of Stage I (see Figures 6.3C top right & left and 6.4C). Moreover, the film thickness curve was smoothed at the point in time when the skin and coalesced layer appeared (see the red arrows in Figure 6.3C top right & left); and even after 136 min when the coalesced layer appeared, the film thickness continued to decrease linearly (see Figure 6.4C), indicating that the particles on the film top became deformed but not fully coalesced yet (so that water evaporated freely through the boundaries between the packed particles).

3) SLS's effects on the thickening of coalesced layer

As shown in Figures 6.3 A, B & C – top right, after the skin and coalesced layer appeared on the film top, the coalesced layer thickness (h_{coal}) increased with time. With more post-added amount of SLS, h_{coal} increases faster with time, the same trend was found for the model PEM latex in Figure 5.3 (Chapter 5). This can be explained by the effect of added SLS surfactant on delaying the particles' coalescence: with the coalescence retarded or delayed, less water would be trapped in the wet domain (i.e. k_w^* is smaller in Equation 6.1)

below the matured skin with coalesced particles and low permeability which is formed after the delay-time is reached. By fitting the measured h_{coal} curves in Figure 6.3 using the coalesced layer thickening model (see Equation 6.1 in Section 6.1 above), the A_{coal}'s (the coalesced layer thickening prefactor) of PLB, PLB+0.5%SLS and PLB+1%SLS are derived as 10.9, 13.2 and 93.8 μm/min$^{0.5}$, respectively, with their t_{coal}'s (the fitted point in time at which h_{coal} begins to increase) as 180 min, 374 min and 234 min, respectively. With the WVP = 6.0×10^{-11} g/(cm · min · Pa) for all coalesced layers (Table 6.4 in Section 6.3.3 showing similar WVP's of the dried latex films for both PLB+2%SLS and PLB), p_0 = 3169 Pa at 25 °C and ΔRH's (93% for PLB, 57% for PLB+0.5%SLS and 65% for PLB+1%SLS due to the different drying humidity values), the effective water content in the wet domain below the skin or coalesced layer k_w^*'s ($k_{w,eff}^*$'s) were derived theoretically using Equation 6.1 in Section 6.1 and found to be 22.9% for PLB, 11.1% for PLB+0.5%SLS and 0.28% for PLB+1%SLS. While the theoretically determined $k_{w,eff}^*$'s for PLB and PLB+0.5%SLS are a bit larger than their experimentally determined $k_{w,infl}$'s (17.07% for PLB and 9.28% for PLB+0.5%SLS in the drying curves in Figures 6.3A and B – bottom left), and the $k_{w,eff}^*$ for PLB+1%SLS is far lower than its $k_{w,infl}$ (6.55% in the drying curve in Figure 6.3C – bottom left). Thus, in order to better fit the coalesced layer's thickening process, the mathematical model needs to be improved with the considerations of the amount of strong-bonded water in the coalesced layer, the non-uniform water distribution in the wet domain and even the time-evolving WVP of the coalesced layer.

6.3.2 The use of drying curves to determine the coalescence delay times (Δt_{del}) of PLB+additive latex films

In Section 5.2.8 (Chapter 5), the coalescence delay time (Δt_{del}) was determined from the difference of k_w's at the inflection points ($k_{w,infl}$'s on the continuous drying curves) between the original latex and the latex with a post-added surfactant. However , since some drying curves are discrete in this chapter (see Figure 6.5B), the k_w's at 2000 min ($k_{w,2k}$'s) are used to determine Δt_{del}; if the drying data is not measured exactly at 2000 min, $k_{w,2k}$ can be obtained as the value at 2000 min on the line connecting the two adjacent k_w points near 2000 min (see the intersections of the black dashed line and the colored dashed lines that connect the two adjacent k_w points near 2000 min in $k_w(t)$ curves in Figure 6.5B). The reason is that the difference of $k_{w,infl}$'s is actually about the same as that of $k_{w,2k}$'s. In the example of the $k_w(t)$ curves of PLB and PLB+2%SLS in Figure 6.5A, the $k_{w,infl}$ difference is 12.81% - 4.29% = 8.52%, which is similar to the $k_{w,2k}$ difference as 11.59% - 3.12% = 8.47% (see Figure 6.5B). Therefore, by replacing $k_{w,infl0}$ and $k_{w,infl1}$ with $k_{w,2k0}$ ($k_{w,2k}$ of the original latex) and $k_{w,2k1}$ ($k_{w,2k}$ of the latex with a post-added additive) in Equation 5.23 (Chapter 5), the Δt_{del}'s of the PLB+SLS latex series and the PLB+(other additive) latexes are derived as:

$$\Delta t_{del} = \frac{m_s}{v_0} \cdot \frac{k_{w,2k0} - k_{w,2k1}}{\left(1 - k_{w,2k0}\right)\left(1 - k_{w,2k1}\right)} \qquad (6.4)$$

where v_0 is the initial drying rate of free water (7.0×10^{-5} g/(cm^2 · min)) and m_s is the solid mass in the latex per unit area (0.1 g/cm^2 with 1 mm dried film thickness herein). The results of Δt_{del}'s which are derived from the drying curves of all latex films given in Figure

6.5 are listed in Table 6.3 (Section 6.2.2). The coalescence delay times Δt_{del}'s are plotted in Figure 6.6 (Section 6.3.3) as a function of percent particles' surface coverage with post-added SLS surfactant and also as a function of weight ratios of all additives versus PLB's solids. It should be noted that in Table 6.3, the Δt_{del} of the PLB+2%SLS film determined by the continuous drying curve in Figure 6.5A (141.3 min) is similar to that determined by the discrete drying curve in Figure 6.5B (146.3 min), which shows more confidence that the two types of drying curves are giving almost the same results.

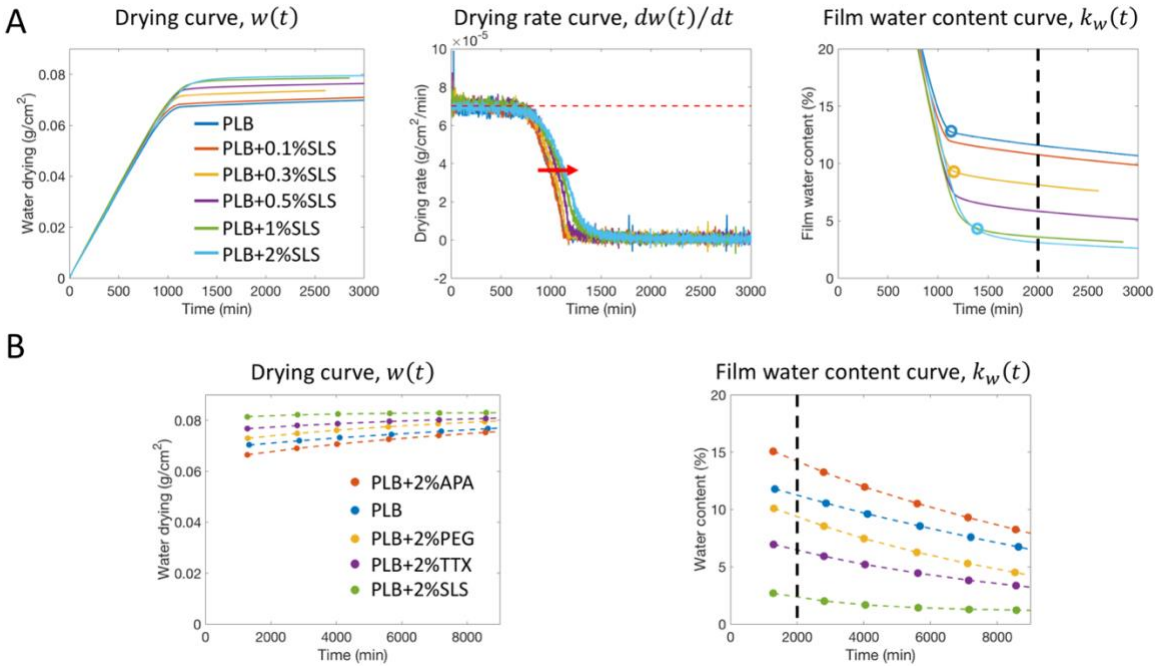

Figure 6.5: (A) The drying curves ($w(t)$), the drying rate curves ($dw(t)/dt$) and the film water content curves ($k_w(t)$) of PLB latex, PLB+SLS latexes. (B) The $w(t)$, $dw(t)/dt$ and $k_w(t)$ curves of PLB+2%APA, PLB, PLB+2%PEG, PLB+2%TTX, PLB+2%SLS latexes. All the latex films had an initial wet thickness at ~1.8 mm (so that the thickness of dried latex film is expected to be 1 mm), and were measured in the controlled environment (23 °C and 50% RH without wind). The red arrow in (A) denotes the rightward shift of the $dw(t)/dt$ curves in the regions where the drying rates drop. The circles on the $k_w(t)$ curves in (A) denote the inflection points (t_{infl}'s) of the PLB, PLB+0.3%SLS and PLB+2%SLS latexes. The black dashed lines in both (A) and (B) denote the vertical lines at 2000 min.

6.3.3 Interpretation of the role of post-polymerization additives in drying PLB latex films based on coalescence delay times (Δt_{del})

As demonstrated in Figure 5.6 (Chapter 5), the post-added surfactant into the latex system can shorten the film drying time by delaying the particles' coalescence; that is: the longer the coalesce delay time (Δt_{del}, relative to the original latex film), the more water evaporates freely before the particles on the film top coalesce into a low-permeable matured skin layer, thus the less water is trapped below the skin and coalesced layer (i.e., lower water content in the wet domain below the skin or coalesced layer, or k_w^* in Equation 6.1), the faster the coalesced layer thickens with time, and the less time is needed for the entire latex film to become dried. In Figure 6.6, the data of Δt_{del}'s of all PLB+additive latex films (determined in Section 6.3.2 and listed in Table 6.3 in Section 6.2.2) are plotted as a function of SC_{SLS} (percentage of latex particles' surface covered by post-added SLS surfactant molecules) for the PLB+SLS series, and as a function of $k_{add/s}$ (weight ratio of additive versus PLB's solids) for all PLB+additive latexes.

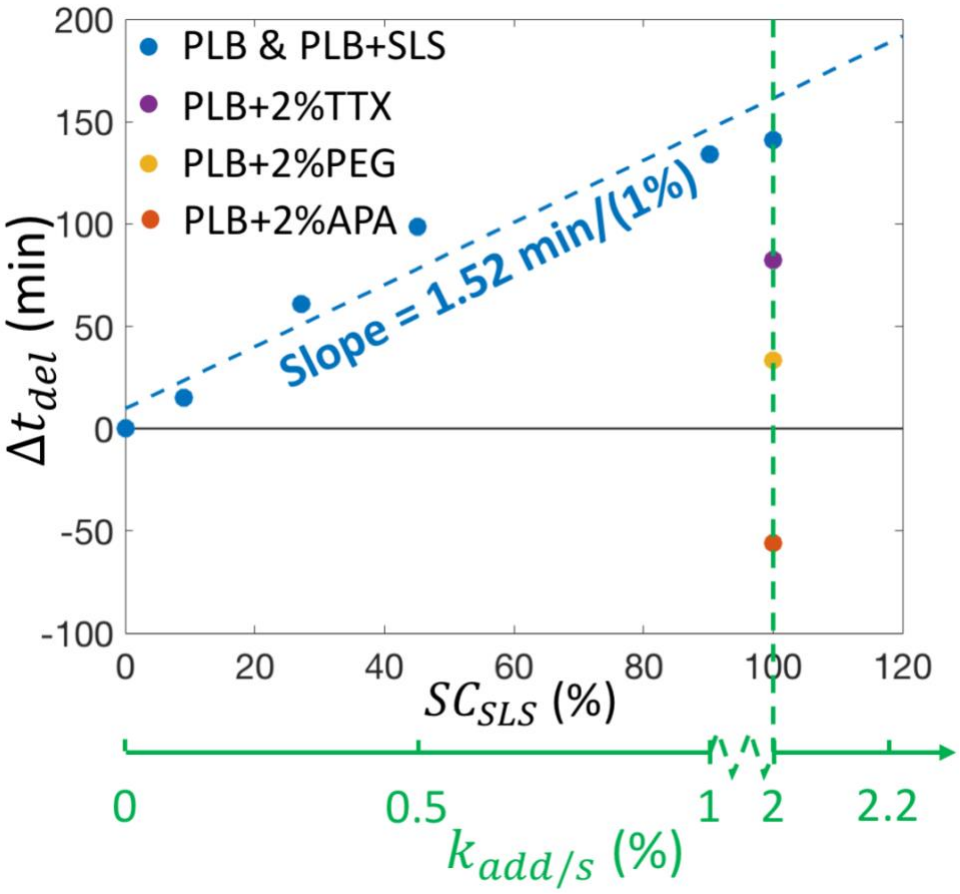

Figure 6.6: Coalescence delay times Δt_{del}'s as a function of percent particles' surface coverage with poste-added surfactant (SC_{SLS}) for the PLB+SLS series, and as a function of weight ratios of all additives versus PLB's solids ($k_{add/s}$) for all PLB+additive latexes (data abstracted from Table 6.3). The blue circles are the results of PLB, PLB+0.1%SLS, PLB+0.3%SLS, PLB+0.5%SLS, PLB+1%SLS and PLB+2%SLS latex films. The blue, purple, yellow and red circles (given along the vertical dashed green line) are the results of PLB+2%SLS, PLB+2%TTX, PLB+2%PEG and PLB+2%APA latex films, respectively. The data of Δt_{del}'s, which are listed in Table 6.3 in Section 6.2.2, were derived based on the drying curves in Figure 6.5 by the method documented in Section 6.2.4.

For the PLB+SLS latex series, the drying curves in Figure 6.5A show that the post-added SLS surfactant moved the region of the drying rate's drop rightwards (see the red arrow in Figure 6.5A center), and lowered the k_w (water content in the film) at the inflection point when the drying rate was impeded by the matured skin (see the circles in Figure 6.5A right). This is similar to what was found for the effects of surfactants on the drying curves of PEM latex films in Section 5.2.7 in Chapter 5. As shown in Figure 6.6, Δt_{del} increases mostly linearly with SC_{SLS}, giving the "coalescence delay efficiency" ($\widetilde{\Delta t}_{del}$, fitting slope of Δt_{del} versus SC_{SLS}) as 1.52 min/(1%) (see the blue dashed line in Figure 6.6), which is similar but a bit lower than the $\widetilde{\Delta t}_{del}$ for PEM+SLS latex series (1.90 min/(1%), see Figure 5.4 in Chapter 5). It is interesting that the PLB+2%SLS latex formed a coherent film after its inflection point (1380 min), while the PEM+2%SLS latex film was still re-dispersible in water even after being dried for 3000 min, although the SLS amounts in both PLB+2%SLS and PEM+2%SLS were more than enough to reach 100% SC_{SLS}. Such difference may be related to the difference of the surfactant types in the original latexes, i.e. a mixture of ionic and non-ionic ethoxylated surfactants in PLB, versus SLS in PEM. SLS can be more effective in impeding particles' coalescence than the ethoxylated surfactant (Triton X-100), as found in Section 5.3.2 in Chapter 5.

For the PLB+2%SLS, PLB+2%TTX and PLB+2%PEG latexes with $k_{add/s}$ = 2%, the PLB+2%SLS film gave the longer Δt_{del}, the delay-time for PLB+2%TTX film was in the middle and the PLB+2%PEG film gave the shorter delay-time (see the Δt_{del} data at $k_{add/s}$ = 2% in Figure 6.6). This indicates that the PEG (polyethylene glycol), although not as effective as the surfactants (TTX and SLS), can delay the latex particles' coalescence. The mechanism might be complicated: the polyethylene glycol (PEG) molecules can be

adsorbed on the latex particles' surface through the hydrogen-bonding with the chemically bound carboxyl groups on the particles' surface[6], which can increase the repulsive forces between particles due to steric effects and in turn impede the particles' coalescence. In addition, the PEG molecules that are soluble in the aqueous phase may be trapped in the interstices between particles which can also provide a barrier to retard polymer chains' inter-diffusion. On the other hand, the PLB+2%APA latex film gave a negative Δt_{del} (see the red circle at $k_{add/s}$ = 2% in Figure 6.6), meaning that the particles' coalescence of PLB+2%APA latex happened earlier than that of PLB latex, leading to a higher water content in the wet domain below the low-permeable matured skin layer. It took ~14 days for the PLB+2%APA film to get 95% of water evaporated compared to ~12 days for the original PLB film. It is believed that the APA (ammonium polyacrylate) molecules can interact with surfactants, carboxyl groups on particles' surface and other water-soluble molecules (such as oligomers and salts) in the aqueous phase through both ionic and hydrogen bonds[6]. Understanding such effects on the drying process of PLB latex film requires further investigation beyond the scope of this dissertation.

6.3.4 Water absorptions of dried PLB+additive latex films

Figure 6.7 shows the water absorption curves of the dried films of PLB, and PLB with various post-added additives, which are plotted as a function of both t and $t^{1/2}$ (A and B, respectively). Similar to what was found for the PEM+surfactant latex films in Chapter 5 (see Figure 5.5B), the R_{abs} data of the PLB+additive latex films in this chapter are mostly proportional to $t^{1/2}$ (see Figure 6.7B), corresponding to the Fickian absorption kinetics[5]. The water absorption efficiencies ($\tilde{R}_{abs}$'s, the linear fitting slopes of R_{abs} versus $t^{1/2}$) are

derived and given in Table 6.4. Interestingly, the PLB dried film ($\tilde{R}_{abs}$ = 0.016 day$^{-0.5}$) has a similar water absorption as the PEM dried film ($\tilde{R}_{abs}$ = 0.017 day$^{-0.5}$ measured in Section 5.3.3 in Chapter 5), suggesting that the dried latex film of PLB (poly(40LMA/35BA/24MMA/1MAA)) has a similar hydrophobicity to that of PEM (poly(64EHA/35MMA/1MAA)). Moreover, due to the similar values of $\tilde{R}_{abs}$'s and WVP's for both PLB film and PLB+2%SLS film (see Table 6.4), the post-added SLS surfactant (up to 2% relative to the latex solids) in the PLB does not compromise the water resistance of the dried latex film. The same also applies on the PLB+2%TTX film with $\tilde{R}_{abs}$ = 0.020 day$^{-0.5}$, which is similar to the $\tilde{R}_{abs}$ of the PLB film (0.016 day$^{-0.5}$).

On the other hand, as shown in Figure 6.7B, the post-added APA and PEG increase the water absorption of the dried latex film much more than the other additives do, as reflected by the relatively high $\tilde{R}_{abs}$'s of PLB+2%APA and PLB+2%PEG dried films given in Table 6.4. This is probably due to the ethoxylate groups associated with PEG and the carboxyl groups from APA's molecules that are trapped within the latex polymer film. However, it is surprising that the TTX surfactant molecules with ethoxylate groups do not increase the water absorption of the dried PLB film that much, while as shown in Figure 5.5 (Chapter 5) the post-added TTX increases the water absorption of the dried PEM film significantly.

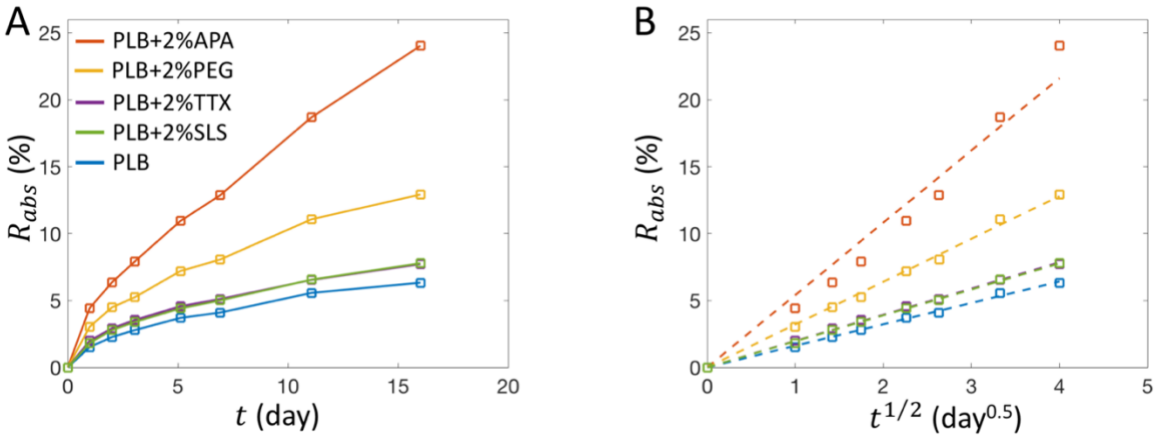

Figure 6.7: the relative absorbed water masses (R_{abs}) in dried latex films of PLB, PLB+2%APA, PLB+2%PEG, PLB+2%TTX and PLB+2%SLS (with 1 mm dried film thickness), as a function of immersion time (A) and square root of immersion time (B). It should be noted that R_{abs}'s of PLB+2%TTX are very close to those of PLB+2%SLS, so that the purple data points overlap with the green ones in (A) and (B).

Table 6.4: The water absorption efficiencies ($\tilde{R}_{abs}$) and the water vapor permeabilities (WVP) of dried latex films of PLB and PLB with various post-padded additives

Latex	$\tilde{R}_{abs}$ (day$^{-0.5}$)	WVP (10^{-11} g/(cm · min · Pa))
PLB	0.016	6.0
PLB+2%APA	0.054	/
PLB+2%PEG	0.032	/
PLB+2%TTX	0.020	/
PLB+2%SLS	0.019	5.9

As discussed in Sections 5.3.2 and 5.3.3 in Chapter 5, the particle surface coverage by surfactant molecules and the hydrophilic natures of the additives trapped between particles may not be the sole reasons for the effects of the post-added additives on the latex's drying process (i.e. coalescence delay time) and the dried film's water resistance (i.e. water absorption). The carboxyl and sulfate groups (or other chemically bound groups) on the particles' surface, the surfactants, salts and oligomers that are soluble in the aqueous phase, may also play a role. Just as important, the interactions between the additive molecules and the existing water-soluble species in the original latex (such as surfactants, salts and oligomers) can affect the surfactant adsorption on particles' surface (and perhaps its desorption and redistribution) and the rheological properties of the aqueous medium between particles, which in turn influence the drying process and the film's water resistance. In this chapter using the PLB latex system, the surfactants (both ionic SLS and non-ionic TTX) are found to be most effective in shortening the film drying time by delaying the particles' coalescence, while not compromising the water resistance of dried latex film. PEG also shortens the film drying time, but the dried film has a high water absorption. By contrast, the post-polymerization addition of APA is found to increase both the film drying time and water absorption of the dried film.

6.4 Conclusions

This chapter investigates the effects of post-polymerization additions of ionic and non-ionic surfactants such as sodium lauryl sulfate (SLS) and Triton X-100 (TTX), respectively, and other water-soluble additives such as ammonium polyacrylate (APA) and polyethylene glycol (PEG) on the drying process of the commercial PLB latex with a wet film thickness

in the millimeter range, as well as the water resistance (or water absorption) of the dried latex films. Similar to Chapter 5, both the OCT-Gravimetry-Video characterizations and the drying curve measurements under the controlled environment of 23 ℃ and 50% RH without wind were performed. The post-addition of SLS into the PLB latex decreased the water content in the wet domain (k_w^*) under the matured skin layer and increased the thickening rate of the coalesced layer thickness (h_{coal}), leading to a shorter film drying time. Such results are explained by the time delay of particles' coalescence (see schematic illustration given in Figure 5.6 in Section 5.4 of Chapter 5): the longer the coalescence delay time (Δt_{del}), the more water evaporates freely through the incipient skin layer before it becomes matured, the lower the water content in the wet domain below the skin or coalesced layer (k_w^*), thus the faster the increase of h_{coal} with time according to the coalesced layer thickening model (Equation 6.1), as well as the shorter film drying time. Based on the measurements of the latex films' drying curves and the surfactant's adsorption isotherms, Δt_{del} was found to increase almost linearly with the percentage of particles' surface coverage by SLS surfactant (SC_{SLS}). The TTX surfactant also increases Δt_{del} significantly. PEG and APA show opposite effects on the drying process: $\Delta t_{del} > 0$ for PEG, while $\Delta t_{del} < 0$ for APA. As for the water resistance of the dried latex films, SLS and TTX do not compromise the water resistance, while APA and PEG increase the water absorption significantly. There is no direct correlation between Δt_{del} and the dried film's water absorption regarding varied types of water-soluble additives. It should be noted that the effects of post-polymerization additives on the latex film formation process and the dried film's water resistance are more complex than just consideration of the ability of adsorption of these additives on the latex particles' surface and/or their hydrophilicity. In

fact consideration should be given to the molecular interactions between the post-added additives and the water-soluble species in the original latex that may influence the properties of the complex fluids in the interstices between latex particles during the drying process.

6.5 References

1. Lau, W. Frontiers in Emulsion Polymerization for Coatings. *The Dow Chemical Company*
2. Mark, J. E. *Physical Properties of Polymers Handbook*. (Springer New York, 2007).
3. Ller, B. M. & Poth, U. *Coatings Formulation: An International Textbook*. (Vincentz Network, 2011).
4. Zong, Z., Wall, S., Li, Y.-Z., Ruiz, J., Adam, H., Badre, C. & Trezzi, F. New additives to offer freeze–thaw stability and increase open time of low/zero VOC latex paints. *Prog. Org. Coat.* **72,** 115–119 (2011).
5. van der Wel, G. K. & Adan, O. C. G. Moisture in organic coatings — a review. *Prog. Org. Coat.* **37,** 1–14 (1999).
6. Napper, D. H. *Polymeric stabilization of colloidal dispersions*. (Academic Press, 1983).

7 Chapter 7 Conclusions and Recommendations

7.1 Conclusions

Waterborne latex is a colloidal system of polymer particles (usually with diameters < 1 μm) that are suspended in an aqueous medium. After being dried at a temperature higher than the polymer T_g, the fluidic latex can be transformed into a coherent solid polymer film, which has been widely used in industrial applications such as paints, coatings, adhesives, carpet backing, etc.. The latex is also used as inks, cosmetics and pharmaceuticals. However, during the drying process, the spatial distribution of latex particles is inhomogeneous and evolving with time, causing defects in the latex film. In this dissertation, studies were conducted on the drying inhomogeneity during the film formation of waterborne latex systems, especially the process of skin layer formation. Skin layer formation is usually encountered by drying a low-T_g thick latex film (when the Peclet number $Pe > 1$ and $\bar{\lambda} < 1$, see Equations 1.1 and 1.2 in Chapter 1), during which the latex particles on the film top (film/air interface) become dried early and coalesce into a polymer skin that traps water in the wet domain beneath the skin layer. Since the skin usually has a very low water vapor permeability (WVP), the film's drying rate can be impeded and the film drying time can be extended from days to weeks which is unacceptable in many applications. For example, in the architectural and roofing applications for waterproofing purpose, the dried film thicknesses of low-T_g latex coatings are often in the millimeter range, leading to the skin layer formation during drying at room temperature.

In this dissertation, model latex systems with different polymer T_g's and particle sizes were synthesized and characterized, including PS latex (with a copolymer

composition of 99 wt% styrene (St) and 1 wt% of methacrylic acid (MAA)), PBM latex series (with varied copolymer compositions of n-butyl acrylate (BA), methyl methacrylate (MMA) and 1 wt% MAA) and PEM latex (with a copolymer composition of 64 wt% 2-ethylhexyl acrylate (EHA), 35 wt% MMA and 1 wt% MAA) (Chapter 2); the OCT-Gravimetry-Video method was established by combining both microscopic and macroscopic characterizations in order to monitor the film's drying process of the high-T_g PS model latex system at room temperature and investigate the various types of drying inhomogeneity (Chapter 3); the drying process of the low-T_g model latex system with a latex film thickness in the millimeter range was studied using the OCT-Gravimetry-Video method, with the process of skin layer formation explained and a mathematical model of film formation developed (Chapter 4); the effects of post-added surfactants (added into the latex after emulsion polymerization) on the skin layer formation and the film's drying process of the model latex system were investigated (Chapter 5); the drying process and skin layer formation of a commercial low-T_g latex (PLB latex, with a copolymer composition of 40 wt% lauryl methacrylate (LMA), 35 wt% BA, 24 wt% MMA and 1 wt% MAA) were studied, and the effects of both post-added surfactants and other water-soluble additives were investigated (Chapter 6). In addition, concerning the water resistance of dried film for coating applications, the water absorptions of dried films with and without post-added additives were measured and analyzed (Chapters 5 and 6). The conclusions of this dissertation are summarized as follows.

1. A new method was developed by combining optical coherence tomography with gravimetric and video analysis (called "OCT-Gravimetry-Video" method), and used to

study and characterize the various stages during the drying process of the latex systems. The OCT, as a non-destructive and non-invasive optical imaging technique, monitors the internal microstructure of latex in microns' resolution (4.5 μm in this dissertation) in real time based on the back-scattered light intensity; at the same time, the gravimetry by using a digital balance measures the global water mass loss as a function of drying time, and the video camera takes time-lapse photos of the latex from the top view. This method was first applied to investigate the drying process of polystyrene (PS) latex at room temperature. Since PS has a T_g of 106 °C, the latex particles will not deform. The OCT was then used to study the more complex film-forming latex systems (PEM and PLB latexes) with T_g's lower than room temperature. Various types of drying inhomogeneity of high-T_g PS latexes were observed in both the horizontal direction (along the top surface of latex) and the vertical direction (perpendicular to the top surface of latex). These include: (i) the vertical packing process, where the latex particles become packed and restricted in motions from the latex top (latex/air interface) to the latex bottom (latex/substrate interface); (ii) the horizontal drying front, where the particles preferentially accumulate near the latex edge; (iii) the shear bands, where the dislocation of packed high-T_g particles occurs due to the internal compressive stresses; (iv) the drying boundary, which separates the white drier region to the blue wetter region, and propagates along the latex top; and (v) the cracks and the detachment, where the fractures of packed high-T_g particles form and the latex detaches from the substrate due to the internal compressive stresses. The PS particle size was found to significantly affect the packing process, the formation of shear bands and cracks.

2. During drying of a low-T_g thick model latex film (T_g < 0 °C, such as PEM latex) at room temperature, the latex particles on the film top (film/air interface) become dried early and coalesce into a polymer skin layer that traps water beneath it (in the wet domain). This is the process of skin layer formation, one type of drying inhomogeneity in the vertical direction, which occurs when the Peclet number $Pe > 1$ and $\bar{\lambda} < 1$. The OCT-Gravimetry-Video studies of the drying process of the PEM model latex system with a latex wet film thickness of ~2 millimeter show four drying stages: (I) packing of particles (where particles become in contact with each other with their Brownian motions restricted), (II) consolidation of particles (where particles become more densely packed or distorted), (III) formation and then maturation of incipient skin layer (where deformed particles on film top become coalesced into a coherent transparent polymer skin), (IV) thickening of coalesced latex polymer layer (coalesced layer) (where the particles in the wet domain continue coalescence until the entire film becomes dried and transparent). The drying rates during Stages I and II are fast and close to free water evaporation, while those during Stages III and IV are slow and limited by the water vapor permeability (WVP) and the thickness of skin and coalesced layers. A schematic illustration of the drying process of a low-T_g latex film is shown in Figure 4.4 in Chapter 4.

3. The WVP's of the matured skin and coalesced layer are similar to that of the dried latex polymer film. The "coalesced layer thickening model" is developed by assuming the water content in the wet domain is uniform along the vertical direction and the WVP of coalesced layer do not change with time (Equation 4.6, Chapter 4). This model

successfully predicts the increment of the coalesced layer thickness (h_{coal}, which includes the skin layer thickness) with the square root of time ($t^{1/2}$). Since the drying rate is very slow due to the low WVP's of skin and coalesced layer, the total drying time of a thick low-T_g latex film should be dominated by the time it takes for all water in the wet domain (below the skin and coalesced layer) to evaporate, which translates into that the h_{coal} should increase until the entire film becomes transparent. According to this model, the increasing rate of h_{coal} is related to the WVP of latex polymer film, the environmental humidity and the water content in the wet domain (k_w^*). By adjusting those parameters, the film drying time can be controlled and even shortened.

4. As discussed in Chapter 4, according to the coalesced layer thickening model, one effective way to shorten the drying time of a thick low-T_g latex film is by lowering k_w^*, so that h_{coal} can increase faster with time. This can be achieved by delaying the coalescence (interdiffusion of polymer chains) between latex particles. The longer the coalescence delay time (Δt_{del}), the more water evaporates freely before the packed particles on the film top coalesce into a low-permeable matured skin layer, thus the less water is trapped in the wet domain below the skin and coalesced layer (i.e., lower k_w^* in Equation 4.6 in Chapter 4), the faster the coalesced layer thickness (h_{coal}) increases with time, and the less time is needed for the entire latex film to become dried. For example, by drying a latex with a higher T_g (but still slightly below room temperature, for which the polymer chains' mobility is lower) or a larger particle size (for which the internal compressive stress is smaller), it takes longer time for the latex particles to deform and coalesce, so that k_w^* becomes lower and the film drying time is shorter.

5. The post-added surfactants into the original model PEM latex system are found to shorten the film drying time by delaying the particles' coalescence, making k_w^* lower and thus accelerating h_{coal}'s increment with time. Most of the post-added surfactant molecules are found to be adsorbed on the latex particles' surface, with the remaining amount soluble in the aqueous phase. It is proposed that, during the drying process of latex film, the surfactant molecules on particles' surface can increase the repulsive forces between particles so that a larger internal compressive force is required for particle-particle contact to take place and to initiate coalescence (called the "potential energy barrier" effect); surfactant molecules may also desorb from particles' surface as the distance of separation between particles decreases during drying and get trapped within the interstices between particles' boundaries to impede polymers' inter-diffusion (called the "physical barrier" effect).

   The coalescence delay time (Δt_{del}, derived from the difference of the film water contents at the inflection points of drying curves between the original latex and the latex with post-added surfactant) was found to increase linearly with the percentage of particles' surface coverage by surfactant (SC_{sur}, derived from the measured surfactant adsorption isotherms). It was found that at the same percent surface coverage by surfactant molecules, the sodium lauryl sulfate (SLS, an anionic surfactant) gives a longer Δt_{del} than Triton X-100 (TTX, a non-ionic surfactant) does. This may be related to the larger repulsive forces between particles with adsorbed SLS molecules, giving a higher potential energy barrier. And/or, the higher hydrophile-lipophile balance (HLB) value of SLS surfactant located at the interstices between the particles provides a more

hydrophilic physical barrier through which a hydrophobic polymer chains from the latex particles find them harder to penetrate, thus delaying the initiation of particle coalescence. With an appropriate amount of post-added surfactant into the latex, not only was the film drying time found to be shortened, but also the water resistance (especially the water absorption) of the dried latex film was found not to be compromised. However, too much surfactant post-added into the latex either causes incomplete film formation with poor coalescence, or a high water absorption of dried film. A schematic illustration of the effects of post-added surfactants on the drying process of a low-T_g model PEM latex film is shown in Figure 5.6 in Chapter 5.

6. The surfactant molecules that are adsorbed on latex particles' surface should not be the sole reason for delaying the particles' coalescence during the drying process of a low-T_g latex films. The carboxyl and sulfate groups (or other chemically bound groups) on the particles' surface, the surfactants, the salts and oligomers that are soluble in aqueous phase, may also contribute to delaying the latex particles' coalescence. Besides surfactants, other post-added water-soluble additives, such as polyethylene glycol (PEG) and ammonium polyacrylate (APA), were also found to influence the Δt_{del} and the film drying time (see studies reported in Chapter 6 on the film formation of PLB latex). Moreover, the water absorptions of dried latex films depend on the types of post-added additives and the choice of a latex system. Such complications should be the result of molecular interactions between the post-added additives and the water-soluble species in the original latex (including surfactants, oligomers and salts), as well as the carboxyl groups and other chemically bound groups on particles' surface. These molecular interactions can affect not only the surfactant's adsorption on particles'

surface (and perhaps its desorption and redistribution) bust also change the rheological property of the complex aqueous fluid resulting from specific molecular interactions between these species at the interstices between particles, thus impacting the coalescence delay time during the film formation process and the water resistance of the final dried film.

7.2 Recommendations

The drying process and film formation process of a waterborne latex system are complex, depending on the polymer T_g, the particle size, the chemically bound groups on particles' surface, the adsorbed surfactants and the water-soluble molecules in the original latex, as well as the post-added surfactants and other water-soluble additives. This dissertation establishes the "OCT-Gravimetry-Video" as a viable method to monitor the drying process of latex systems, to investigate the process of skin layer formation and film formation of a thick low-T_g latex film, and proposes a mechanism for the role of surfactants and other water-soluble additives on the film formation process, including shortening the latex film drying time through retarding the process of skin layer maturation via post-polymerization additives. In addition to those deliverables, there are several aspects to be recommended for future studies in order to better understand the latex film formation process.

1. With the help of the "OCT-Gravimetry-Video" method, the polystyrene (PS) latex was used as a model system to investigate the packing process of particles, the drying front, and the formations of shear bands and cracks during the drying process (see Chapter 3). Undoubtedly, the particle size and size distribution, the particle's surface charge,

the salts and other water-soluble molecules that alter the interactions between particles can affect the drying behaviors of PS latex dramatically. Further studies are needed to quantitatively correlate those factors to the particles' dynamics during drying. Moreover, the "OCT-Gravimetry-Video" method can be combined with the measurement of the latex film's internal stresses, in order to study the shear-banding and cracking phenomena.

2. The drying process of a thick low-T_g latex film experiences the formation of skin layer and the thickening of coalesced latex polymer layer (coalesced layer), which cause the lengthening of the film drying time due to the slow drying rate through the coalesced layer. The "coalesced layer thickening model" developed in Chapter 4 predicts the coalesced layer thickness as a function of time, and provides some guidelines to control the film drying time by adjusting the parameters used in this model (such as the WVP of coalesced layer, the water content in the wet domain and the environmental humidity). This model can be further improved with considerations of the strong-bonded water within the coalesced layer and the vertical non-uniform water distribution within the wet domain below the skin and coalesced layer, in order to simulate the film formation process more accurately.

3. The post-added surfactants into the latex can shorten the film drying time of a low-T_g latex film by delaying the particles' coalescence in which way less water would be trapped below the matured skin layer. The surfactant molecules adsorbed on particles' surface and trapped between particles can provide barriers (both potential energy and/or

physical barriers) to impede the coalescence. Thus, it would be also interesting to investigate how the chemically bound hydrophilic groups on particles' surface (such as carboxyl groups, sulfate groups and other functional groups) delay the particles' coalescence and influence the film drying time. The pH value of latex, which determines the ionization extent of carboxyl groups, should also play a role and should also be the subject of further investigation.

4. The particle surface coverage by surfactant molecules and the hydrophilic natures of the additive molecules trapped between particles should not be the sole reasons for the effects of the post-added surfactant or other additives on the film drying time (viz. coalescence delay time) and the dried film's water resistance (viz. water absorption). The molecular interactions between the additive molecules, the water-soluble molecules in the original latex, and the chemically bound groups on particles' surface need to be considered and studied in the future, since those interactions may also have a significant impact on the film's drying process and the dried film's water resistance.

5. Due to the resolution limitation (~5 μm) of OCT imaging, the migrations and distributions of surfactant and other water-soluble molecules (with sizes in nanometers) could not be detected. In order to monitor the evolution of those molecules' spatial distributions, especially within the interstices between particles (with interstitial distances changing from tens of nanometers to few nanometers during drying, see Table 5.3 in Chapter 5), a high-resolution imaging technique is needed; moreover, the molecules may have to be tagged with fluorophore. Confocal microscopy with

resolutions > 200 nm cannot resolve the interstices between particles. The near-field scanning optical microscopy with a resolution of tens of nanometers and the environmental scanning electron microscope (ESEM) with a resolution of several nanometers may be employed in future. The cryogenic scanning electron microscope (Cryo-SEM) may also help in detecting the molecules in the interstices between particles that are frozen, especially when the energy-dispersive X-ray spectroscopy (EDXS) is equipped to map out the distributions of chemical elements. Such mapping of molecules in the interstitial spaces will help to explain the effects of surfactants and other water-soluble additives on the coalescence between latex particles and the water resistance of final dried latex films.

6. Besides the water-soluble additives, the effects of post-added pigment/filler particles on the drying process of latex and the water resistance of dried film are also important for practical coating applications; thus it should be part of future studies. Those pigment/filler particles, which are usually made of inorganic materials, do not deform during the film formation process, but may affect the latex particles' coalescence and the porosity of the final dried coatings. Moreover, the interactions between the dispersant molecules and the pigment/filler particles' surface may also show intriguing effects on the latex film formation process.

Appendix I Examples of Calculating Particles' Surface Coverage by Surfactant Molecules (SC_{sur}) of PEM, PEM+1%SLS and PEM+1%TTX latexes

The % surfactant surface coverage (SC_{sur}, percentage of particles' surface covered by surfactant molecules) can be calculated based on the latex % solids content and (k_{s0}) and wt% ratio of surfactant versus latex solids ($k_{sur/s}$). It follows Equations 5.12, 5.13, 5.15, 5.16, 5.17 and 5.18. The PEM latex has an average particle diameter D_p = 176 nm and the densities of polymer, water, and latex are assumed to be the same, $\rho_s = \rho_w = \rho$ = 1 g/cm^3. The surfactant molecular weight (M_{sur}) is 288.4 g/mol for SLS and 625.0 g/mol for TTX. The SC_{sur}'s, the surfactant number densities adsorbed on latex particles' surface ($\varphi_{sur,p}$, number of surfactant molecules per nm^2 on particle surface), the surfactant concentrations in aqueous phase ($c_{sur,aq}$) and the partition coefficients (K_D, the molar amount ratio of surfactant molecules on particle surface versus those in aqueous phase) of PEM, PEM+1%SLS and PEM+1%TTX are determined as follows.

I) the original PEM latex

For the original PEM latex, k_{s0} = 50.37% and $k_{SLS/s}$ = 0.5%. The SLS surfactant has an adsorption isotherm curves with $\tilde{\varphi}_{SLS} = 0.401$ nm^{-2}/mM, $CMC_{serum} = 2.93$ mM, and $\varphi_{SLS,p,max} = 1.175$ nm^{-2}. First, the temporary $c_{SLS,aq}$ ($c_{SLS,aq,temp}$) is calculated by Equation 5.12 (Chapter 5) as:

$$c_{SLS,aq,temp}(k_{s0}, k_{SLS/s}) = \frac{\rho_s \rho_w N_A D_p}{M_{SLS}} \cdot \frac{k_{s0} k_{\frac{SLS}{s}}}{6\rho_w \tilde{\varphi}_{SLS} k_{s0} + \rho_s N_A D_p (1 - k_{s0})}$$

$$= \frac{1\,\mathrm{g/cm^3} \times 1\,\mathrm{g/cm^3} \times 6.022 \times 10^{23}\mathrm{mol^{-1}} \times 176\mathrm{nm}}{288.4\,\mathrm{g/mol}}$$

$$\cdot \frac{50.37\% \times 0.5\%}{[6 \times 1\,\mathrm{g/cm^3} \times 0.401\ \mathrm{nm^{-2}/mM} \times 50.37\% + 1\,\mathrm{g/cm^3} \times 6.022 \cdot 10^{23}\mathrm{mol^{-1}} \times 176\mathrm{nm} \times (1 - 50.37\%)]} = 0.732\mathrm{mM}$$

Since $c_{SLS,aq,temp} < CMC_{serum}$ = 2.93 mM, the surfactant surface coverage should be less than maximum. Thus, $c_{sur,aq} = c_{sur,aq,temp}$ and $\varphi_{sur,p}$ is calculated by Equation 5.13 (Chapter 5) as:

$$\varphi_{SLS,p} = \tilde{\varphi}_{SLS} \cdot c_{SLS,aq} = 0.401\ \mathrm{nm^{-2}/mM} \times 0.73\ \mathrm{mM} = 0.294\ \mathrm{nm^{-2}}$$

Then K_D and SC_{SLS} are calculated by Equations 5.17 and 5.18 (Chapter 5), respectively:

$$K_D = \frac{\varphi_{SLS,p}}{c_{SLS,aq}} \cdot \frac{6\rho_w k_{s0}}{\rho_s D_p (1 - k_{s0}) N_A}$$

$$= \frac{0.294\ \mathrm{nm^{-2}}}{0.732\ \mathrm{mM}}$$

$$\cdot \frac{6 \times 1\,\mathrm{g/cm^3} \times 50.37\%}{1\,\mathrm{g/cm^3} \times 176\mathrm{nm} \times (1 - 50.37\%) \times 6.022 \times 10^{23}\mathrm{mol^{-1}}} = 23.0$$

$$SC_{SLS} = \frac{\varphi_{SLS,p}}{\varphi_{SLS,p,max}} = \frac{0.294\ \mathrm{nm^{-2}}}{1.175\ \mathrm{nm^{-2}}} = 25.0\%$$

Therefore, in the original PEM latex, 25% of particles' surface is covered by SLS molecules.

II) PEM+1%SLS latex

For the PEM+1%SLS latex, k_{s0} = 49.22% and $k_{SLS/s}$ = (0.5+1)% = 1.5% (which includes the SLS in the original PEM latex). $c_{SLS,aq,temp}$ is calculated by Equation 5.12 as 2.19 mM, which is smaller than CMC_{serum} (2.93 mM), and thus $c_{SLS,aq}$ = $c_{SLS,aq,temp}$ = 2.19 mM. By Equations 5.13, 5.17 and 5.18 in Chapter 5, $\varphi_{SLS,p}$, K_D and SC_{SLS} are calculated as 0.88 nm^{-2}, 22.0 and 74.8%, respectively.

III) PEM+1%TTX latex

In the PEM+1%TTX latex with k_{s0} = 49.63%, both SLS surfactant (with $k_{SLS/s}$ = 0.5%) and TTX surfactant (with $k_{TTX/s}$ = 1%) co-exit. Although SLS and TTX molecules interact with each other when they are in contact [Colombié, D., Landfester, K., Sudol, E. D. & El-Aasser, M. S. *Langmuir* **16**, 7905–7913 (2000)], in this dissertation it was assumed that SLS and TTX are adsorbed on particles' surface independently.

For the SLS in PEM+1%TTX latex, it should have the same surfactant distribution as that of PEM latex, which are $c_{SLS,aq}$ = 0.73 mM, $\varphi_{SLS,p}$ = 0.29 nm^{-2}, K_D = 23.0 and SC_{SLS} = 25.0%.

For the TTX in PEM+1%TTX latex with $\tilde{\varphi}_{TTX} = 14.1$ nm^{-2}/mM, $CMC_{serum} = 0.0436$ mM, and $\varphi_{TTX,p,max} = 0.614$ nm^{-2}, $c_{TTX,aq,temp}$ is calculated by Equation 5.12 as 0.0201 mM, which is smaller than CMC_{serum} (0.0436 mM), and thus $c_{TTX,aq}$ = $c_{TTX,aq,temp}$ = 0.0201 mM. By Equations 5.13, 5.17 and 5.18 in Chapter 5, $\varphi_{TTX,p}$, K_D and SC_{TTX} are calculated as 0.28 nm^{-2}, 785.1 and 46.0%, respectively.

Vita

Hao Huang was born to Xiaoshi Huang and Xiulan Jia in 1991 in Luoyang (China). After his primary school, he moved with his family to Ningbo (China), where he entered Zhenhai Middle School. Then he attended East China University of Science and Technology in 2009 in Shanghai (China). He gained the Bachelor of Engineering degree there in 2013. In the same year, he was admitted as a Ph.D. student to Lehigh University in Bethlehem, Pennsylvania (USA). During the first two years of his Ph.D. study, he majored in Bioengineering, performed research on the dielectrophoresis of nano-colloids, and published a paper on *Electrophoresis* (Wiley-VCH). After that, he changed his major to Chemical Engineering, where he focused on his research of the drying inhomogeneity of colloids and the film formation process of latex systems. At the time of the completion of this dissertation, an article based on Chapter 3 was submitted to *Scientific Reports* (Nature Publishing Group) and received favorable reviews, which will be resubmitted for publication. Two to three other articles will be prepared based on Chapters 4 – 6 and will be submitted to *Langmuir*, and *Journal of Coatings Technology and Research*. He also actively attended several national/international conferences (including International Polymer Colloids Group (IPCG) Conference, American Chemical Society (ACS) National Meeting, American Physical Society (APS) March Meeting, American Institute of Chemical Engineers (AIChE) Annual Meeting, American Coatings Conference), where he gave presentations/posters and received several awards. He will graduate in May 2018 with the Doctor of Philosophy (Ph.D.) degree in Chemical Engineering and the Master of Science (M.S.) degree in Bioengineering, after which he will pursue a career in the fields of emulsion polymers, coatings and colloidal matters.